THE EFFECT OF MORPHOLOGY OF α and β PHASES ON SUPERPLASTIC PROPERTIES OF Ti-6Al-4V ALLOY

by

Bradley J. Diak

A thesis presented to
the University of Manitoba
in partial fulfillment of the
requirements for the degree of
Master of Science
in
Mechanical Engineering

Metallurgical Science Laboratories
Winnipeg, Manitoba
1990

ISBN 0-315-71807-2

THE EFFECT OF MORPHOLOGY OF a and B PHASES ON SUPERPLASTIC PROPERTIES OF Ti-6Al-4V ALLOY

BY

BRADLEY J. DIAK

A thesis submitted to the Faculty of Graduate Studies of the University of Manitoba in partial fulfillment of the requirements of the degree of

MASTER OF SCIENCE

ABSTRACT

The effects of morphology of alpha and beta phases on the superplastic properties of the Ti-6Al-4V alloy was examined. Tensile testing of cylindrical specimens at constant strain rates of $5x10^{-3}$ to $1x10^{-4}$ s^{-1} in the temperature range of 875 to 950°C were performed to determine the flow properties of beta annealed, beta quenched and equiaxed material with the same overall chemical composition and similar initial volume fractions of alpha and beta phases. Specifically, the total elongation to failure and the change in strain rate sensitivity values with strain were determined. Optical, scanning, and transmission electron microscopy studies were performed on tensile specimens water quenched from the test temperatures to relate the observed superplastic properties to the observed microstructural changes.

It was revealed that high aspect ratio alpha phase microstructures result in strain softening and initially low strain rate sensitivity values. The strain rate sensitivity values increase as the microstructures become more equiaxed with strain. The break-up of the alpha phase is characterized by alpha/alpha boundary separation by beta cusping and increased beta phase continuity. Activation energy and TEM observations indicate that grain boundary diffusion, dislocation slip and grain boundary sliding occur during deformation The morphology of the alpha and beta phases determine the contributions from each mechanism.

ACKNOWLEDGEMENTS

The author would like to thank Dr. M.C. Chaturvedi for the opportunity to develop this work and for his constant encouragement throughout its course.

As well the author would also like to extend his thanks to Dr. N. Richards of Bristol Aerospace Limited with whom I was able to share my thoughts on this work. Special thanks are also in order to Mukesh Jain for planting the seeds for this thesis and for his friendship.

I would also like to acknowledge the superb support staff in the lab, particularly Messrs. L. Oree, J. Van Dorp , D. Mardis , and R. Hartle for their technical assistance and friendship.

TABLE OF CONTENTS

Page

Page

LIST OF FIGURES

LIST OF TABLES

GLOSSARY

acicular alpha	A product of nucleation and growth from beta to the lower temperature allotrope alpha phase. It may have a needlelike appearance in a photomicrograph and may have needle, lenticular, or flattened bar morphology in three dimensions. Its typical aspect ratio is about 10:1.
alpha	The low temperature allotrope of titanium with a hexagonal, close packed structure. (It occurs below the beta transus temperature.)
alpha-beta	A microstructure which contains both alpha and beta as the principal phases at a specific temperature.
alpha case	The oxygen, nitrogen, or carbon enriched, alpha stabilized surface which results from elevated temperature exposure.
alpha prime	A supersaturated, non-equilibrium hexagonal phase formed by a diffusionless transformation of the beta phase.
alpha stabilizer	An alloying element which dissolves preferentially in the alpha phase and raises the alpha-beta transformation temperature. Aluminum is an alpha stabilizer.
alpha transus	The temperature which designates the phase boundary between the alpha and alpha plus beta fields.
basketweave	Alpha platelets with or without interleaved beta platelets that occur in colonies in a Widmanstätten microstructure.
beta	The high temperature allotrope of titanium with a body-centered cubic crystal structure. (It occurs above the beta transus.)
beta transus	The minimum temperature above which equilibrium alpha does not exist. For beta eutectoid additions, the beta transus ordinarily is applied to hypoeutectoid compositions, or those that lie to left of the eutectoid composition.
blocky alpha	Alpha phase which is considerably larger and more polygonal in appearance than the primary alpha in the sample.
colonies	Regions within prior beta grains with alpha platelets having nearly identical orientations. Colonies arise as transformation products during cooling from the beta field at cooling rates that induce platelet nucleation and growth.
elongated alpha	A fibrous type of microstructure brought about by unidirectional metalworking. It may be enhanced by the presence of grain boundary alpha.

equiaxed microstructure	A polygonal or spheroidal microstructural feature have approximately equal dimensions in all directions.
grain boundary alpha	Primary alpha outlining prior beta grain boundaries. It may be continuous unless broken up by subsequent work. Also may accompany blocky alpha. Occurs by slow cooling from the beta field into the alpha-beta field.
hydride phase	The phase TiH_x formed in titanium when the hydrogen content exceeds the solubility limit. Sometimes reported as an electropolishing artifact.
intergranular beta	Beta phase situated between alpha grains. It may be at grain corners as in the case of equiaxed alpha-type microstructures in alloys having low beta stabilizer contents.
martensite	The alpha product resulting from cooling from the beta phase region at rates too high to permit transformation by nucleation and growth. Martensite is supersaturated with beta stabilizer.
matrix	The constituent which forms the continuous or dominant phase of a two phase microstructure.
prior beta grain	The beta grains established during the most recent beta excursion.
transformed beta	A local or continuous microstructure compromised of decomposition products arising by nucleation and growth processes during cooling from the local or over-all beta transus. Primary and growth alpha may be present. Transformed beta typically consists of alpha platelets which may or may not be separated by beta phase.
Widmanstätten microstructure	A microstructure of alpha platelets or alpha and beta platelets resulting from cooling from a temperature above the beta transus. The platelets will often occur in colonies, giving a basketweave appearance.

LIST OF SYMBOLS

α	alpha phase
α'	alpha prime martensite
α''	alpha double prime martensite
α^m	generic martensite
β	beta phase
β_{tr}	beta transus
BA	material with beta annealed phase morphology
BCC	body centered cubic
BQ	material with beta quenched phase morphology
ε	true strain
ε_a	actual true strain
ε_t	total true strain
$\dot{\varepsilon}$	true strain rate
EQ	material with equiaxed phase morphology
ϕ	alpha aspect ratio
GBS	grain boundary sliding
g.s.	grain size (the mean linear intercept)
HCP	hexagonal close packed
k	material constant
l	length of alpha plate
m	strain rate sensitivity
m^+	strain rate sensitivity determined from incremental test

m^-	strain rate sensitivity determined from decremental test
m_{ave}	average strain rate sensitivity determined from $m+$ and $m-$
M_f	The temperature at which the martensite reaction is complete.
M_S	The maximum temperature at which the alpha prime martensite reaction begins upon cooling from the beta phase
n	strain hardening coefficient
Q	activation energy
R	Universal gas constant
σ	true stress
s^{-1}	per second
t	time or thickness of alpha plates
T	temperature
V_x	volume fraction of phase x

CHAPTER 1
INTRODUCTION

In the last twenty years, superplastic forming technology has provided an effective means of shaping complex structural materials that are usually expensive to machine or join, particularly in the aerospace field. The effort in understanding superplasticity has been made by characterizing alloys in terms of mechanical and microstructural variables, and the relationships between them. Even though general requirements for superplasticity have been settled, no satisfactory model which takes into account all variables, and describes the rate controlling mechanism completely has yet been developed.

It has been observed that a considerable number of microstructural variables such as grain size, grain size distribution, phase fraction, and texture influence superplastic deformation, but the interdependencies among these variables are difficult to separate. Varieties of binary eutectic and eutectoid systems and ternary systems, including Ti-6Al-4V, have been studied extensively. Microstructural variations in Ti-6Al-4V are common in this commercial alloy. Researchers have tried to enhance superplastic deformation characteristics and isolate variables like phase fractions by altering chemical compositions.

The objective of this work was to microstructurally characterize an important α-β titanium alloy, that is known to be superplastic, modify its phase morphology and study its high temperature deformation properties. Taking a novel approach, the microstructural morphology of the alloy was thermally altered, but maintained at the same overall chemical composition and volume fraction of α and β phases to determine the effect of morphology on superplasticity. The quantitative effect of grain size, grain shape, and volume fraction on the change in mechanical properties was fully assessed, with the goal to better understand the influence of morphology on superplastic deformation.

The study was conducted by evaluating the high temperature tensile flow properties of three distinct Ti-6Al-4V morphologies, each containing similar volume fractions, but

measurable microstructural differences at the same initial superplastic conditions. The changes in morphology were observed using optical, scanning, and transmission electron microscopy, and related to the changes in mechanical properties in the superplastic state.

CHAPTER 2
LITERATURE REVIEW

2.1 Introduction

High temperature deformation behaviour of Ti-6Al-4V, particularly the phenomenon of superplasticity has been studied extensively with respect to microstructure in an effort to formulate an understanding of the operating mechanism. Unfortunately, the number of microstructural variables suggested to affect superplasticity are considerable, and very few studies have attempted to completely characterize a microstructure using all the variables.

The purpose of this literature review was four-fold. Firstly, to establish the general requirements for the superplastic behavior of a crystalline material. Secondly, to establish their superplastic flow characteristics. After establishing these requirements, the physical metallurgy of Ti-6Al-4V alloy and particularly the morphology of various phases in the alloy were reviewed. Finally, the effect of microstructural variables on the superplasticity of Ti-6Al-4V alloy has been examined with an emphasis on the relationships between microstructural features, deformation variables and superplastic characteristics, and their similitude to other microduplex alloy systems.

2.2 General Superplasticity

2.2.1 Observation of Superplasticity

The ability of some materials to deform at relatively low stresses, to large elongations without necking under specific deformation conditions, is known as superplasticity. Earliest observations of superplasticity were made by Hargreaves [1,2], Jenkins on eutectic Cd-Zn and Pb-Sn alloys[3], and by Pearson on Pb-Sn and Bi-Sn alloys [4] in the 1928 to 1934 period. Unfortunately, it was not until Underwood [5] published a review article in 1962 of some of this early work that interest was rekindled in the area.

Since the late sixties, a considerable amount of work has been done, to the extent that various reviews on superplasticity now list wide numbers of superplastic materials indicating tensile elongation for one alloy greater than 5500 percent [6-10]. With all the activity in superplastic studies, few structural alloys have made the transition from the laboratory to industrial forming applications. The ability to use the technology has superceded the understanding of the phenomenon, and at the present time the mechanism for superplasticity has not yet been satisfactorily identified. In the move to commercialize the superplastic deformation behavior of titanium alloys, their mechanical property parameters have been quantified to a greater extent then microstructural parameters. It was not until Paton and Hamilton's work in 1979 [11] that microstructural parameters other than initial grain size were considered in Ti-6Al-4V superplasticity studies.

To fully evaluate superplasticity in a material, both microstructural and mechanical property parameters must be fully characterized. However, it is essential to first establish the mechanical properties that characterize superplasticity.

2.2.2 Mechanical Characteristics

Superplastic flow characteristics are best demonstrated by the relationship between stress and strain rate and to a lesser extent by the qualitative relationship between elongation to failure and strain rate. For the latter, total elongation to failure is a measure of the enhanced ductility prevalent in superplastic materials where values must be greater than 200 percent [10]. Superplastic materials in general exhibit a sigmoidal relationship between the logarithm of flow stress, σ, versus the logarithm of strain rate, ε, as shown in Figure 2.1. This curve exhibits three distinct regions. The three regions are characteristically different with respect to strain rate, stress and temperature. Region II is deemed superplastic, because of the high strain rate sensitivity, m, which corresponds to the maximum slope of the stress versus strain rate plot defined as follows.

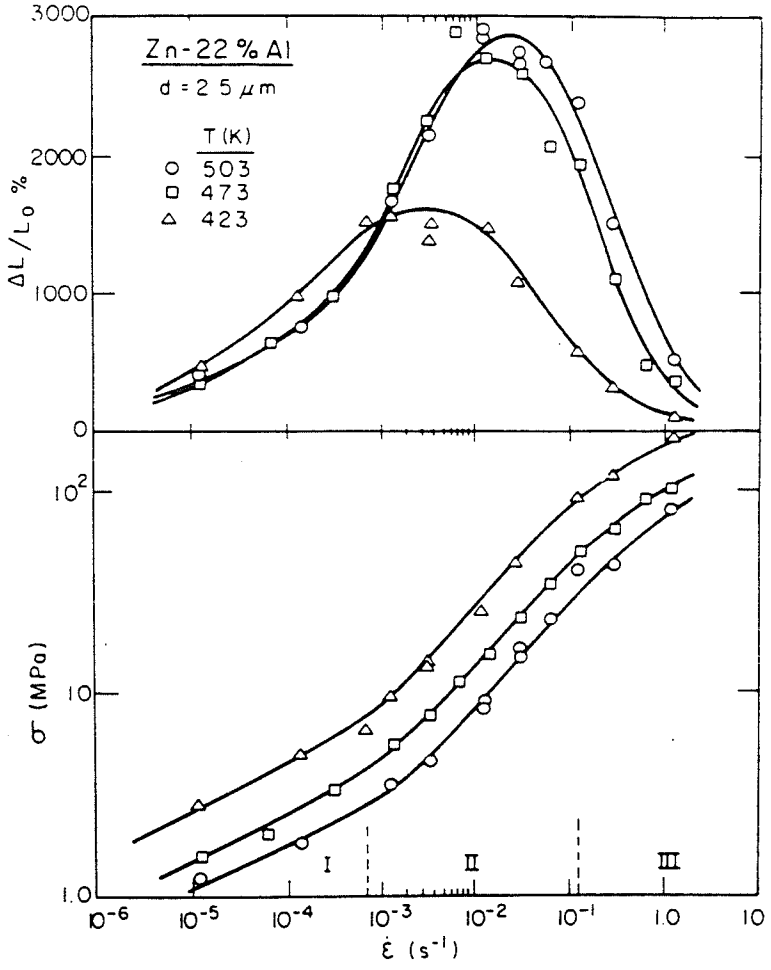

Figure 2.1: Typical Flow Properties of Zn-22 wt. pct. Al [6].

$$\sigma = k\dot{\varepsilon}^{m} \varepsilon^{n} \Big|_{T} \tag{2.1}$$

where,

σ = flow stress

k = material constant

$\dot{\varepsilon}$ = strain rate

m = strain rate sensitivity

ε = strain

n = strain hardening coefficient

T = temperature

If n=0, then the flow stress can be expressed as,

$$\sigma = k\dot{\varepsilon}^{m} \Big|_{T,\varepsilon}, \tag{2.2}$$

and therefore the strain rate sensitivity, m, follows as,

$$m = \left(\frac{\partial \ln \sigma}{\partial \ln \dot{\varepsilon}} \right) \Big|_{T,\varepsilon}. \tag{2.3}$$

Materials that exhibit superplasticity have a characteristically high strain rate sensitivity at a constant strain and temperature. Strain rate sensitivity values for superplastic materials are typically greater than or equal to 0.3, with the typical range being between 0.4 to 0.8. The strain rate sensitivity was first inferred to relate substructure deformation to mechanical test data [12], but it was Backofen *et al.* [13,14] who established its importance to superplasticity. It follows from equation (2.3) that m values are determined at constant temperature and strain.

The temperature requirement for superplasticity is fundamentally significant, being typically greater than one half the melting point of the alloy [6]. The three regimes can be expressed by their temperature dependance in an Arrhenius plot, where strain rate depends on temperature and flow stress. Figure 2.2 shows the Arrhenius plots for a Zn-22 weight percent Al alloy. The reason for the three regimes can be linked to the corresponding activation energies. Regime I typically exhibits activation energies, Q, similar to those for lattice self diffusion. Regime II, where the high strain rate sensitivity exists, has activation energy values near those for grain boundary self diffusion. Finally, Regime III exhibits lattice self diffusion activation energies similar to those in Regime I.

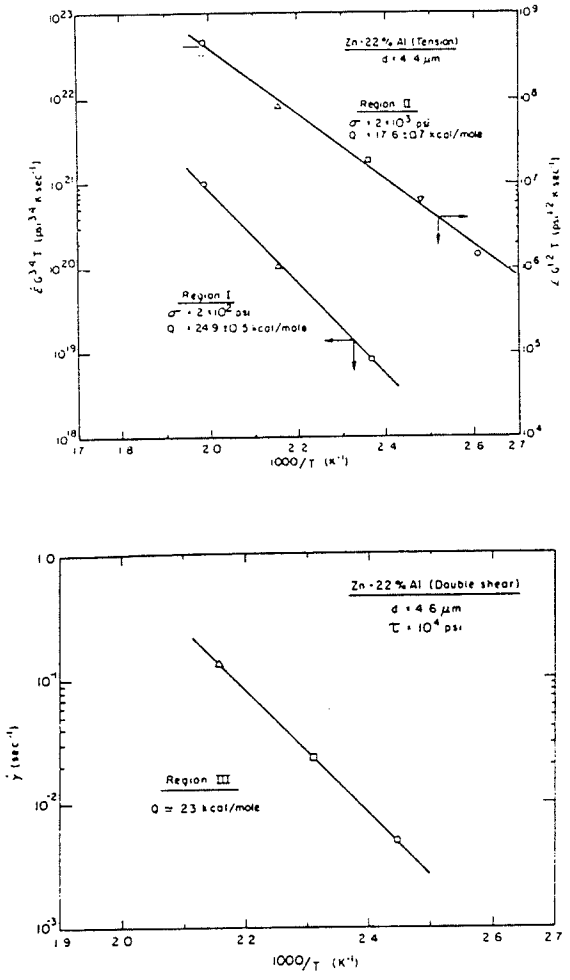

Figure 2.2: Arrhenius Plots for Zn-22 wt. pct. Al [15].

The other factor that must be constant when determining m is the strain. The fact that strain must be constant suggests the obvious conclusion that the microstructural state of the material is important, and suggests that the microstructure can change with time and strain. It is pertinent therefore, to review the microstructural requirements that are necessary for existance of superplasticity.

2.2.3 Microstructural Requirements

One of the first recognized microstructural requirements for superplasticity was observed to be a small, equiaxed, stable grain size less than 10 μm. [6,7]. Considering the high temperatures at which deformation must take place, the maintenance of a fine grain size is difficult, so most materials exhibiting superplasticity are either two phase or single phase containing a fine dispersion of second phase particle. These second phases, or in the case for single phase materials, particles, tend to stabilize grain size during deformation [16,17]. For the Ti-6Al-4V alloy, partitioning of the substitutional alloying elements between alpha and beta phases slows grain coarsening when substantial volume fractions of both phases are present [18]. For example, without the presence of a second phase, the beta phase in Ti-6Al-4V alloy will rapidly grow to diameters well in excess of 50 μm at temperatures above 760°C. Since small grain size is a requirement for superplasticity some researchers have used new processing methods to achieve ultra-fine grain sizes in order to evaluate their effect on superplasticity. Peters *et al.* [19] showed that decreasing the α grain size in the Ti-6Al-4V alloy to one to two micrometers from the conventionally processed sheet with grain sizes between 10 to 20 μm lowered the flow stress. More significantly, higher strain rate sensitivities were achieved at lower temperatures. Unfortunately, no elongation data was presented regarding the increased ductility due to the smaller grain size.

In contrast, large grain materials have also shown superplasticity with m values approaching unity [20]. Beta titanium and β brass alloys tend to develop large grain sizes

at superplastic deformation temperatures, but develop subgrains that enhance material flow. Unfortunately, large grains are not satisfactory for optimum superplasticity, since holding at these temperatures allows grain coarsening which reduces superplastic flow properties. Lee and Backofen demonstrated that holding the Ti-6Al-4V alloy at temperature for an extended period of time increased the α or β grain size from 6.6 μm to 19.8 μm, and consequently reduced the m from 0.8 to 0.6 at a strain rate of $1x10^{-4}$ s^{-1} [21].

Beside grain size, other microstructural variables have been suggested as essential in characterizing superplastic behavior, particularly for systems that have complex microstructures. As well, most commercial alloys produced in the forms of sheets or bar and having undergone processing to achieve small grain sizes contain what have been deemed as anomalies like banding and have grain size distributions that adversely affect superplastic deformation. So the question arises, what microstructural variables must be characterized for a superplasticity study?

Rosenblum *et al.* have suggested volume fraction of α and β phases, size, distribution, shape of grains and their contiguity must be characterized [22]. Ghosh and Hamilton [23] went a little further by adding to the previous list the need to also characterize texture, and grain growth kinetics. Some materials tend to cavitate during superplastic deformation, and so an evaluation of their cavitation behaviour is also sometimes necessary. The type of microstructural morphologies possible in the Ti-6Al-4V alloy are varied, but distinct. So before reviewing the effect of these variables on superplasticity of Ti-6Al-4V, an understanding of the possible morphologies for each phase is necessary.

2.3 Ti-6Al-4V Alloy

2.3.1 Equilibrium Phases

Ti-6Al-4V is a near alpha - alpha plus beta titanium alloy. Alpha(α) is a hexagonal close packed(HCP) phase, while the higher temperature phase, beta(β), is body centered cubic(BCC). In pure titanium, HCP-α undergoes an allotropic transformation to BCC-β at a temperatures of 882°C [24]. Alloying additions of aluminum increase the α-β transformation temperature while the isomorphous vanadium lowers the transformation temperature. Hence, aluminum and vanadium are alpha and beta stabilizers, respectively. Ti-6Al-4V contains both types of stabilizers, so α and some β can coexist at room temperature. It is in effect temperature which determines the percentage of phases present at equilibrium [25]. Varieties of thermal treatments can be designed to vary the mechanical properties of Ti-6Al-4V by controlling the fraction of phases and their compositions. Work done by Fopiano *et al.*, reported in Table 2.1, demonstrates the change in volume fraction of phases present and their compositions after solution treating and water quenching.

TABLE 2.1: Phases Present in Ti-6Al-4V and Their Compositions at Various Solution Temperatures [26]

Sol'n temp,	Phases present	vol%β +/or α'	α wt %		β wt %		M_S
°C	after quench		Al	V	Al	V	°C
750	α,β	8	6	3	1	14	
800	α,α',β	14,5	7	3	1.5	11	480
850	α,α'	25	8	2.5	2	8	655
900	α,α'	38	9	2.5	2	6.5	710
950	α,α'	64	10	2	4	5	825
1000	α'	100			6	4	916

Alpha prime(α') in this table is the non-equilibrium product derived from the non-equilibrium cooling of β. During equilibrium cooling, α precipitates from β by a diffusion controlled nucleation and growth mechanism [24,27,28]. The α phase usually nucleates

as Widmanstätten plates in the β phase. It will be shown that the nature of the β to α transformation itself can be used to control the alloy morphology. That is, the morphology of α and β phases depends upon whether the transformation occurs by nucleation and growth, martensitic or a combination of the two.

2.3.2 Non-equilibrium Phases

Besides the equilibrium α and β phases found in Ti-6Al-4V, transformations under non-equilibrium conditions can lead to formation of martensitic phases. It has been reported that rapid cooling from the β to the α plus β field and crossing the start of the martensitic transformation, M_S, will result in a complete transformation of beta to alpha prime(α') or alpha double prime (α") martensite [26]. The phase α' is hexagonal, while α" is reported to have an orthorhombic crystal microstructure [29]. When reference is made to the transformation product and the crystal microstructure is not mentioned, the symbol α^m is often used. Unlike a nucleation and growth mechanism, this martensitic transformation involves cooperative movement of atoms from one crystal lattice to another. The transformation morphology is a function of M_S which decreases with increasing cooling rate and increasing amounts of β stabilizing elements [24]. High M_S results in martensites forming as colonies of parallel-sided platelets. Low M_S results in a characteristically more random microstructure consisting of individual units or platelets.

Slower cooling forms grain boundary and Widmanstatten α, which is similar to martensites in orientation. Two cases to consider are the effects of high and low transformation temperatures on slow cooling. High transformation temperature and slow cooling results in large colonies of α, which nucleate at β grain boundaries resulting in a coarse aligned microstructure within the prior beta grain. Low transformation temperatures combined with slow cooling produce smaller colonies, which contain fewer parallel-sided platelets, and appear to nucleate independently of the grain boundaries resulting in the basketweave microstructure.

The β phase in Ti-6Al-4V has been shown to transform completely to α' when water quenched from above 800°C [26]. The concentration of β stabilizers in the β phase determine whether or not the β transforms directly to α' or remains as β upon cooling. For example, at a temperature high in the α plus β phase field, there exists a considerable amount of β phase in Ti-6Al-4V alloy. The concentration of vanadium in the β phase at the higher temperature is lower than that expected at a lower equilibrium temperature, because there is simply a larger volume fraction of β. With increasing volume fraction of β, the concentration of β stabilizing element vanadium decreases, and so the β has a greater tendency to not be retained during non-equilibrium cooling.

2.3.3 Effect of Thermal Treatments

Thermal treatments involve coordination of temperature and time with known phase transformations to control the phase morphology and volume fraction. Many temperature-time combinations exist, but one of the most important treatments involves the solution treatment.

Without considering a specific phase morphology and or the effect of phase transformations, solution treatment at various temperatures in the range from 600°C to 1020°C results in a fixed volume fractions of α, α and β, or β phases. A point of discrepency in the literature, is in the time required to attain phase equilibriation. Realizing that the time for a material to attain an equilibrium temperature is dependant upon the physical mass of the material and its thermal conductivity, TABLE 2.2 was compiled, which lists the solution treatment times for Ti-6Al-4V used by several investigators after what is assumed to be equilibrium temperature was attained. Note that the starting microstructure will vary in all cases so it must be considered as a factor in the total solution treatment times.

TABLE 2.2: Solution Treatment Times at Temperature for Ti-6Al-4V

Temperature (°C)	Time (minutes)	Workers	Reference
875-950,1020	60,2	Diak	[30]
875-950	30	Jain *et al.*	[31]
802-927	200-66.7	Ito *et al.*	[32]
955	30	Weiss *et al.*	[33]
760-940	40	Cope and Ridley	[34]
927	<30	Ghosh and Hamilton	[35]
925	120-1500	Rosenblum *et al.*	[22]
927	10,>1500	Hamilton and Ghosh	[36]
580-900	suitable period	Furushiro and Hori	[37]
800-1000	10	Lee and Backofen	[21]
954-1010	60	Sherman and Kessler	[38]

For an equiaxed Ti-6Al-4V microstructure, two phase equilibrium is attained when the volume fraction of each phase is that dictated by a Ti-Al-V ternary phase diagram. Figures 2.3 and 2.4 demonstrate just how significant the change in volume fraction of phases in Ti-6Al-4V is with time. Therefore, solution treatment time at a given temperature should be defined as that resulting in either phase fractions that correspond to the phase diagram or phase fractions that do not change appreciably with time. The latter is more realistic, because holding the material for periods up to 24 hours to attain equilibrium will result in a considerable increase in grain size and thus deteriorate the superplastic flow properties, accordingly.

Varieties of other heat treatments have been designed to produce microstructural variations in Ti-6Al-4V. TABLE 2.3 summarizes the most common heat treatments for α plus β titanium alloys, and the resulting microstructures.

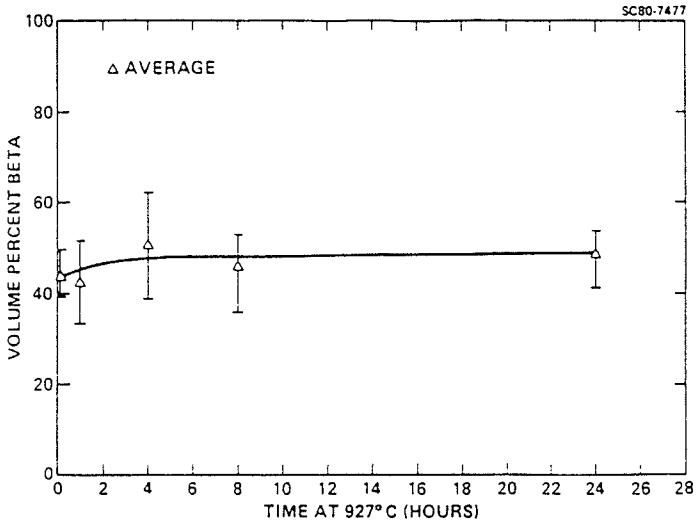

Figure 2.3: Volume fraction of the beta phase as a function of time at 927°C [37].

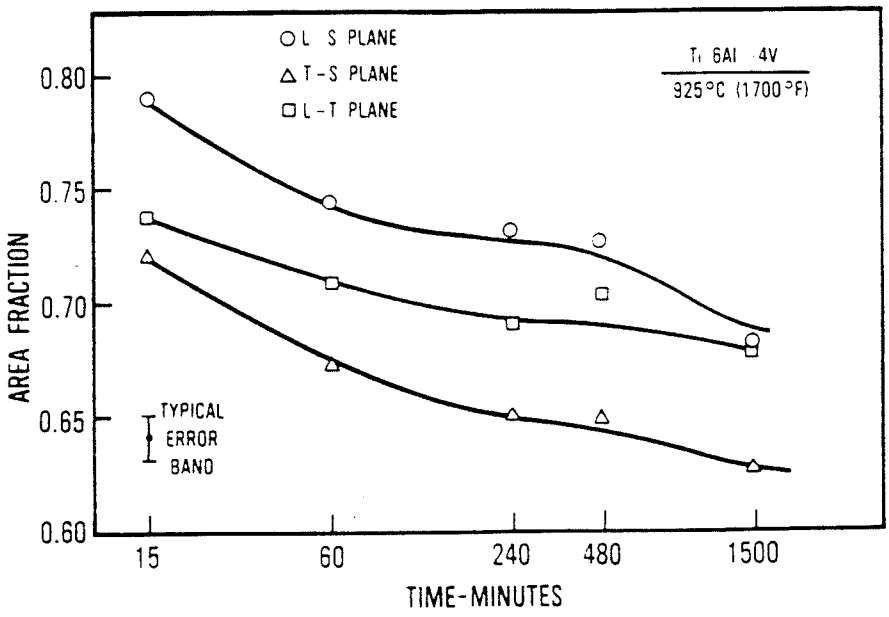

Figure 2.4: Variation of area fraction with time, measured on three axes of the Ti-6Al-4V mill annealed sheet [22].

TABLE 2.3: Summary of Heat Treatments for $\alpha + \beta$ Ti Alloys [27]

Heat Treatment Designation	Heat Treatment Cycle	Microstructure
Duplex anneal(DA)	Solution treat at 50-75°C below T_β(a), air cool and age for 2-8 h at 540-675°C	Primary α, plus Widmanstatten $\alpha + \beta$ regions
Solution treat and age (STA)	Solution treat at ~40°C below T_β, water quench(b) and age for 2-8 h at 535-675°C	Primary α, plus tempered α' or a $\beta + \alpha$ mixture
Beta anneal (BA)	Solution Treat at ~ 15°C above T_β, air cool and stabilize at 650-760°C for 2 h	Widmanstatten $\alpha + \beta$ colony microstructure
Beta quench (BQ)	Solution treat at ~15°C above T_β, water quench and temper at 650-760°C for 2 h	Tempered α'
Recrystallization anneal (RA)	925°C for 4 h, cool at 50°C/h to 760°C, air cool	Equiaxed α with β at grain boundary triple points
Mill anneal (MA)	$\alpha + \beta$ hot work + anneal at 705°C for 30 min to several hours and air cool	Incompletely recrystallized α with a small volume fraction of small β particles

(a) T_β is the β-transus temperature for the particular alloy in question. (b) In more heavily β-stabilized alloys such as Ti-6Al-2Sn-4Zr-6Mo or Ti-6Al-6V-2Sn, solution treatment is followed by air cooling. Subsequent aging causes precipitation of a phase to form an $\alpha + \beta$ mixture.

Three thermal treatments worth considering, are those that produce the so called mill-annealed microstructure, and the lamellar microstructures, designated as beta annealed and beta quenched. The mill-annealed designation has been used considerably if not carelessly in the past until recently [22], while the lamellar morphologies have been considered more in terms of transformation studies.

The mill-annealed microstructure is at best "ill defined" since the variations possible in the as-received microstructures depend upon the working history of the material [22]. Material fitting this designation is a result of hot working in the alpha plus beta temperature range and annealing at 705°C for several hours. The final microstructure is a function of pre-strain, temperature and the α phase size before deformation. Recrystallization response can be varied, and create a non-uniform microstructure, due to incomplete recrystalliztion. Consequently, the microstructure can vary from a heavily worked microstructure to one with equiaxed grains, and therefore no meaningful grain size can be attached to the mill annealed microstructure.

Beta quenched(BQ) microstructures require solution treating about 15°C above the beta transus and then water quenching. Water quenching produces a completely martensitic microstructure, which is then heat treated at 650-760°C for two hours, resulting in tempered martensite. Tempering of martensite results in a two stage decomposition, first reported by Williams and Blackburn [39], involving reversion of the α' phase to β phase and the final precipitation of the α phase. The α phase is precipitated as plates parallel to $\{110\}_\beta$ while the Burgers orientation relationship between the two phases is observed. Final equilibrium microstructure consists of relatively coarse α phase in a β matrix.

Beta annealing (BA) requires solution treating about 15°C above the beta transus and air cooling to the 650 to 760°C range and holding at that temperature for two hours. A review by Hammond and Nutting [24] indicated that slow cooling from the β region results in the transformation of metastable β to grain boundary and acicular alpha, resulting in a coarse aligned α microstructure. In between the plates are layers of retained β phase. The

thickness and continuity of the retained β layers depend upon cooling rate and alloy content. Also reported first in 1975 by Rhodes and Williams [40], and subsequently verified by Sridhar *et al.* [28] and disputed as an electropolishing artifact in a transmission electron microscopy study by Shelton and Ralph [41], was an interface phase and/or phases that formed on furnace or air cooling after solution treatment above the beta transus. Shelton and Ralph attributed one of three phases observed to electropolishing, while Sridhar *et al.*'s study indicated water quenching from above the beta transus did not yield any interface phases.

Recognizing the possible morphologies of the phases in these three microstructures is essential in making any reasonable effort in understanding their deformation.

2.4 Behaviour of Ti-6Al-4V at Superplastic Temperatures and Strain Rates

2.4.1 Superplastic Deformation Characteristics

Since superplasticity was first recognized in Ti-6Al-4V by Lee and Backofen [21] in 1967, a considerable amount of work has been done in characterizing the conditions needed for optimum superplasticity in this alloy. Work to date has shown the two typical flow characteristics for the superplastic deformation of Ti-6Al-4V in tension. Figure 2.5 indicates considerable work hardening, with no observable steady state stress plateau for a Ti-6Al-4V alloy of varying initial grain sizes and varying strain rates at 927°C. In contrast, results for a slightly larger grain size and similar strain rates at 900°C in Figure 2.6 indicate that the flow stress reaches a steady-state plateau quickly after an initial flow softening and maintains this level with increasing strain. Figure 2.7 displays the effect of temperature on the ductility of the Ti-6Al-4V alloy. These variations in behaviour are significant, and tend to reflect some of the conflicting observations during the superplastic deformation of Ti-6Al-4V. TABLE 2.4 defines the generally accepted conditions for the presence of superplasticity in Ti-6Al-4V and other α plus β and β titanium alloys as presented in a review by Pilling and Ridley [10].

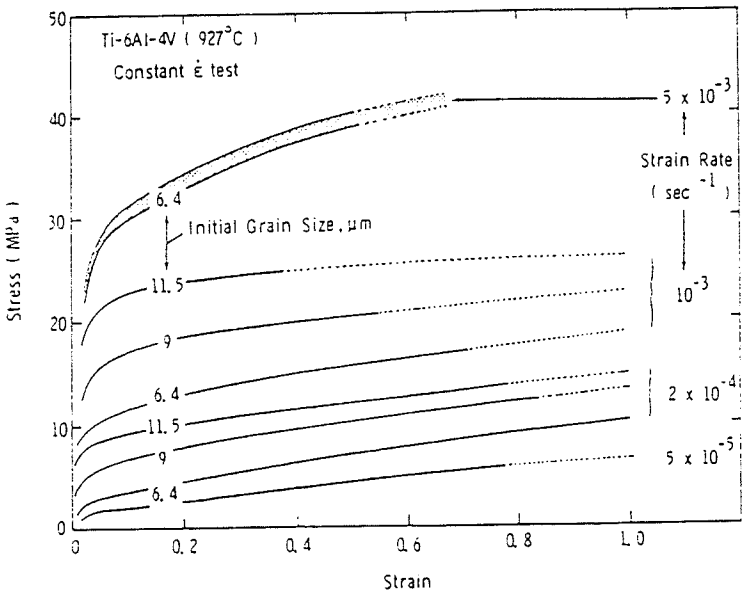

Figure 2.5: True stress-strain curves for three initial grain sizes of 6.4, 9, and 11.5 μm, respectively... The dotted part indicates significant strain gradient developing in the specimen [36].

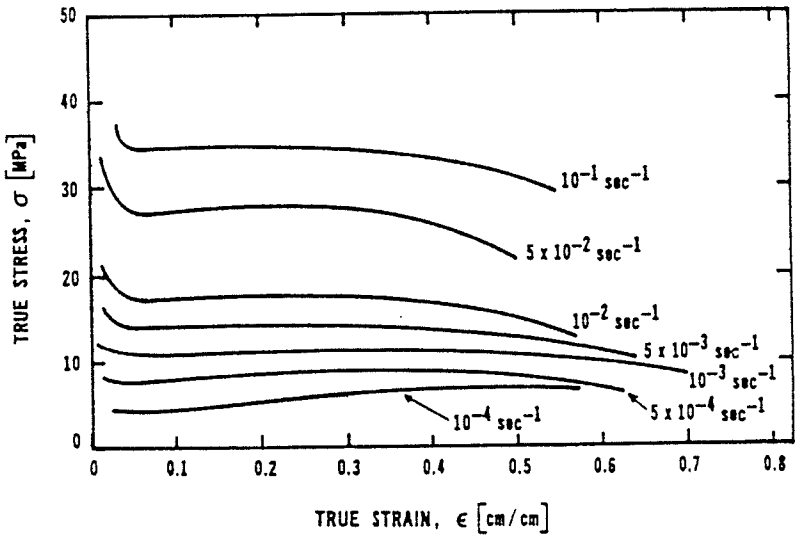

Figure 2.6: True stress versus true strain plot for different strain-rates at 1173 K with an initial grain size of 14.0 μm[42].

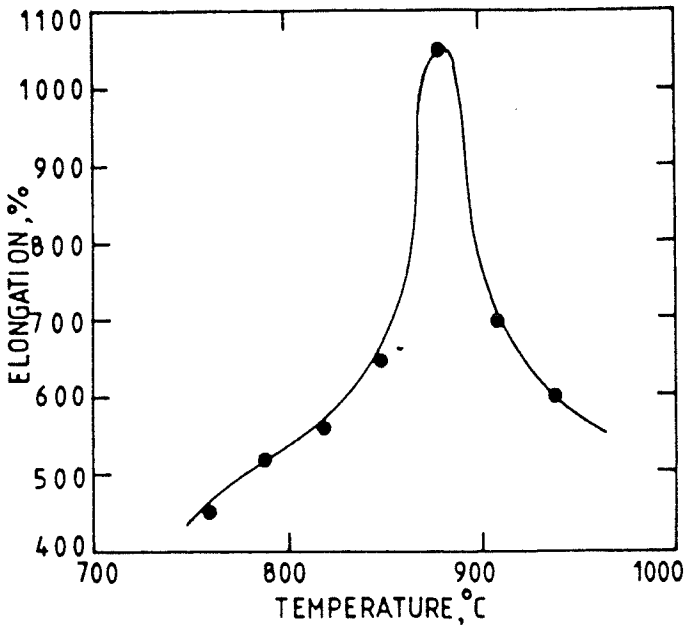

Figure 2.7: Variation of elongation to failure with deformation temperature at a constant strain rate of 2.3×10^{-4} s^{-1} [34].

TABLE 2.4: Summary of the conditions under which superplasticity is observed in titanium-based alloys (Upper section - α/β alloys: Lower section - fully β alloys) [10]

Alloy	Temperature °C	Strain rate %/min	m	Elongation %
Ti-6Al-4V	790 - 940	0.6 - 6	0.8	700 - 1400
Ti-6Al-5V	850	5	0.7	>700
Ti-6Al-2Sn-4Zr-2Mo	900	0.6 - 6	0.6 - 0.7	>500
Ti-4.5Al-5Mo-1Cr	840 - 870	1.2	0.8	>500
Ti-6Al-4V-2Co	815 - 950	0.6 - 6	0.75 - 0.85	720
Ti-6Al-4V-2Ni	815 - 950	0.6 - 6	0.7 - 0.95	670
Ti-6Al-4V-2Fe	815	1.2	0.54	650
Ti-5Al-2.5Sn	900 - 1100	1.2	0.5	>400
Ti-4Al-4Mo-2Sn-0.5Si	880 - 930	0.6 - 6	0.48 - 0.65	500 - 1200
Ti-15V-3Cr-3Sn-3Al	760 - 850	1.2 - 6	0.5	200
Ti-13Cr-11V-3Al	800			150
Ti-8Mn	750		0.43	150
Ti-15Mo	800		0.6	100

It should be noted that summary tables such as these are misleading, because values for strain rate sensitivities and elongations are dependant upon other variables that can vary with each study. For example, percent elongation values can vary between constant cross-head deformation tests and constant strain rate tests. It should also be noted that flow characteristics are not only dependant upon simple microstructural variables like initial grain size, but on other variables, which will be reviewed next.

2.4.2 Grain Size Effects

As noted by Ghosh and Hamilton [23], superplasticity of metals is most strongly influenced by grain size. The smaller the grain size, the lower the flow stress, and generally the higher the strain rate sensitivity. Usually larger strain rate sensitivities correspond to the greatest elongations for the same temperature-strain rate conditions, but they do not always correspond [17]. This could be attributed to considering only a maximum m and not a normalized average. Figure 2.8 demonstrates the relation between strain rate sensitivity and elongation for the Ti-6Al-4V alloy and other alloys. As mentioned before, initial average grain size measurements are inadequate to characterize a material's

response to superplastic deformation, especially commercial alloys like Ti-6Al-4V where variations in different heats of the same alloy contain considerably different microstructures [23].

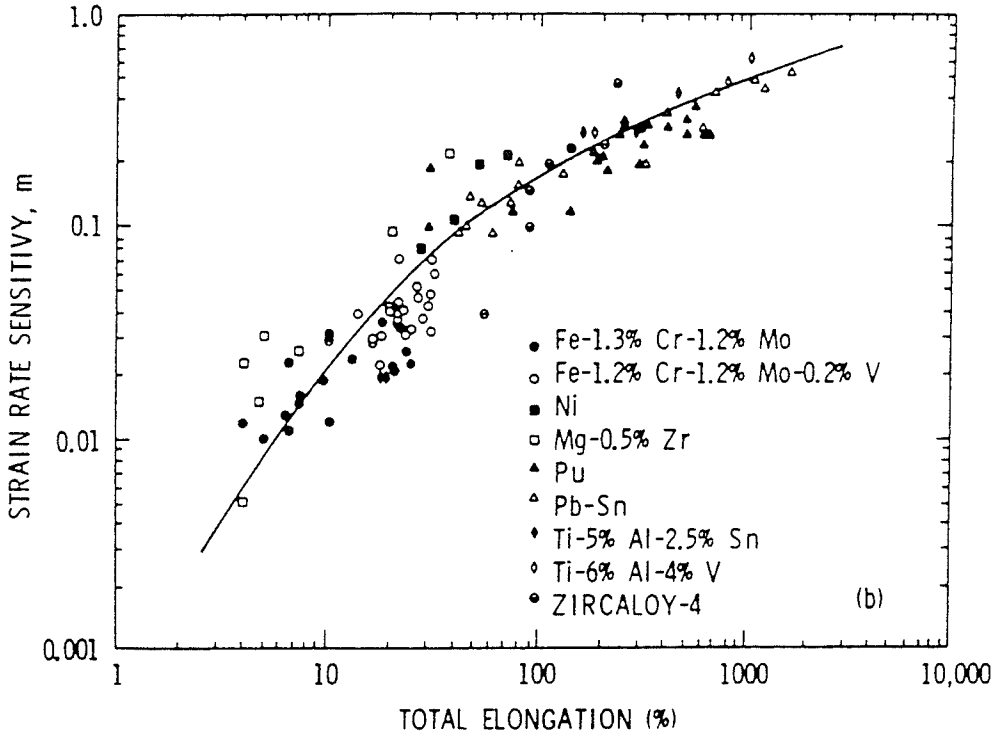

Figure 2.8: Relation between strain rate sensitivity and ductility [43].

The effect of grain size distribution on the superplastic behaviour of the Ti-6Al-4V alloy was first noted by Paton and Hamilton [11]. They observed that microstructures with smaller grain size, but larger grain size distributions had lower m values than a larger more uniform grain size. It was postulated that large and small grains deformed differently and therefore composite effects would be observed. Ghosh and Raj [44] applied these ideas to a model that considered bimodal distributions, where large grains could support large stresses(power law creep) and fine grains sliding by diffusional processes

would support the lower stresses. Support for different mechanisms operating in different sized grains is given by Chokshi and Mukherjee's work on an Al-Li alloy [44]. It was found that for a bimodal microstructure, in the superplastic regime, coarse grains elongated and grain movement suggested intragranular creep, while fine grains in the bimodal microstructure deformed by an intragranular creep mechanism and showed no elongation. In contrast, strain rates characteristic of Regime III caused coarse grains to elongate as before, but the fine grains also displayed elongation, and underwent intragranular deformation. For a microstructure consisting of large equiaxed grains with a uniform distribution it would be expected that grain elongation might occur, but instead very little elongation has been observed [20].

Beside grain distributions, the shape of non-equiaxed grains must be considered. Typical non-equiaxed shapes found in α plus β titanium alloys include blocky alpha and acicular alpha. Blocky alpha is characterized by large, polygonal and/or non-equiaxed shaped grains. Acicular alpha has a distinct needle-like or lenticular shape, and occurs frequently as well-defined plates. Consequently, a parameter is needed that can characterize these morphologies. The grain aspect ratio is one such parameter and can be defined as the ratio between the length and the thickness of a plate. Grain aspect ratios varying from 30 to one have been reported for the Ti-6Al-4V alloy [33].

The significance of this parameter can be seen in data for Ti-6Al-4V alloy. Grain aspect ratios greater than one for the alpha phase reduced superplastic properties for material that had a typically smaller grain size than a smaller aspect ratio microstructure with large grain size [11]. More specifically, tensile samples with an α titanium aspect ratio of six, developed non-uniform deformation as exemplified by multiple neck formations. Even after superplastic deformation, the banding persisted. It should be noted that banded microstructures usually contain elongated grains, but could also consist of equiaxed grains in a contiguous morphology, aligned parallel to the rolling direction. McDiarmid *et al.* [46] observed the effect of phase contiguity on plastic anisotropy during superplastic

deformation of round, tensile specimens of the Ti-6Al-4V alloy. After tensile straining at temperatures in the range from 900 to 928°C at strain rates of $4x10^{-4}$ s^{-1}, the cross sections were reported to become elliptical, which reflects the diametral strain anisotropy. The tendency for the material to exhibit multiple necks is believed to be due to more contiguous alpha phase occupying a greater fraction of the test piece cross-section. Kashyap and Murty [47] showed that banded, non-equiaxed, microstructures are unstable during high temperature of a Pb-Sn eutectic, and the microstructure tended toward an equiaxed one during deformation. The flow stress was found to be dependant upon strain, but they did not evaluate any changes in strain rate sensitivity with strain. Kashyap and Murty's observations are contrary to Paton and Hamilton's observations for the Ti-6Al-4V alloy, since they reported the banding persisted in the alloy [11]. This contradiction could be due to the intrinsic difference in alloy systems, but is more likely to be due to a variation in the amount of banding in the starting microstructures. The reduction or persistance of banding in initially banded microstructures, after superplasticity, suggests the importance of the starting microstructure, and exactly how much banding can be accomodated (ie. not deter superplasticity)? Lamellar and acicular microstructures represent some of the most excessive cases of banding.

At this time, few researchers have attempted to study deformation of titanium alloys with lamellar microstructures at temperatures and strain rates typical of superplastic deformation conditions for an equiaxed microstructure. This is probably due to the fact that initial work showed that acicular microstructures, in general, showed reduced superplasticity [21]. No concern was expressed for the change in these structures during deformation, the primary goal was to improve superplastic properties, by determining what variables gave the best flow conditions. Lamellar microstructural deformation studies can be divided into two categories if the creep region is neglected: (1) high strain rate deformation($>1x10^{-2}$ s^{-1}) with the purpose of producing an equiaxed microstructure and (2) superplastic strain rate regime deformation. The former will be reviewed first.

Equiaxed alpha-beta titanium microstructures can be produced by deforming and then annealing an initially lamellar microstructure. Many authors have verified that the final degree of grain refining depends upon the lamellae width and aspect ratio, deformation temperature, and amount of pre-strain [33,48]. Studies have concentrated on the parameters relating initial microstructure to the final equiaxed microstructure. It should be noted that the working temperatures used in the thermomechanical processing are in the α plus β phase field, and are typically in the superplastic deformation temperature range. The basic high temperature interest in the lamellar microstructure is in producing the equiaxed microstructure. Processing methods can include extrusion, forging, and rolling, so that deformation rates for hot working are considerably higher than those characteristic of the superplastic regime. Nevertheless, the microscopic changes during these processes should be considered.

After deformation of a beta-quenched lamellar microstructure, the alpha lamallae are bent, distorted and sheared. The nature of the plastic flow during extrusion forces the alpha plates to align along the extrusion axis. As well, the aspect ratio decreases with true strain as shown in Figure 2.9.

The break-up of the α phase occurs by heterogeneous and homogeneous action due to intense shear bands and dislocation substructure, respectively. Shearing regions become alpha/alpha grain boundaries or if penetrated by the beta phase, will result in complete severance into alpha regions separated by beta phase. Consequently, beta phase becomes continuous just as reported after superplastic deformation. The flow curve is characteristic of the process; a high initial stress is followed by flow softening with increasing strain. Malcor and Montheillet [49] attribute the softening to break-up of the α needles.

Chen and Coyne [50] studied the deformation of both "globular" and acicular Ti-6Al-4V alloy under isothermal forging conditions for initial strain rates of 6.7×10^{-3} and 6.7×10^{-2} s^{-1} and a temperature range of 816°C to 982°C. A "globular" microstructure is similar to an equiaxed microstructure. Generally, the globular microstructure demonstrated

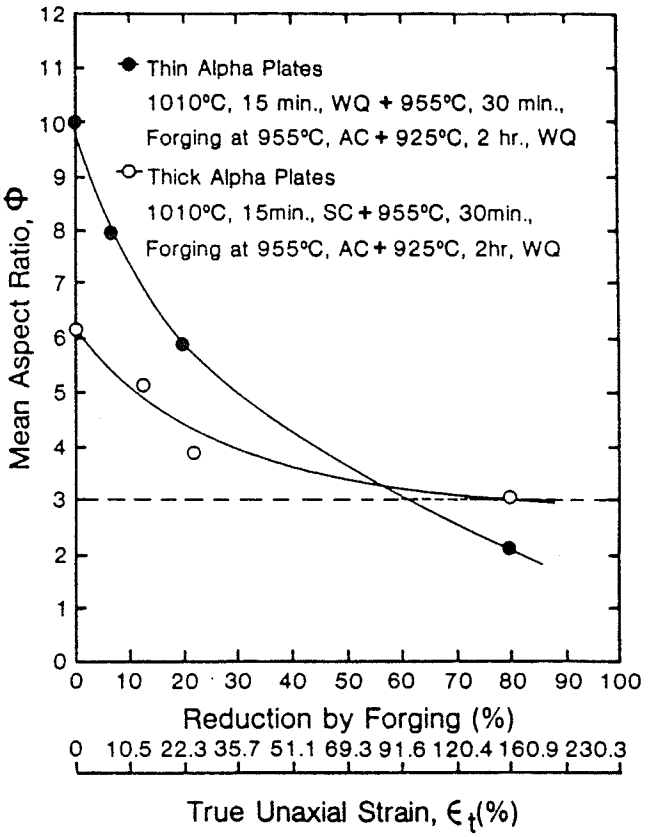

Figure 2.9: The effect of forging reduction or true strain on the mean aspect ratio of the alpha phase, in materials with thick and thin initial lenticular microstructure [33].

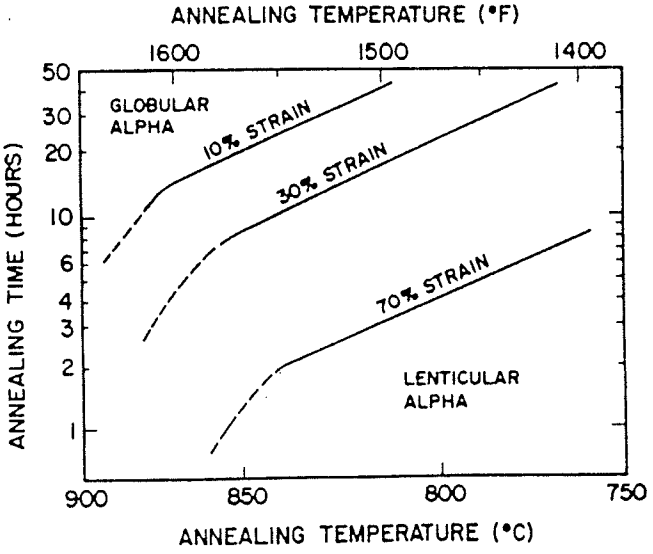

Figure 2.10: Relationship of alpha morphology to annealing time and temperature after various amounts of deformation in the alpha-beta field [48].

more strain hardening then the acicular microstructure. The strain rate sensitivity associated with both microstructures, referred to as the ram rate sensitivity in their paper, was used to evaluate the ease of reducing the material strength as ram rate is increased. Their results showed that ram rate sensitivities measured at yield and 0.36 strain increased with temperature. The increase was greatest in the globular microstructure. Microstructural response due to forging was temperature sensitive, indicating the deformation mechanism associated with the forging appears to be thermally activated. The energies associated with it were typically those of dynamic recrystallization, and the increasing temperature promoted recrystallization. Optically, the acicular microstructure after deformation appeared ragged, indicating alpha recrystallization. A later study reported that the degree of deformation effects the temperature at which recrystallization occurs. Froes and Highberger [48] demonstrated the effect of deformation and annealing time in converting a lenticular alpha microstructure in Corona 5 titanium alloy to a globular microstructure. Figure 2.10 summarizes their results.

At lower strain rates Paton[51] examined the effect of strain rate on flow stress for 'mill-annealed' and beta treated Ti-6Al-4V alloy. He simply found that the latter treatment gave strain rate values less than 0.3 and was therefore deemed not superplastic. Ito *et al.* [32] and Ro *et al.* [58] also superplastically deformed the Ti-6Al-4V alloy with lamellar microstructures, but neither provided any useful parameters to characterize the microstructure.

Ma and Hammond investigated the superplastic deformation of IMI 550 α plus β titanium alloy, with equiaxed and coarse transformed beta microstructures [52]. Deformation resulted in distinct flow curves for each initial microstructure. The coarse transformed microstructure showed higher initial flow stress in the acicular microstructure than the equiaxed microstructure at the same temperature and strain rate conditions, but the flow stresses decreased with strain, indicating break-up of the aciclular alpha. Interestingly, it was reported that the equiaxed and coarse transformed β microstructures

became similar with respect to both grain size, shape and α/β volume fraction as strain increased. The distributed β phase became continuous after deformation. Unfortunately, no quantitative evidence was reported for the α/β grain size or volume fraction. The strain rate sensitivity was reported to increase with strain, as the material changed from being non-superplastic to superplastic during deformation. No attempt was made to correlate the strain rate sensitivity change to the change in microstructure.

Ma and Hammond's study did not take the material to failure and so the final grain size was not evaluated, as well, the strain rate sensitivity before failure was not determined. Their study does suggest some final microstructural similarities in the deformation of the two microstructures, including volume fraction, grain size and continuity of β phase.

2.4.3 Grain Growth Kinetics

One metallurgical variable that must be considered during the superplastic deformation is concurrent grain growth, or the increased grain growth during superplastic deformation. Under static conditions, most materials will not demonstrate appreciable grain growth over the periods of time needed to superplastically deform a material, but grain growth due to the deformation has been reported by several workers [53-55].

Since mean grain size does not remain constant, the initial grain size effect is lost during deformation. Therefore, the initial grain size itself is not adequate in describing the microstructure of the material. The concurrent evolution of the microstructure during superplastic deformation has been found to depend directly on strain and strain rate. Usually increasing the strain rate increases the grain growth due to deformation, but deformation of a δ/γ duplex stainless steel with decreasing strain rate coarsened the microstructure [56]. This could be due to the increased time at temperature caused by the slower deformation rates. Clearly the effect is alloy system dependant, but nevertheless the effect of the grain growth must be considered. In the Ti-6Al-4V alloy, grain growth has an adverse effect on strain rate sensitivity, and leads to a transition from diffusional to

power law creep. Some phases grow more rapidly than others. Beta phase in Ti-6Al-4V coarsens more rapidly than α at higher temperatures, and so in any system it is important to determine if concurrent grain growth is the product of high temperature activity or due to the strain and strain rate.

In a Cu-Al alloy [57], grain growth has been found to increase the resistance to neck growth, and hence improve superplastic properties. Coronze 638 tested at lower strain rates experienced grain growth, which resluted in what was deemed sufficient hardening to compensate for the low strain rate sensitivities, and subsequently prevent sharp neck development.

Finally, it has been reported by Ro *et al.* that for varying initial grain sizes, fracture in superplastic Ti-6Al-4V occurred when the grain size reached a critical value [58]. Heriot *et al.* made a similar observation for a Cu-P system [59]. They noted that rapid necking occurs when a sample grain size exceeds the maximum permissable superplastic grain size. When this occurs, the strain rate sensitivity can decrease from 0.5 to 0.2.

2.4.4 Contiguity

Contiguity as expressed by Rosenblum *et al.*, and first established by Gurland [60], is the consideration of boundary sharing between phases in a material. Its importance lies in the consideration of grain boundary sliding and the potential rates of sliding between similar and dissimilar phases. This parameter can be quantified for a material by direct measurements, but has not been done to any large extent for Ti-6Al-4V alloy due to the difficulty in delineating alpha/alpha and beta/beta grain boundaries. Jain *et al.* [31] theoretically calculated the potential grain boundaries present for a range of volume fractions of α and β phases present in superplastic Ti-6Al-4V, and qualitatively correlated the number of boundaries and triple points to observed superplastic behaviour. They theorized that in the 900/925°C range, which experimentally demonstrated the optimum superplasticity, there exists a maximum number of $\alpha\beta$ grain boundaries and $\alpha\alpha\beta/\alpha\beta\beta$

triple points. Lower or higher temperatures, which correspond to decreasing or increasing volume fractions of β, would theoretically decrease the number of these boundaries. TEM work demonstrated that αα/αββ triple points and αβ grain boundaries seemed to be preferential sites for the emission of dislocations that accomodated the grain boundary sliding. A large number of these boundaries are therefore expected to enhance superplastic properties.

2.4.5 Texture

The mechanical properties of titanium alloys are strongly dependant upon their texture. Texture is the tendency of a material's polycrystalline aggregate to align identical planes in a specific direction or more appropriately have a preferred orientation. The texture is variable because: (1) it is usually present when commercial material is first recieved, (2) can change upon thermomechanical treatments before superplastic deformation, and (3) can change during superplastic deformation and consequently alter post-formed properties.

Texture is easily developed in the hexagonal close packed titanium-α phase through such forming operations as rolling and swaging, and can lead to definite anisotropic properties. The pole figures most frequently cited for hexagonal metals are the $(001)_\alpha$ and $(100)_\alpha$, also referred to as the basal and and prism-plane pole figures. The $(100)_\alpha$ plane is an active slip plane in the α-Ti phase at room temperature [61]. After rolling, the basal $(001)_\alpha$ planes can align themselves parallel to the sheet normal or align in the plane of the sheet with respect to the transverse direction. The latter is called transverse texture, while the former is basal texture [27].

Beside hot working, simple transformations used in titanium alloy morphology manipulation can effect material texture. Fujishiro and Nadiv [62] showed that for pure titanium, variations in the heating and cooling rates above and below the beta transus could develop basal texture in α titanium along the direction of the temperature gradient.

Converesely, Peters and Luetjering were able to eliminate as-recieved textures in a Ti-6Al-4V alloy plate by a β quench treatment [63]. These observations add to the complexity of controlling texture during titanium alloy hot working.

The existence of texture and its effect on room temperature material properties in conventionally formed sheets warrants consideration of texture changes after or during superplastic deformation. Interestingly enough, one of the first attempted correlations between texture changes before and after superplastic deformation was made during one of the initial observations of superplasticity. Reported as an addendum to the original Pearson paper [4], O'Neill found that the Pb-Sn eutectic deformed by Pearson displayed no preferred orientation before or after superplastic deformation. Since this initial observation, conflicting evidence has been presented regarding the effect of superplastic deformation of textured and un-textured material, particularly titanium alloys. Some workers report that for the Ti-6Al-4V alloy, the role of texture in superplasticity is minor [11]. Others note considerable differences in superplastic ductility of strongly textured Ti-6Al-4V [64]. In one of the more exhaustive studies on an alpha-beta titanium alloy, Ingelbrecht *et al.* found that sheet orientation of the sample to the tensile axis determined whether texture increased or decreased during superplastic deformation of IMI 550 [65].

Each of the previous studies varied the degree of textural analysis. For valid textural studies, complete texture evaluation using full pole figures is a necessity [7], as opposed to less intensive techniques where simple intensity measurements of major diffracting planes in Ti-6Al-4V alloy bar and their manipulation have been cited as measurements of texture changes [66].

2.4.6 Volume Fraction

Volume fraction of phases is one variable that has recieved considerable attention for two phase alloy systems in superplastic studies, primarily due to the ease with which it can be measured. In Ti-6Al-4V alloy, the volume fractions of α and β phases, and the phase

compositions were found to be temperature dependant. Superplastic deformation itself has been shown to be temperature dependant, and hence the relationship of volume fraction to temperature represents an important interdependent variable. Belzunce and Suéry noted that the intrinsic effect of temperature is very difficult to separate from that of grain size or that of the phase proportion, these being dependant upon temperature [66].

Volume fraction as a variable is best considered by reviewing its direct effect on superplastic properties, its relation to other microstructural variables that are related to superplastic properties, and the methods used to study the relationship.

In the Ti-6Al-4V alloy with two phase equiaxed microstructure, the maximum strain rate sensitivity has been reported to occur when the α to β volume ratio is around unity[43,68], while 20 to 40 percent β results in the maximum elongations [64]. Hamilton reasoned that the difference in the values of volume fraction of β phase for which a maximum m and maximum percent elongation is observed is due to the grain growth effect. Another consideration is that m values quoted in the literature represent maximum or steady state values at low strains, and so when compared to total elongation data they do not take into account changes in m with strain. The strain rate sensitivity has been shown to change with strain, so m values should be normalized with respect to total elongations before being compared. An alternative approach is to base the final elongation on the final instantaneous m [43,68].

For comparable systems like α-β brass, 50/50 phase ratios have been shown to exhibit optimum superplasticity [69,70]. Alpha-beta brass is similar to α-β Ti-6Al-4V alloy in that self-diffusion in β brass is more rapid than α brass [69]. Similarly for Ti-6Al-4V, deformation is reported to take place in β [64,71,72], and the value of the coefficient of self-diffusion in the β phase is almost 100 times that of the α phase. Generally, the inter-diffusion rate between α and β in titanium differs by a factor of two [20]. Maximum ductility may be due to the presence of α, which stabilizes the grain growth, and the high diffusivity of β in α. The balance gives the good superplastic deformation properties.

Volume fraction of phases can also be linked to other microstructural variables like contiguity, number of grain boundaries, and grain size. Ro *et al.* reported that the average grain size depended upon the volume fraction of the phase [58].

The effects of volume fraction variations have been studied in several ways. First, for a fixed alloy composition, variation in temperature in the α plus β field at which the alloy is held, alters the volume fractions and chemical compositions of alpha and beta phases. Unfortunately, the change in temperature influences the diffusivity in the various phases, and the temperature dependance on superplasticity is difficult to separate from that of volume fraction. Subsequently, alloying additions to the alloy have been used to suppress phase formation at a given temperature. Hamilton, Paton and Mahoney doped Ti-6Al-4V with varying compositions of hydrogen, which is a beta stabilizer, and tested at a single temperature [73]. The results showed that for all alloys containing entirely α or all β phases, the strain rate sensitivity values were very low and the flow stresses were higher. Similarly, Wert and Paton [18] made two percent additions of Fe, Co, and Ni to lower the beta transus, and thus lower the superplastic deformation temperature. They concluded that the volume fraction of β phase and the morphology of the α and β phases are among the factors that control the superplastic properties. However, it should be noted that in all these cases the chemical composition of the two phases changed with alloying addition.

Ro *et al.* studied Ti-Al-V alloys that contained the same phase compositions at 900°C as Ti-6Al-4V, but distinctly different volume fractions in an effort to clarify the effect of α-β volume fractions and to determine, which alloy composition had the best superplastic properties [58]. They found that Ti-5.3Al-5V alloy had the best superplastic properties at this temperature with an α-β phase ratio of one to one.

So far however, no attempt has been made to use the same alloy, thus not changing its overall chemical composition at superplastic temperatures, but altering its grain morphology solely by thermal treatments to explore the effect of alpha-beta morphology and volume fraction on superplastic properties. It has been shown that Widmanstätten

structures can be produced in alpha-beta alloys like Ti-5.25Al-5.5V-0.9Fe-0.5Cu alloy such that the volume fraction can be varied by time at a given temperature.[74,75]. The problem that exists is in measuring the volume fraction of the phases in some alloys. Sridhar et al. stated that after air cooling of Ti-6Al-4V alloy to produce a beta-annealed microstructure, they observed via transmission electron microscopy only five to six percent β, while the β and interface phase volume fraction total was between 15 to 19 percent [28]. Optically this interface phase could be mistaken for β, if only α and β are expected. Therfore, care must be exercised in measuring volume fraction of phases, but the possible variations in α/β morphology with similar phase fraction suggests further studies on the effect of morphology on superplasticity.

2.4.7 Cavitation

The initiation and growth of small intergranular voids at grain boundaries and particles during superplastic deformation is called cavitation. Cavitation has been found to influence superplastic deformation of microduplex stainless steels [76] and alpha-beta brasses [69,77]. In the stainless steel study a considerable amount of quantitative work indicates that cavity volume fractions increase with increasing strain, decreasing strain rate, increasing temperature, and increasing grain size.

A number of studies have been carried out to assess the effect of cavitation on superplastically deformed Ti-6Al-4V alloy [32,77,78,79]. No conclusive evidence has been observed for cavitation affecting superplastic properties and subsequently influencing ductility. Some studies even indicate no evidence of cavitation after superplastic deformation of Ti-6Al-4V alloy [35,46,80]. The contradictory reports on cavitation in the Ti-6Al-4V alloy indicate that quantitative work must be done to verify this factor, but the tendency to not observe significant cavitation suggests that only quantitative aspects be considered.

2.5 Superplastic Deformation Mechanisms

2.5.1 Review of Observed Superplastic Deformation Mechanisms

Observation of superplastic deformation indicates that grain boundary sliding, grain growth and grain rotation are characteristic of the process. This behaviour allows grains to remain essentially equiaxed during deformation. These observations have lead to the development of various models describing both the mechanism and supplementary accommodation processes. The accommodation processes are deemed necessary to account for the large tensile elongations that cannot be due solely to grain boundary sliding. Grain boundary sliding has been reported to contribute to about 60 percent of specimen elongation [80]. Considering that grain boundary sliding(GBS) is present, it is assumed that it itself cannot be responsible for the rate controlling aspect of superplasticity, because GBS cannot occur continuously on all interfaces [81]. Subsequently, other process or processes must be responsible for the rate controlling aspect of superplasticity.

The search for a separate mechanism arose from the three distinct regions demonstrated in ln stress versus ln strain rate curves. Sastry *et al.* [82] have shown experimentally that in the Ti-6Al-4V alloy the intermediate region(Regime II) coincides with Nabbaro-Herring creep or diffusion accommodated grain boundary sliding, while the higher strain rate regime is characterized by dislocation-climb controlled deformation. The transition between the two mechanisms is simply the superposition of the two.

Determining whether diffusion or dislocation motion is the prominent accommodation mechanism stems from experimentally measured values of activation energy. Using an Arrhenius type stress dependance such as,

$$\sigma = k\dot{\varepsilon}^{m} \exp\left(\frac{-Q}{RT}\right) \qquad (2.4)$$

where,

σ = flow stress

k = material constant

$\dot{\varepsilon}$ = strain rate

m = strain rate sensitivity

Q = activation energy

R = Universal Gas Constant

T = temperature(K)

and plotting $\ln(\sigma/\dot{\varepsilon}^m)$ versus (1/T) at constant $\dot{\varepsilon}$ and m should give a straight line. The slope of this line is characteristic of the activation energy, (-Q/R). Unfortunately, some difficulties arise interpreting the plots. For example, if more than one mechanism is operating it becomes difficult to distinguish the contribution from each mechanism. Their contribution will depend upon temperature, strain rate and various microstructural parameters. As well, care must be exercised in selecting the stress value, σ, for equation (2.4) when constructing the Arrhenius plot. The stress must correspond to the steady state flow condition such that at a constant strain rate, $\partial\sigma/\partial t$ is constant. When material strain hardens during superplastic deformation, which was illustrated in section 2.4.1 for the Ti-6Al-4V alloy, a steady state flow is not reached until the attainment of ultimate stress. If constant cross-head velocity experiments are performed, the material flow stress varies with the decrease in strain rate, which occurs monotonically during the test. The stress corresponding to the strain rate, though is not constant with respect to time and therefore does not represent a steady state. Such experimental differences could be responsible for the irregular behaviour reported for the Ti-6Al-4V alloy [79].

Generally, the interpretation of the activation energy values induced the different approaches of modelling accommodation processes with the superplastic deformation mechanism, whether by diffusion, dislocation motion or a combination of both. A considerable number of models have been proposed, but only two, one diffusion based and

the other dislocation based, will be considered. Most of the more recent modelling attempts have arisen from modification of the following two, thus demonstrating their original importance.

2.5.2 Qualitative Descriptions of the Ashby-Verall and Gifkins Models for Superplasticity

Qualitative models proposed by Ashby and Verall [83] and by Gifkins[84,85] to explain the superplasticity mechanism consider grain boundary sliding to be an essential part of the process, but differed in the explanation of accommodation.

Accommodation was suggested by Ashby and Verall [83] to occur by diffusion such that grain switching is accommodated by diffusion along grain boundaries to maintain continuity. The diffusion allows material transport to maintain phase compatibility. Figure 2.11 shows the topological unit steps for the Ashby-Verall model in two dimensions for a single phase.

In Gifkins' model[84,85] grain boundary sliding takes place by the motion of grain boundary dislocations that pile-up at triple points. The pile-ups are accommodated by creating new dislocations at the stress concentrations that climb in or near the grain boundary. With these actions, the core of the grain remains relatively free of dislocations, while all dislocation activity is confined to the region near the grain boundary. Topologically, this model used a three dimensional approach that predicts grain emergence from other layers. This is shown in Figure 2.12 for a single phase material.

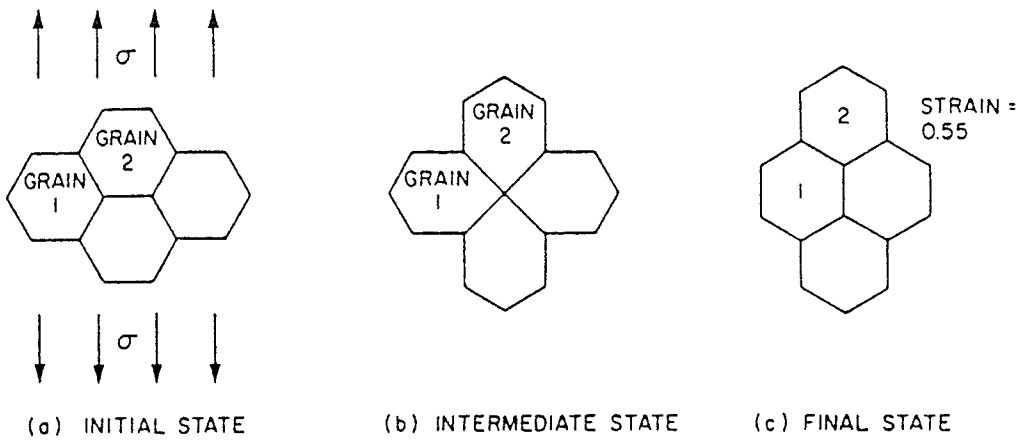

Figure 2.11: The unit steps in Ashby-Verall's grain switching process. (a) Initial configuration of sliding grains;(b)intermediate or "saddle configuration; (c) final configuration after true strain of about 0.55 [8].

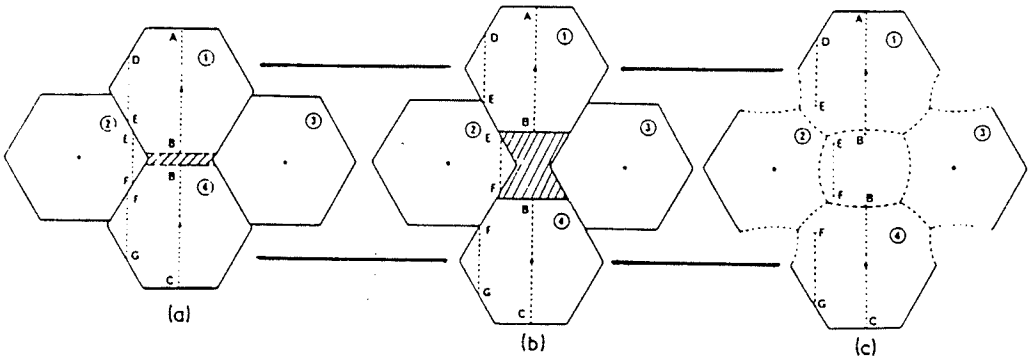

Figure 2.12: Specimen elongation by GBS and accommodation by movement of grains from one layer to the next "emerging" grains. (a) After a small amount of deformation, a small narrow fissure forms; (b) this gap is enlarged and filled by an emerging grain; (c) the grain boundary network adjusts to maintain correct dihedral angles [85].

2.5.3 Application of Models to Ti-6Al-4V Alloy

Both the Ashby-Verall and Gifkin models have been criticized on several grounds [8,86]. This criticism has resulted in modification of the models to fit experimental data, including observations for two phase alloys. The microstructural and topological predictions of Ashby and Verall's model for large strains appear to match those observed in Ti-6Al-4V by Paton and Hamilton [11], Ghosh and Hamilton [23], and Wert and Paton [18].

Modelling of the mechanisms and comparison to mechanical property data is invaluable, but more direct methods of observation are essential to our understanding of the phenomena. One technique, transmission electron microscopy(TEM), has until recently been applied sparingly in the study of superplasticity. The next section reviews some of the relevant TEM work performed on superplastically deformed Ti-6Al-4V alloy.

2.6 Microstructural Observations (TEM)

2.6.1 High Temperature Microstructure Retention

Transmission electron microscopy of superplastically deformed Ti-6Al-4V has been used to deduce internal microstructure and relate it to the mechanism of deformation. Part of the dilemma of commenting on high temperature mechanisms is retaining the high temperature microstructure at room temperature if in situ work is not possible. For Ti-6Al-4V alloy the α phase can be retained, but the β phase transforms on cooling subsequently thus destroying all the evidence of its high temperature microstructural state. Various methods of retaining the high temperature microstructure have been used. Air cooling, helium cooling [21], and argon cooling [79] to room temperature are too slow, in that some β probably transforms to α. These techniques will not guarantee that the room temperature α volume fraction is the same as the high temperature microstructure. Water quenching has been used [58,86] such that the material retains the α phase depending upon the initial temperature before quenching, and all the β transforms to martensite. The β to martensite

transformation induces internal stresses in the material due to the volume change and must be considered in any microstructural interpretation. Still water quenching does not guarantee locking all the dislocations in their dynamic high temperature state, considering the small distances they must travel to reach a sink. Consequently, water quenching under load has been attempted to freeze the dislocation structures in their dynamic state[31]. Nevertheless, the observations to date are quite limited, and even one of the most accepted characteristics of superplasticity has not been verified for the Ti-6Al-4V alloy by transmission electron microscopy.

2.6.2 Equiaxed Microstructures

Generally, grain boundary sliding is not evident in transmission electron microscopy studies due to the difficulty in performing marker experiments [8]. For essentially equiaxed microstructures recrystallization has been observed in alpha grains with alpha recrystallized near alpha/beta grain boundaries at temperatures between 800 and 900°C and strain rates around $5x10^{-4}$ s^{-1} [32,71]. At lower temperatures of 750°C, alpha phase grain refinement and dynamic recrystallization is evident [79]. More recently, Jain *et al.* [31] demonstrated that dislocations are generated at grain boundaries and triple points during superplastic deformation of the Ti-6Al-4V alloy. Specifically, plastic incompatibility between α and β phases during superplastic deformation appeared to generate more dislocations between α/β boundaries than α/α or β/β.

2.6.3 Lamellar Microstructures

Beside equiaxed microstructures, lamellar microstructures have been deformed with the purpose of producing an equiaxed microstructure during a post annealing treatment. Recrystallization during annealing after deformation forms the equiaxed grains[63]. A study by Shakhanova *et al.* [87] suggests that structural changes during hot deformation of lamellar Ti-6Al-4V are due to polygonization of the β phase, under the action of

deformation over the whole temperature range, accompanied with dynamic recrystallization at temperatures greater than 920°C and strain rates less than $1x10^{-2}$ s^{-1}. It is theorized that new β grains in the plate-like structures are placed as layers between the deformed α plates. This size being comparable to the width of the β layers. The non-uniformity of the recrystallization is attributed to the initial thickness of the alpha-plates. Thicker plates result in more twinning of α phase, and consequently more non-uniformity of recrystallization.

Sastry et *al.* [82] deformed beta annealed Ti-6Al-4V at a strain rate of $5x10^{-2}$ s^{-1} and observed that the deformation substructure at 700°C is characterized by extensive dislocation activity in the α phase, continuity of slip in the β phase, and the absence of polygonization result in profuse shearing of the β phase. Above 850°C, both dynamic recovery and recrystallization occur, in both equiaxed and beta annealed microstructures as demonstrated by hexagonal dislocation networks in the α phase, the formation of small equiaxed α and the absence of shearing of the β phase. Results from higher temperature and lower strain rate experiments more typical of the superplastic regime for the Ti-6Al-4V alloy were not indicated.

The observation that deformation of both equiaxed and acicular microstructures at superplastic temperatures and strain rates results in similar microstructural behaviour suggests that the differences in mechanical deformation of varied morphologies at the same temperature and strain rate conditions could provide some insight into the superplastic deformation and accommodation mechanisms for the Ti-6Al-4V alloy.

2.7 Scope of Study

It is recognized from the literature presented in the review that microstructural variables such as volume fraction, grain size and grain shape have a major influence on superplasticity in two phase titanium alloys. The volume ratio of alpha and beta phases is dependant upon temperature, time and alloy composition so that the interdependency between these variables are difficult to separate when evaluating their effects on

superplasticity. Volume fraction studies on superplasticity to date have varied the volume fraction of alpha and beta phases at fixed temperatures, by modifying the alloy chemical composition and subsequently altering the diffusion properties of each phase. Others have altered the overall chemical composition of the alloy, but produced identical phase compositions for various volume fractions at a fixed temperature. No one at this time has purposely varied the alloy phase morphology at a fixed temperature, but kept the overall composition and volume fraction constant.

Volume fraction of alpha is known to effect the grain size of α and β titanium alloys. Small, equiaxed grain size typically less than 10 μm, is a recognized requirement for superplastic behaviour. This applies particularly to equiaxed morphologies which have been studied extensively since they provide the optimum superplastic properties. Unfortunately, producing a completely equiaxed microstructure is difficult, and titanium alloys can be processed to produce a variety of morphologies, including lamellar microstructures, which are characterized by grains of high aspect ratios. Grain aspect ratio effects on superplasticity in titanium alloys are recognized as being important, but little quantitative work has been accomplished. At typical superplastic conditions for material with equiaxed morphologies, material with lamellar morphologies has been characterized by high yield stresses and low values of m. In most cases, the initial microstructures for these morphologies prior to deformation have not been fully characterized by volume fraction and grain aspect ratio distribution measurements. Observations reported in the literature have been made that quantify the evolution of material with lamellar morphologies to equiaxed ones, where the final grain size at fracture for lamellar morphologies is equal to those for equiaxed ones at the same conditions. These observations suggest that an understanding of the evolution of microstructure in material with different morphologies by comparison to mechanical test data could explain the inherent initial differences and final similarities in their superplastic properties. A complete mechanical behaviour study, which not only examines the ductility of the material with lamellar morphologies, but also the

change in strain rate sensitivity with strain at typical superplastic deformation conditions is lacking.

Therefore, this study will investigate the effect of initial morphology and volume fraction of α and β phases on flow properties during the high temperature deformation of the Ti-6Al-4V alloy in the typically superplastic regime. The purpose of the investigation is to determine if with varied morphologies, the superplastic behaviour of fixed volume fractions of alpha and beta phases maintains the same temperature dependance. As well, this study relates the differences and similarities in mechanical behaviour to both observed microstructural evolution and the test methods themselves.

The method used in this study involved testing a Ti-6Al-4V alloy with three different morphologies, but similar volume fractions of α/β phases at typically superplastic temperature and strain rate conditions. Material with three different morphologies was produced by varying the temperature time paths leading to the final superplastic deformation temperature. The final superplastic deformation temperature determines the volume fraction of α and β phases. Unidirectional tensile tests at constant strain rates of $5x10^{-3}$, $1x10^{-3}$, $5x10^{-4}$, $1x10^{-4}$ s^{-1} were performed at 875, 900, 925 and 950°C. The mechanical tests were designed to evaluate the material ductility and the variation of strain rate sensitivity with strain. Considerable data exists for equiaxed Ti-6Al-4V alloy in the literature, so in these experiments material with an equiaxed morphology was used as the standard by which mechanical test results for the material with the two lamellar morphologies could be evaluated.

CHAPTER 3

EXPERIMENTAL PROCEDURE

3.1 Material

The Ti-6Al-4V commercial alloy used in this study was supplied by RMI Titanium. The material's production history included hot rolling, and annealing, and was received in the form of 1.27 cm diameter rods. The chemical composition for the alloy is shown in TABLE 3.1. The beta transus specified by RMI and verified experimentally was 1005°C.

TABLE 3.1: Chemical Composition for Ti-6Al-4V Alloy

Element	wt.%	Element	ppm
C	0.03	Y	<50
N	0.012	B	<30
Fe	0.22		
Al	6.2		
V	3.8		
Cu	<0.01		
Si	0.02		
O	Top-0.156		
	Bottom-0.166		

Initial microstructure of the alloy in the as received state is shown in Figure 3.1 for completion, but is not important since all material underwent various pre-deformation treatment, and these starting microstructures are described later.

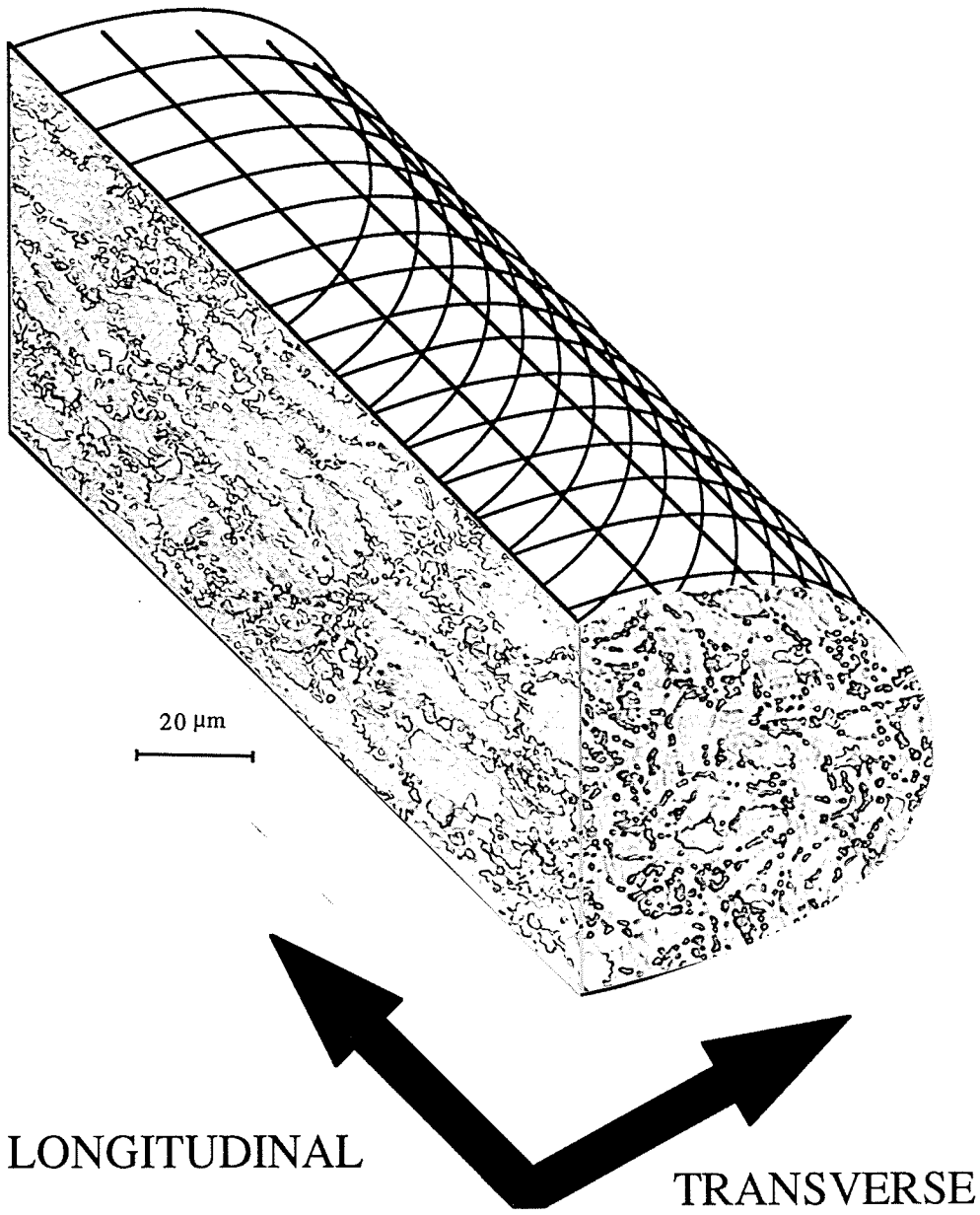

Figure 3.1: Microstructure of the Ti-6A1-4V as received material with respect to the rod orientation.

3.2 Heat Treatments

Three different heat treatment schedules, referred to as BA, EQ, and BQ, were performed on the machined tensile test specimens in order to give the material three distinct morphologies at the same test temperature. These Paths are illustrated in Figure 3.2. A full description is given below.

BA involved heating the material above the beta transus to 1020°C for 20 minutes, and then step quenching to 870°C by air cooling at a rate 12.5°C per second. Once this temperature was reached the material was immediately heated to the prescribed test temperature (875, 900, 925, or 950°C) and held for one hour. The treatment was similar to that specified for beta annealing [27], and consequently all material treated by this schedule was referred to as BA.

EQ consisted of heating the as received material to the test temperature and holding for one hour before testing. This treatment was used to stabilize the as received material at the test temperature, and the resulting microstructure was expected to be equiaxed. Therefore, material treated by this schedule was referred to as EQ.

Figure 3.2(c) shows that the BQ schedule is the most complicated of the three. BQ treatment consisted of heating the material to 1020°C for 20 minutes and then water quenching to room temperature. The water quenched material was then heated to the test temperature and held for one hour. The treatment was similar to that specified for beta quenching [27], and consequently all material treated by this schedule was referred to as BQ.

3.3 Specimen Preparation

Specimens for tensile testing were designed to facilitate subsequent observations by optical microscopy, scanning electron microscopy and transmission electron microscopy as described in the following sections.

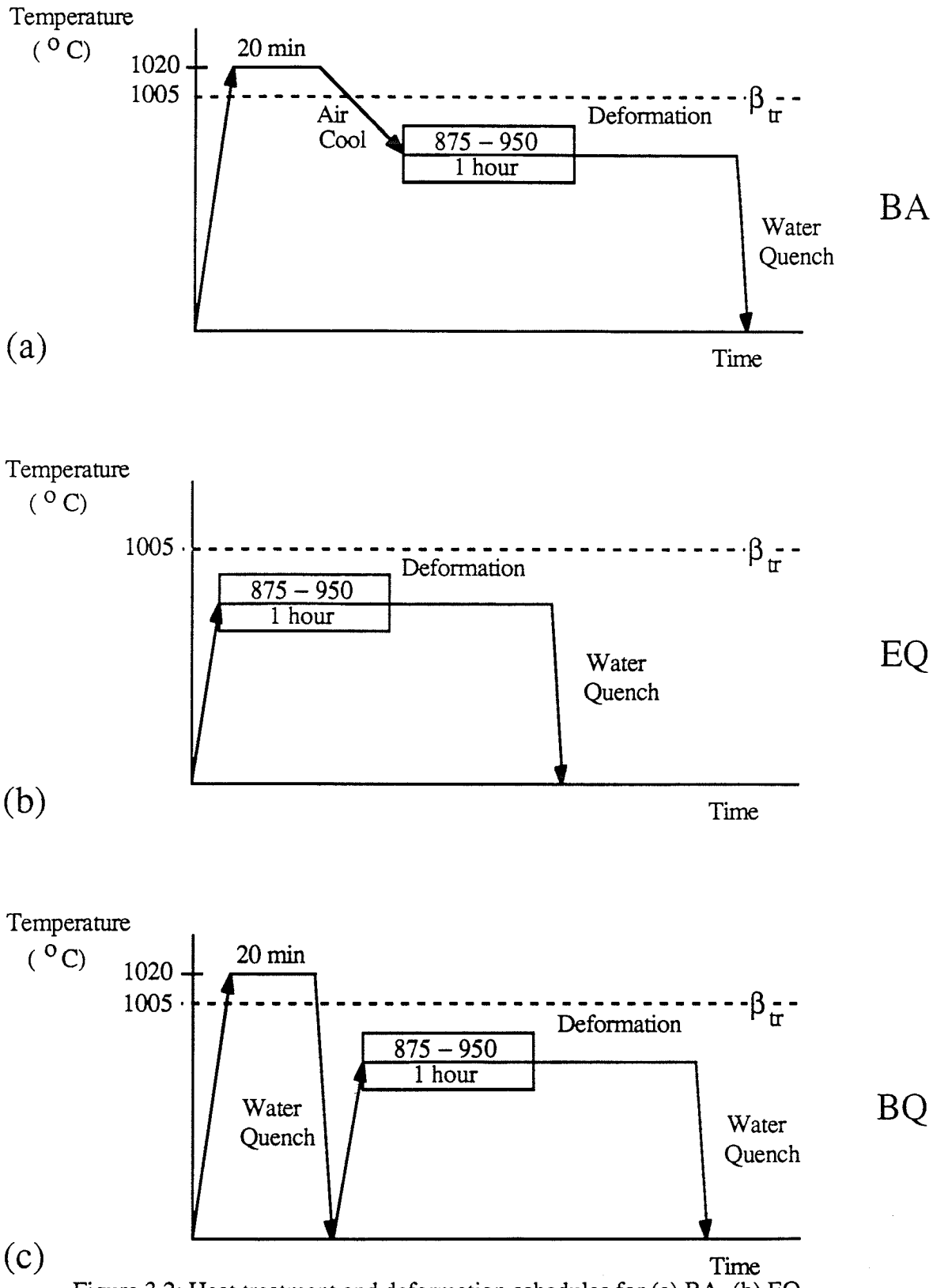

Figure 3.2: Heat treatment and deformation schedules for (a) BA, (b) EQ, and (c) BQ.

3.3.1 Tensile Samples

Cylindrical tensile samples were prepared from the rod stock by machining it to produce threaded samples with 1.0 cm guage length and 5.0 mm guage diameter as detailed in Figure 3.3. The specimen dimensions are similar to those used by Ro *et al.* [58]. They were chosen to enable maximum tensile elongations to remain in the constant temperature zone of the split furnace depicted in section 3.4, and to minimize deformation of the head.

Before tensile testing, all specimens underwent the required heat treatment, as described in section 3.2. The heat treatments took place in an argon atmosphere furnace mounted on the Instron test frame for all schedules except the one specified BQ. The first step of BQ involved encapsulating individual specimens in Vycor glass containing an argon atmosphere, and heating each specimen to 1020°C for 20 minutes in a box furnace . After 20 minutes, the specimen was water quenched by rapid transfer of the capsule to a water quench bath and instantaneous breaking of the tube on impact with the bath bottom to ensure rapid quench. These specimens were then mounted on the test frame for the remainder of the heat treatment as specified in section 3.2.

3.3.2 Optical Metallography Specimens

Optical metallography specimens were required to characterize initial and deformed microstructures in the static and dynamic conditions with respect to volume fractions of alpha and beta phases, alpha and beta grain size and alpha aspect ratio. Figures 3.4(a) and 3.4(b) show where optical specimens were taken from initial and deformed tensile specimens, respectively. Statically annealed specimens were taken from the tensile gauge head after deformation. Sectioning was done using a slow-speed diamond saw. The sections were then mounted in bakelite and mechanically polished using silicon carbide papers, diamond pastes and aluminum oxide powder to a final surface finish of 0.05 μm. Etching was performed prior to observation with 10 ml of H_2O_2 added to a ten percent NaOH solution at 80°C.

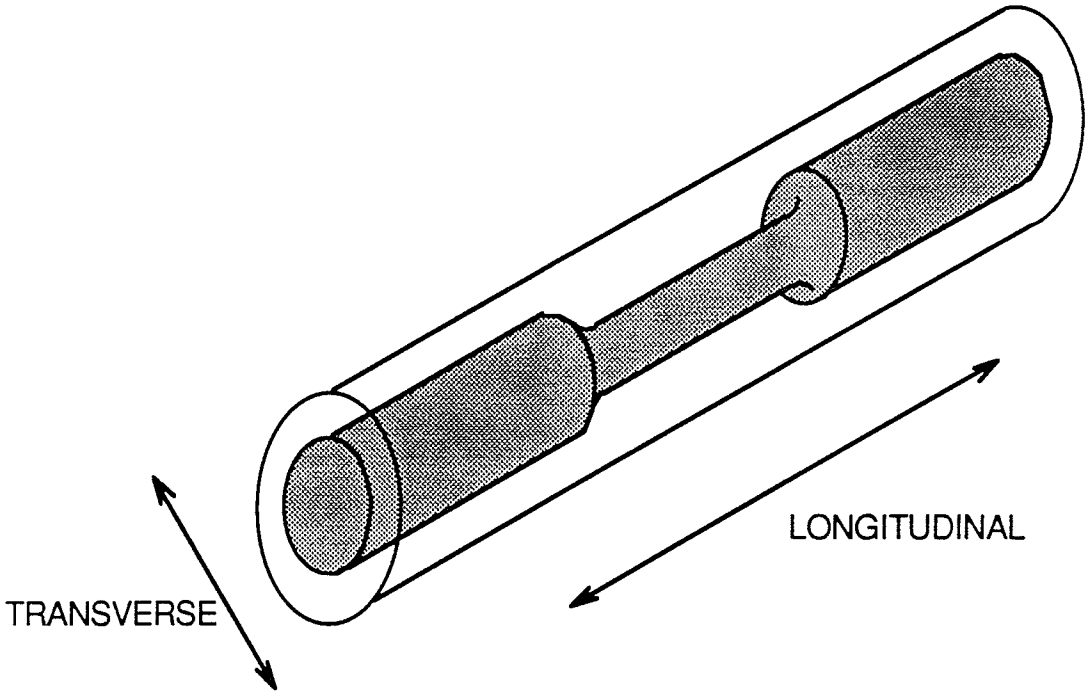

(a) Specimen orientation with respect to rod stock.

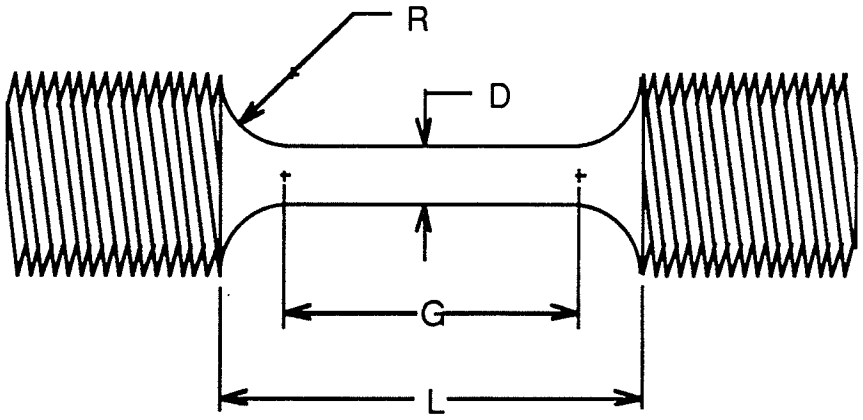

D = 5.00 ± 0.05 mm
G = 10.00 ± 0.05 mm
L = 15.0 ± 0.10 mm
R = 2.50 ± 0.05 mm
3/8" UNF Threads

(b) Specimen dimensions.

Figure 3.3: Cylindrical tensile test sample detail.

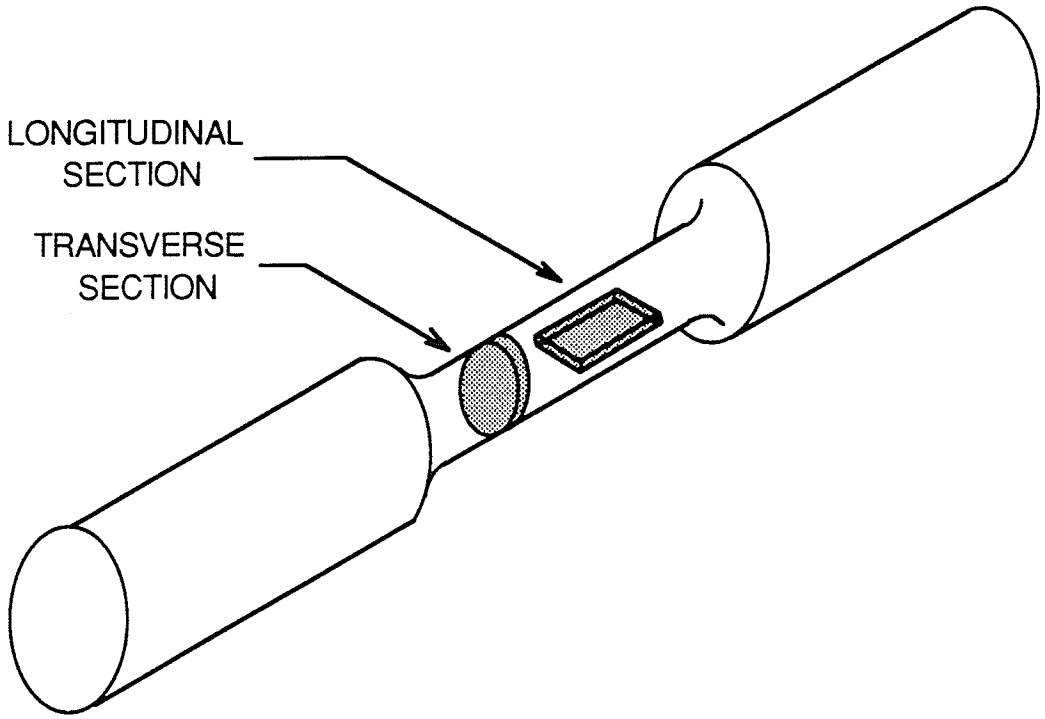
LONGITUDINAL
SECTION
TRANSVERSE
SECTION

(a)

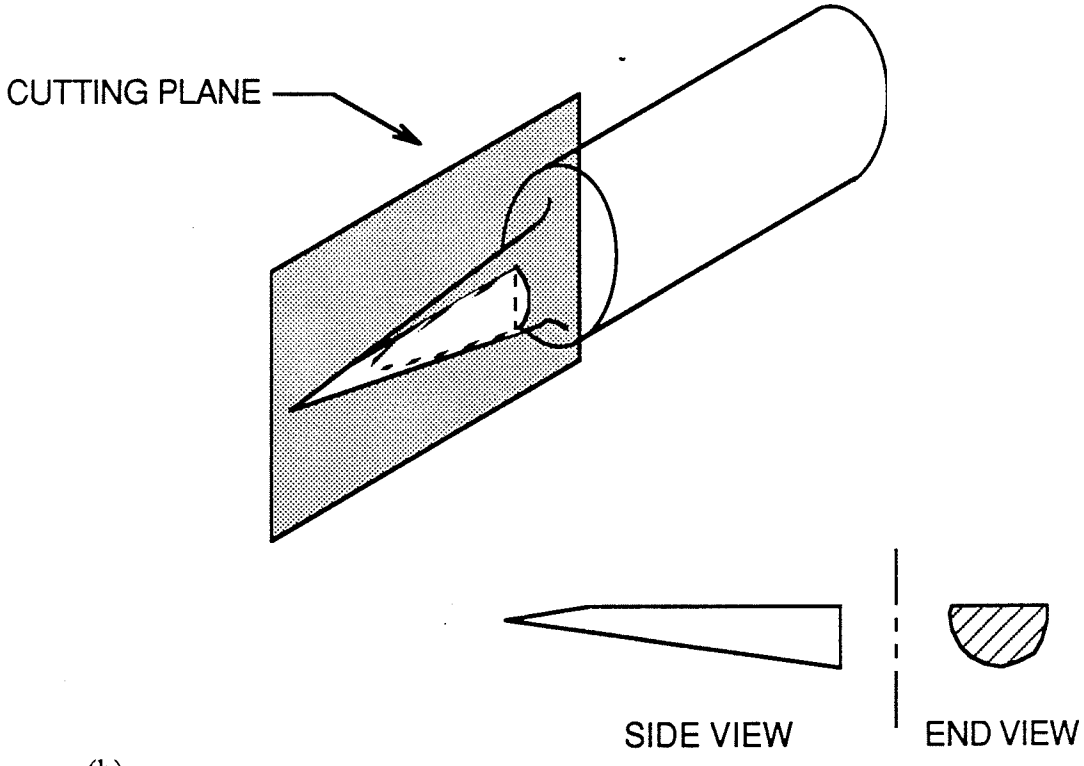
CUTTING PLANE
SIDE VIEW
END VIEW

(b)

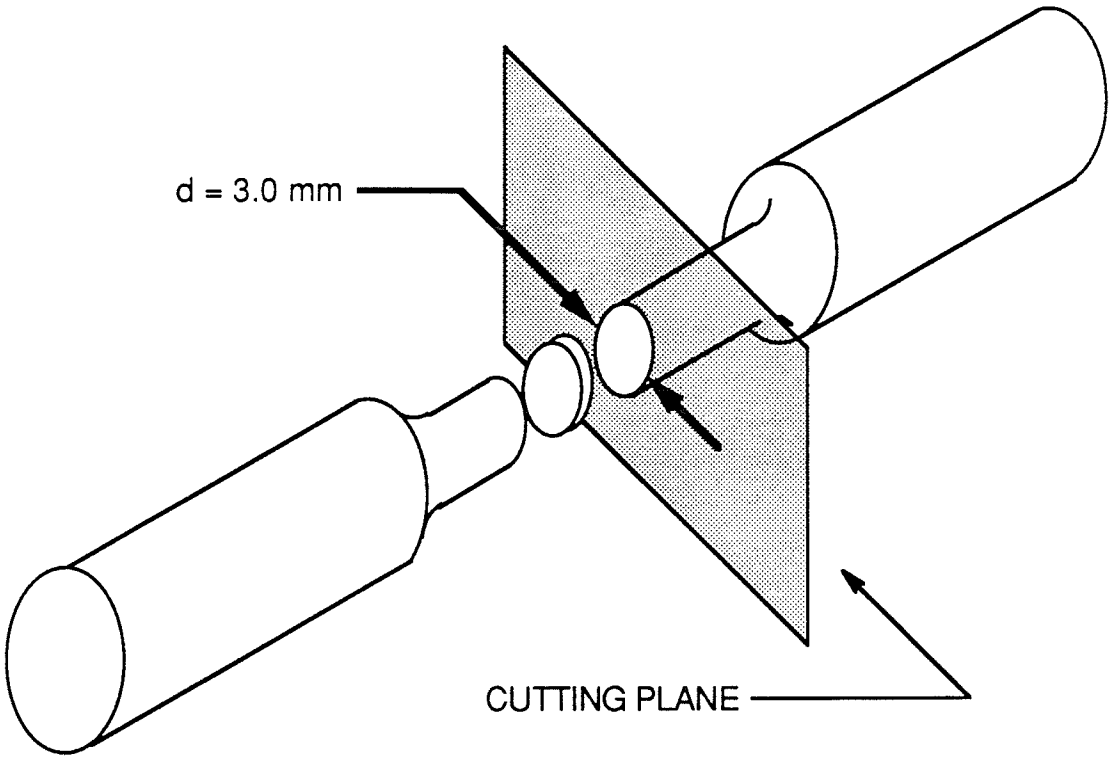

(c)

Figure 3.4: Metallography specimens.

(a) Specimens removed from undeformed tensile sample.

(b) Transverse specimen removed from failed tensile sample.

(c) TEM specimen removed from partially deformed tensile sample.

3.3.3 Scanning Electron Microscopy Specimens

Scanning electron microscopy samples were required for cavitation and final microstructural studies. These samples were selected from the tensile specimens pulled to failure, as shown in Figure 3.4 (b). For cavitational studies, slices parallel to the longitudinal direction were taken from one of the fracture ends to the gauge head. Specimens were mounted in bakelite and polished to a 0.05 μm finish following the same procedure as used for optical metallography specimens. The specimens were not etched in order to prevent dissolution of cavities. After the cavitational study, samples were etched as described in section 3.3.2 to examine other microstructural features.

3.3.4 Transmission Electron Microscopy Specimens

Transmission electron microscopy (TEM) specimens were prepared from tensile specimens deformed to a fixed strain and water quenched under load. The method, detailed in section 3.5, improves the probability of locking dislocations in their high temperature configuration. Figure 3.4(c) showed how 0.30 mm thick specimens were sectioned from the deformed guage length in areas where the guage diameter was 3 mm. This method removed the need to actually cut the 3 mm disc and disturb the dislocation structure. These slices were mechanically thinned to about 0.15 mm using 600 grit silicon carbide paper, and stored in ethanol until ready for electropolishing. The discs were electropolished just before TEM observation to minimize potential contamination. The polishing unit used to perforate the TEM foil was a Metalthin Thin Foil Preparation Unit. The electropolishing conditions used were as follows. It should be noted that special precautions must be taken when using perchloric acid [88].

Electrolyte: 13.5 vol.% perchloric acid (70)
15.5 vol.% butanol
71.0 vol.% methanol

Temperature: -40 to -45°C

Voltage: 30V

Jet Speed: 5 to 6 units

Electropolished foils were washed in methanol, ethanol, and stored in a vacuum desiccator.

3.4 Tensile Testing

Uniaxial tensile testing was performed to characterize the flow properties of three different starting morphologies in a range of temperature and constant strain rate conditions.

3.4.1 Apparatus

Tensile testing was conducted on a screw driven Instron model #1137 testing machine interfaced to a microcomputer-based data acquisition system. The frame was specially modified, as per Jain *et al.* [31], to allow testing in temperature regimes of up to 1020°C. Ti-6Al-4V alloy tensile specimens were threaded into 316L stainless steel grips, using a high temperature nickel compound as an intermediate to prevent bonding between the specimens and the grips at high temperatures. The specimens were enclosed in an argon filled chamber in which the sample could be water quenched from the test temperature. The argon atmosphere was maintained at a positive pressure to prevent high temperature oxidation of the Ti-6Al-4V. A split 3-zone furnace with a constant temperature zone length of 10 cm was used to heat the specimens and assembly with an accuracy ±1°C. This meets the requirements summarized by Hamilton for temperature control [9]. The time for the specimen to reach equilibrium temperatures between 875°C to 1020°C from room temperature was 15 to 17 minutes. Typically, after the heat treatment and the mechanical test, samples were water quenched, by removing the furnace and filling the chamber with water. Quenching from test temperature occurred either under load if the

specimen was not taken to failure or unloaded after tensile fracture. The cooling rate on water quenching was measured to be 100°C s^{-1}. For interrupted tests, slight unloading during the tests initiated the automatic water quench control. A custom designed slip rod system allowed thermal contraction on quenching without sample loading.

3.4.2 Test Conditions

Uniaxial tensile tests were performed for the three morphologies at 875,900,925, and 950°C for the constant strain rates of $5x10^{-3}$, $1x10^{-3}$, $5x10^{-4}$, and $1x10^{-4}$ s^{-1}. Tensile testing consisted of two series: (1) total elongation tests by constant strain rate to failure, and (2) strain rate sensitivity tests by strain rate change tests to a fixed strain value.

3.4.3 Elongation to Failure

One measure of superplasticity is a material's percentage elongation to failure for some of the proposed temperature-strain rate conditions. Selected temperature - strain rate conditions were chosen to evaluate the trends, if any, between the phase morphology, the flow characteristics and the percent elongations. The total elongations also provided some guide into preparing the strain rate change tests over fixed intervals. Failed samples were water quenched and used for post deformation studies.

3.4.4 Strain Rate Sensitivity Determination

Strain rate change tests as proposed by Hamilton, Ghosh and coworkers [11,23,35,36,89] for strain rate sensitivity determination, were performed to determine the strain rate sensitivity of the three morphologies at all the proposed temperatures and strain rates. Tests were started at a constant strain rate, referred to as the base strain rate, and at fixed strains for fixed intervals during the test the strain rate was increased by multiples of 2 and then decreased back to the base stain rate. The strain rate sensitivity, m , follows from the test using the flow relation presented earlier by equation (2.3). Strain rate

sensitivity values were calculated from true stress - true strain plots of the test data. Typical flow curves for (a) strain hardening, (b) constant stress with strain, and (c) strain softening are shown in Figure 3.5. The m values calculated represent the average, m_{ave} of the up-step(m^+) and down-step(m^-) values. Selected specimens were pulled to a maximum of 250 percent elongation (or less depending upon the predicted onset of fracture) and subsequently a maximum number of 3 mm discs were retrievable from the specimen for TEM (250 percent uniform deformation of a 5 mm diameter specimen gives 3mm discs). Specimens were water quenched under load as detailed in section 3.4.1. Other samples were taken to failure to determine the variation of m_{ave} with strain.

3.5 Microstructural Examination

3.5.1 Optical Microscopy

Optical Microscopy was performed to determine the distribution and morphology of the α and β phases present in the three starting morphologies at the four temperatures. Specifically, the prior β grain size, the volume fraction of phases, the mean linear intercept of each phase and α aspect ratios of the lamellar morphologies were quantified. All optical metallographic samples were prepared according to section 3.3.2, and first examined using a Nikon Epiphot reflecting light microscope at magnification from 50X to 1500X. Images were recorded using an attached 35mm photographic system. Quantitative metallography was performed on etched samples as outlined in section 3.6.

3.5.2 Scanning Electron Microscopy

Scanning electron microscopy (SEM) was used for enhanced resolution studies of the post deformed microstructures. Specifically, cavitational behavior and final deformed morphology were observed using the SEM. Specimens were prepared as per section 3.3.3

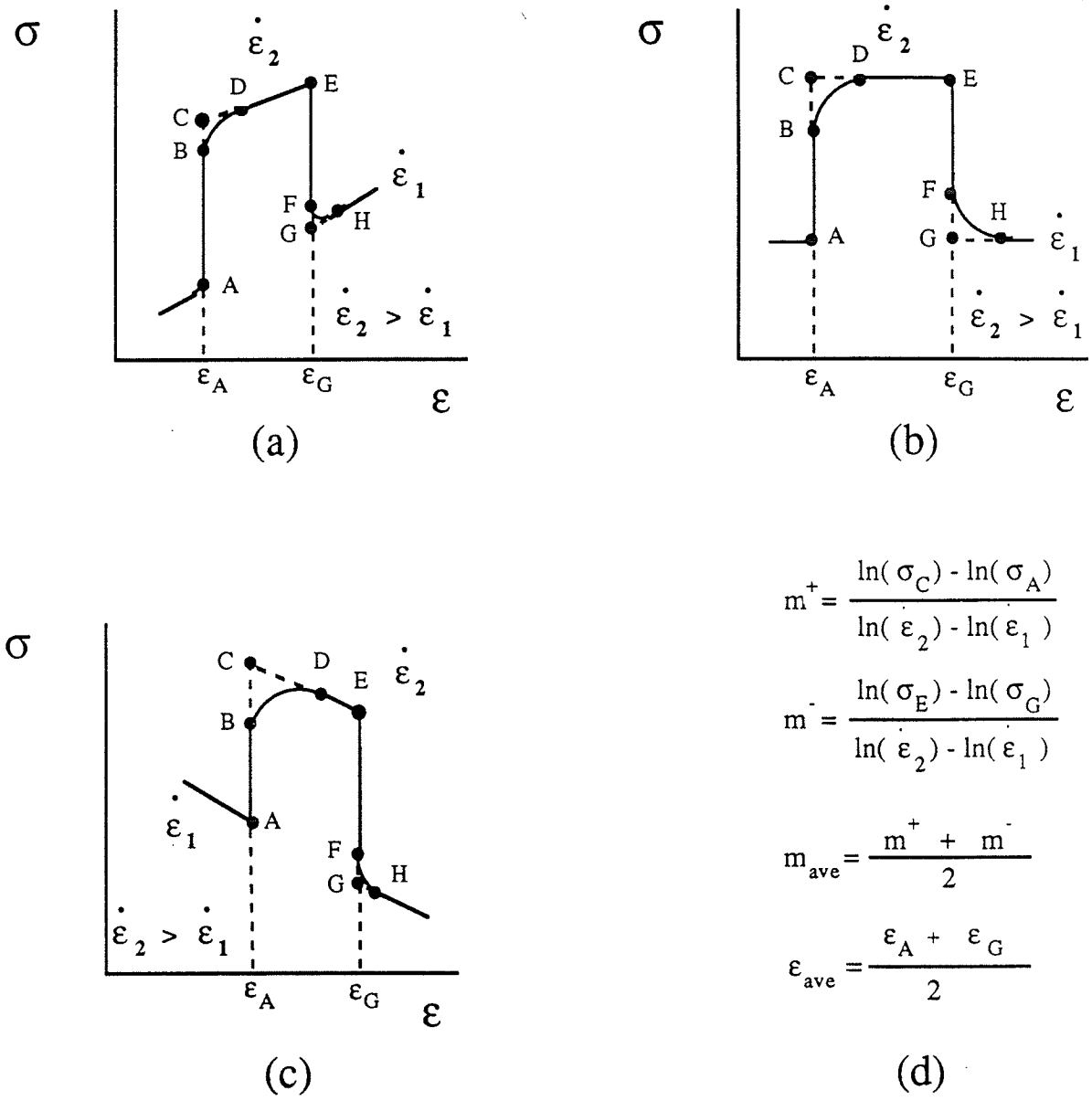

Figure 3.5: Schematic representation of a typical strain rate change tests showing, (a)strain hardening, (b)constant stress with strain, (c)strain softening, and (d)the algorithm used to determine the average strain rate sensitivity, m_{ave} for all conditions.

and examined in a Jeol JXA-840 scanning microanalyzer operating at 20.0 KV using both secondary and backscattered electron detectors.

3.5.3 Transmission Electron Microscopy

The purpose of the transmission electron microscopy (TEM) study was to qualitatively characterize the changes in the α and β phases of the three morphologies after deformation to a fixed strain. A particular emphasis was placed on studying dislocation substructure, and dynamic recrystallization. Microscopy was performed on a Jeol 2000 FX TEM/STEM with a tungsten source operating at 200 KV. Bright field, darkfield, and selected area diffraction techniques were used to derive most of the information.

3.6 Quantitative Metallography

Quantitative metallography was used to statistically describe the macrostructual and microstructural features considered for the three Ti-6Al-4V alloy morphologies, viewed either optically or by SEM.

All image analysis, except aspect ratio measurements, was performed using a LEITZ/TASIC automated image analyzer interfaced to a DEC (PDP-11) computer. Analysis was performed directly on the sample or on traced images to enhance poorly detected grain boundaries. The microstructural parameters measured included α/β volume fraction, α/β and prior beta mean linear intercept, and α aspect ratio. The macrostructural parameter measured was the tensile sample necking profiles.

3.6.1 Prior Beta Grain Size

Prior beta grain size was measured on specimens held above the beta transus for varying periods of time and water quenched. The water quenching resulted in transformation of β to martensite. The relative orientation of the martensite plates in the structure identifies the prior grain boundaries. Fifteen fields at 50X magnification were

photographed for each condition, and the prior beta grains were hand traced on acetate transparencies. The planar prior beta grain size was determined using a mean linear intercept method [90]. The mean linear intercept was found by taking the average length of lines intercepting prior beta grains at angles 0°, 120° and 240°, as shown in Figure 3.6.

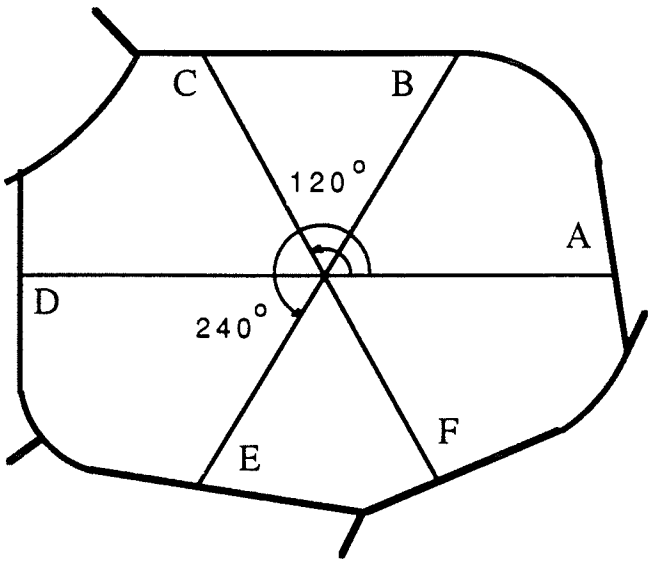

$$\text{mean linear grain size} = \frac{\overline{AD} + \overline{BE} + \overline{CF}}{3}$$

Figure 3.6: Schematic of linear intercept measurements used to determine the mean linear intercept of a grain.

3.6.2 Volume Fraction of α and β Phases

Volume fractions of α and β phases were measured by the point count or intersecting grid line technique, and statistically analyzed as outlined by Abrams [91] to attain 95 percent confidence levels. An image analyzer was used to systematically move a grid consisting of 100 points over 6 to 8 randomly chosen bulk areas. All samples considered were quenched from the test temperature as detailed in section 3.2. The volume fraction of high temperature β is assumed to be represented by the martensitically transformed microstructure at room temperature.

3.6.3 Alpha and Beta Grain Size

The grain size of material with equiaxed α and β morphology was determined by measuring each phase's mean linear intercept. The mean linear intercept for a grain was expressed in Figure 3.6. Optical/SEM specimens used for the measurements were prepared according to sections 3.3.2 and 3.3.3. Image analysis was used to optically detect variations in phase contrast, allowing either α or β grain size to be evaluated. Ten fields consisting of approximately 150 grains of either phase were analyzed to attain grain size distribution plots at 95 percent confidence levels.

3.6.4 Alpha Plate Aspect Ratio

The phase morphology for EQ material is typically equiaxed, but the BA and BQ morphologies are characterized by lamellar α and β phases. Alpha phase aspect ratios were determined for material with BA, EQ and BQ morphologies using the technique demonstrated by Weiss *et al.* [33] for similar microstructures. The morphology was characterized by considering the shapes of individual alpha plates defined in three dimensions by its length(l), width(w), thickness(t), and the aspect ratio (ϕ), where

$$\phi = \frac{l}{t} \quad . \tag{3.3}$$

In the metallographic cross-section it was not possible to distinguish between width and thickness, due to random sectioning of the alpha plates. The t values reported are the average section thickness, and the l values are the average section lengths, since the angle of plate inclination to the metallographic surface could not be determined. The length and thickness of 1000 individual plates were physically measured from optical photomicrographs for the 875, 900, 925, and 950°C BA, EQ, and BQ starting conditions to obtain the mean plate thicknesses, and the ϕ distributions.

3.6.5 Neck Profiles

Image analysis was performed on deformed samples in order to measure the variation of deformation along the gauge length of tensile specimens deformed to either fixed strains or failure. Figure 3.7 shows a schematic of a typical deformed cross-section. Measurements consisted of measurements on the UU' axis and rotating the sample 90° to measure the VV' axis to evaluate possible anisotropy. Measurements were taken at 1.0 mm intervals along the length. Variation in dimensions a and b, including cross sectional area, πab assuming an ellipse, were plotted against length along sample. Fracture surface cross-sections were not measured, and are assumed zero in all analyses.

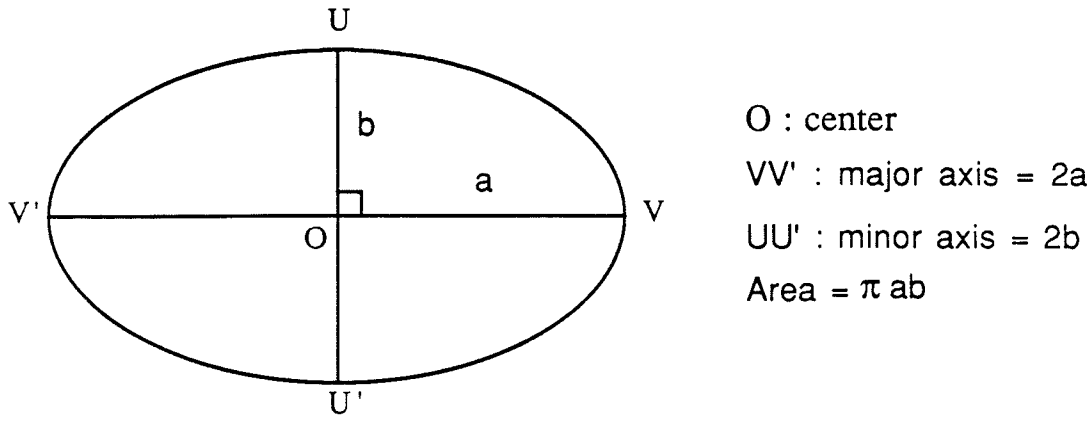

Figure 3.7: Dimensions of deformed cross-section

CHAPTER 4

EXPERIMENTAL RESULTS

4.1 Starting Microstructures

4.1.1 Prior Beta Grain Size

It is recognized that increasing grain size reduces superplasticity in Ti-6Al-4V. It was observed that if uninhibited, beta grains grow rapidly at temperatures above the beta transus. In the first stage of the heat treatment for the BA and BQ morphologies, the material must spend enough time above the beta transus to transform completely to β phase, yet maintaining the smallest possible grain size. Figure 4.1 shows the prior beta grain size as a function of time at constant temperature, while Figure 4.2 shows the transformed beta structure resultant from holding the material at 1020°C for 20 minutes followed by a water quench. Experiment showed that all α in the alloy could be completely transformed to β after two minutes at temperatures above the beta transus, but the treatment was not consistently reproducible. It was found that at least 10 to 20 minutes at temperatures above 1005°C were needed to ensure complete α to β transformation. Figure 4.1 indicates that the β grain size after two minutes increased from its as received size of approximately two micrometers to almost 200 μm for temperatures ranging from 1005 to 1060°C. Increasing the holding time from 10 to 20 minutes did not increase the beta grain size much further, and so based upon these results it was decided that a 1020°C - 20 minute treatment was justified. The 1020°C - 20 minute beta treatment used for the tensile samples produced a prior β grain size of 240 μm.

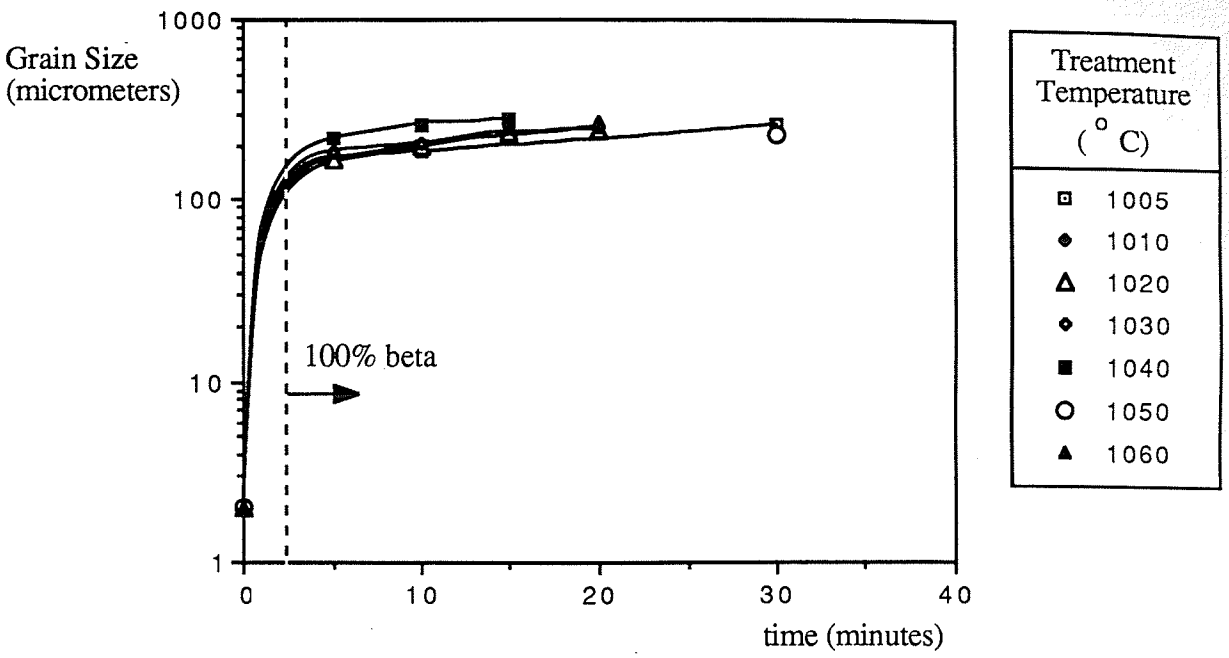

Figure 4.1: Prior beta grain size for Ti-6Al-4V alloy as a function of time at constant temperature.

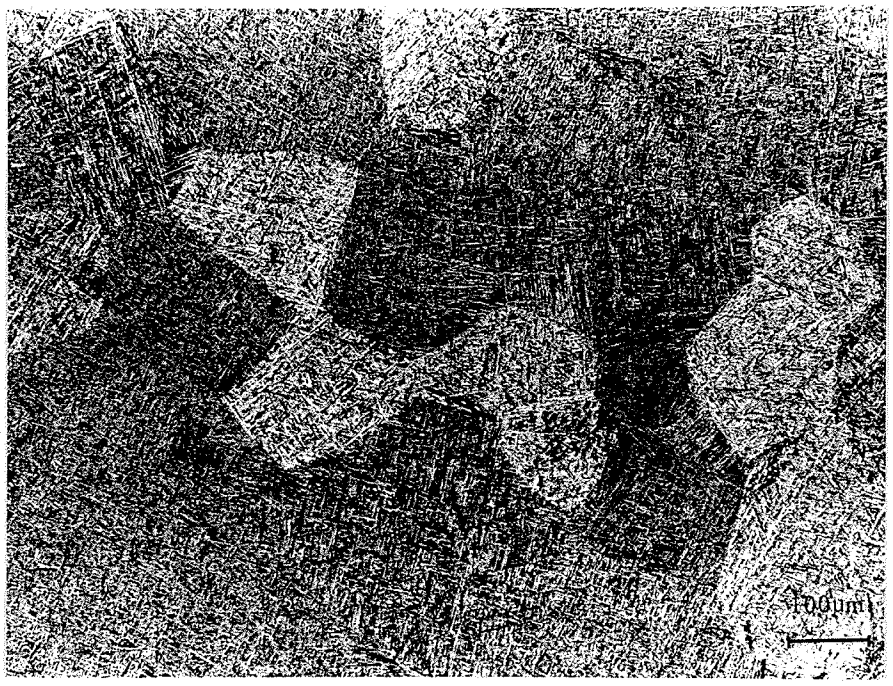

Figure 4.2: Transformed beta microstructure showing prior beta grain boundaries.

4.1.2 Microstructure Before Deformation

TABLE 4.1 lists the measured microstructural parameters for the three starting morphologies: beta-annealed, BA; equiaxed, EQ; beta-quenched, BQ. Figures 4.3 to 4.5 show respectively the micrographs for the BA, EQ and BQ morphologies after one hour treatment at 875, 900, 925, and 950°C followed by a water quench. In Figure 4.3, the BA morphology is characterized by plate-like α(light) and intergranular transformed β(dark). The EQ morphology in Figure 4.4 is characterized by equiaxed α grains(light) in a transformed β matrix(dark). Finally, the BQ morphology in Figure 4.5 consists of acicular α(light) in a transformed β(dark) matrix in what is typified as a basketweave morphology. Qualitatively, the microstructures for each morphology appear different, but quantification is needed. Morphologies were characterized by volume fraction of α, and either mean linear intercept and aspect ratio or plate thickness and aspect ratio measurements of α. Mean linear intercept and aspect ratio measurements were used for the EQ morphology which appeared isotropic. The BA and BQ morphologies were characteristically anisotropic so mean plate thickness measurements were substituted for the mean linear intercept. The volume fraction of alpha is an important parameter because it indicates the relative proportions of α and β phases at the four test temperatures.

For each of the three morphologies the volume fractions of α and β phases were comparable after one hour at the same temperature. The volume fractions tended to deviate at the higher temperatures, but more importantly the volume fraction ratio ranges appeared distinct for each temperature. For example, the mean volume fraction of α for all the morphologies at 900°C ranged from 52.1 to 56.2 percent. At 925°C, the α volume fraction ranged between 40.9 and 47.8, and no overlap occurred between this range and the ones at 900 or 950°C. Figure 4.6 demonstrates the phase volume behaviour for alpha and beta phases for the three morphologies in the 875 to 950°C temperature range.

TABLE 4.1: Initial Microstructural Parameters

Temp. (°C)	Morphology	Grain Size (μm) α	Grain Size (μm) β	Volume Fraction (%) α	ϕ α	t (μm) α
	BA			58.9±4.4	18.0±2.1	1.36
875	EQ	3.63±0.13	1.97±0.06	66.3±4.1	1.52±0.07	
	BQ			62.0±4.4	9.71±1.0	1.36
	BA			52.1±4.8	12.3±1.3	3.28
900	EQ	4.53±0.15	3.20±0.11	56.2±4.8	1.46±0.09	
	BQ			54.0±4.7	15.1±1.6	1.23
	BA			40.9±5.3	9.3±1.0	2.74
925	EQ	3.87±0.13	4.08±0.14	43.0±5.2	1.51±0.10	
	BQ			47.8±5.0	15.1±1.7	1.18
	BA			29.7±5.8	13.5±1.2	3.13
950	EQ	3.62±0.14	7.26±0.29	34.2±5.6	1.51±0.11	
	BQ			39.3±5.4	14.5±1.5	1.21

The temperature range at which 50 percent α and β coexist is between 905 and 920°C. It should be noted that the volume fraction results for the EQ morphology are similar to those reported by others [32,34,79].

For the material with the BQ morphology the volume fraction of α reported here is higher by about 15 percent than that reported by Ito *et al.* [32] at the same temperatures, but higher solution treatment times. No data was found in the literature for volume fraction measurements on BA type morphologies for the Ti-6Al-4V alloy. With equal volume fractions at the four test temperatures, differences in grain size, α-plate thickness and α aspect ratio are needed to differentiate the three morphologies.

Figures 4.7 and 4.8 display the alpha and beta mean linear intercept distributions for the EQ morphology. The mean α grain size remained in the 3.5 to 4.6 μm range at all temperatures. Increasing the solution treatment temperature from 875 to 900°C increased the alpha grain size from 3.63 to 4.53 μm, which is indicated by the shift in the mean linear alpha intercept distribution from Figure 4.7(a) to (b). Further increase in temperature

resulted in a decrease in alpha grain size to 3.87 and 3.62 μm at 925 and 950°C, respectively. At all temperatures at least 50 percent of the α grains were less than 5 μm with no observed grain exceeding 15 μm.

The EQ morphology β phase behaved differently than the α phase. Increasing the treatment temperature from 875 to 950°C increased the β grain size considerably, from 1.97 μm to 7.26 μm. The increase in β grain size with temperature is linked to the decrease in volume fraction of α which tends to restrict β growth. More importantly, the beta grain size distribution plots indicate that the grain size distribution widens at higher temperatures such that almost 20 percent of the beta grains are larger than 10 μm.

For the BA and BQ morphologies, mean linear intercept measurements were not made for reasons expressed earlier, so the mean α plate thickness values are used instead. TABLE 4.1 indicates that the BQ plates tend to be thinner than the BA plates. For the BA morphology, the plate thickness, t is 1.36 μm at 875°C. Increase in treatment temperature from 900 to 925, and 950°C increased the plate thickness from 1.36 μm to 3.28, 2.75, and 3.21 μm, respectively. The plate thickness values are within the EQ morphology mean linear intercept range. For the BQ morphology, the mean α plate thickness at 875°C is the same as the BA morphology plate thickness, but with increasing temperature the α plate thickness for this morphology remains relatively stable between 1.18 to 1.36 μm.

The final microstructural parameter assessed for all morphologies was the α aspect ratio, ϕ. For the BA morphology, Figures 4.9(a) to (d) show the ϕ distributions after the four treatment temperatures. Where the plate thickness tended to increase with increasing temperature, the ϕ shows a decrease from 875 to 925°C. At 950°C, there is a noted increase in α aspect ratio with 25 percent of the alpha plates having ϕ values greater than 20.

For the EQ morphology Figures 4.9(e) to (h) indicate that ϕ is constant at all temperatures, ranging from 1.52 to 1.46. This supports the labelling of this morphology as equiaxed(EQ).

The ϕ distributions for the BQ morphology are given in Figures 4.9(i) to (l). The ϕ shows a marked increase from 9.71 to 17.5 when the treatment temperature is increased from 875 to 900°C. Further increase in treatment temperature gradually reduces the ϕ from 17.51 at 900°C to 15.1 and 14.5 at 925 and 950°C, respectively. The ϕ at 875°C is low compared to those at the higher temperatures. The expected trend would be for the ϕ to decrease with increasing treatment temperature, since the martensitic microstructure in Figure 4.2 is the start of this treatment. The low ϕ measurement could be due to interpretation of the α plate lengths at 875°C. The microstructure consists of a basketweave morphology, which when revealed by chemical etching makes length measurements difficult. Alpha plates overlap so that measured lengths are less then actual lengths. At higher temperatures, the reduced volume fraction of α and increased volume fraction of β improved total α plate visualization.

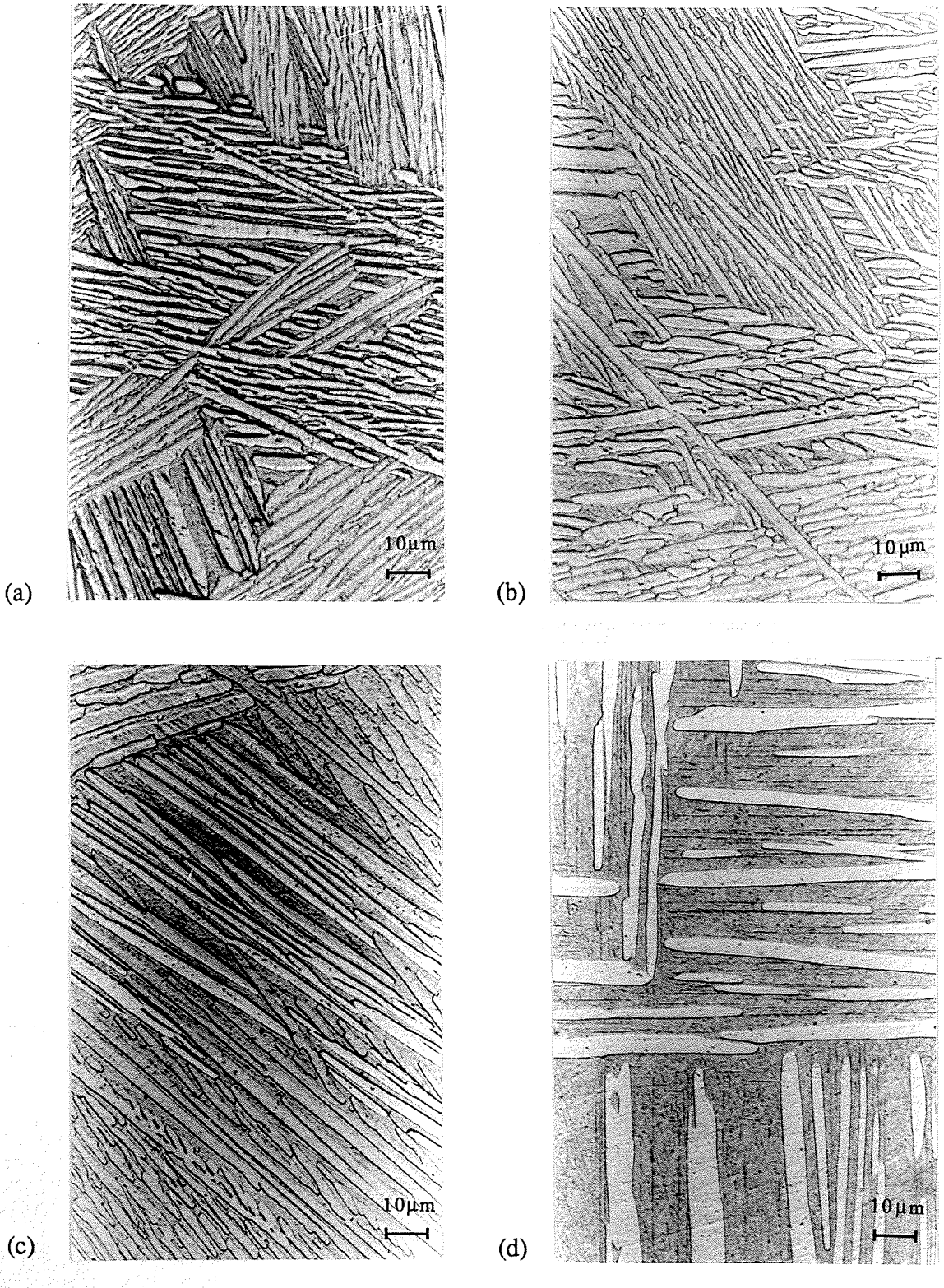

Figure 4.3: Beta-annealed(BA) microstructures at (a) 875, (b) 900, (c) 925, and 950°C.

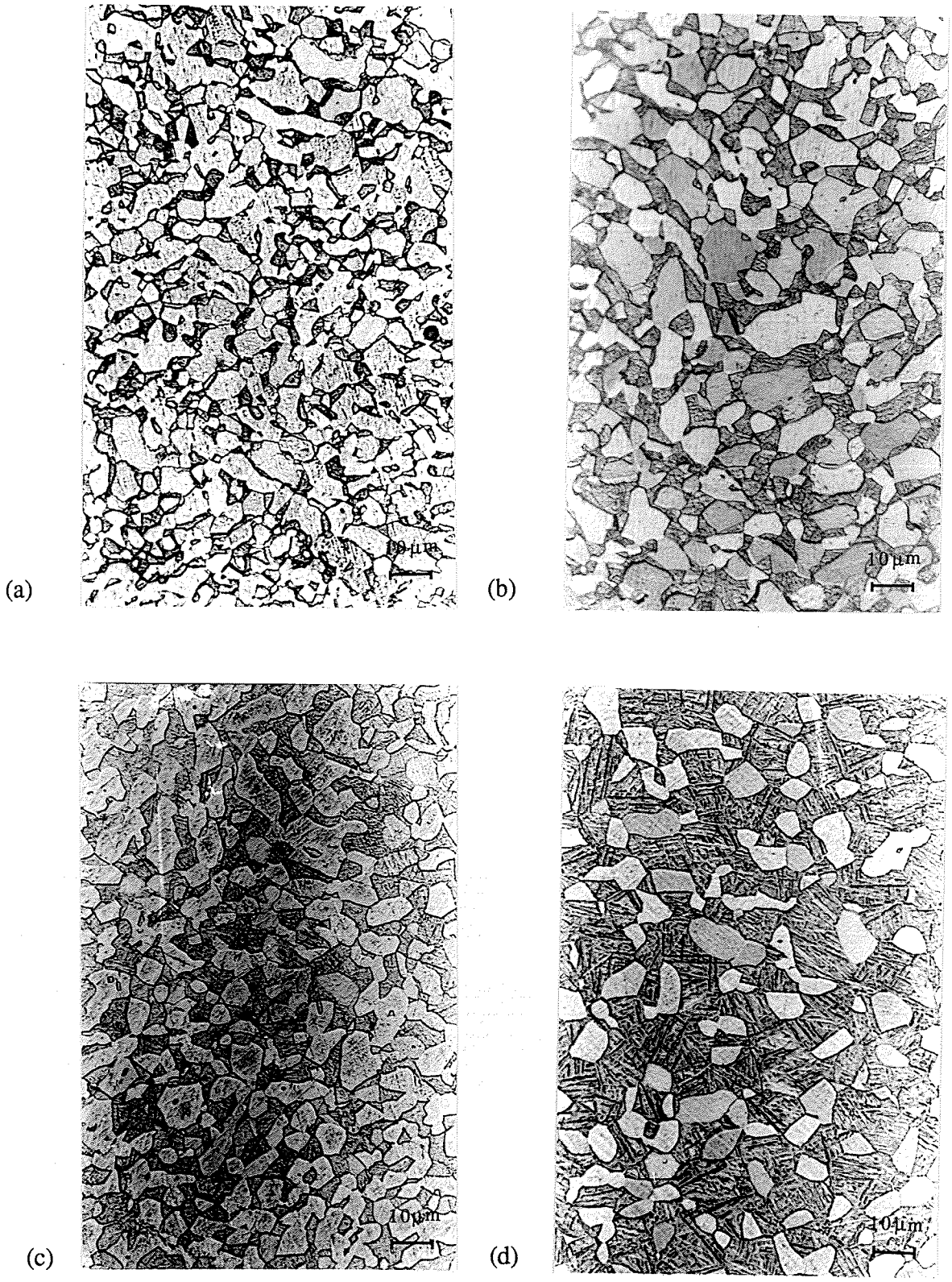

Figure 4.4 Equiaxed(EQ) microstructures at (a) 875, (b) 900, (c) 925, and 950°C.

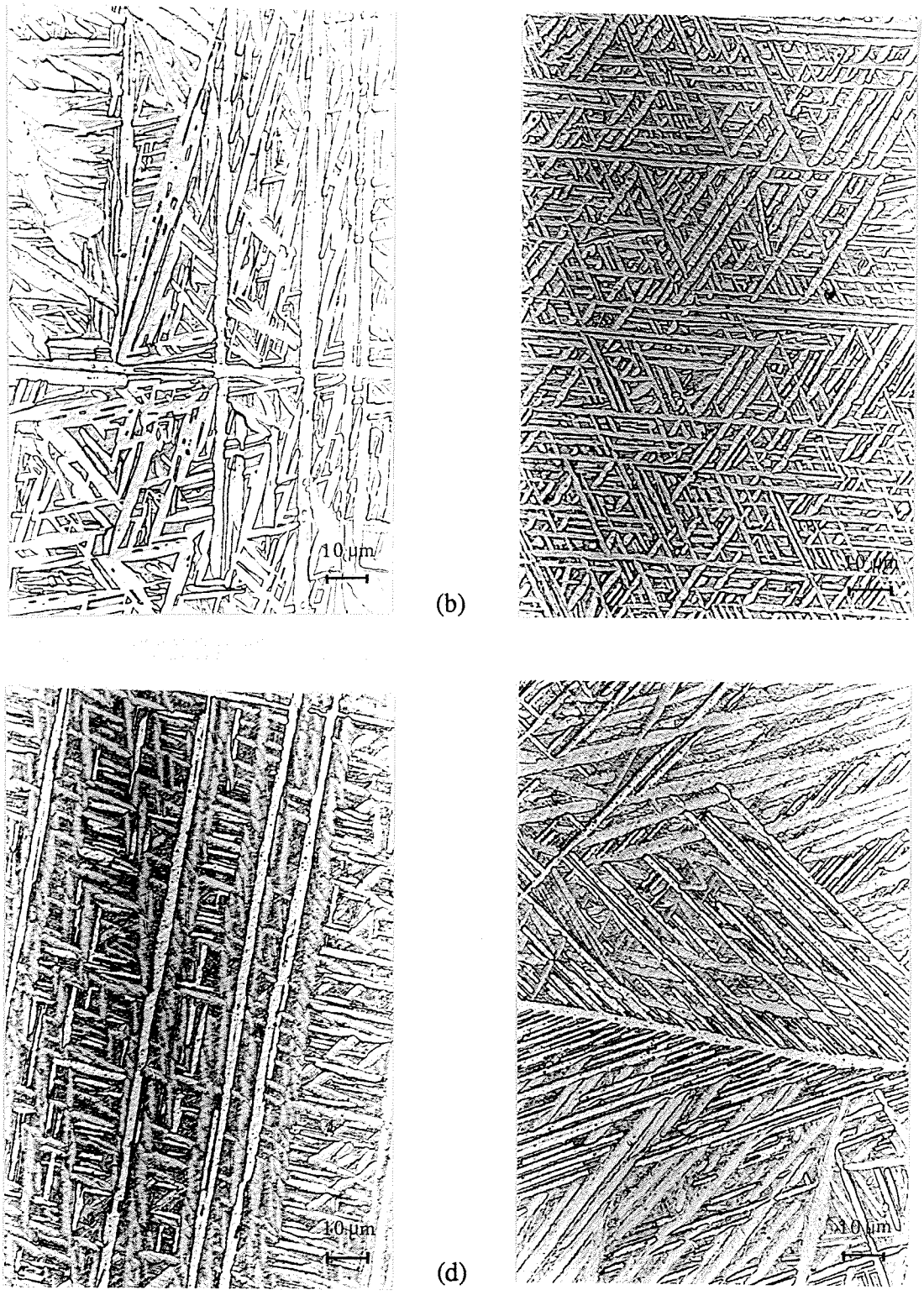

Figure 4.5: Beta-quenched(BQ) microstructures at (a) 875, (b) 900, (c) 925, and 950°C.

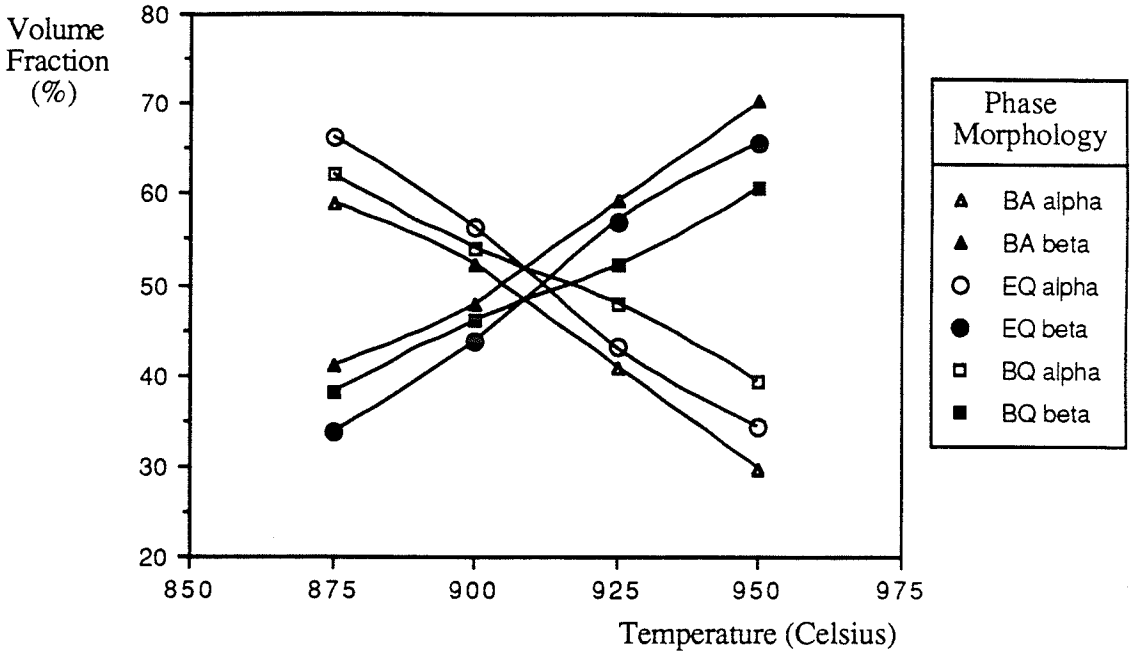

Figure 4.6: Volume fraction of alpha and beta phases versus temperature for BA, EQ, and BQ morphologies after one hour static treatments.

(a)

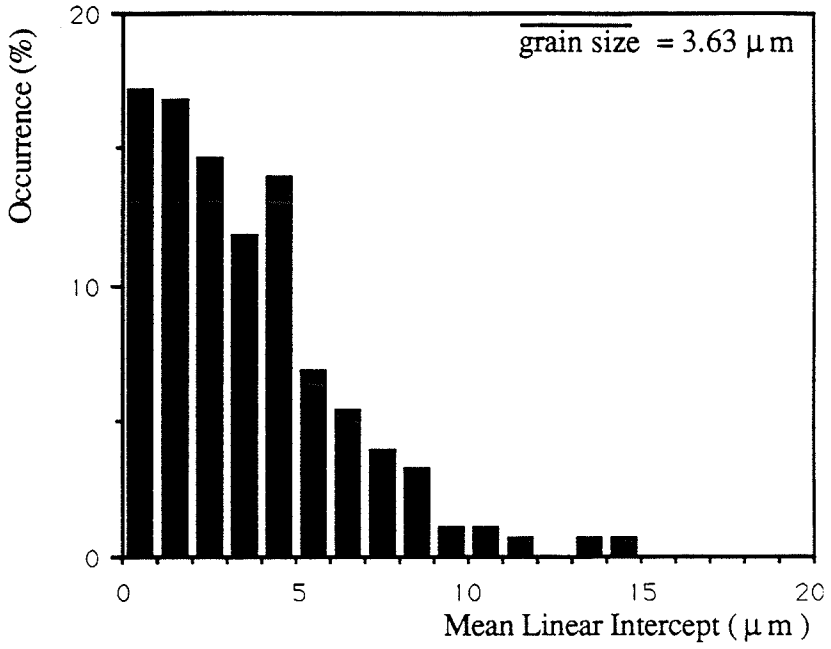
grain size = 3.63 μm
Occurrence (%)
20
10
0
0
5
10
15
20
Mean Linear Intercept (μ m)

(b)

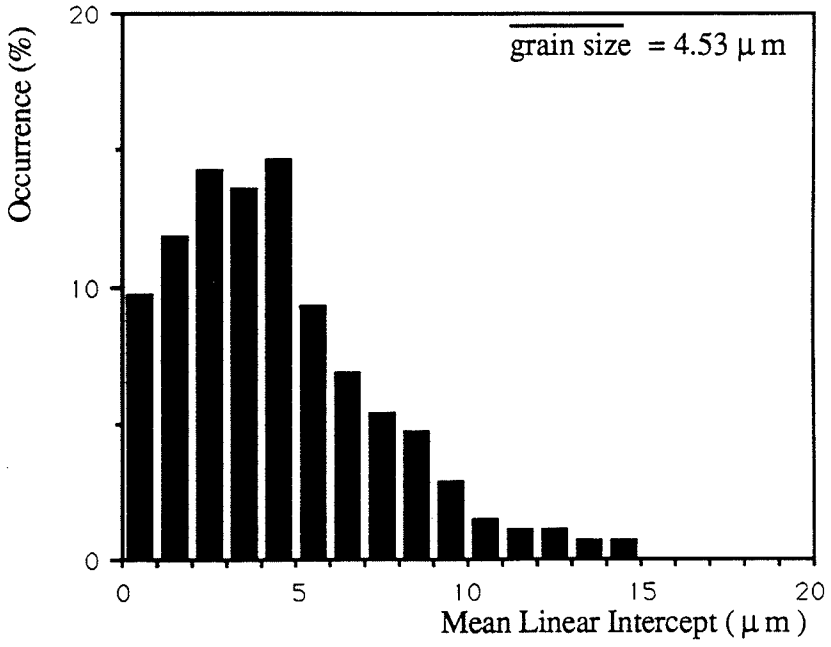
grain size = 4.53 μm
Occurrence (%)
20
10
0
0
5
10
15
20
Mean Linear Intercept (μ m)

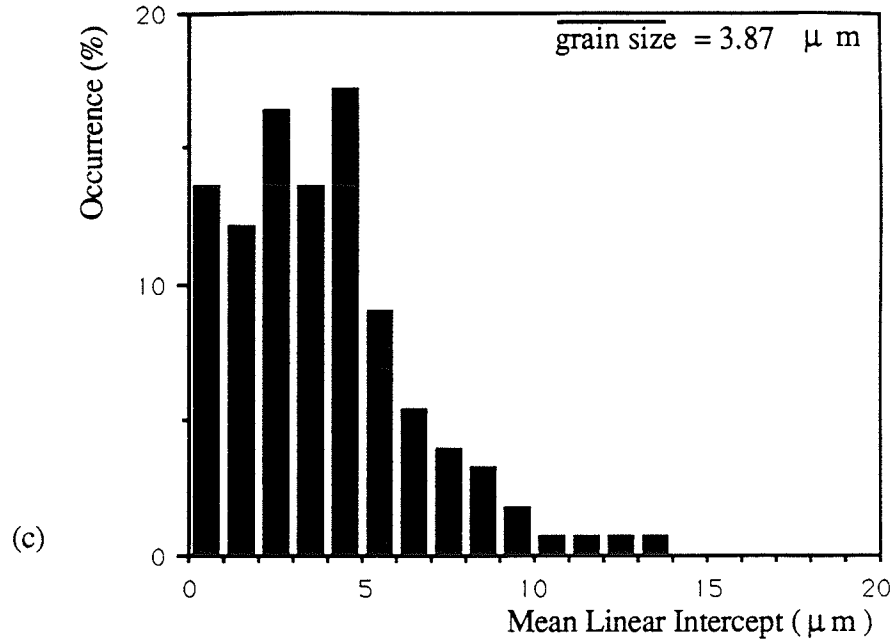

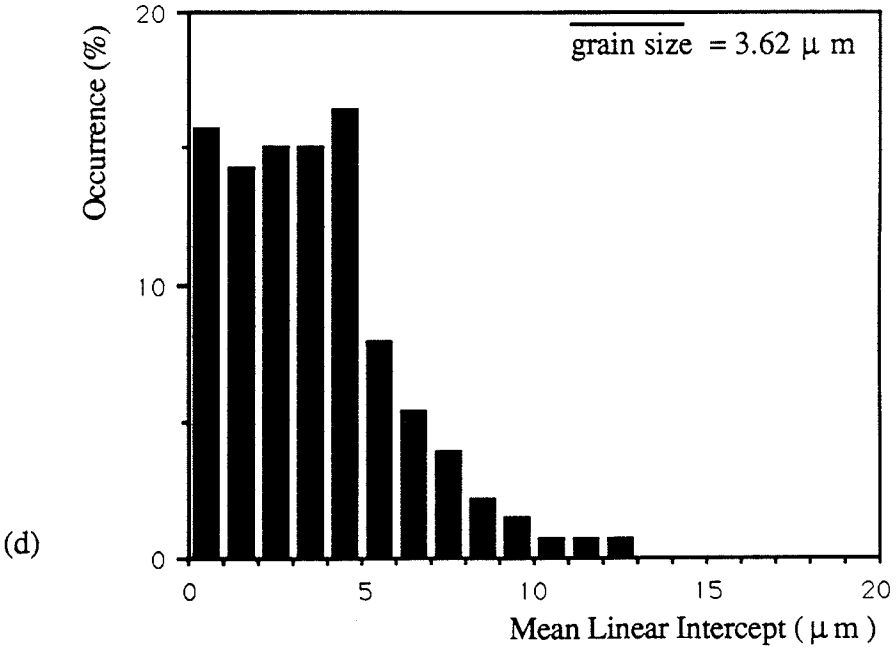

Figure 4.7: Distribution of alpha mean linear intercept for EQ starting morphologies at (a) 875, (b) 900, (c) 925, and (d) 950°C.

(a)

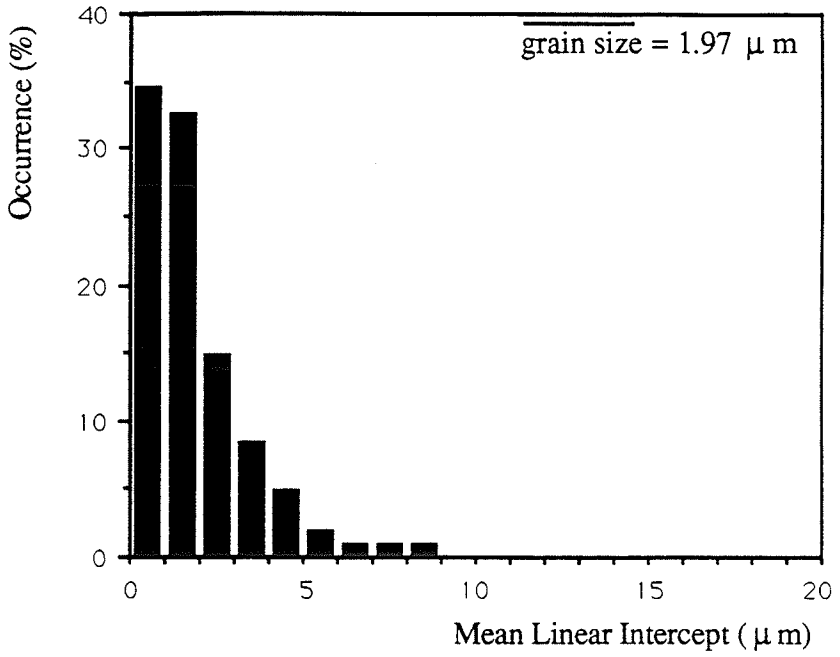
grain size = 1.97 μ m
Occurrence (%)
40
30
20
10
0
0
5
10
15
20
Mean Linear Intercept (μ m)

(b)

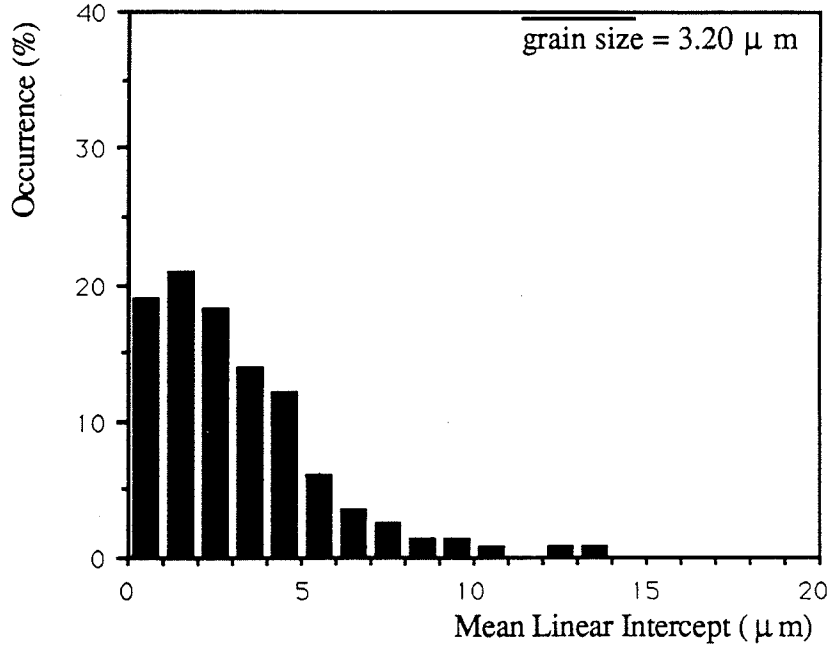
grain size = 3.20 μ m
Occurrence (%)
40
30
20
10
0
0
5
10
15
20
Mean Linear Intercept (μ m)

(c)

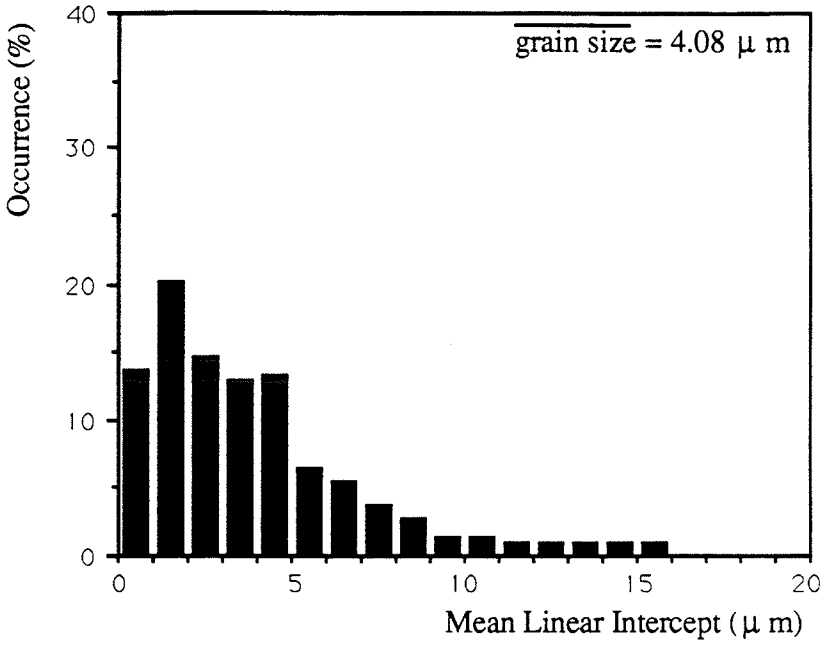

(d)

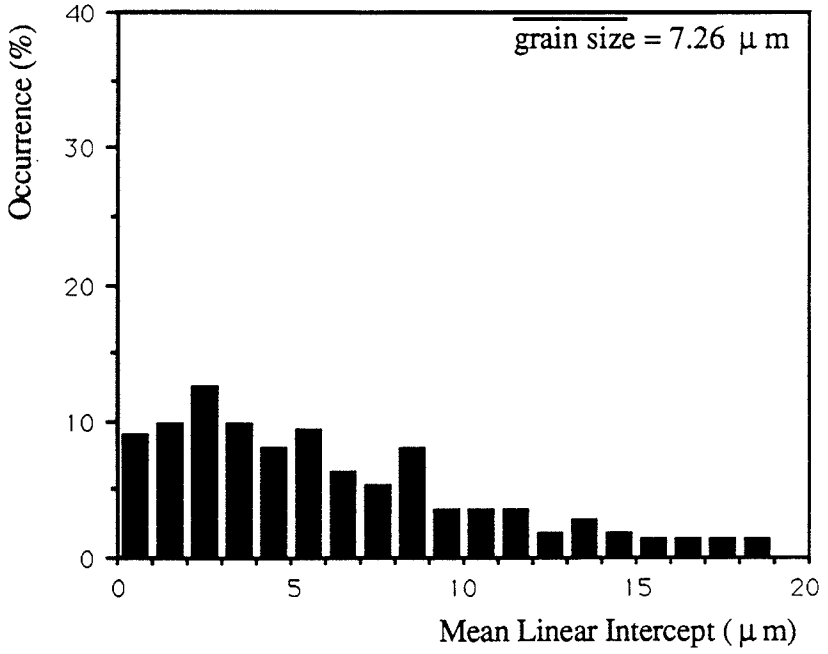

Figure 4.8: Distribution of beta mean linear intercept for EQ starting morphologies at (a)875, (b) 900, (c) 925, and (d) 950°C.

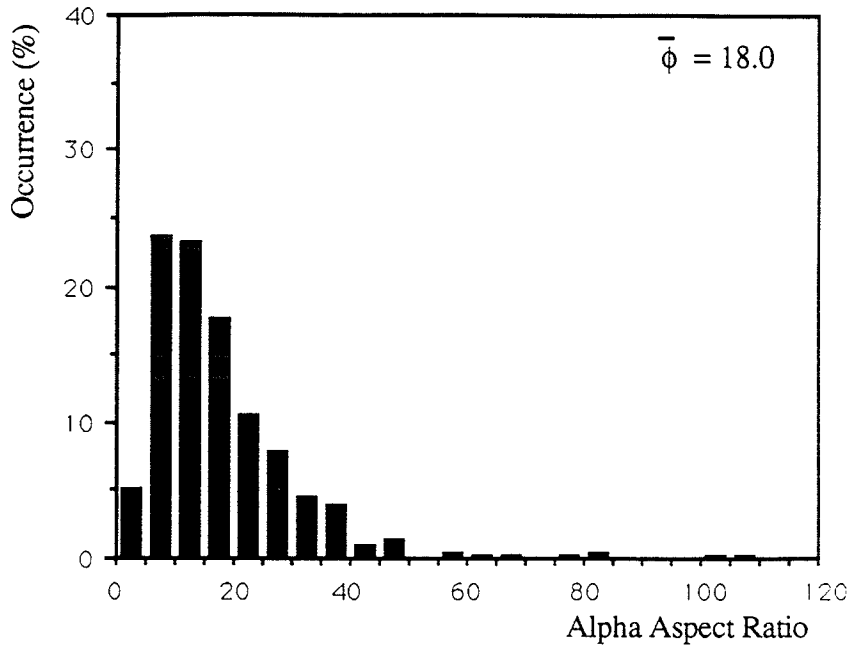

(a) BA morphology at 875°C.

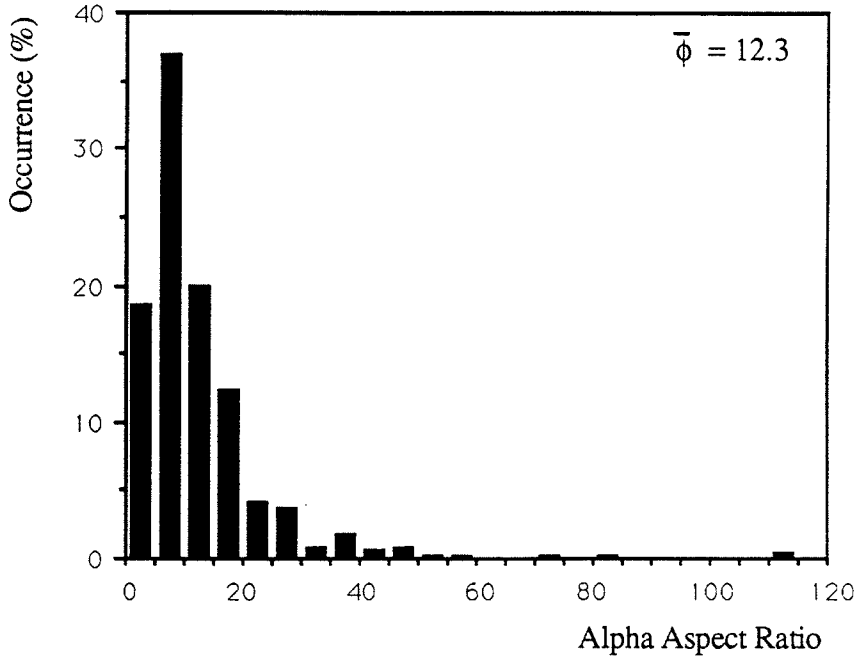

(b) BA morphology at 900°C.

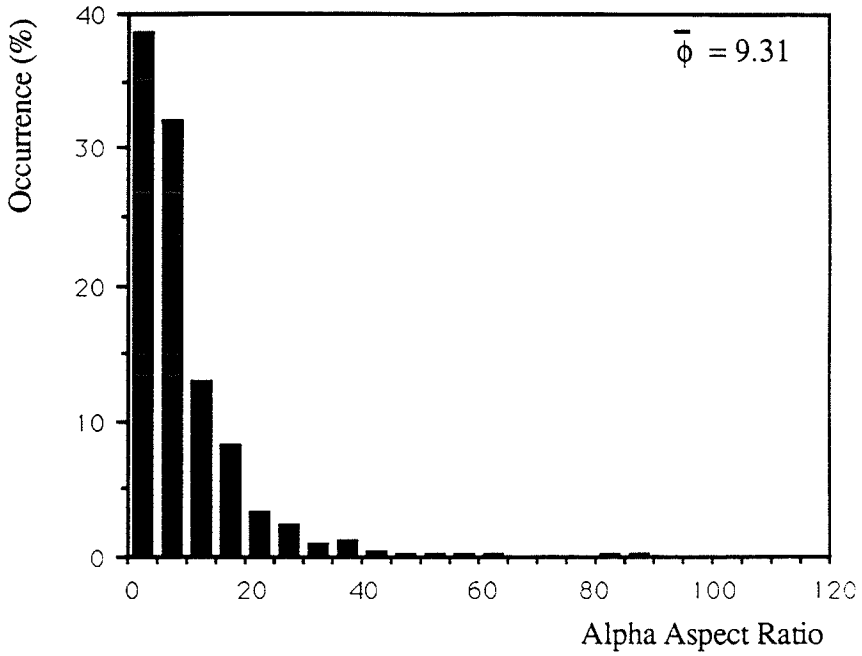

(c) BA morphology at 925°C.

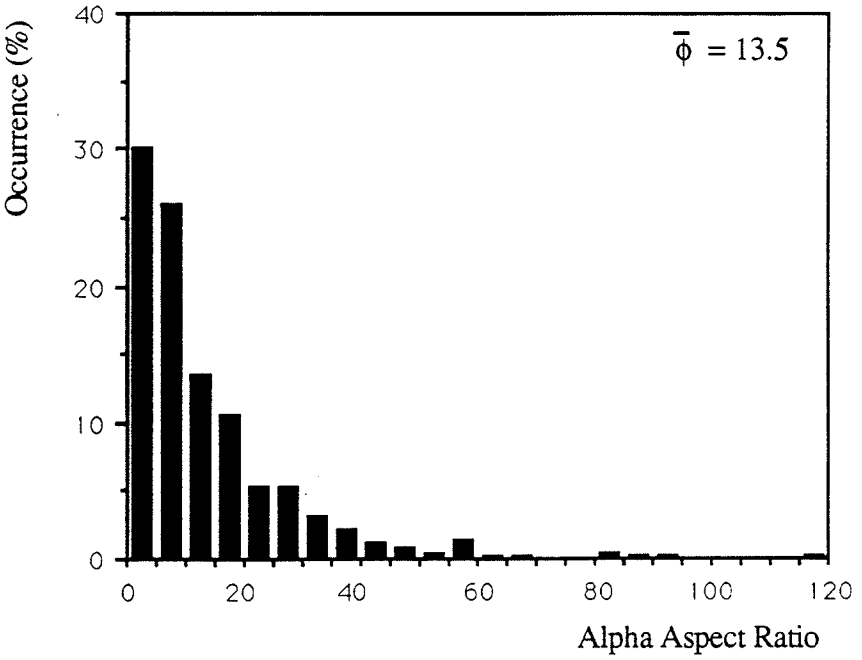

(d) BA morphology at 950°C.

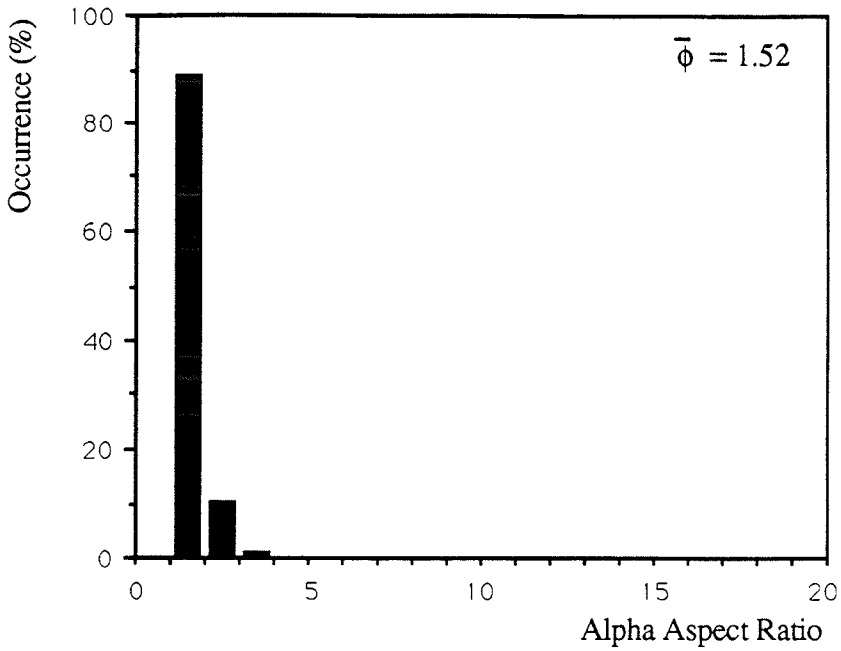

(e) EQ morphology at 875°C.

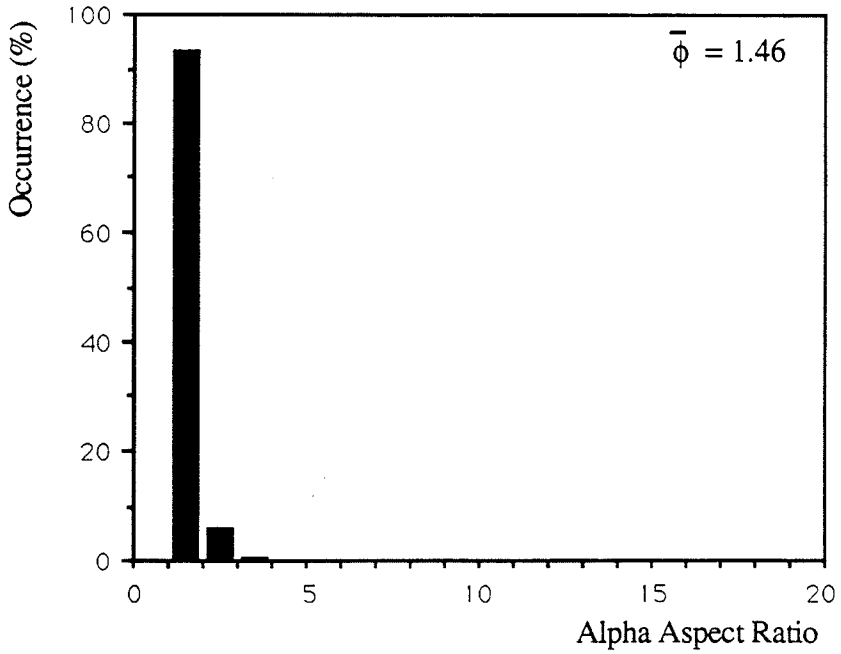

(f) EQ morphology at 900°C.

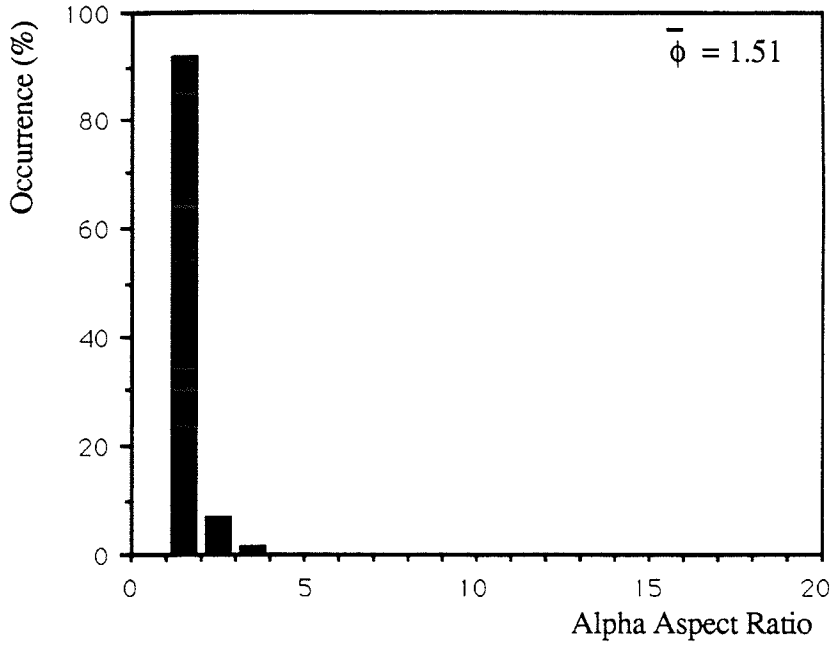

(g) EQ morphology at 925°C.

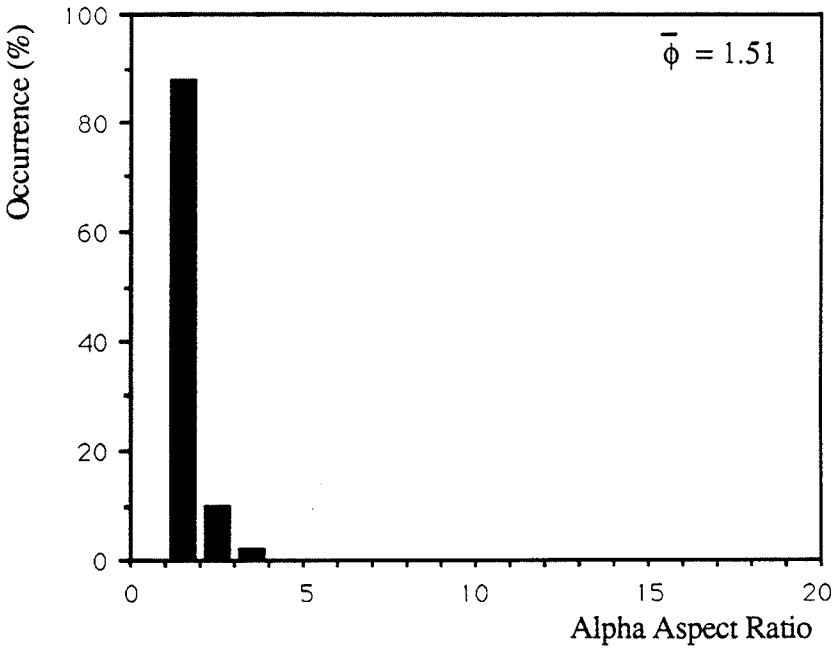

(h) EQ morphology at 950°C.

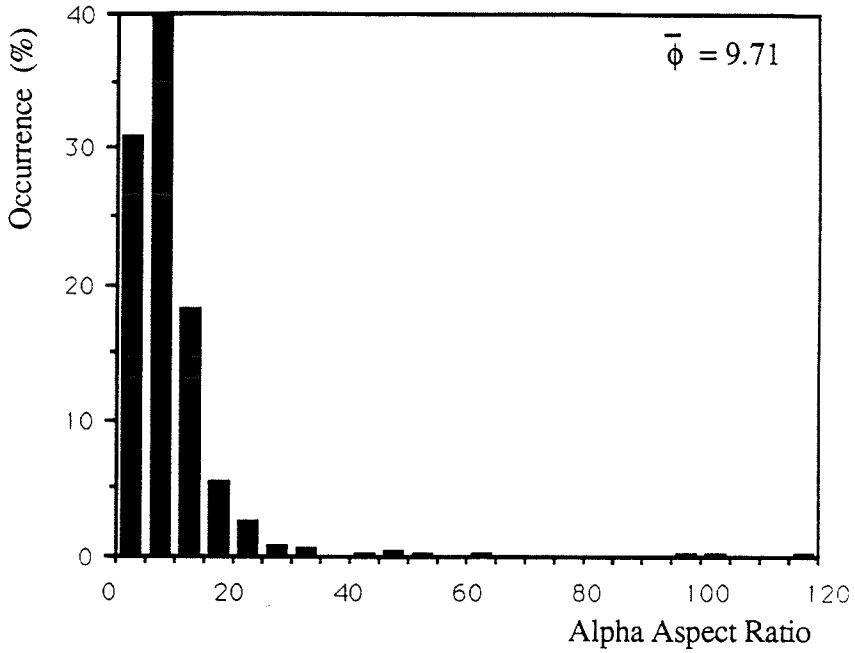

(i) BQ morphology at 875°C.

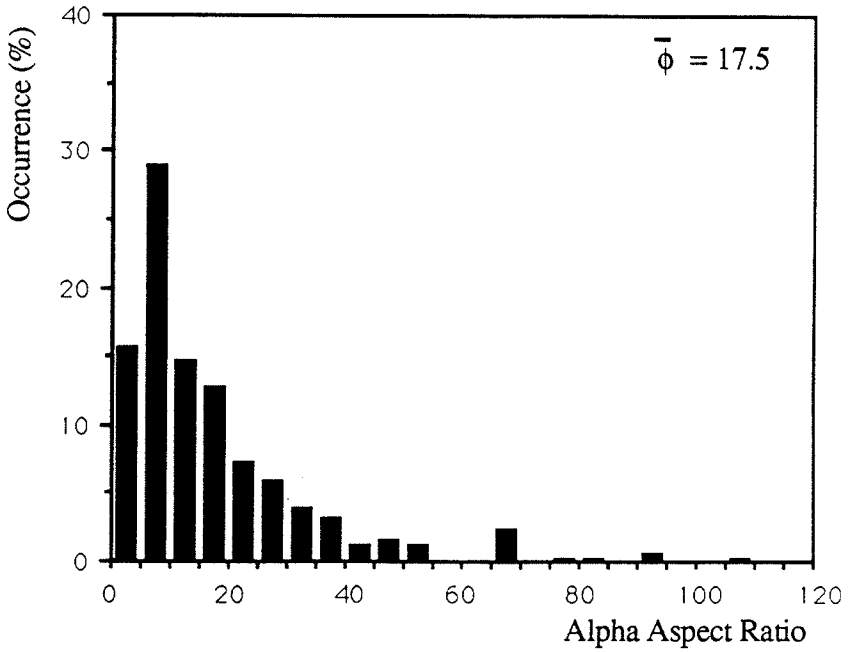

(j) BQ morphology at 900°C.

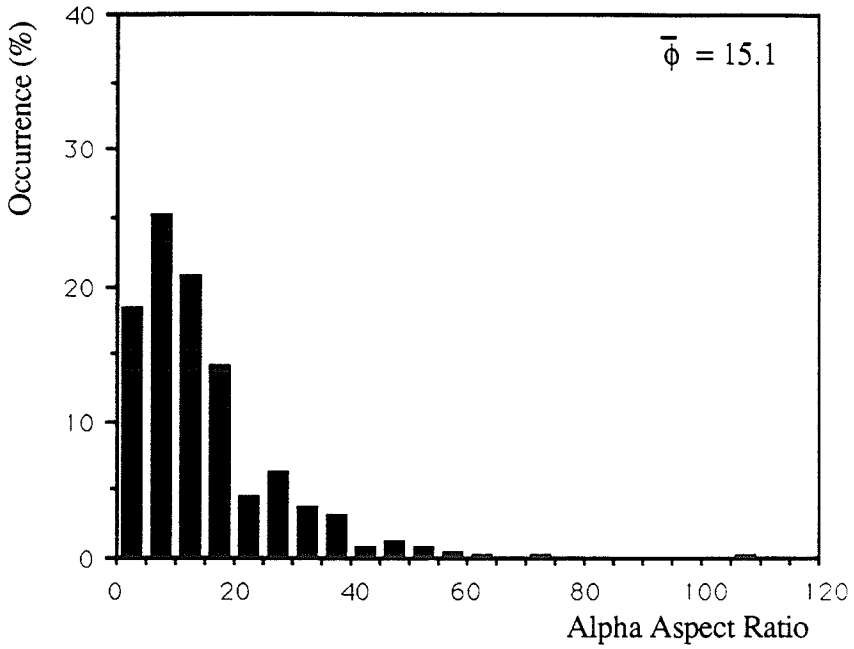

(k) BQ morphology at 925°C.

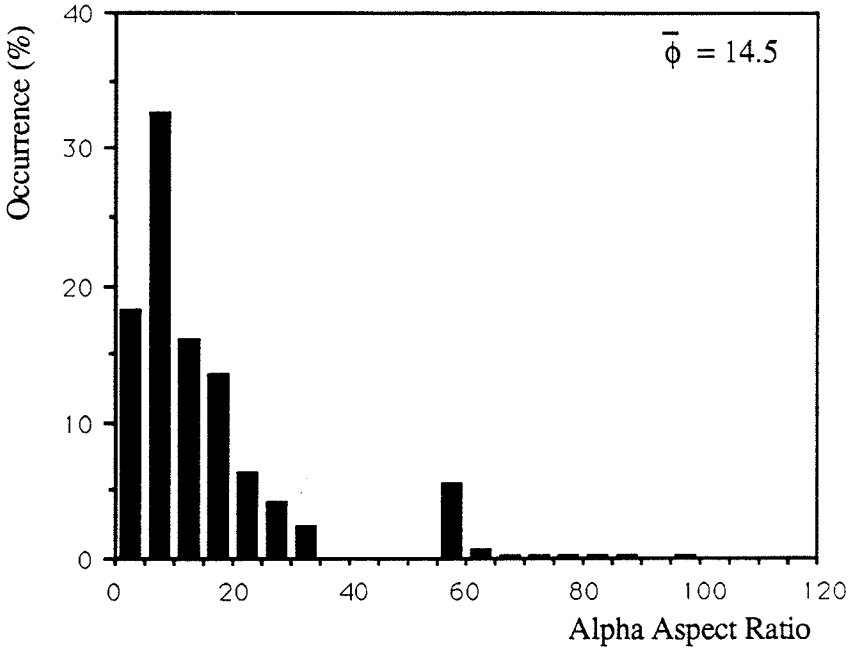

(l) BQ morphology at 950°C.

Figure 4.9: Distribution of alpha aspect ratio for (a)-(d) BA, (e)-(h) EQ, and (i)-(l) BQ starting morphologies at temperature.

4.2 Mechanical Testing

4.2.1 Continuous Tensile Tests

A series of tensile tests was performed to evaluate the stress-strain characteristics of the Ti-6Al-4V under uniaxial tensile load. Specifically, the tests were taken to failure and were used to evaluate the ductility of the material with a particular morphology. Material with the three characteristic phase morphologies were strained uniaxially in tension at temperatures of 875°C, 900°C, 925°C and 950°C. The constant strain rates applied for each temperature were $5x10^{-3}$, $1x10^{-3}$, $5x10^{-4}$, and $1x10^{-4}$ s^{-1}. Figures 4.10, 4.11 and 4.12 display the characteristic flow curves for the BA, EQ and BQ morphologies, respectively. Some flow curves are appended with a dashed line(-------) indicating that the tests were terminated prematurely. These tests were stopped either to preserve the microstructure at the selected strain, or in the case of the EQ morphology tested at the $1x10^{-4}$ s^{-1} strain rate, because the tensile sample started to slip from the grips. This in fact occurred for all the EQ $1x10^{-4}$ s^{-1} tests except for one at 925°C. This test though was characterized by considerable deformation of the gauge head. A revised tensile sample size consisting of a larger diameter head would be necessary to complete these tests. The most notable qualitative characteristics of the tensile tests were that the BA and BQ morphologies experienced strain softening, while the EQ morphology experienced notable strain hardening during deformation. Quantitatively, the continuous tensile tests provided flow stress and ductility information.

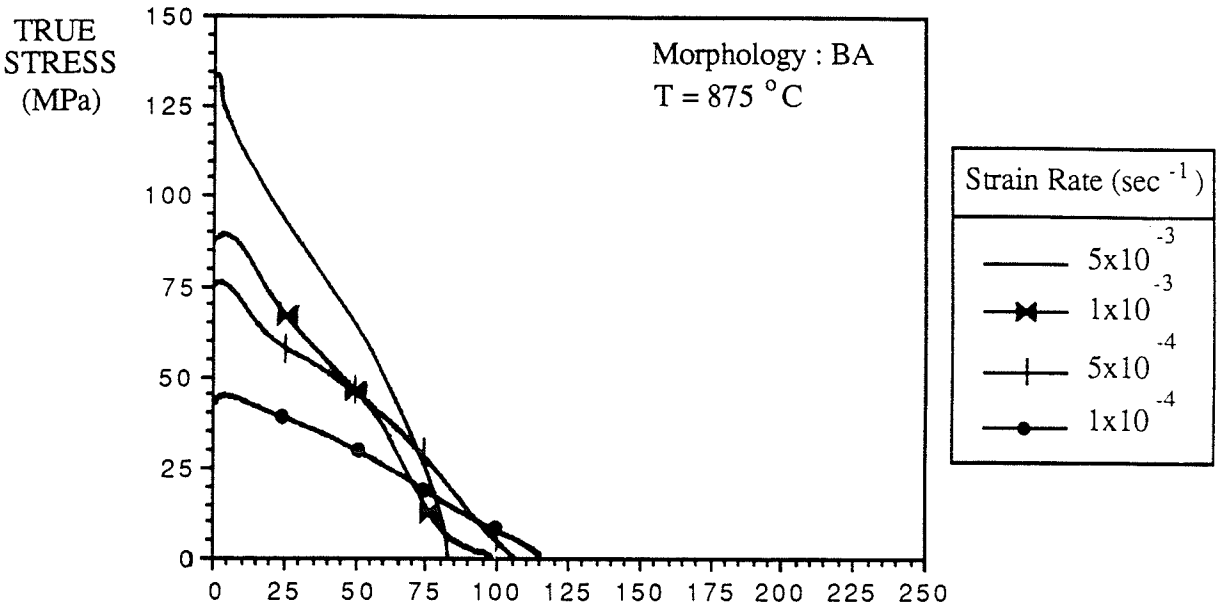
TRUE
STRESS
(MPa)
150
125
100
75
50
25
0
Morphology : BA
T = 875 °C
Strain Rate (sec -1)
5x10 -3
1x10 -3
5x10 -4
1x10 -4
0 25 50 75 100 125 150 175 200 225 250
TRUE PLASTIC STRAIN (%)

(a)

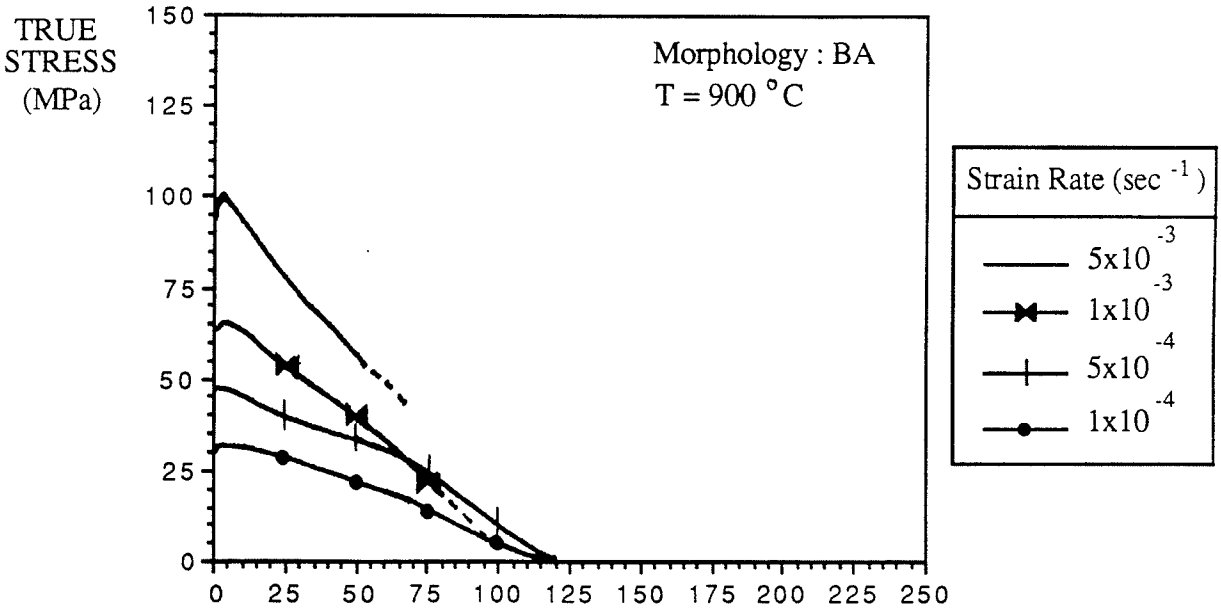
TRUE
STRESS
(MPa)
150
125
100
75
50
25
0
Morphology : BA
T = 900 °C
Strain Rate (sec -1)
5x10 -3
1x10 -3
5x10 -4
1x10 -4
0 25 50 75 100 125 150 175 200 225 250
TRUE PLASTIC STRAIN (%)

(b)

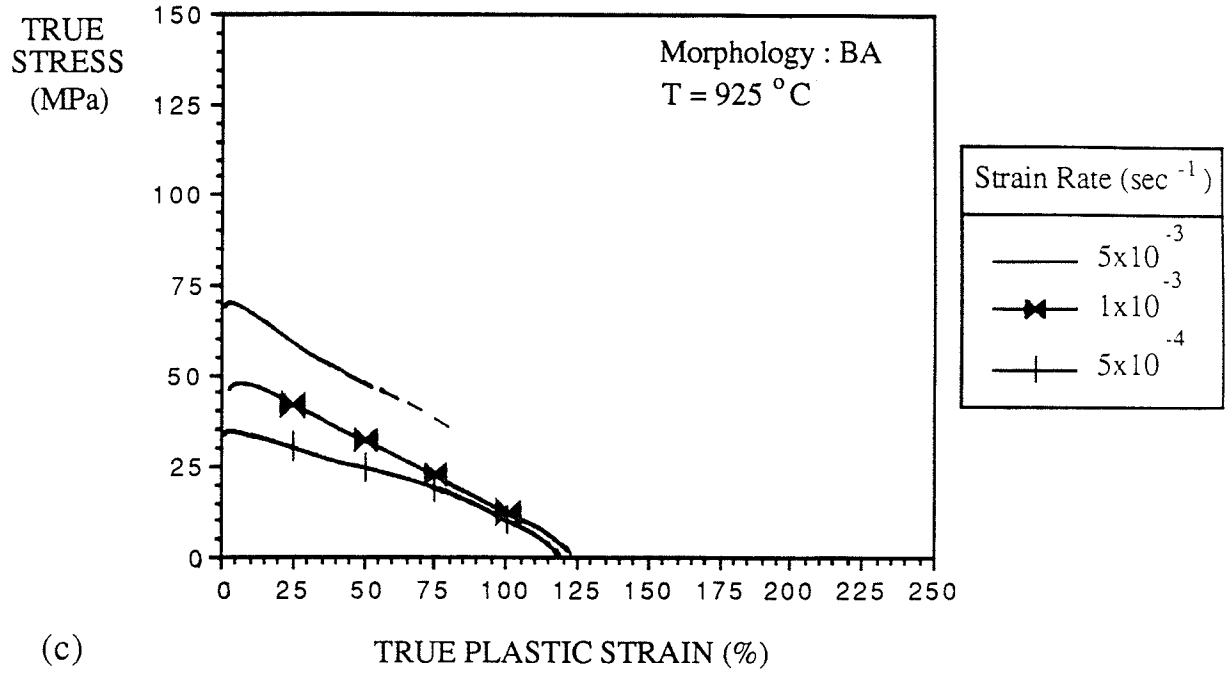

(c)

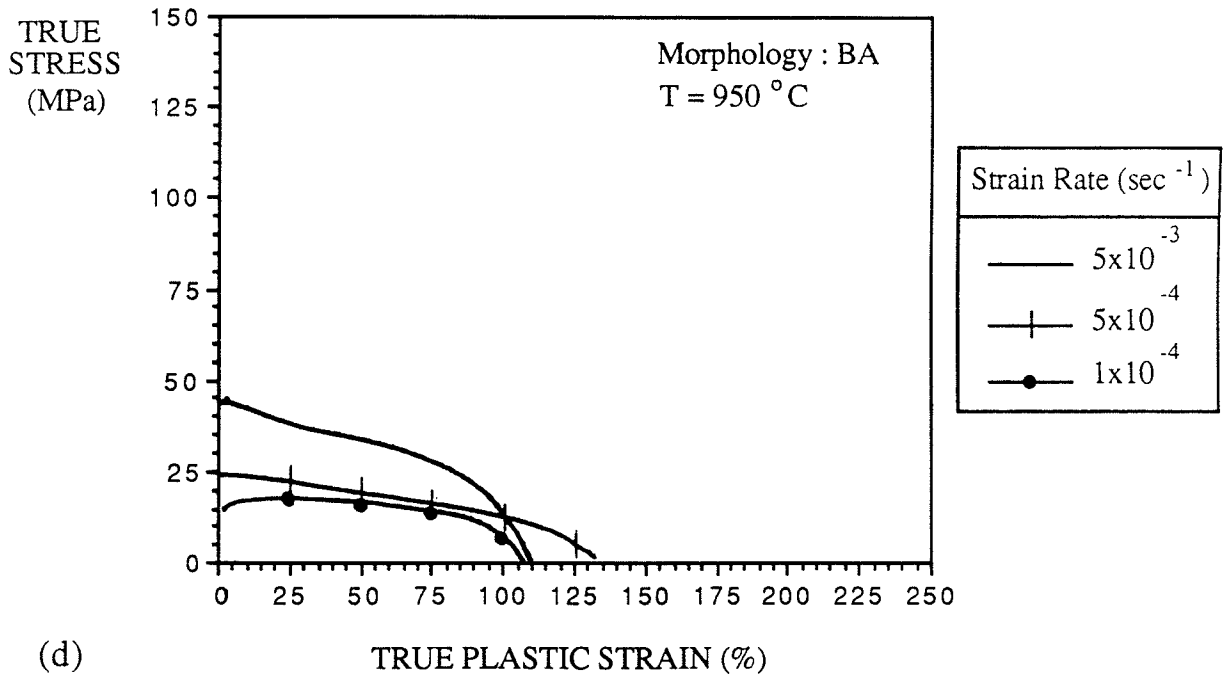

(d)

Figure 4.10: True stress versus true strain for the BA morphology at (a) 875,(b) 900, (c) 925, and (d) 950°C.

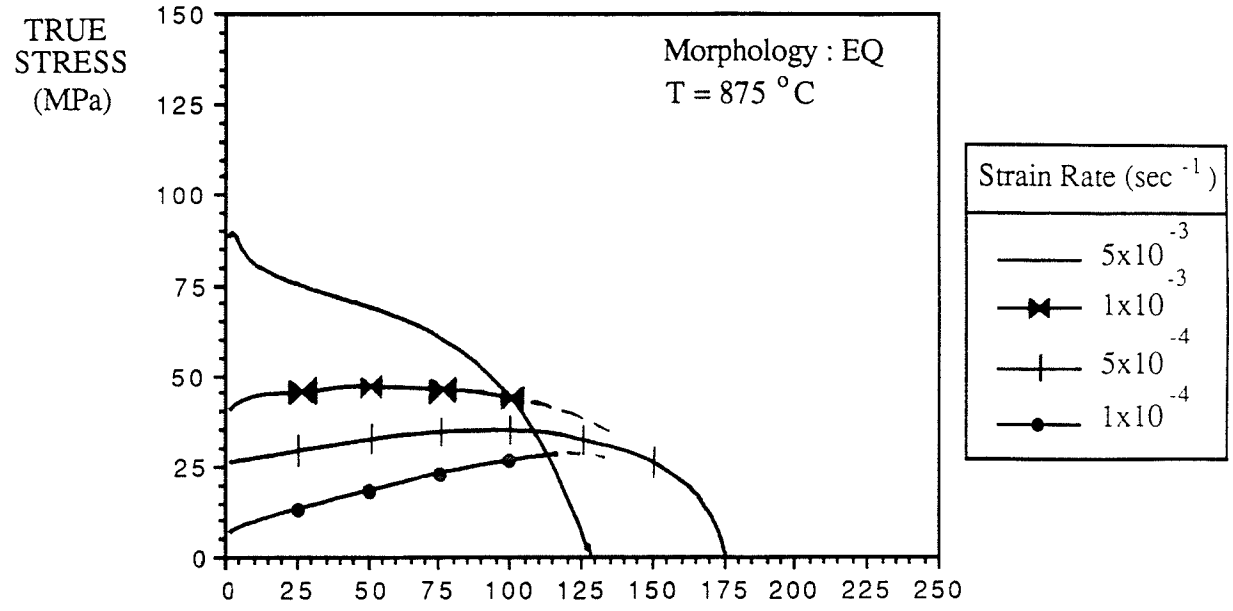
TRUE STRESS (MPa)
Morphology : EQ
T = 875 °C
Strain Rate (sec -1)
5x10-3
1x10-3
5x10-4
1x10-4
0
25
50
75
100
125
150
175
200
225
250
TRUE PLASTIC STRAIN (%)

(a)

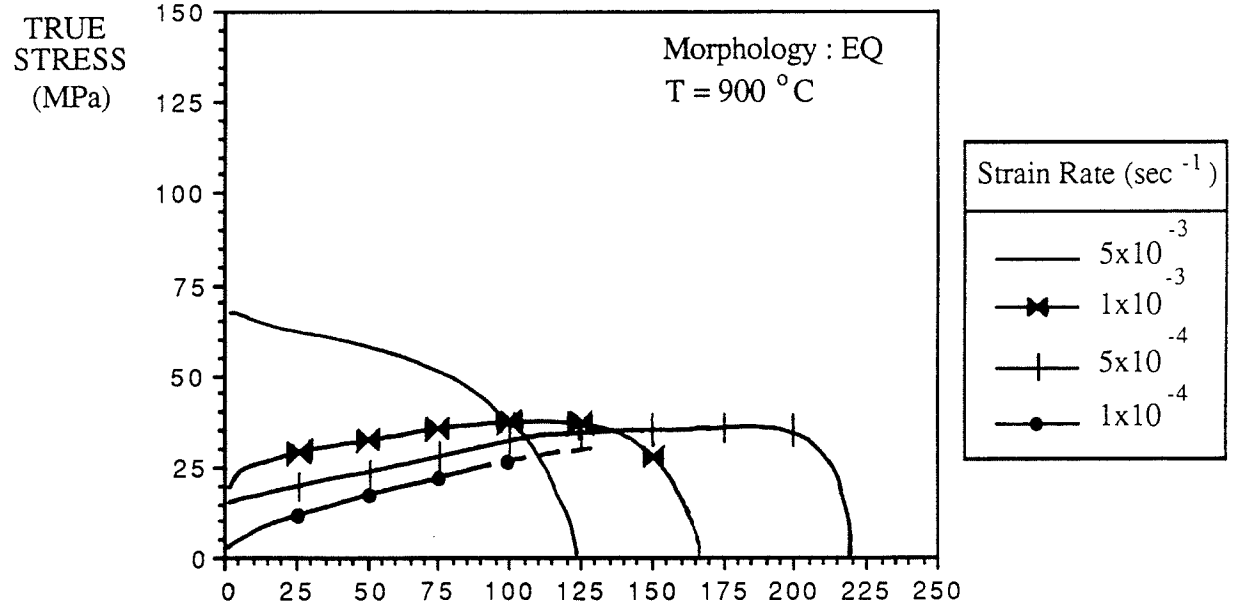
TRUE STRESS (MPa)
Morphology : EQ
T = 900 °C
Strain Rate (sec -1)
5x10-3
1x10-3
5x10-4
1x10-4
0
25
50
75
100
125
150
175
200
225
250
TRUE PLASTIC STRAIN (%)

(b)

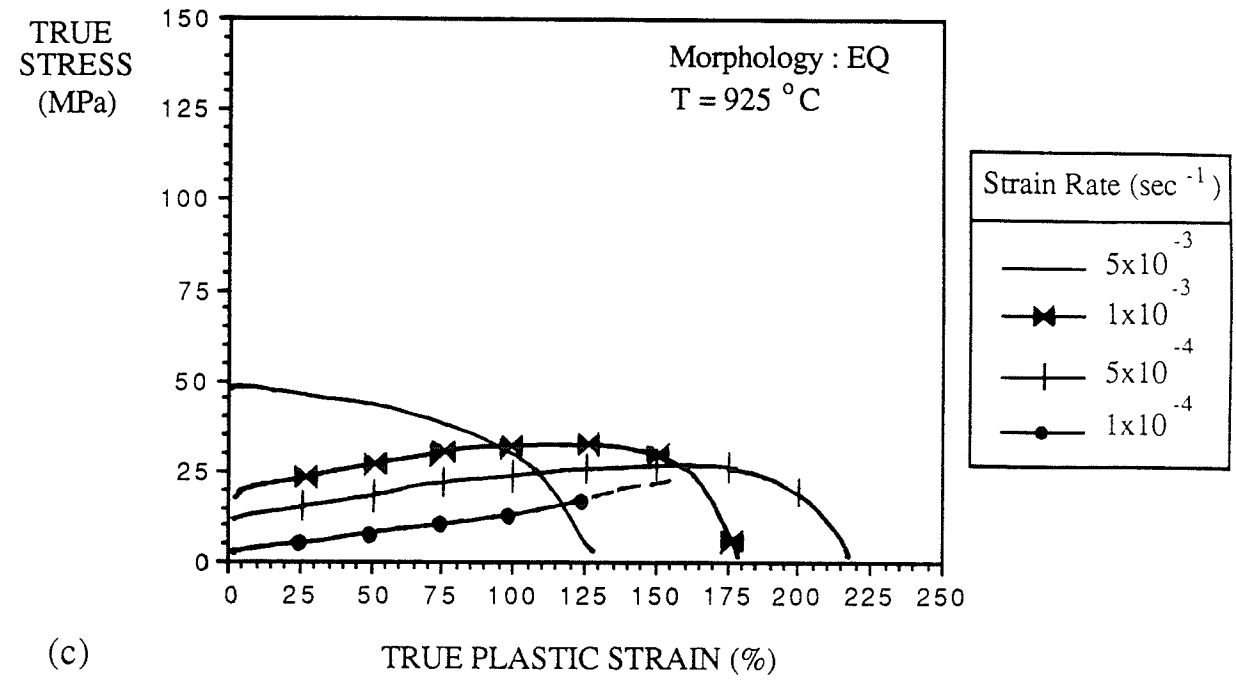

(c)

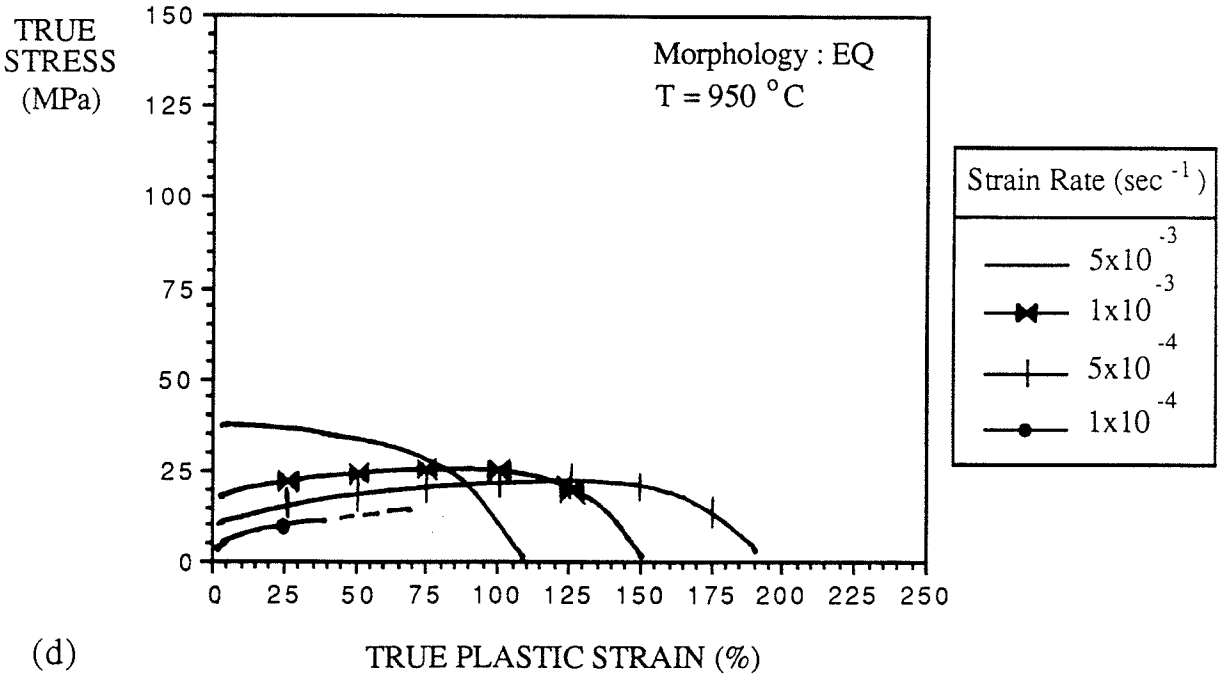

(d)

Figure 4.11: True stress versus true strain for the EQ morphology at (a) 875,(b) 900, (c) 925, and (d) 950°C.

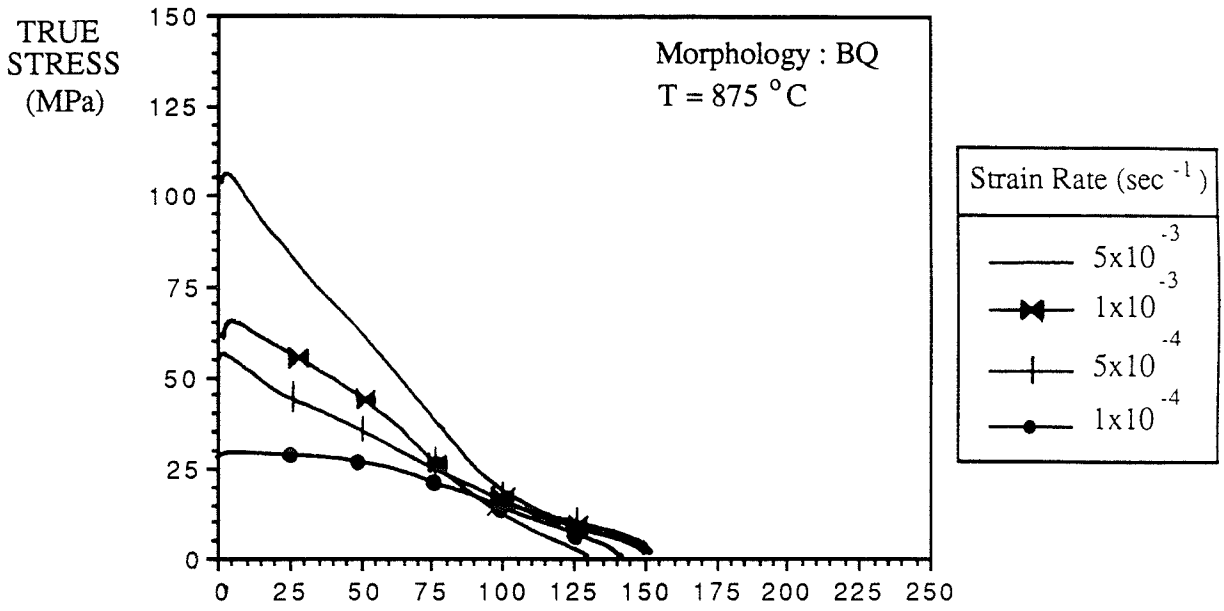
TRUE
STRESS
(MPa)
Morphology : BQ
T = 875 °C
Strain Rate (sec -1)
5x10 -3
1x10 -3
5x10 -4
1x10 -4
150
125
100
75
50
25
0
0 25 50 75 100 125 150 175 200 225 250
TRUE PLASTIC STRAIN (%)

(a)

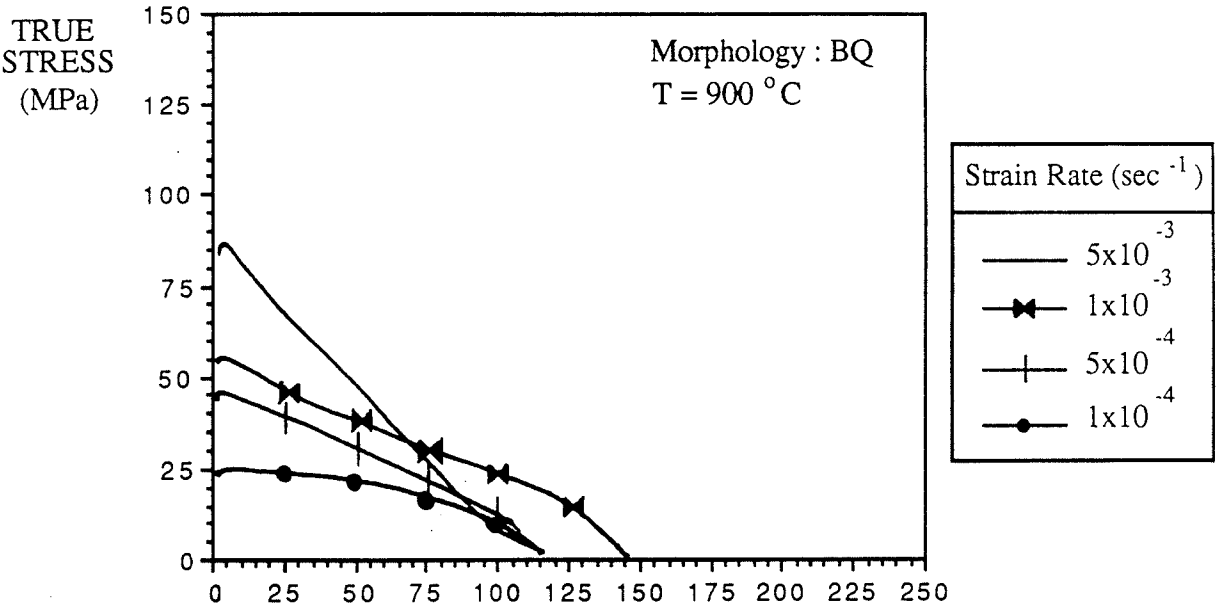
TRUE
STRESS
(MPa)
Morphology : BQ
T = 900 °C
Strain Rate (sec -1)
5x10 -3
1x10 -3
5x10 -4
1x10 -4
150
125
100
75
50
25
0
0 25 50 75 100 125 150 175 200 225 250
TRUE PLASTIC STRAIN (%)

(b)

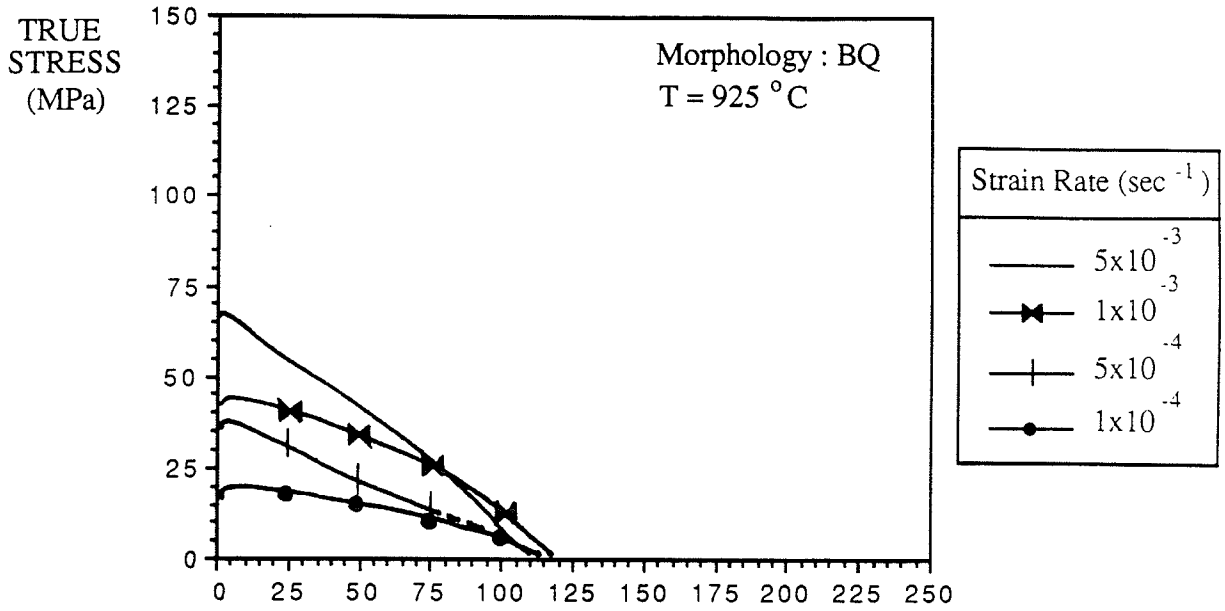

(c)

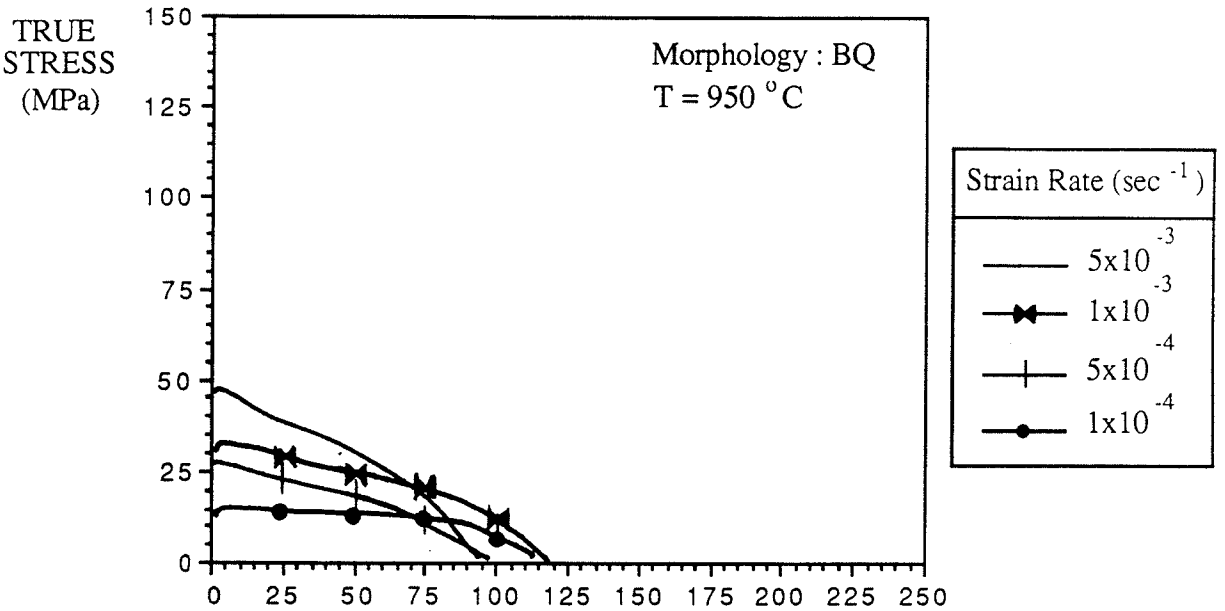

(d)

Figure 4.12: True stress versus true strain for the BQ morphology at (a) 875,(b) 900, (c) 925, and (d) 950°C.

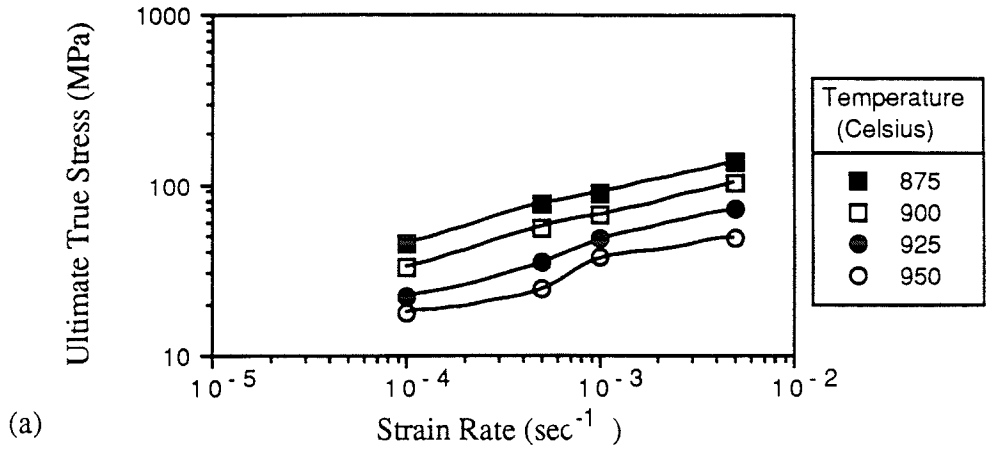

(a)

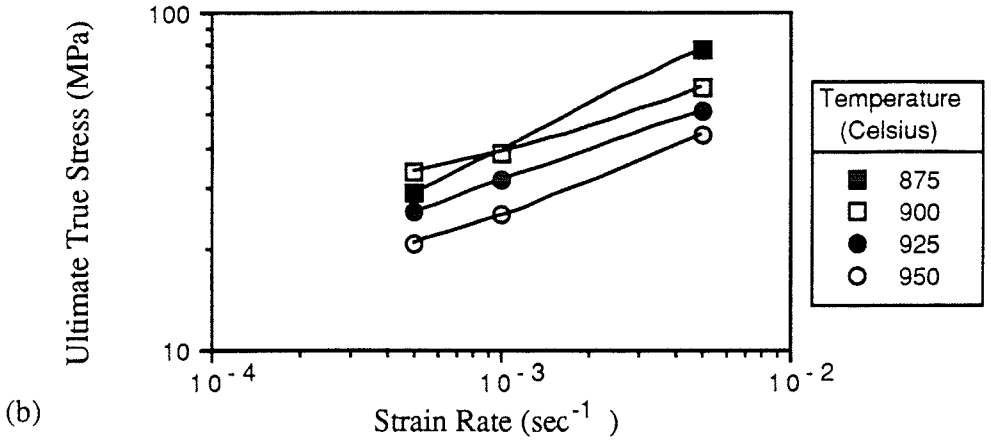

(b)

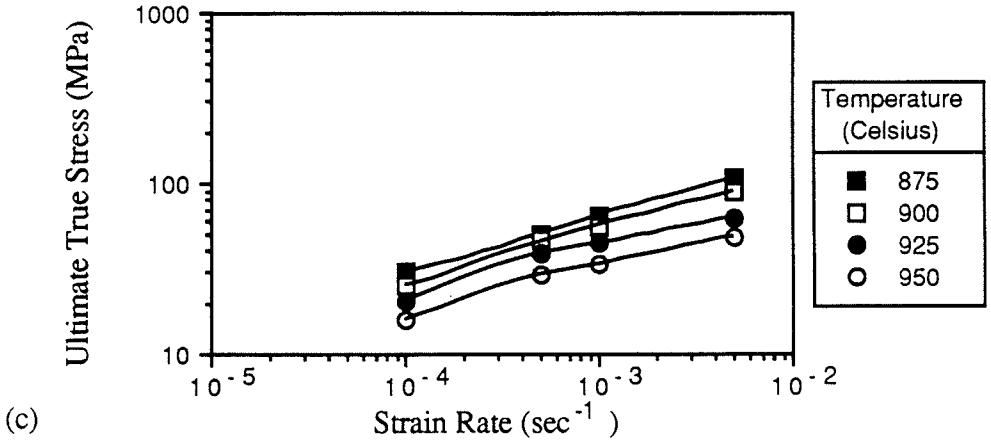

(c)

Figure 4.13: Ultimate true stress versus strain rate for (a)BA, (b)EQ, and (c)BQ morphologies at 875, 900, 925, and 950°C.

Figures 4.13(a) to (c) are log-log plots of ultimate true stress versus strain rate. These plots as mentioned earlier have been shown to demonstrate the sigmoidal relationship between stress and strain rate associated with superplasticity. One noticeable difference in these plots as compared to those in the literature is the use of ultimate true flow stress versus strain rate. The ultimate true flow stress has been used, because it is the actual point of steady state flow. At this point there is no strain hardening or softening and consequently this is defined as steady state flow. The test results indicate that increases in temperature from 875 to 950°C or decreases in strain rate from $5x10^{-3}$ to $1x10^{-4}$ s^{-1} reduced the ultimate true stress for all morphologies.

Finally, TABLE 4.2 summarizes the total percent elongation of the various morphologies at some of the temperature/strain rate conditions being investigated. The percent total elongation is a measure of the total sample gauge elongation, both uniform and non-uniform that occurs in the gauge length of the sample. It was calculated by the following expression.

$$\% \text{ total elongation } = \frac{\text{final gauge length - initial gauge length}}{\text{initial gauge length}} \times 100 \qquad (4.3)$$

TABLE 4.2 reveals that of the three materials, the one with EQ morphology failed after the longest elongations. The material with BQ morphology demonstrated the second overall ductility, while the one with BA morphology showed the least ductility. More specifically, at a constant strain rate of $5x10^{-3}$ s^{-1}, all the materials failed at elongations less than 300 percent, except for the one with BQ morphology at 875°C, which elongated to 385 percent before failure. The most important trend from the results is that the greatest ductility is experienced by all the three materials in the 900 to 925°C range, at a strain rate of $5x10^{-4}$ s^{-1}, indicating similar influence of temperature, volume fraction and strain rate on deformation. Figure 4.14 summarizes the effect of temperature on the ductility of the material with BA, EQ and BQ morphologies at a constant strain rate of

TABLE 4.2: Summary of Total Percent Elongation to Failure for Ti-6Al-4V Alloy

Strain Rate(s^{-1})		$5x10^{-3}$	$1x10^{-3}$	$5x10^{-4}$	$1x10^{-4}$
Temperature (°C)	Morphology				
875	BA	135	-	213	215
	EQ	232	-	474	-
	BQ	385	252	169	300
900	BA	-	-	253	210
	EQ	219	277	743	-
	BQ	215	330	387	218
925	BA	-	-	283	250
	EQ	286	481	706	654
	BQ	212	225	450	210
950	BA	215	-	303	210
	EQ	-	-	526	-
	BQ	162	-	177	230

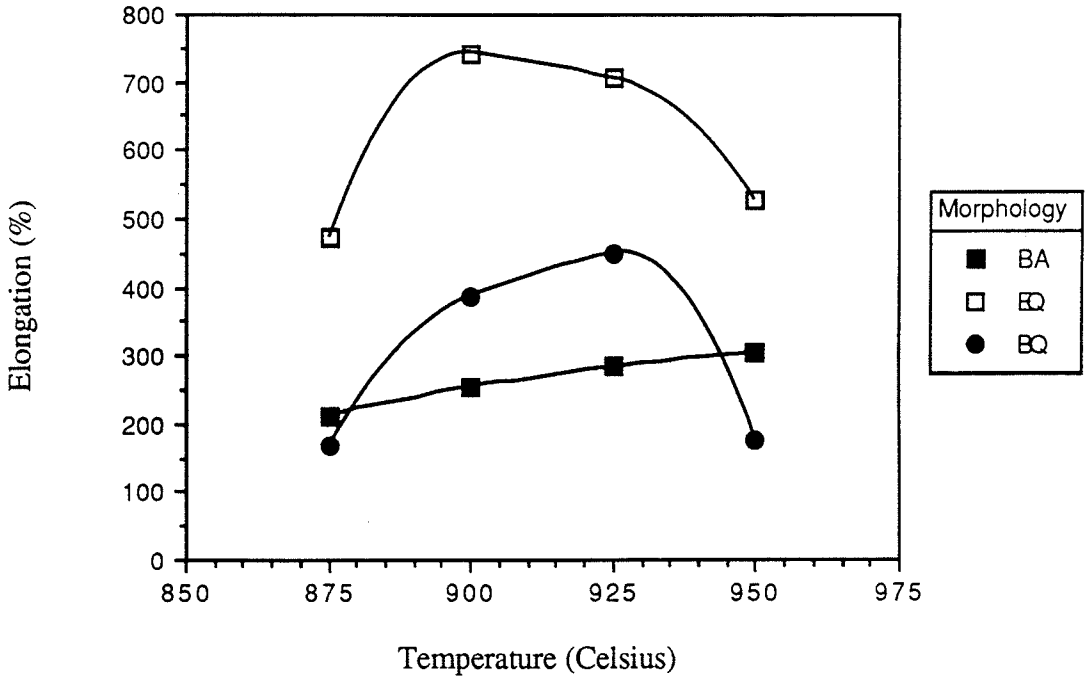

Figure 4.14: Percentage elongation versus temperature for the BA, EQ and BQ morphologies at a constant strain rate of $5x10^{-4}$ s^{-1}.

$5x10^{-4}$ s^{-1}. The difference in total deformation between the material with EQ morphology and the others is evident, but the similarity in profiles between the material with EQ and BQ morphologies, and the dissimilarity between the material with BQ and BA lamellar morphologies is interesting. Since the three materials contained the same volume fractions and were tested at the same temperature and strain rate conditions, it would appear that the difference in morphology influenced the deformation behaviour. This though is not an indication of the same mechanism operating in each material during deformation. To better understand the deformation behaviour of material with these morphologies, the strain rate sensitivity behaviour was evaluated.

4.2.2 Differential Strain Rate Tests

The purpose of the differential strain rate tests was to determine the material strain rate sensitivity, m , as it varied with strain. Figures 4.15 to 4.18 demonstrate the variation of m with the percentage true strain at constant strain rates. Not all tests took the tensile sample to failure, because the computer program used, limited the number of steps detailed in section 3.4.4 to 16. A limited number of steps reduces the number of times during the test that m can be sampled. Subsequently, the m just before failure is not always known, but the tests that did go to failure are indicated by 'X' marks at the end of each m versus percentage true strain curve. The figures are presented so that variation in m with strain is comparable between morphology at each test temperature which corresponds to identical initial volume fraction.

Most notable of the general trends is the fact that EQ strain rate sensitivities are constant or decrease with increasing strain while the BA and BQ strain rate sensitivities increase with increasing strain. Figure 4.15(a) indicates that at 875°C the value of m increases with strain for the material with BA and BQ morphologies, but tends to decrease for the material with EQ morphology with increasing strain. Specific attention should be paid to the initial m values which range from 0.25 to 0.30 for BA and 0.25 to 0.35 for BQ

at all strain rates. The m value for the material with the EQ morphology is considerably lower at the $5x10^{-3}$ s^{-1} strain rate than at strain rates lower than $5x10^{-3}$ s^{-1}.

At 900°C the general trends continue, m increases with strain for the BA and BQ cases, but decrease for the material with the EQ morphology. Once again the initial value of m for the material with BA and BQ morphology ranges from 0.25 to 0.30 and 0.25 to 0.35, respectively. For material with the EQ morphology, the highest initial value of m of 0.75 occurs at $5x10^{-4}$ s^{-1}, and the lowest of 0.35 occurs at a strain rate of $5x10^{-3}$ s^{-1}.

Figures 4.17(a) to (c) display the variation of m with strain at 925°C. The value of m for the BA and BQ morphology materials increase with strain, but the increase is less than that at the lower temperatures. In fact by 100 percent true strain, the value of m has not reached 0.5. This reduced change in the value of m could indicate a reduced change in microstructure. The EQ morpholgy material at this temperature shows the highest initial value of m of all conditions at a strain rate of $5x10^{-4}$ s^{-1}. At $5x10^{-3}$ s^{-1} the m value remains largely unaffected in the temperature range of 875 to 950°C indicating no temperature sensitivity at this strain rate.

Finally, at 950°C Figures 4.18(a) and (c) indicate similar initial values of m for the BA and BQ morphology materials but noticeably lower m values for the EQ morphology material. The value of m for material with the EQ morphology decrease below 0.5 after deformation to 75 percent true strain at a strain rate of $5x10^{-4}$ s^{-1}.

The variation in the value of m with strain might give some insight in relating strain rate sensitivity to total elongation. From this data it is evident that initial strain rate sensitivity alone is not enough to predict total elongation. As an example, all the BA and BQ morphology materials show initial strain rate sensitivities around 0.3, but the BQ morphology demonstrated considerably more ductility at specific temperature - strain rate conditions. This will be discussed later. It is also agreed in the literature that high m values are necessary for a uniform flow. With this in mind, a study of the uniformity of deformation of tensile samples was carried out.

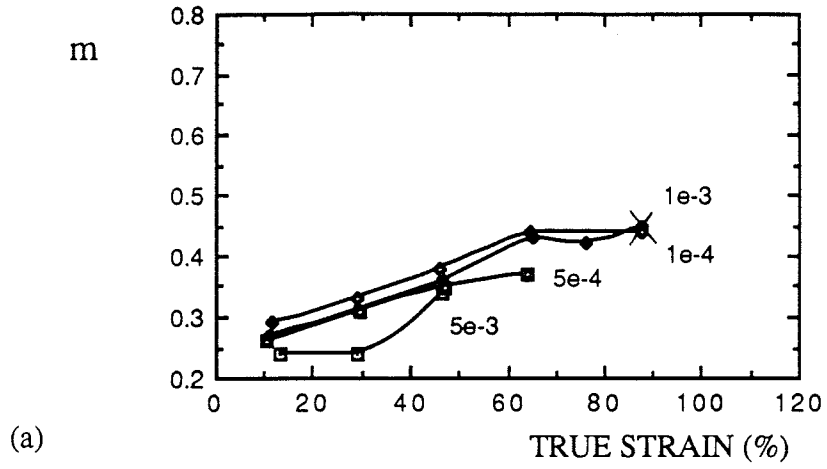

(a)

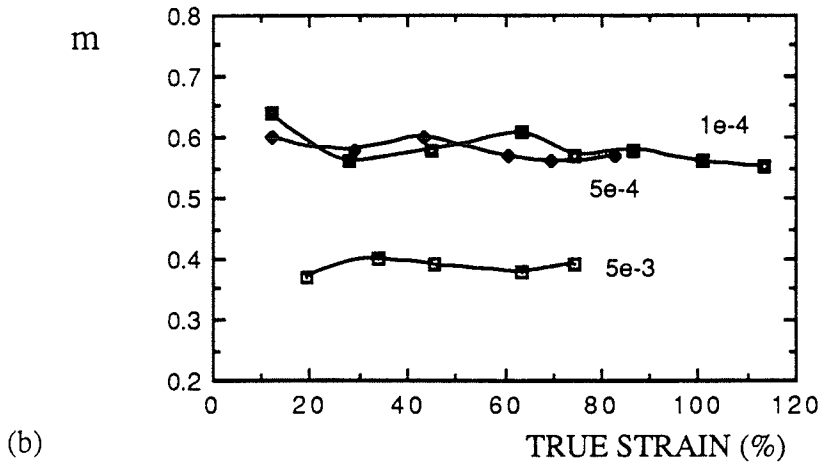

(b)

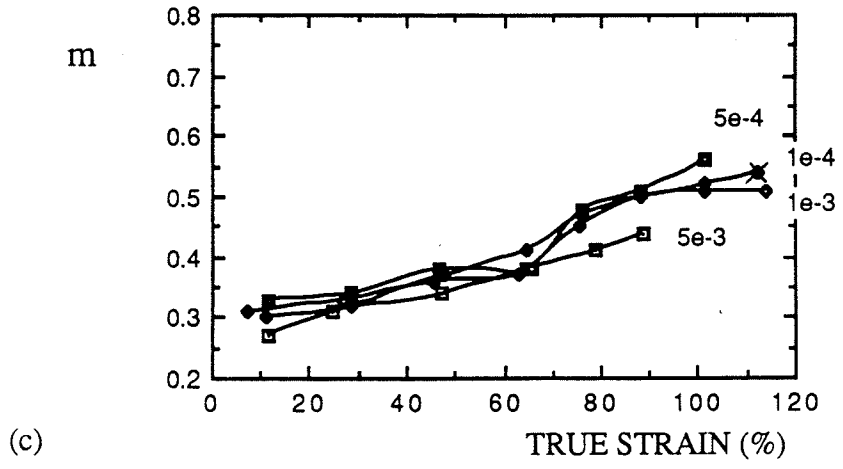

(c)

Figure 4.15: Variation of strain rate sensitivity with strain at different strain rates(s^{-1}) for (a) BA, (b) EQ, and (c) BQ morphology at 875°C.

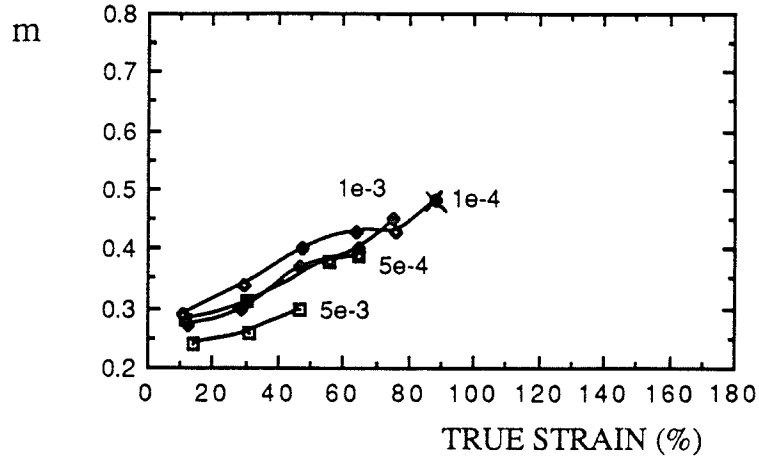

(a)

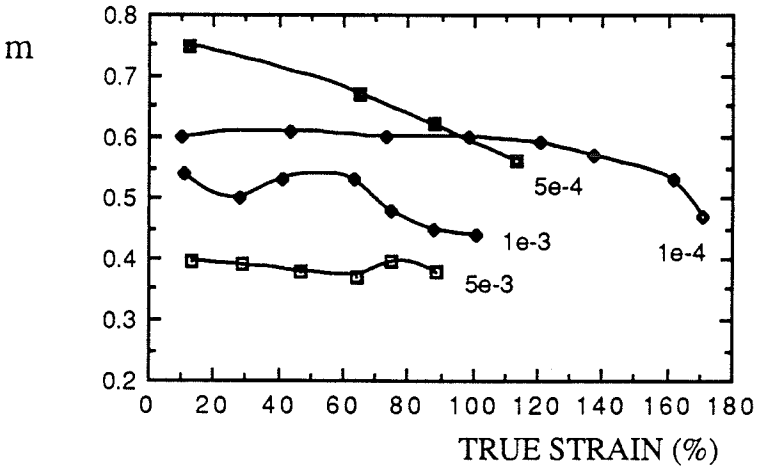

(b)

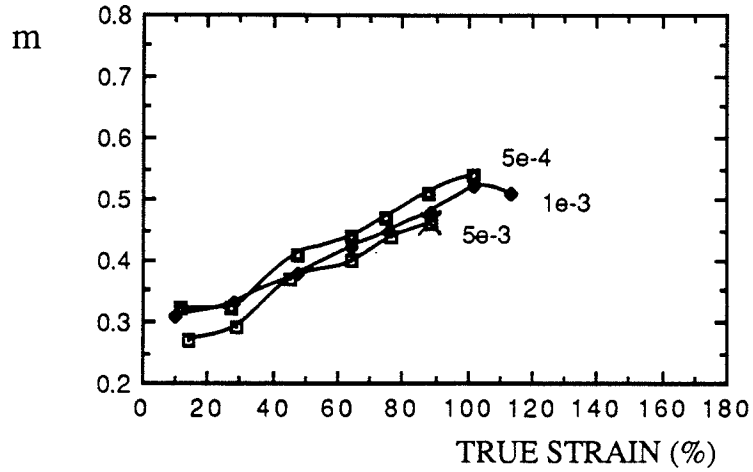

(c)

Figure 4.16: Variation of strain rate sensitivity with strain at different strain rates(s^{-1}) for (a) BA, (b) EQ, and (c) BQ morphology at 900°C.

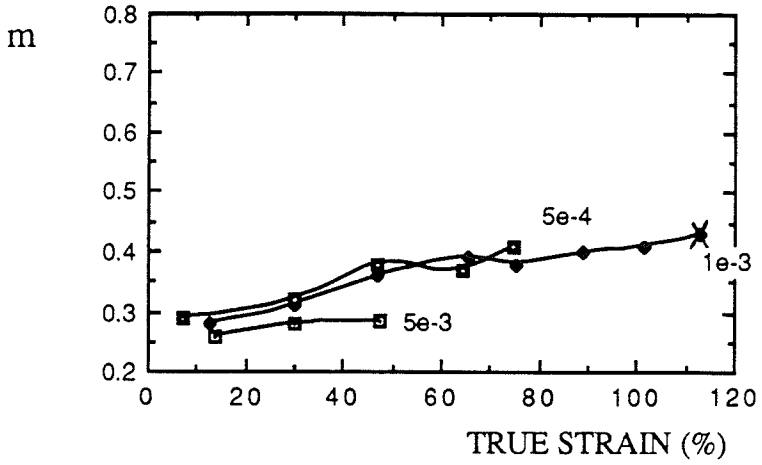

(a)

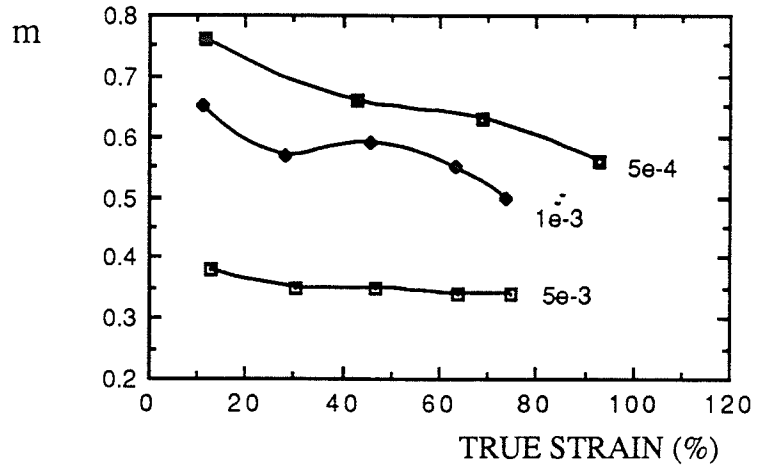

(b)

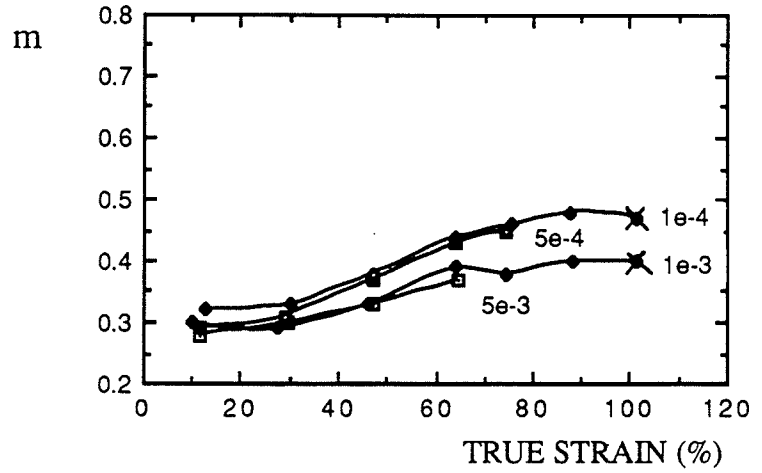

(c)

Figure 4.17: Variation of strain rate sensitivity with strain at different strain rates(s^{-1}) for (a) BA, (b) EQ, and (c) BQ morphology at 925°C.

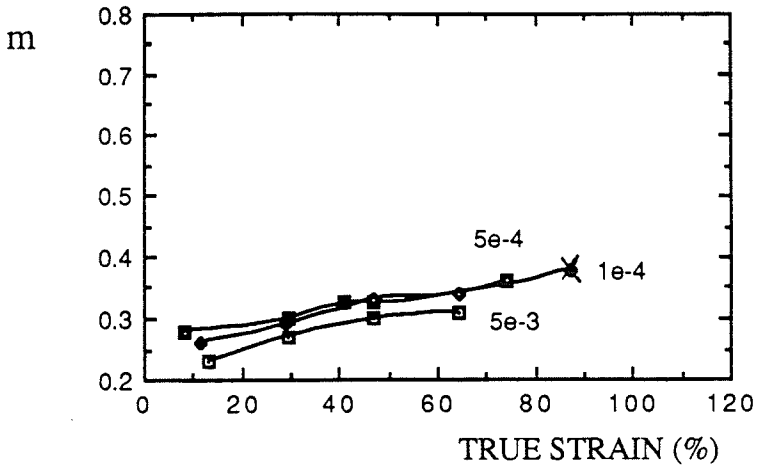

(a)

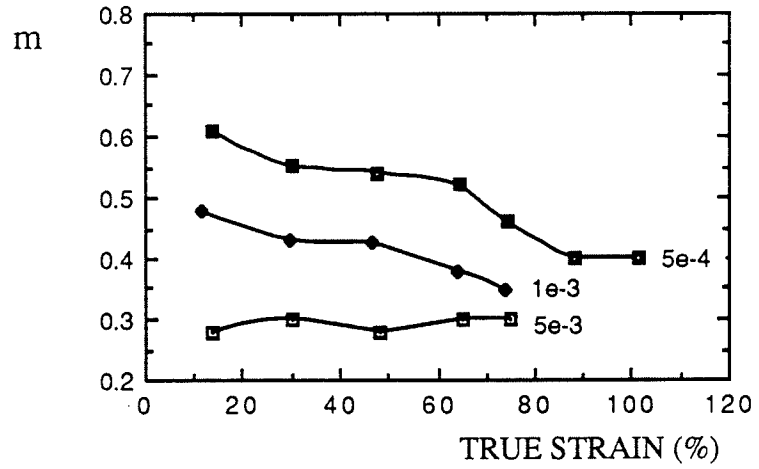

(b)

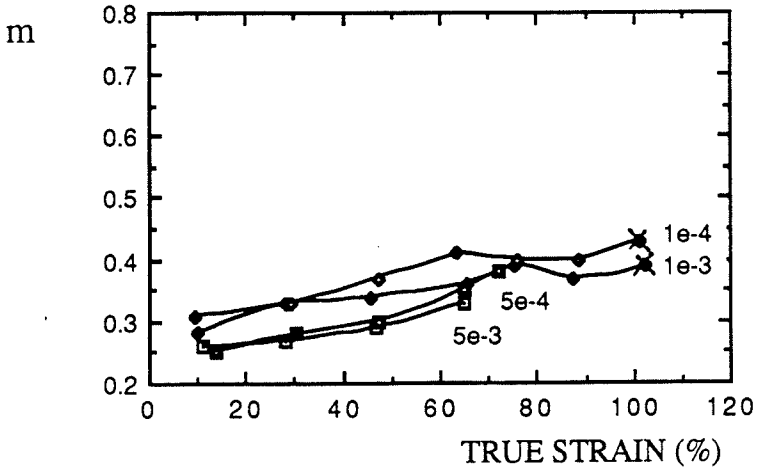

(c)

Figure 4.18: Variation of strain rate sensitivity with strain at different strain rates(s^{-1}) for (a) BA, (b) EQ, and (c) BQ morphology at 950°C.

4.3 Neck Profile Development

4.3.1 Instability Shape

With round tensile samples it was found informative to examine the necking profiles of the samples after deformation. Figures 4.19 to 4.26 display the macroscopic cross-sectional data of all the three morphologies deformed at the four test temperatures and at $5x10^{-3}$ and $5x10^{-4}$ s^{-1} constant strain rates. Measurements were conducted on all samples, but the conditions presented here best typify the best and worst case conditions for the material with three morphologies. The profiles depict the variation of radial and cross-sectional area geometry from the point of instability or necking, defined as the observed minimal cross-sectional area, along the gauge length. The profiles demonstrate two important characteristics. First, the radial dimensions a and b , indicate possible microstructural anisotropy that influences deformation. For example, if a and b remain equal along a deformed length then no deformation influenced by anisotropy is inferred. Secondly, and most notably, the cross-sectional area curves can be characterized in either "V" or "U" shapes. The "U" shape represents the more uniform sample deformation, while the "V" configuration indicates the presence of a pronounced instability which has reduced the uniformity of deformation. The strain produced at a tensile instability usually differs from the average strain of the whole tensile specimen. The actual strain in a cross-section can be determined from the final cross-sectional area, A_f using the simple relation,

$$\varepsilon = \ln(\frac{A_o}{A_f}), \qquad (4.4)$$

where A_o is the starting cross-sectional area.

The next two sections examine the necking profiles in more detail.

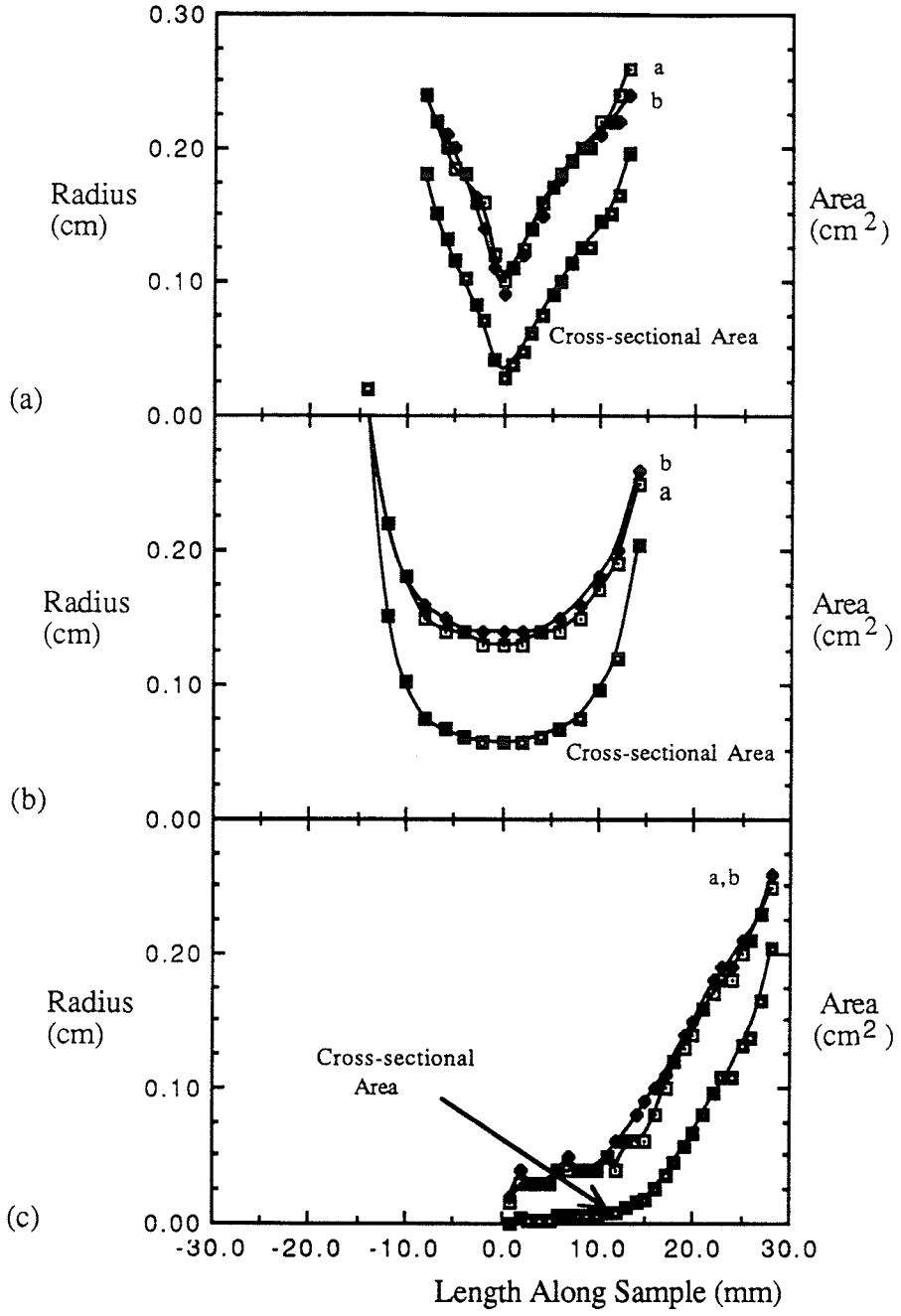

Figure 4.19: Variation of tensile sample cross-sectional geometry along its length at 875°C for (a) BA, (b) EQ, and (c) BQ morphologies after deformation at a constant strain rate of $5x10^{-3}$ s^{-1}.

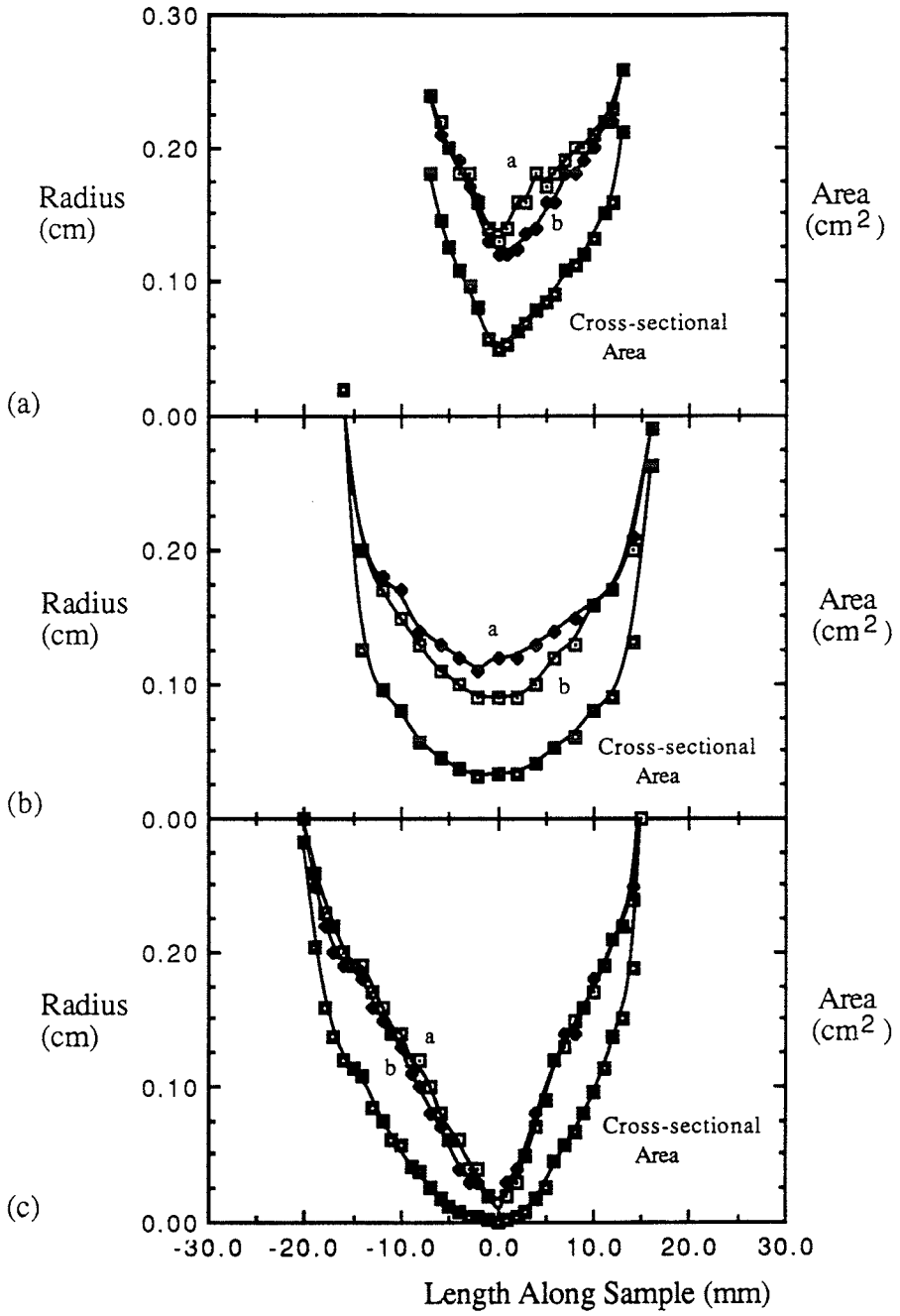

Figure 4.20: Variation of tensile sample cross-sectional geometry along its length at 900°C for (a) BA, (b) EQ, and (c) BQ morphologies after deformation at a constant strain rate of $5x10^{-3}$ s^{-1}.

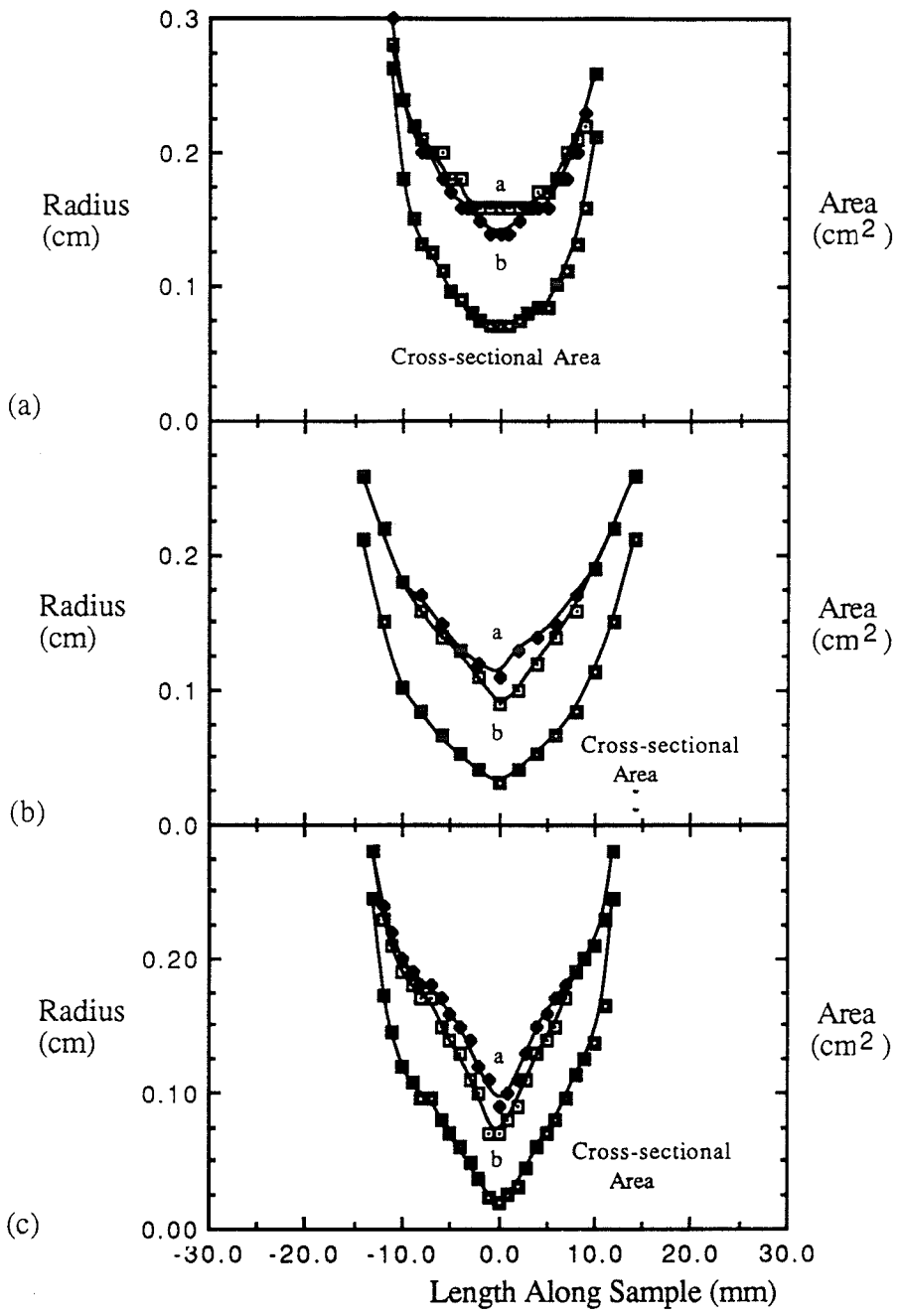

Figure 4.21: Variation of tensile sample cross-sectional geometry along its length at 925°C for (a) BA, (b) EQ, and (c) BQ morphologies after deformation at a constant strain rate of $5x10^{-3}$ s^{-1}.

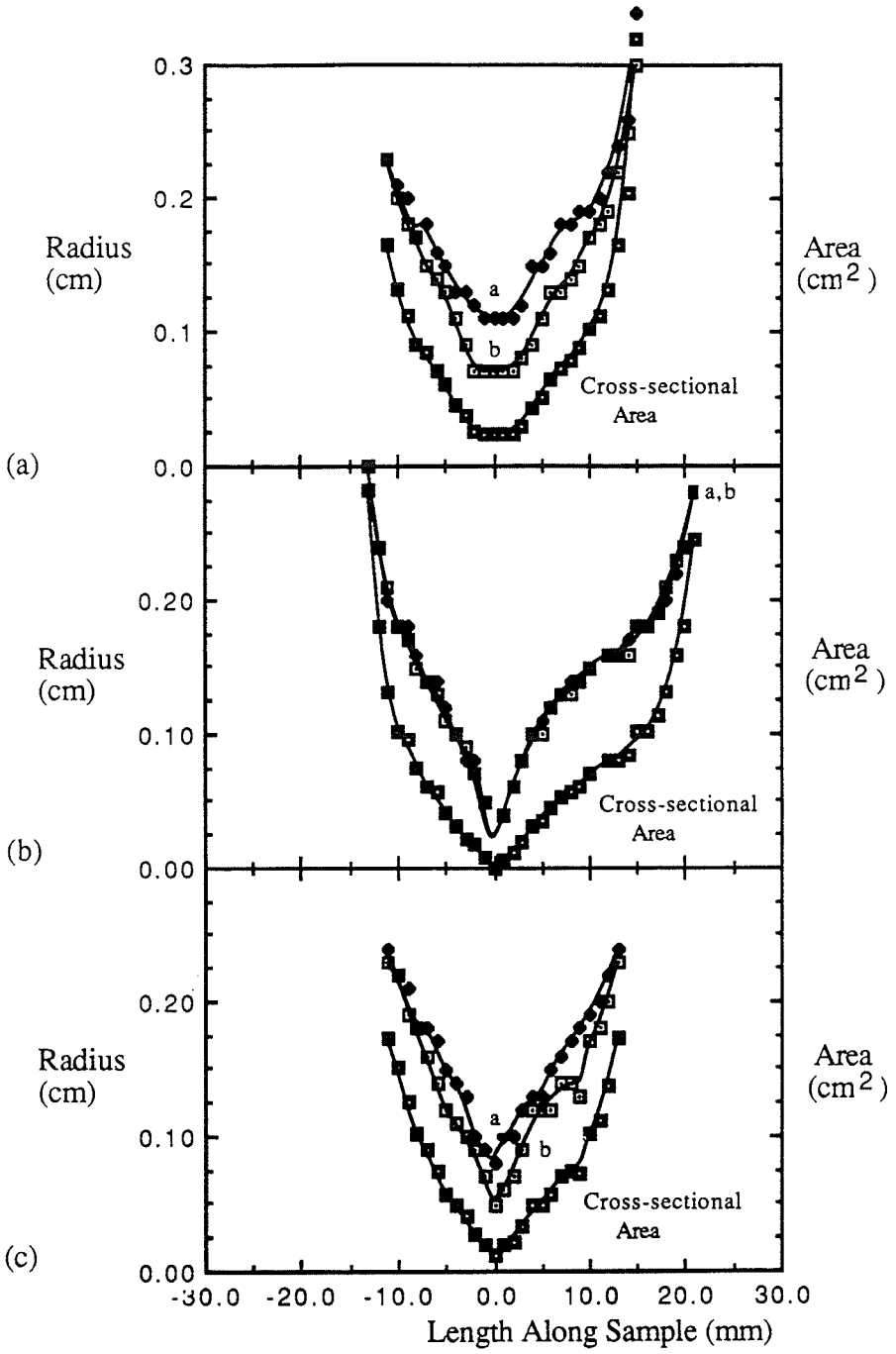

Figure 4.22: Variation of tensile sample cross-sectional geometry along its length at 950°C for (a) BA, (b) EQ, and (c) BQ morphologies after deformation at a constant strain rate of $5x10^{-3}$ s^{-1}.

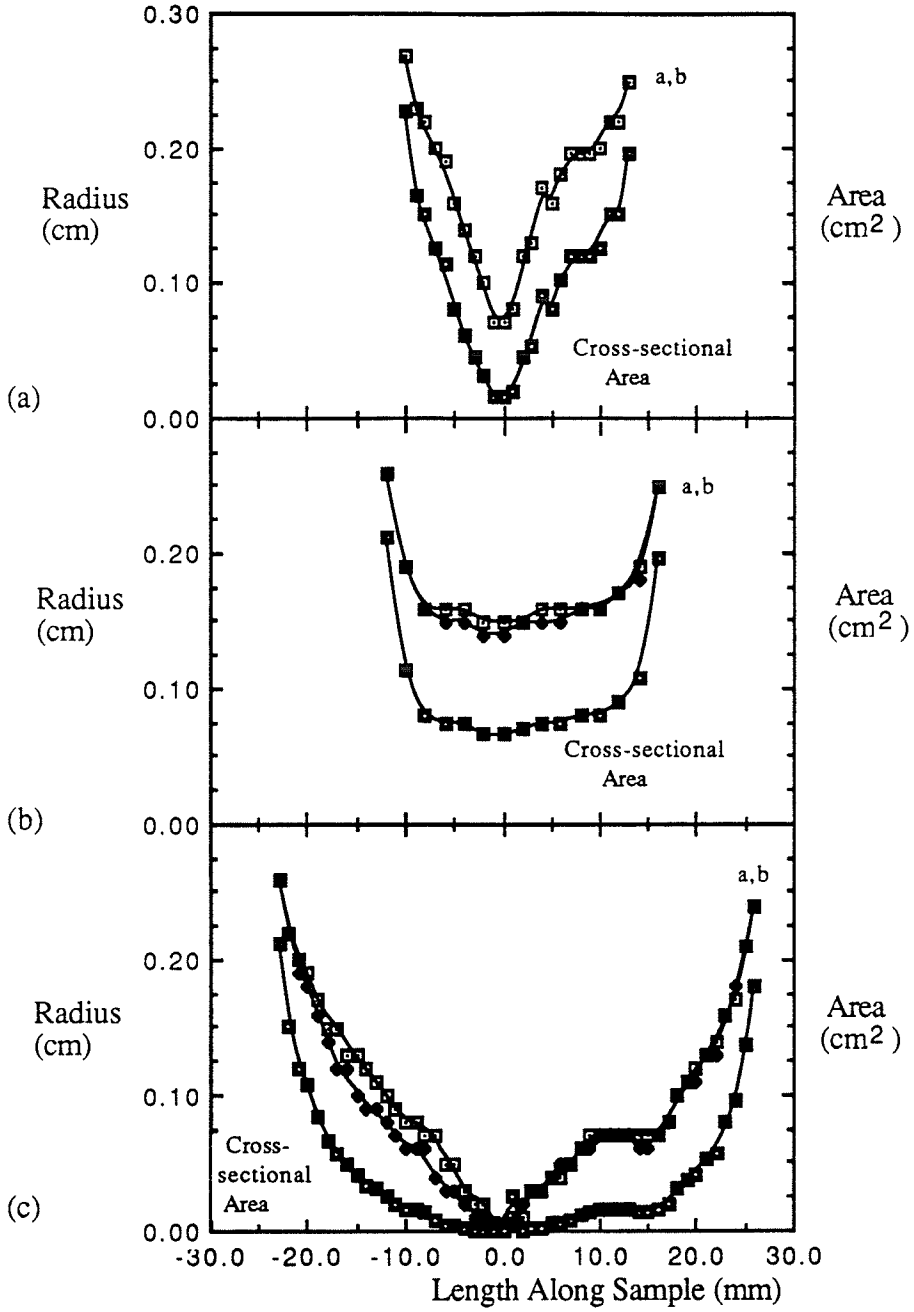

Figure 4.23: Variation of tensile sample cross-sectional geometry along its length at 875°C for (a) BA, (b) EQ, and (c) BQ morphologies after deformation at a constant strain rate of $5x10^{-4}$ sec^{-1}.

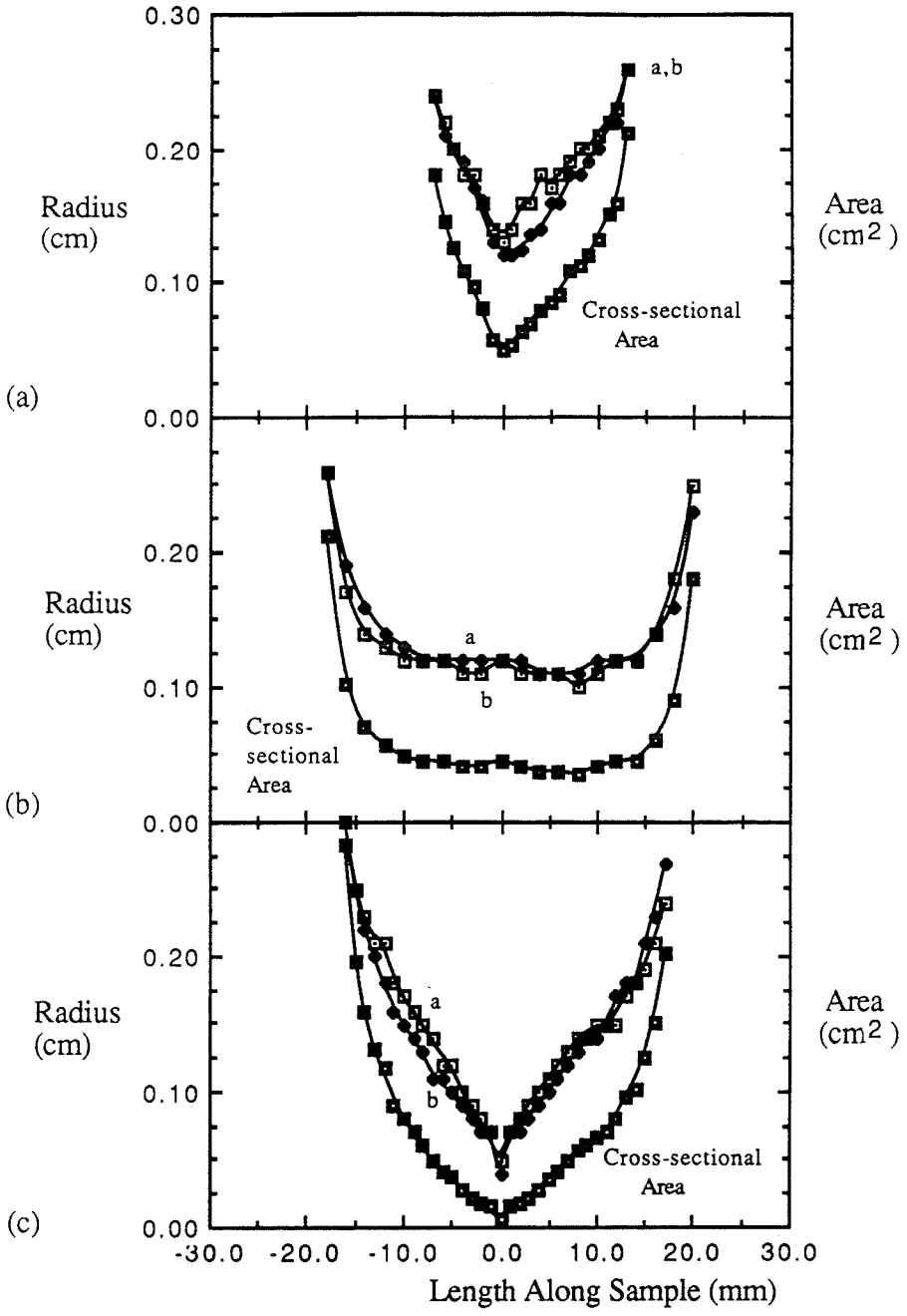

Figure 4.24: Variation of tensile sample cross-sectional geometry along its length at 900°C for (a) BA, (b) EQ, and (c) BQ morphologies after deformation at a constant strain rate of 5×10^{-4} s^{-1}.

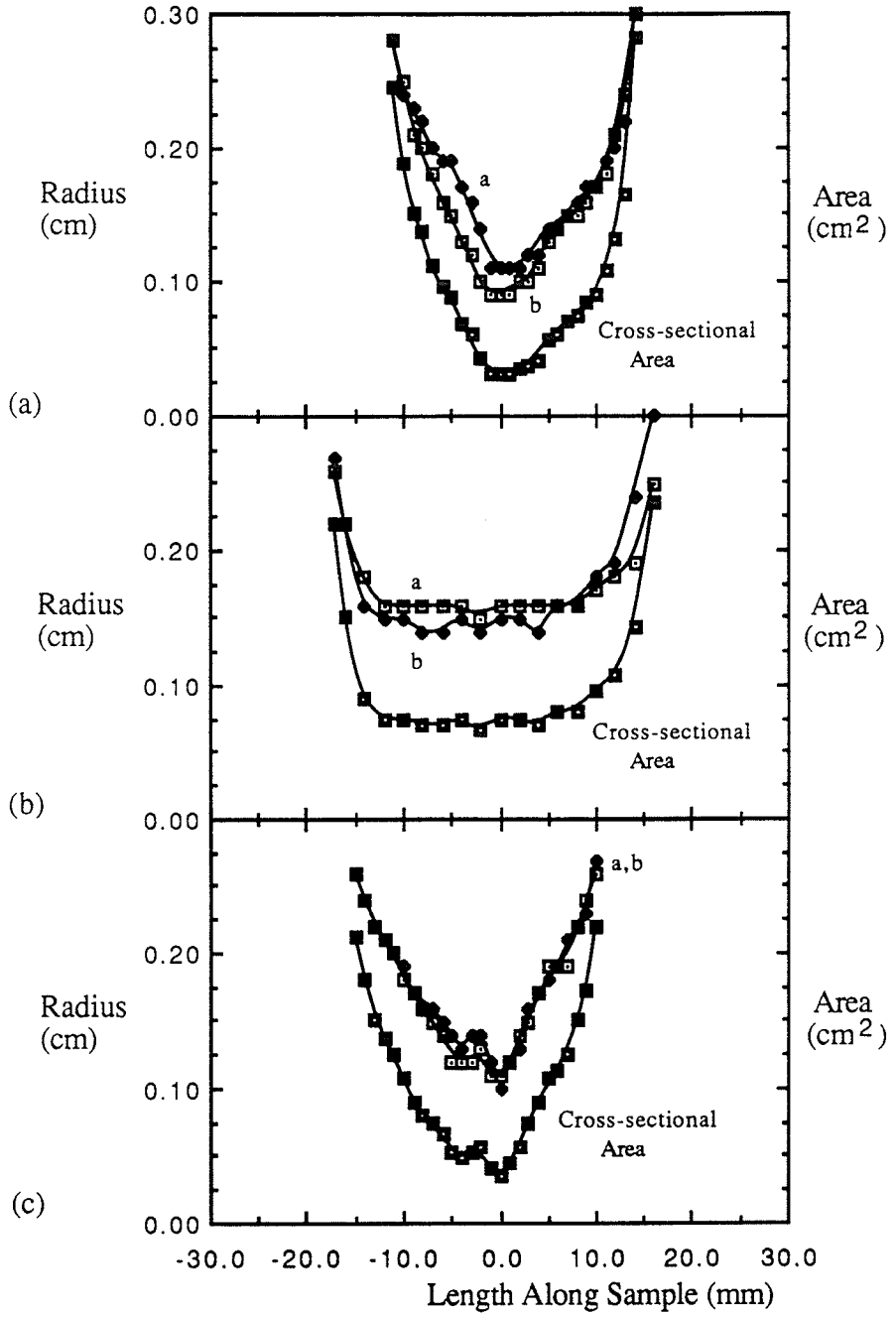

Figure 4.25: Variation of tensile sample cross-sectional geometry along its length at 925°C for (a) BA, (b) EQ, and (c) BQ morphologies after deformation at a constant strain rate of 5×10^{-4} s^{-1}.

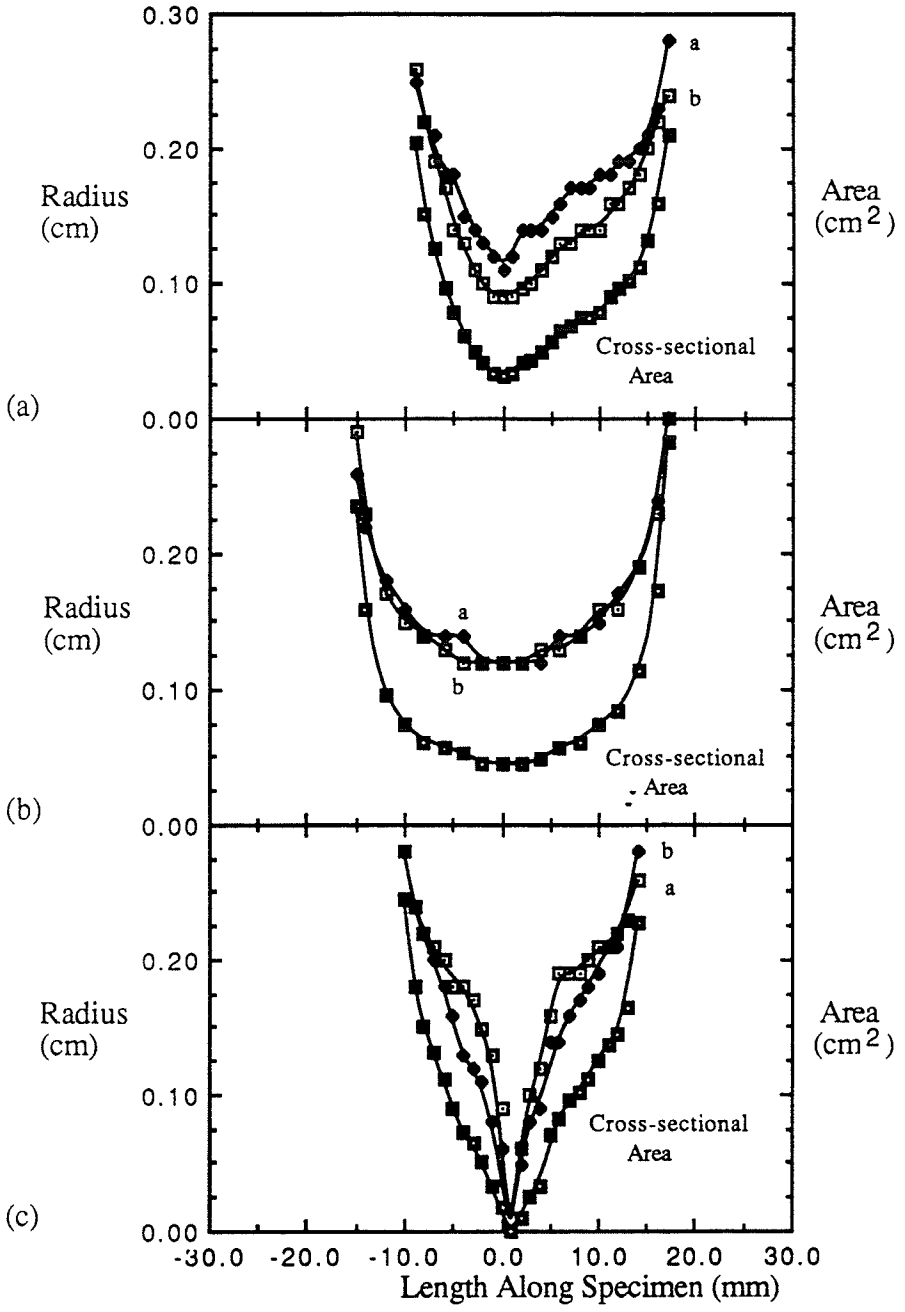

Figure 4.26: Variation of tensile sample cross-sectional geometry along its length at 950°C for (a) BA, (b) EQ, and (c) BQ morphologies after deformation at a constant strain rate of $5x10^{-4}$ s^{-1}.

4.3.2 $5x10^{-3}$ s^{-1} Strain Rate

At $5x10^{-3}$ s^{-1}, the highest constant strain rate tested, the relative ductilities of all specimens were lower than those at $5x10^{-4}$ s^{-1}. The flow curves for the materials with three different morphologies were similar in shape. All indicated flow softening with strain. Nevertheless, the BA morphology materials, as indicated in Figure 4.19(a), has experienced a major instability, while Figure 4.19(b) suggests that the EQ morphology material has deformed rather uniformly after a similar amount of strain. The BQ sample was taken to failure, but only half of its cross-section is shown in 4.19(c). This morphology material approaches the "U" configuration. Increasing the temperature from 875 to 950°C (Figures 4.20 to 4.22) which also signifies an increase in the volume fraction of beta, indicates that the BA morphology material begins to deform more uniformly, as is evident from the "U" shaped curve. The material with the EQ morphology experiences less uniform deformation with increasing temperature, culminating in larger effects of instability. The BQ morphology material, consisting of α plates thinner than the BA morphology shows necking profiles similar to the EQ morphology material. An increase in initial volume fraction, reduces its uniformity of deformation.

With respect to anisotropy, increasing temperature increased BA anisotropy considerably. Figures 4.19(a) and 4.19(d) indicate an increase in the difference between dimensions a and b. The EQ morphology material demonstrated a considerable increase in anisotropy with temperature, too. At 900°C, the maximum difference between *a* and *b* is almost 2.5 mm. At 950°C though the anisotropy difference is reduced. For the BQ morphology material, an increase in temperature results in increased anisotropy.

4.3.3 $5x10^{-4}$ s^{-1} Strain Rate

At 875°C, Figure 4.23(b) indicates that the EQ morphology material has deformed most uniformly, with little anisotropy when compared to the materials with (a)BA and (c)BQ morphologies. The uniformity of flow, remains highest for EQ material with

temperature, but the BA morphology material also demonstrates increased uniformity. Figure 4.23(c) is slightly misleading, when compared to the other cases at this temperature, because the BQ morphology was taken to a different strain than the BA and EQ samples. Figures 4.24 and 4.25 overcome this problem. These figures indicate that at a strain rate of $5x10^{-4}$ s^{-1} and in the range between 900 to 925°C, more than one instability is present. Multiple necks have been reported to occur during superplastic deformation[46], but a noted aspect of this deformation is the ability of material to prevent these instabilities from leading to a premature failure. In fact when one or more instabilities form and seem to be controlling the deformation of the material strain hardening occurs simultaneously reducing the instability growth. An example of this behaviour is given in Figure 4.25(c). This profile is "W" shaped, which indicates that more than one instability has developed in the BQ morphology specimen under these testing conditions, and either instability could lead to failure of the tensile sample. This behaviour was not observed at the higher strain rate conditions, indicating some dependance on strain rate.

Reduced anisotropy is expected at the optimum superplastic condition, which occurs at $5x10^{-4}$ s^{-1} and in the 900 to 925°C temperature range, but Figures 4.24(b) and 4.25(b) do indicate differences between a and b. It should be noted though that the highest total elongation reported in TABLE 4.2 was for the 900°C condition, and not the 925°C test. Figures 4.24(b) and 2.25(b) show that the material exhibits less anisotropy at 900°C and not at 925°C and therefore reduced anisotropy is associated with the greater elongation.

4.3.4 Additional Observations

The anisotropy characterized in the plots of the material with BA and BQ morphologies was greater than that observed in material with the EQ morphology at the same testing conditions, but this measurement is overly simplified. The assumption that the tensile sample cross-sections deformed elliptically is applicable for the EQ morphology

samples, but actual tensile cross-sections for the BA and BQ deformed morphologies were not elliptical.

For the specimens with BA and BQ morphologies, tensile tests demonstrated a higher initial flow stress then the EQ morphology specimen tested under the same conditions, followed by strain softening. From the macro-examination, it appears that one major instability seems to have lead to failure. This instability forms very early in the stage of deformation, probably right at the point of ultimate stress, after which further strain is characterized by strain softening. The initial value of m for material with these two morphologies ranged between 0.25 to 0.35, but increased with strain to values in some cases over 0.5.

The observed differences in mechanical properties indicate that microstructural changes are occurring and the next section examines these changes with respect to the mechanical properties.

4.4 Microstructural Study of Deformed Material

4.4.1 Introduction

The microstructural studies were designed to further study the observed mechanical behaviour of the materials with the three morphologies. Most notably, explanations were needed for the observed strain softening and strain hardening, the variation of m with strain and the non-uniformity of tensile deformation. Optical and scanning electron microscopy were used to initially study a variety of deformed specimens for qualitative evaluation of microstructure. The higher magnification and enhanced depth of field capabilities of SEM were exploited to study cavitation and phase morphology. Quantitatively, tensile sample cross-sections were examined after deformation at 925°C - $5x10^{-3}$ s^{-1} to a fixed strain of 1.0 for the three morphologies to evaluate any changes in volume fraction of α and β phases and to compare the relative effect on each morphology. Finally, TEM was used to

make substructural observations on the material with three different morphologies deformed to a fixed strain at the same strain rate and temperature.

4.4.2 General Morphological Changes

Deformed specimens sectioned along their length according to Figure 3.4(b) were examined. This approach allowed the variation in microstructure with change in diameter of the tensile specimen to be observed which is an indication of the actual true strain, ε_A. For all micrographs the tensile axis extends from left to right, unless otherwise noted. All test times, which represent the period of time from the start of deformation to the final quench, are also included. The results of the examination of the specimens with the BA, EQ and then the BQ morphologies are provided next.

The observation of material with BA morphology suggests that at high strain rates ($5x10^{-3}$ s^{-1}) the α colonies, which are defined as the group of parallel α plates in a prior β grain, tend to behave as a unit. Figure 4.27(a) shows an optical micrograph of the BA morphology specimen deformed to failure at 950°C and $5x10^{-3}$ s^{-1} after 0.2 actual true strain. The microstructure consists of α plates(light) in a transformed β matrix(dark). The large percentage of α grains near the specimen surface should be noted. The colonies of α plates behave as one large entity or "grain", demonstrated by the distinct flow lines of each colony, but the prior alpha grain boundaries appear to control the deformation of the colonies. Figure 4.27(b) shows α plates in a transformed β matrix at a point in the same where the actual true strain was 1.3. Some of the plates appear to have broken up into continuous $\alpha/\alpha/\alpha$ configurations. A secondary electron SEM image of a region where actual true strain was 2.0 shows a colony of α plates(white) aligned with the stress axis in a matrix of transformed β. Note the acicular α in the transformed β matrix. Colony unity has concentrated the alpha plates in the matrix in the form of a band. The α plates have wavy or serrated α/β interfaces and many are not continuous plates, but have become lower aspect ratio grains.

Decreasing the strain rate seemed to have little effect on the elongation to failure of BA morphology material at most temperatures. Figures 4.28 and 4.29 illustrate the microstructural variation in the BA morphology material after deformation at 925°C and $5x10^{-4}$ s^{-1}. Figure 4.28(a) shows the microstructure of the head part of the tensile specimen. It represents the static or zero strain case. Figure 4.28(b) shows a field along the same specimen corresponding to an actual true strain of 2.2. The microstructure is characterized by mostly equiaxed α grains and regions of α plates in a transformed β matrix. A secondary electron SEM micrograph in Figure 4.29(a) of the same area gives more details on the α plate break-up. Phase identification is more difficult in this figure. The micrograph reveals alpha on three layers with respect to the matrix surface: below the surface, at the surface, and above the surface. The two alpha plates at the center of the micrograph are undergoing break-up. Visible are relatively sharp α/α interfaces that can be due to subboundary formation across the plate and/or the interjection of β between the α/α grains. The distance between these interfaces appears to be proportional to the plate thicknesses, such that α plates would become essentially equiaxed after break-up. Figure 4.29(b) displays a continuous band of equiaxed α grains at an actual true strain of 2.8. These α grains contain sharp α/β and α/α interfaces, indicating that either the α plates have been recently cusped by β or that new recrystallized α grains have formed. It should be noted that the microstructure is characterized by a large number of α/α grain boundaries, but the individual α grains surrounded by the transformed β are characteristically more rounded. Finally, Figure 4.29(c) shows a relatively equiaxed microstructure at the fracture tip with a distribution of both large and small grains. Most of the α/α grain boundaries appear to have become α/β.

The previous microstructural results indicate that for material with the BA morphology grain refinement and subsequent reduction of initial α aspect ratio with increasing strain is prevalent. What must be considered when making these observations is that the necking evident from the tensile sample macro-behaviour indicates that the strain

(a)

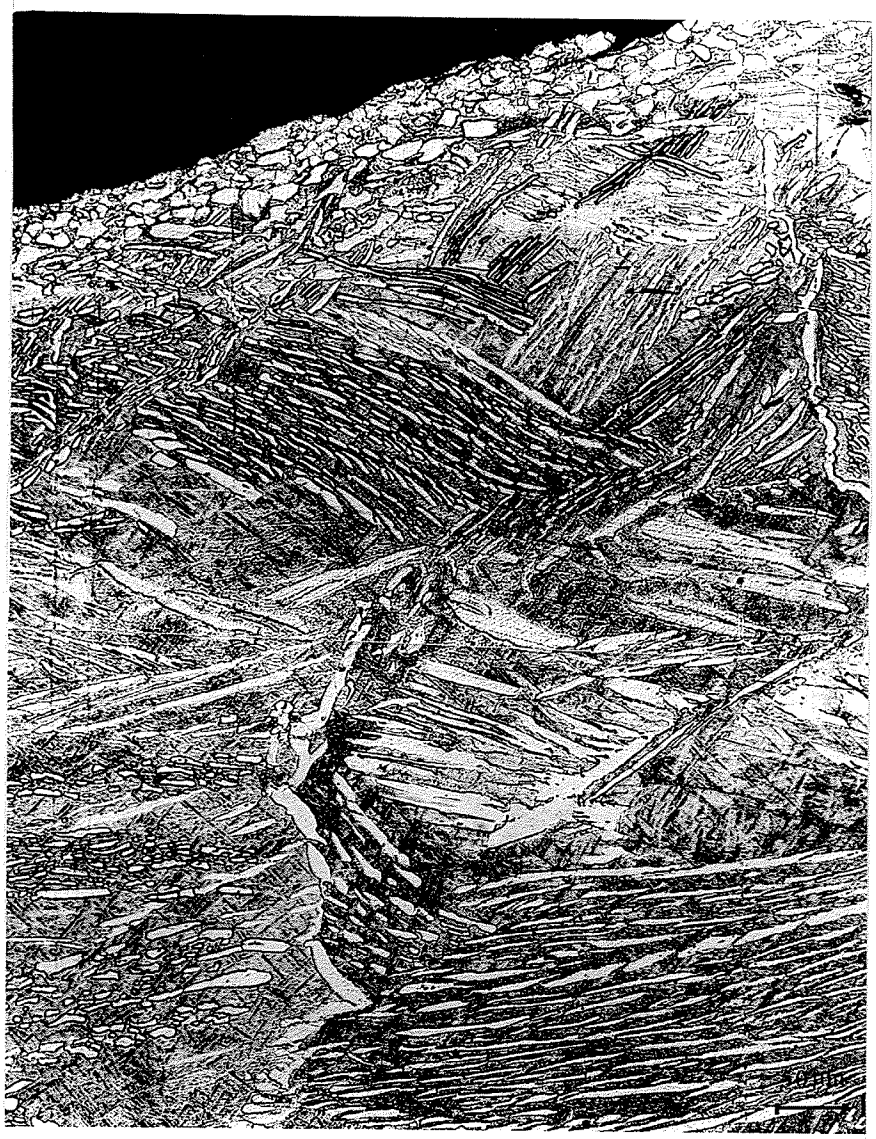

(b)

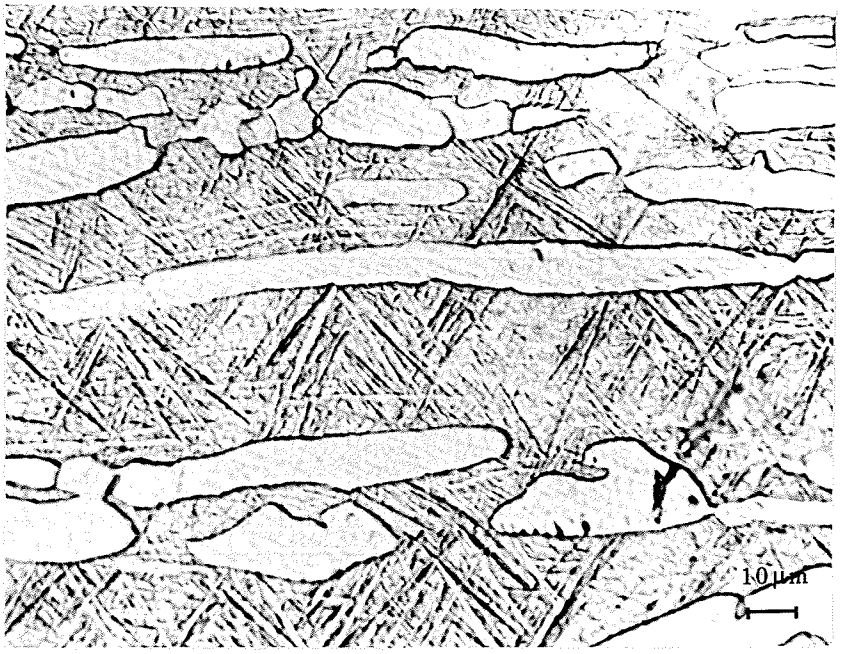

(c)

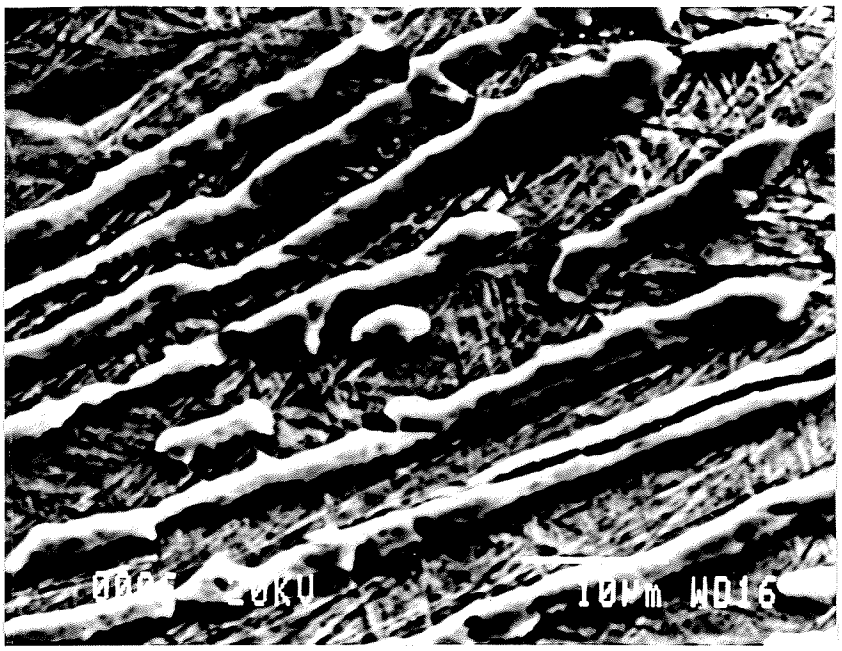

Figure 4.27: Optical micrographs showing longitudinal section of Ti-6Al-4V alloy with BA morphology , 950°C, $5x10^{-3}$ s^{-1}, ε_t =1.14, test time = 4.8 minutes at (a)ε_A=0.2 and (b)ε_A=1.3. SEM secondary electron image of same sample at (c)ε_A=2.0.

(a)

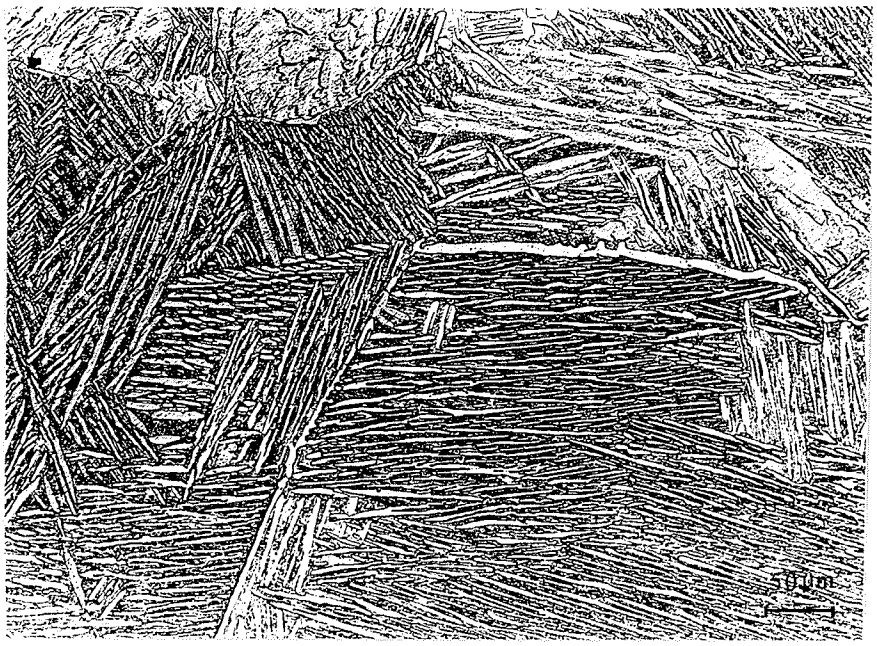

(b)

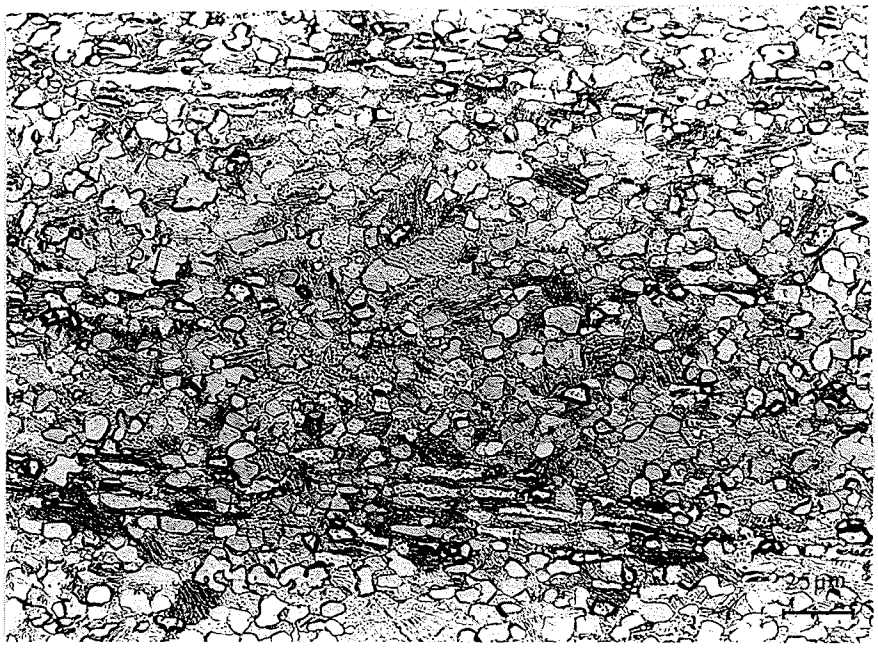

Figure 4.28: Optical micrographs showing longitudinal section of Ti-6Al-4V alloy with BA morphology , 950°C, $5x10^{-3}$ s^{-1}, $\varepsilon_t = 1.34$, test time = 42.2 minutes at (a)ε_A=0.0, (b)ε_A=2.6.

(a)

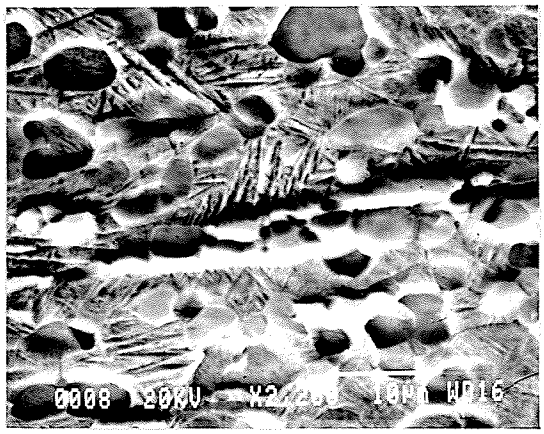

(b)

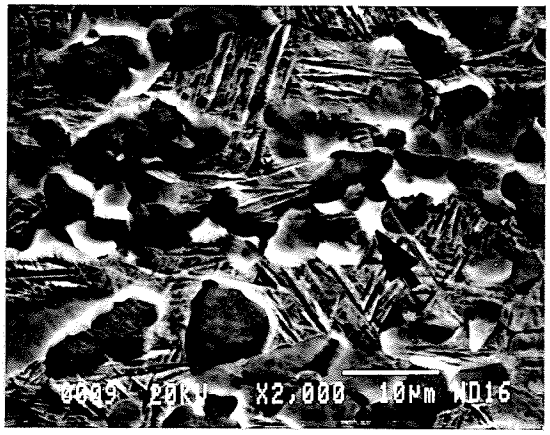

(c)

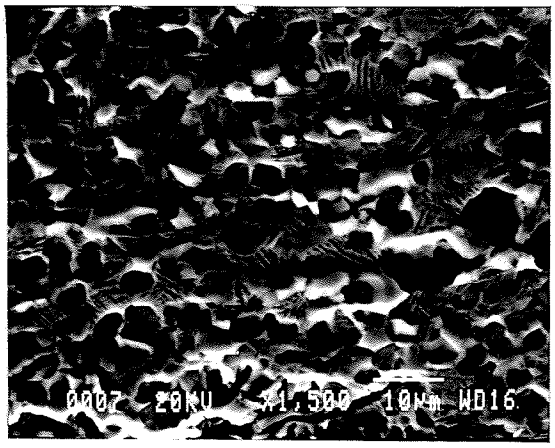

Figure 4.29: Secondary electron SEM micrographs showing longitudinal section of Ti-6Al-4V alloy with BA morphology , 950°C, $5x10^{-3}$ s^{-1}, ε_t = 1.34,test time = 42.2 minutes at (a)ε_A=2.6, (b)ε_A =2.8, and (c)near fracture.

rate is actually higher at the necked regions than that controlled by the cross-head. Therefore, recrystallization effects could be high strain rate($>1x10^{-2}$ s^{-1}) induced and not due to the supposed constant strain rate.

Material with the EQ morpholgy was also characterized by strain softening at all temperatures for the strain rate of $5x10^{-3}$ s^{-1}. Figures 4.30(a)-(c) examine the variation of microstructure with strain for the material with the EQ morpholgy deformed at 900°C and $5x10^{-3}$ s^{-1}. Figure 4.30(a) shows the microstructure taken from the head of the tensile sample representing zero strain. The micrograph reveals a bimodal α grain size distribution and a considerable number of aligned α grains, typical of a banded microstructure. Figure 4.30(b) illustrates the microstructure at an actual true strain of 1.2. Qualitatively there appears to have been an increase in the number of smaller α grains. These smaller grains could be due to α break-up or recrystallization. It should be noted that specimens polished and etched after deformation appear to have thicker grain boundaries. The increase in grain boundary thickness with strain would indicate that diffusion is enhanced in this area during superplastic deformation and thus suggests that the grain boundary plays an important role in the deformation [85]. Near the fracture tip the microstructure is representative of Figure 4.30(c). The dark bands parallel to the tensile axis are cavities.

Decreasing the strain rate and temperature to 875°C and $5x10^{-4}$ s^{-1} reduced the tendency of the material to strain soften. Figure 4.31(a) shows that at an actual true strain of 1.2 the number of elongated α grains appears less than after the same amount of strain at the lower strain rate, but the number of α/α grain boundaries is still considerable indicating little separation of α by β. Figure 4.31(b) reveals the microstructure near the fracture tip. Apparently the α grain size is smaller than that in Figure 4.31(a), indicating grain refinement in the necked region.

Material with the BQ morphology was also characterized by strain softening, but at all temperatures and strain rates tested.

Figures 4.32 (a)-(d) demonstrate the variation of microstructure along the length of a tensile sample deformed at 925°C and $5x10^{-4}$ s^{-1} to failure. These deformation conditions resulted in the highest elongation to failure for material with this morphology. Figure 4.32(a) shows the microstructure at the grip section corresponding to zero strain. Figure 4.32(b) shows both equiaxed and lamellar α(light) at 2.3 actual true strain. The distribution of lamellar and equiaxed α appears quite uniform. Near the fracture tip(Figure 4.32(c)), the α and β grains appear equiaxed. A secondary electron SEM image presented in Figure 4.32(d) of the microstructure near the fracture tip demonstrates a pocket of lamellar α(dark) and β(light) that has remained and not broken up during deformation. Specifically, note the one α plate that is partitioned by six equally spaced beta(white) plates. The break-up of alpha lamellae has been characterized throughout by this β intervention or grooving.

4.4.3 Case of 925°C, $5x10^{-4}$ s^{-1}, ε =1.0

One reported characteristic of superplasticity is the increase in volume fraction of β with increasing strain [79]. The analysis of the change in microstructure along tensile sections provides a quick overview of the changes with strain, but no quantitative measurements can effectively be made because of the variation in strain across a field of study. As well, comparison to other morphologies at the same conditions and strains is difficult, because tensile samples can fail after varying periods of time. Grain size and volume fraction are two variables dependant upon time. Varying tensile testing time of material with different morphologies will therefore make direct comparisons difficult. This section evaluates the change in volume fraction of alpha and beta for the three morphologies deformed at identical conditions(925°C - $5x10^{-4}$ s^{-1}) to a fixed total strain of 1.0, and water quenched. Considering that the uniformity of deformation for each sample varies, the samples were sectioned to reveal the cross sections in the area that corresponds to an actual true strain of 1.0. Figures 4.33 to 4.35 show back-scattered electron images for the three

(a)

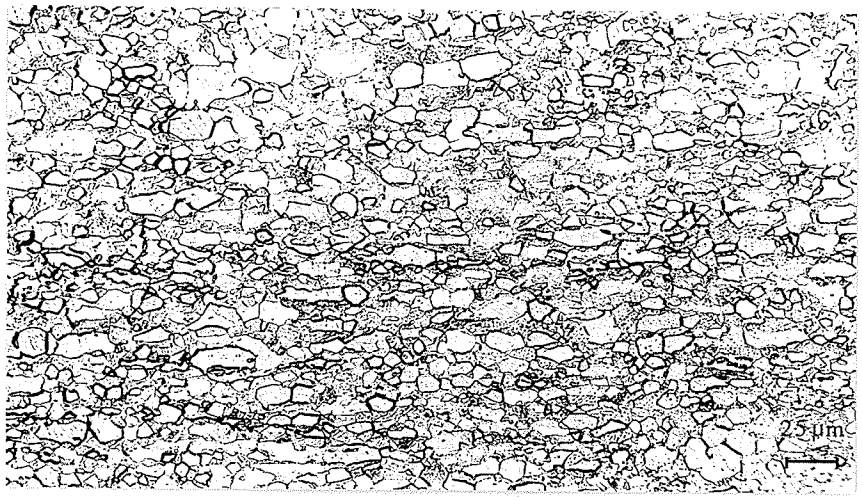

(b)

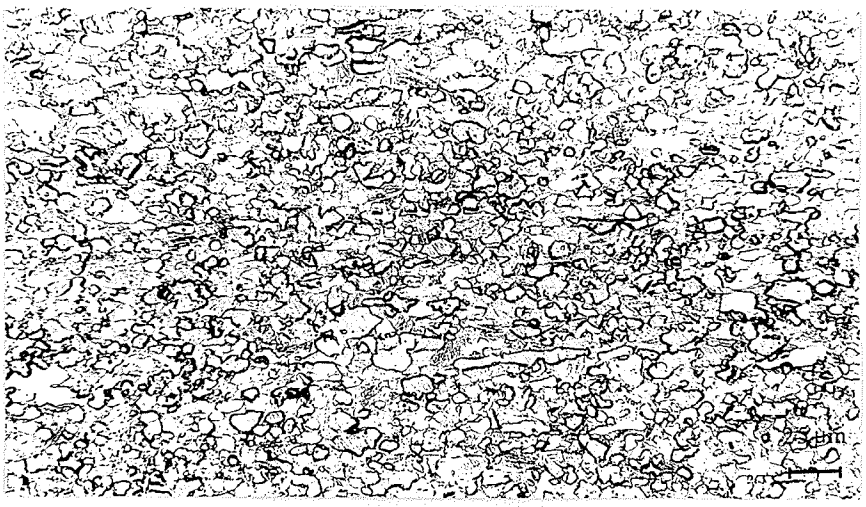

(c)

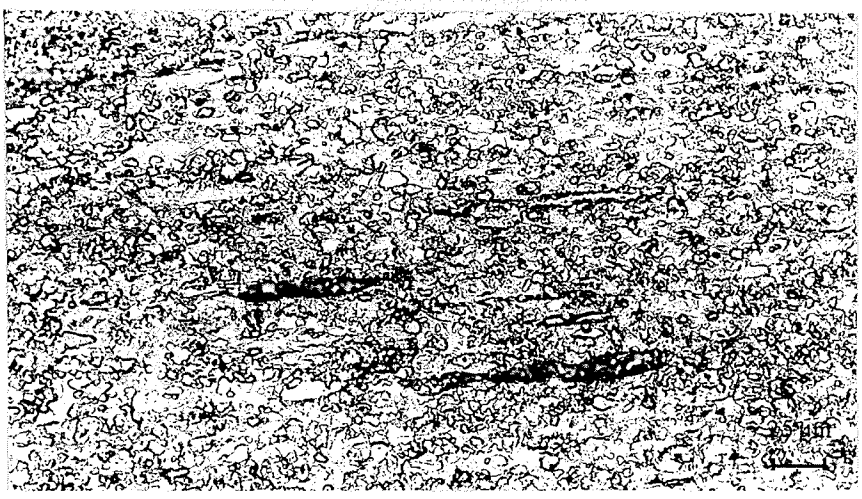

Figure 4.30: Optical micrographs showing longitudinal section of Ti-6Al-4V alloy with EQ morphology , 900°C, $5x10^{-3}$ s^{-1}, ε_t = 1.16, test time = 6.0 minutes at (a)ε_A=0.0, (b)ε_A=1.2, and (c)near fracture.

(a)

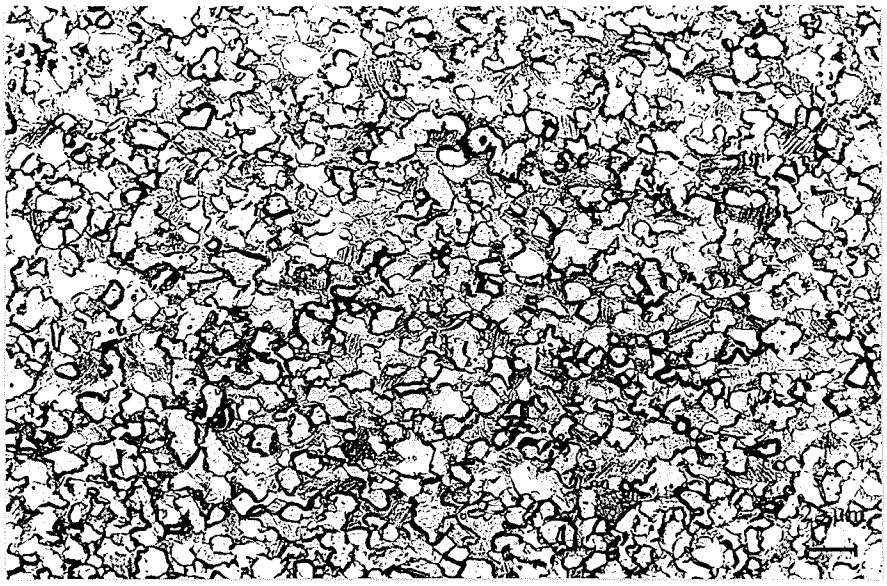

(b)

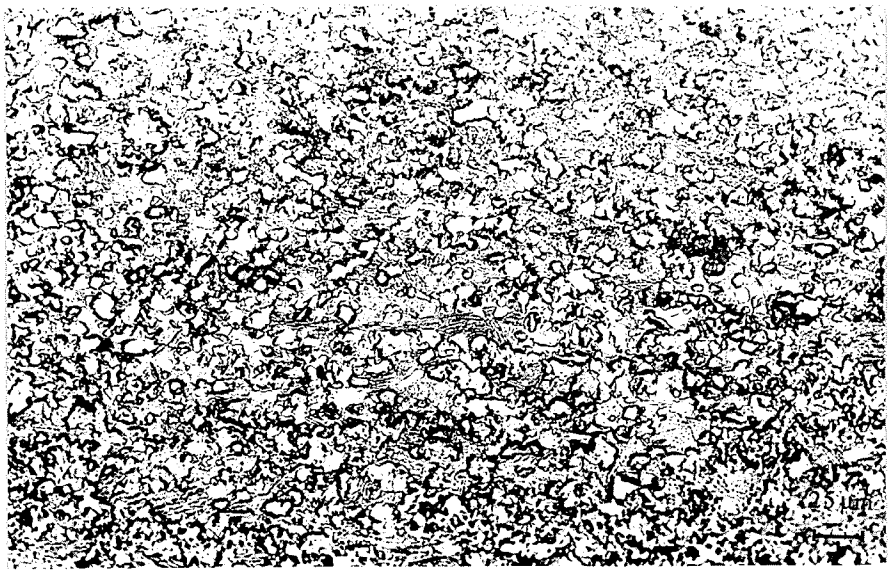

Figure 4.31: Optical micrographs showing longitudinal section of Ti-6Al-4V alloy with EQ morphology , 900°C, $5x10^{-3}$ s^{-1}, ε_t = 1.78, test time = 62.0 minutes at (a)ε_A=1.2, and (b)near fracture.

(a)

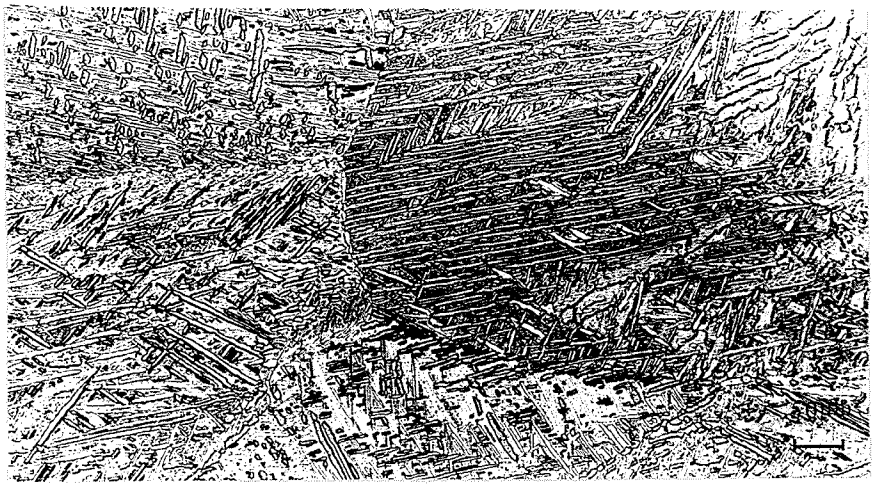

(b)

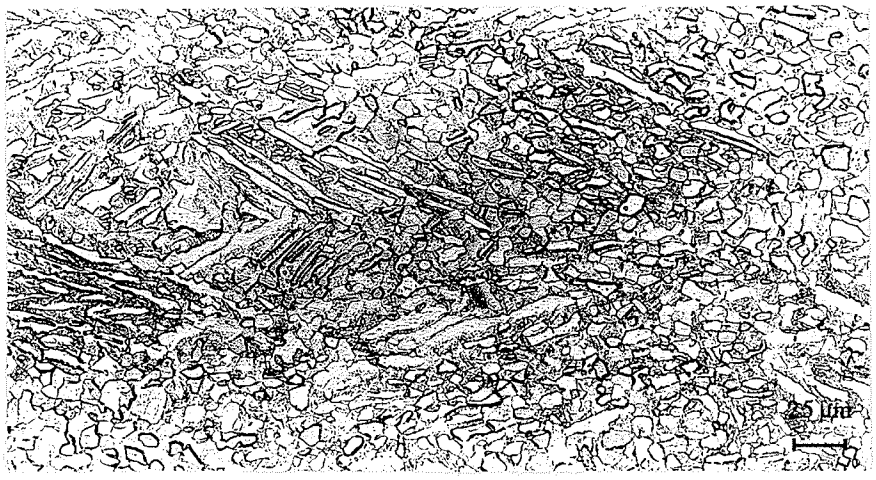

(c)

(d)

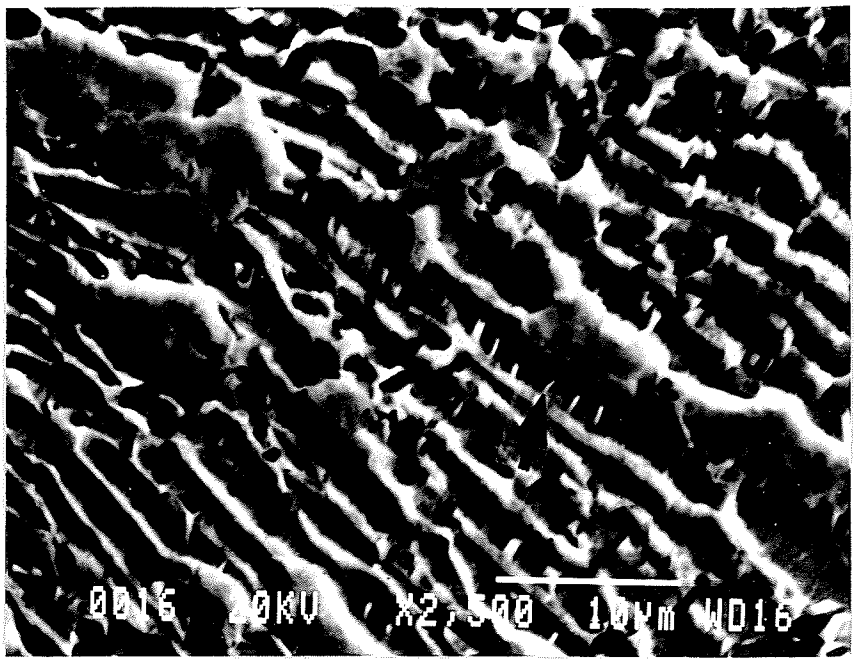

Figure 4.32: Optical micrographs showing longitudinal section of Ti-6Al-4V alloy with BQ morphology , 925°C, $5x10^{-4}$ s^{-1}, ε_t = 1.70, test time = 47.0 minutes at (a)ε_A=0.0, (b) = 2.3, and (c)near fracture. (d) Secondary electron SEM image of same sample near fracture.

(a)

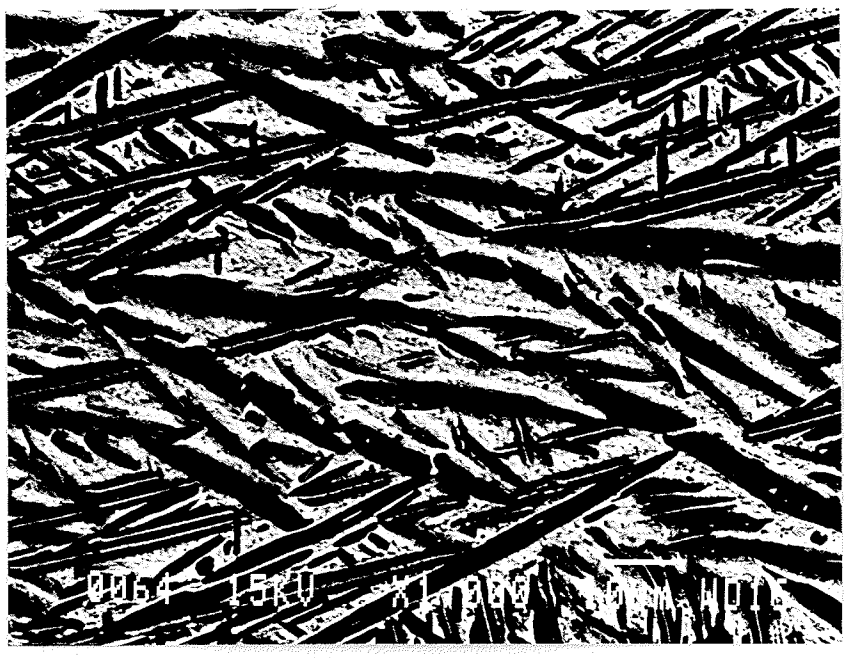

(b)

Figure 4.33: Backscattered electron SEM micrographs of Ti-6Al-4V alloy with BA morphology, 925°C, $5x10^{-4}$ s^{-1}: (a)ε = 0.0, (b)ε =1.0.

(a)

(b)

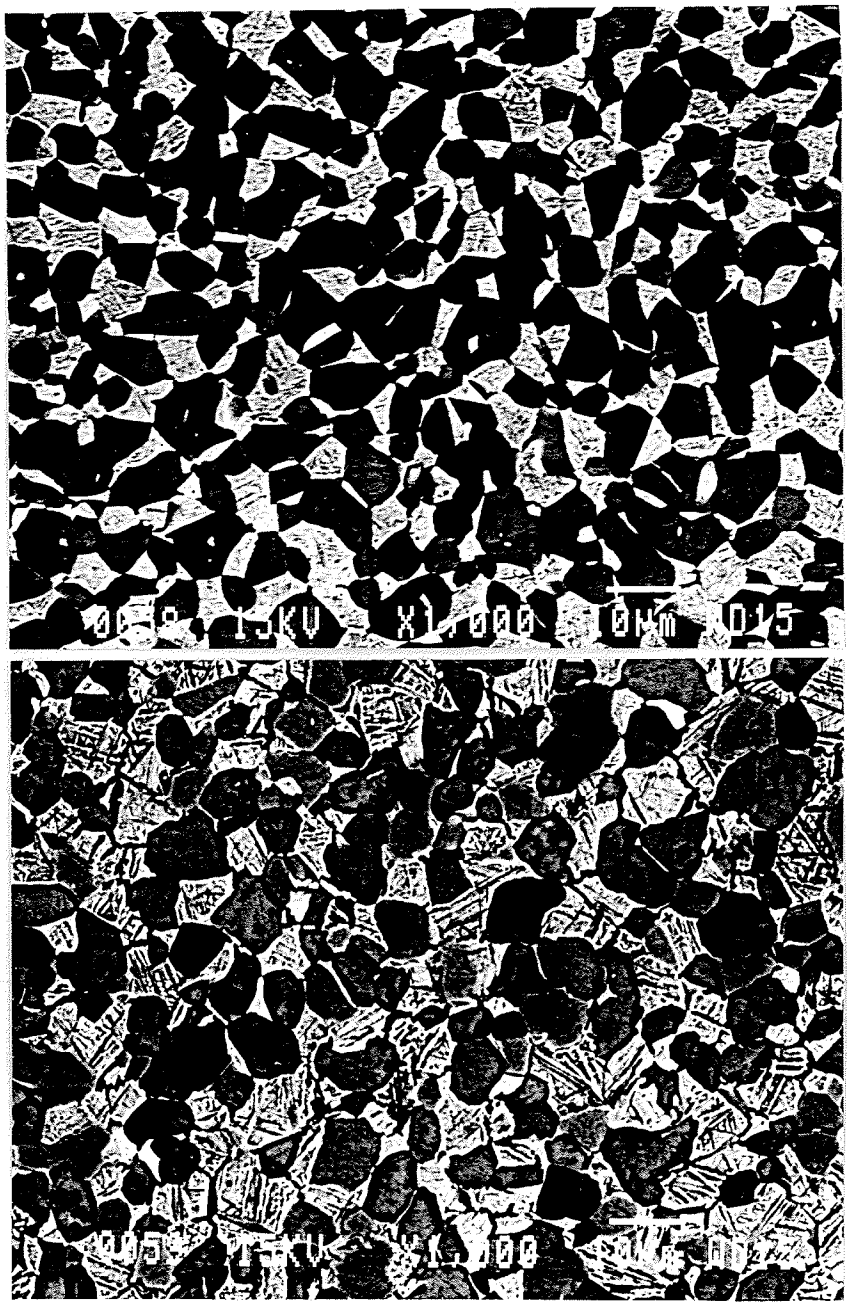

Figure 4.34: Backscattered electron SEM micrographs of Ti-6Al-4V alloy with EQ morphology, 925°C, $5x10^{-4}$ s^{-1}: (a)ε = 0.0, (b)ε =1.0.

(a)

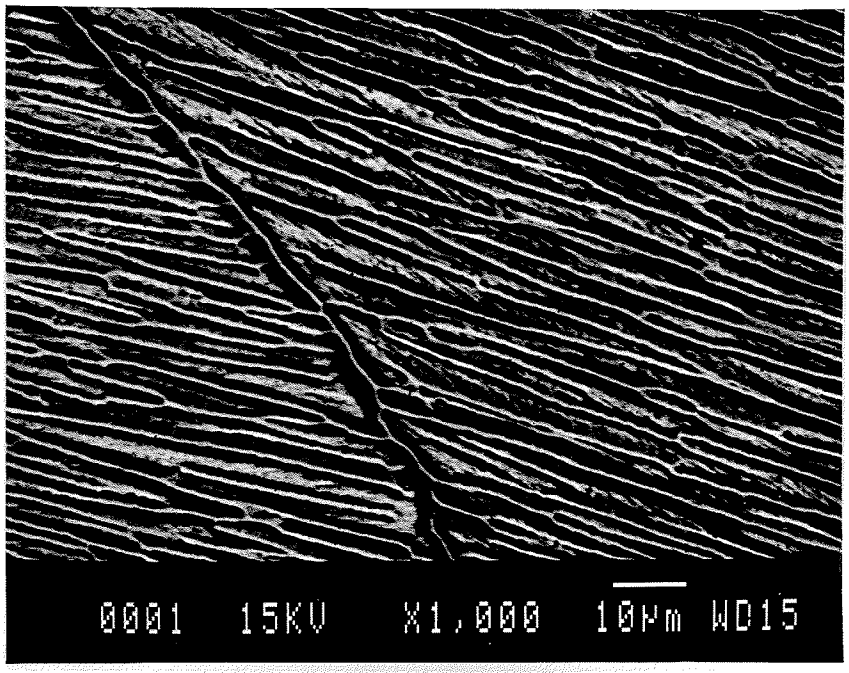

(b)

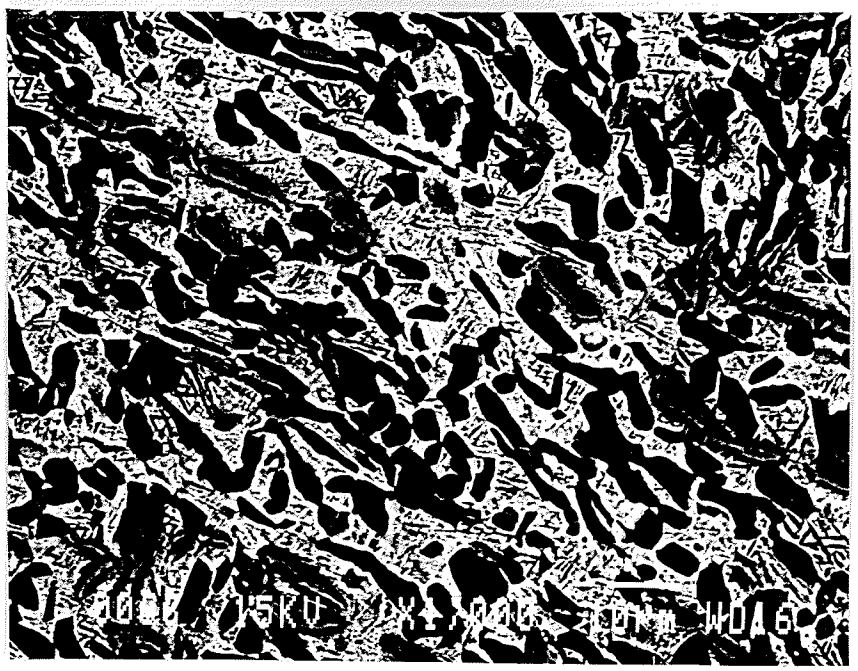

Figure 4.35: Backscattered electron SEM micrographs of Ti-6Al-4V alloy with BQ morphology, 925°C, $5x10^{-4}$ s^{-1}, (a)ε = 0.0, (b)ε =1.0.

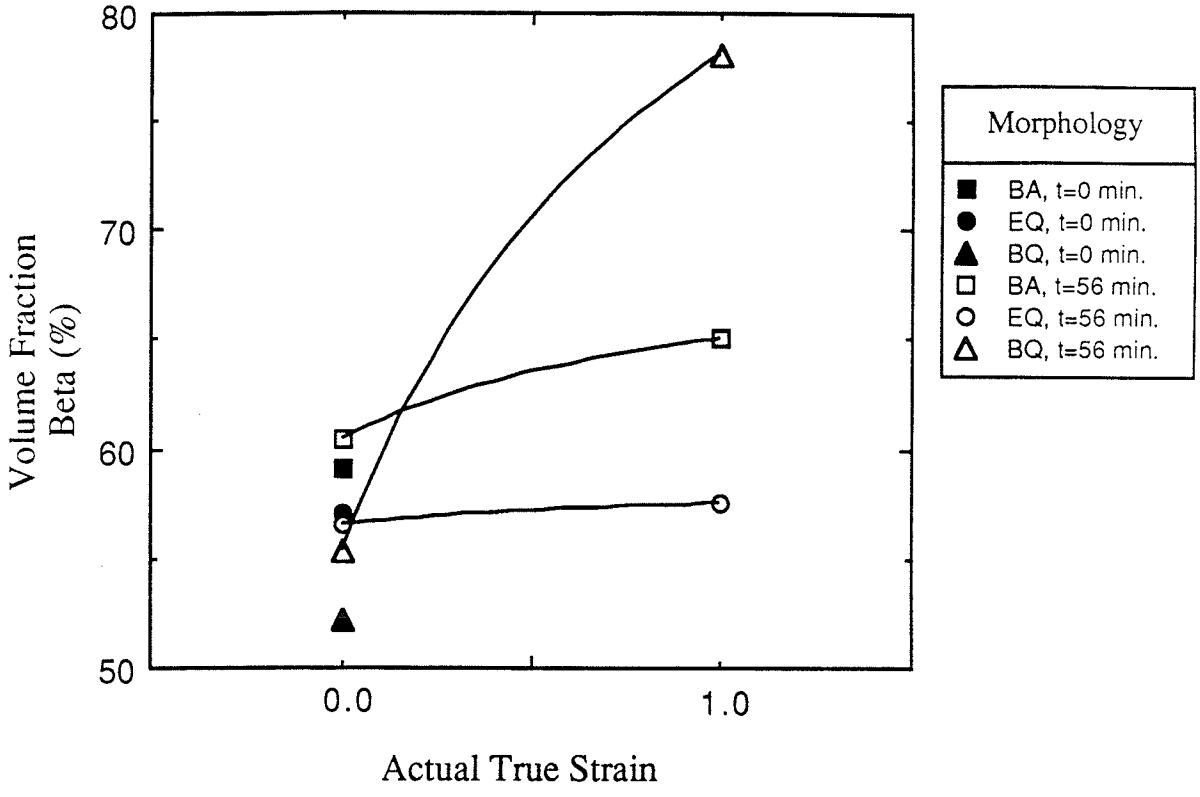

Figure 4.36: Volume fraction of β in Ti-6Al-4V alloy with BQ, EQ, and BA morphology at varying states of deformation at 925°C, 5x10-4 s^{-1}.

morphologies at (a)the gauge head, corresponding to zero strain and at (b)the point of 1.0 strain. Figure 4.36 shows the variation of beta volume fraction with time and strain. It is seen that the volume fraction of β remains constant with increase in time at the test temperature, but increases with strain for material with the BA and BQ morphologies.

4.4.4 Cavitation

Specimens taken to failure with final elongations ranging from 210 to 743 percent were examined qualitatively for cavitation. Other experimentors trying to observe cavitation usually did not take material to failure due to equipment limitations. Initial attempts made to detect cavities using optical microscopy worked well for the cavitational behaviour observed in the lamellar microstructures but did not reveal any cavities in the deformed EQ morphology at superplastic conditions. To overcome the limitation of optical microscopy, the SEM, which supplies high magnification with exceptional depth of field, was utilized. The analysis considered longitudinal and transverse sections. The following observations were made for the longitudinal study.

Material with lamellar morphologies exhibited cavitation after deformation, but only for two conditions examined did it appear to contribute to failure. The material with BA morphology taken to failure at 875 and 950°C at a constant strain rate of $5x10^{-3}$ s^{-1} cavitated readily, indicating that an increase in temperature did not reduce cavitation. Figure 4.37(a) displays the general void morphology near the fracture surface along the tensile axis after deformation to failure at a temperature and strain rate of 875°C and $5x10^{-3}$ s^{-1}, respectively. To the right is the edge of the fracture tip outlined in white, demonstrating its relatively broad cross-section. Most smaller voids form parallel to the tensile axis, while larger voids appear to have coalesced from the smaller voids. The cavitation appears to be controlled by the prior β grain boundaries. Closer examination of one of the voids in Figure 4.37(b) indicate that it formed at the α/β interfaces. More specifically, Figure 4.37(c) displays a prior β grain boundary(↑), where two small cavities (labelled **a** and **b**) have formed near the β plates (white). A larger cavity is visible on the boundary at the bottom of the micrograph. At this strain rate void initiation can take place at prior β grain boundary triple points and propagate along individual α colonies. Reduction of the strain rate changes the morpholgy of the cavities at fracture. Figure 4.38(a) shows a large number of cavities extending along the tensile axis for

(a)

(b)

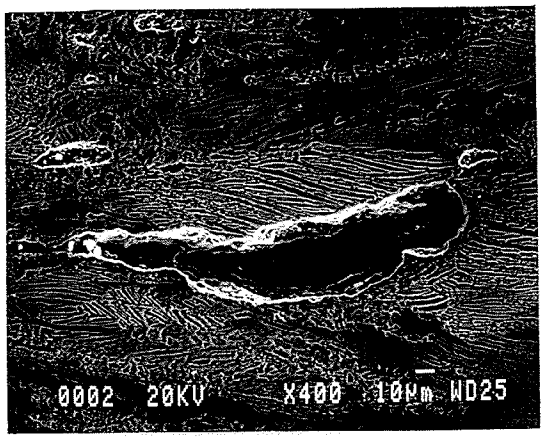

(c)

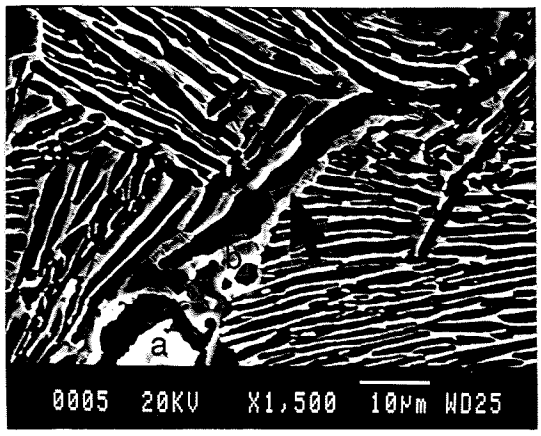

Figure 4.37: Void formation on transverse section for morpholgy BA after failure at 875°C, $5x10^{-3}$ s^{-1}.

(a)

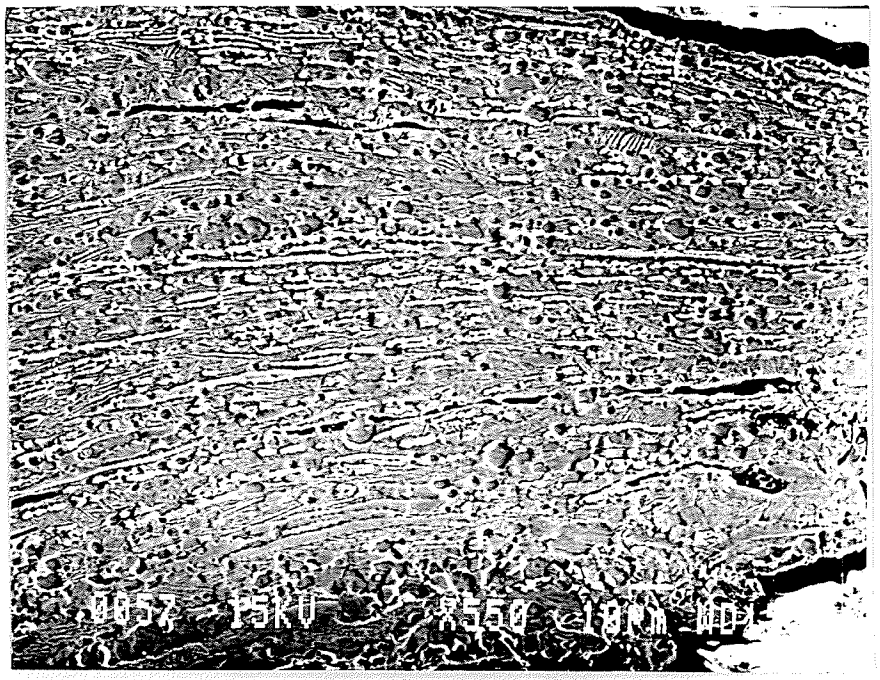

(b)

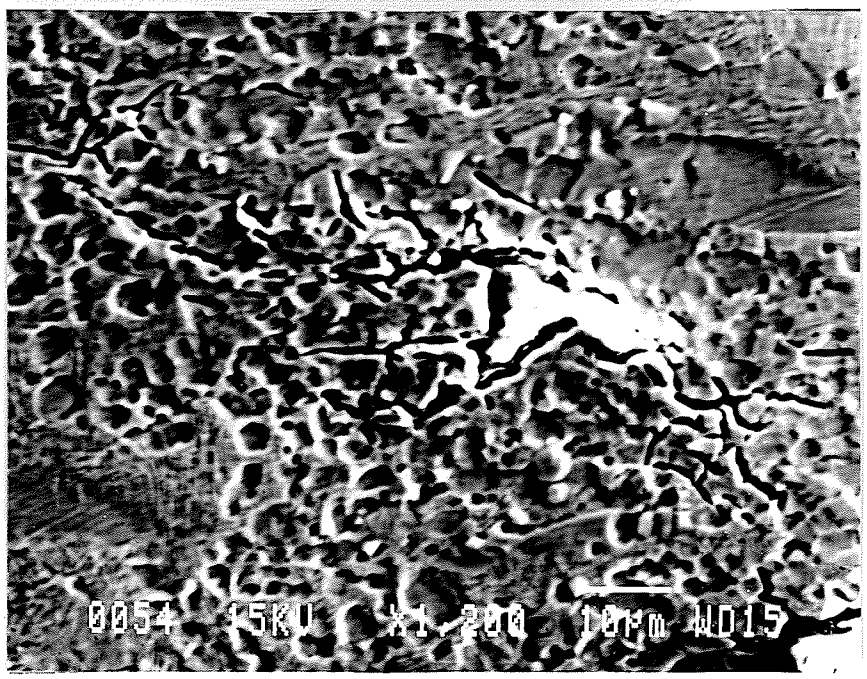

Figure 4.38: Void formation on transverse section for morpholgy BA after failure at 950°C, $5x10^{-3}$ s^{-1}.

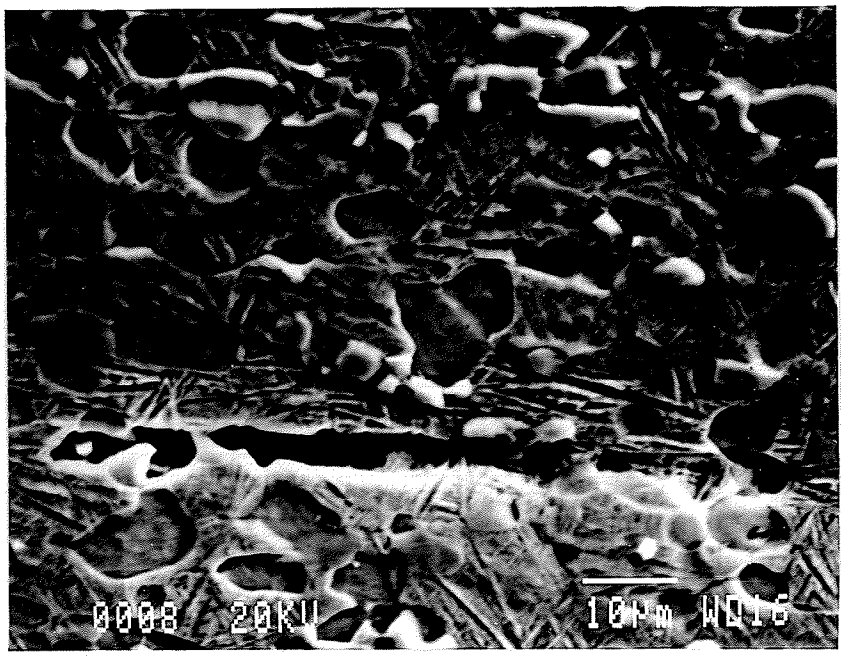

Figure 4.39: Void formation on transverse section for morpholgy BQ after failure at 950°C, $5x10^{-4}$ s^{-1}.

(a)

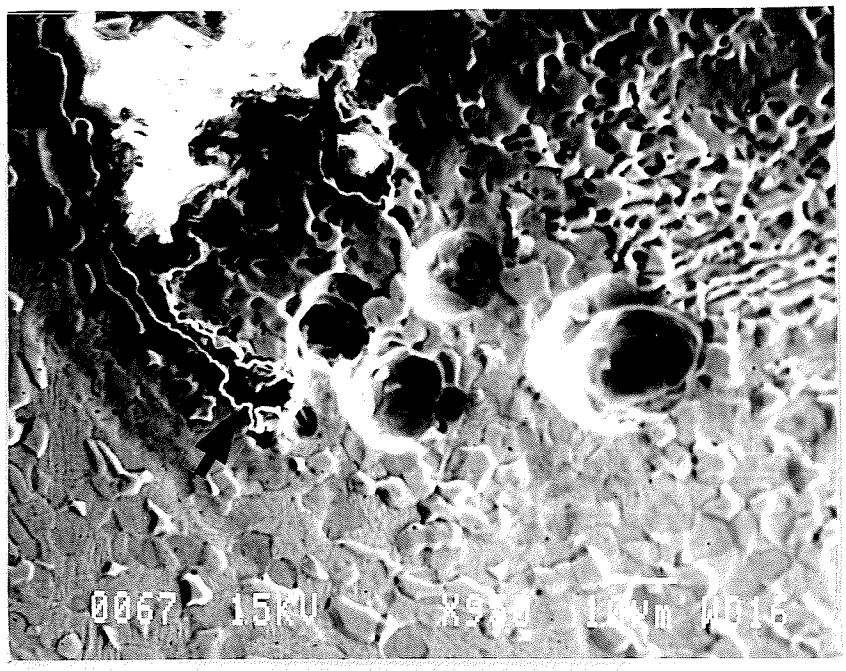

(b)

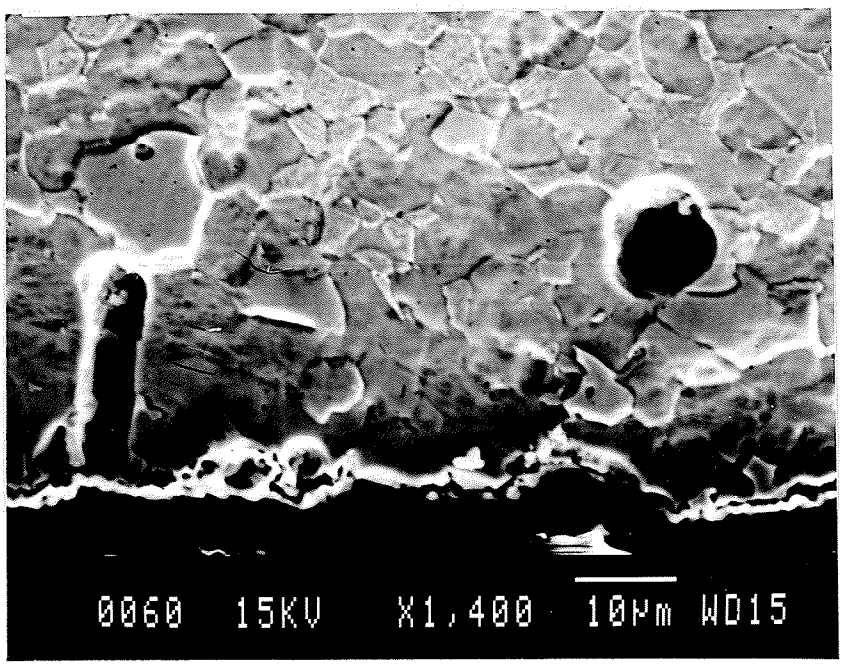

Figure 4.40: Void formation near tensile cross-section surface after deformation at 925oC, 5x10-4 s-1 to an actual true strain of 1.0 for material with (a)BQ and (b) EQ morphologies.

material with a BA morphology deformed at $5x10^{-4}$ s^{-1}. These voids are parallel to the observed α and β plates, and no cavity appeared to propagate perpendicular to the tensile axis or across the plates. Closer to the fracture tip, Figure 4.38(b) shows the transgranular interlinking of voids that have lead to final failure.

For the BQ morphology, cavities were also observed, but not to the extent as material with the BA morphology. Typically, one to two cavities were observed after deformation to failure at all temperatures and a $5x10^{-3}$ s^{-1} constant strain rate. These cavities were observed within one to two millimeters of the fracture tip, and the general morphology was such that they remained centered on the tensile axis. Figure 4.39 shows an observed cavity that is surrounded by β_{tr}. Possibly this void formed early during deformation and was arrested. The explanation for the arrest is not available.

Cavities were not observed with SEM in the EQ morphology material tested at 875, 900, 925 or 950°C and at strain rates greater than $5x10^{-3}$ s^{-1}. This behaviour confirms the observations by Ito *et al.* [32] who found few or no cavities at these conditions. At a strain rates of $5x10^{-3}$ s^{-1}, the material demonstrated reduced ductility, and cavities similar to those in Fig. 4.29(c) were prevalent.

A cavitational study was also performed on the transverse cross-sections of material with the three morphologies deformed at 925°C, $5x10^{-4}$ s^{-1} and taken to 1.0 actual true strain. Examining a tensile cross-section allows examination of regions near surface instabilities that cannot normally be examined with longitudinal studies. Figure 4.40(a) shows the formation of four circular voids near an instability tip at the surface of the BQ specimen. This behaviour was prevalent in the BA morpholgy as well. Figure 4.40(b) shows two examples of the many voids that were present near the surface of material with the EQ morphology after deformation to an actual true strain of 1.0. The actual observation of voids at this condition contradicts most other studies to date. These cavities suggest that the outer surface undergoes considerable deformation during the tensile test, which is a manifestation of the reduced cross-sectional area and increased specimen surface area

characteristic of superplastic deformation. Whether these cavities remain and contribute to failure or disappear during deformation has not been determined.

4.4.5 TEM Study

To better understand the mechanical behaviour of the Ti-6Al-4V alloy with the three morphologies, a TEM analysis was performed. The TEM work performed in this study was restricted to the examination of the material with BA, EQ, and BQ morphologies after deformation at a $5x10^{-4}$ s^{-1} constant strain rate to 1.0 actual true strain. These conditions generally resulted in the optimum observed superplastic properties for each morphology. This optimum behaviour appeared related to the initial volume fraction of α and β phases for each individual morphology. It should be reasserted here that the material observed with the TEM was water quenched at 925°C under load and any evidence of polygonization and recrystallization is not due to cooling. As well, most high temperature evidence was destroyed in the β phase that transformed to α^m with the water quench, leaving most of the emphasis of the study on the α phase.

Mechanically, the material with the lamellar morphologies experienced considerable strain softening, while material with the EQ morphology strain hardened. Optical and scanning electron microscopy suggest that strain softening can be attributed to (1) grain refinement by subgrain formation, and (2) β rearrangement by β cusping. Strain hardening has been reported to be due to (1) grain growth, (2) increase in β content, and (3) dislocation interaction and polygonization [79].

Material with the BA morpholgy had thicker α plates than the BQ morphology at 925°C. Figure 4.41(a) shows the characteristic microstructure before deformation. It depicts parallel α plates(light) surrounded by β that has transformed to α^m by water quenching. The α^m is characterized by dense dislocations that have destroyed the high temperature β microstructure. After deformation to 1.0 actual true strain, the material developed considerable substructure across its α plates (Figure 4.41(b)). At sub-

boundaries, sharp curved interfaces can be seen where β intersects the α plates. The plate itself appears sheared and bent, a definite sign of deformation. Figures 4.41(c) and (d) indicate other substructure development suggesting dynamic polygonization and recrystallization. Figure 4.41(c) shows a dense dislocation network at an α/α grain boundary. Figure 4.41(d) shows a bamboo cell structure forming perpendicular to the α/β grain boundary. Some α plates did not develop such intense polygonal substructure but instead displayed limited slip planes activated across α plates between two β plates. Figure 4.42(a) shows an hexagonal network crossing an α plate. Some small irregular shaped equiaxed α grains are expected if recrystallization occurs. Figure 4.42(b) shows a small α grain relatively free of dislocations surrounded by other α grains(light) and β_{tr}(dark). Tilting of the thin foil revealed that the presence of dislocations in the surrounding α plates suggest that the irregular shaped α grain is newly recrystallized. Figures 4.42(c) and (d) offer a different perspective between the relation of α and β plates. A β_{tr} plate cross-section is found in the middle of an α plate indicating that in three dimensions the β plate would extend normal to the plane of the micrograph. The β plate in the center of the α plate either formed during the initial transformation before deformation or emerged through during deformation. The former is more likely because initial microstructural characterization before deformation revealed β plates within α plates. During deformation some interaction would be expected between the two phases, and some straight dislocations and dipoles can be seen in the α interior between the two β plates.

The material with BQ morphology is shown prior to deformation in Figure 4.43(a). After tensile deformation to 1.0 actual true strain the material with the BQ morphology shows characteristically more β, lower aspect ratio α grains, more α/β interfaces, and more β cusping of α than the material with the BA morphology.

Like the material with the BA morphology, recovery was observed within the α plates for the material with the BQ morpholgy. Figure 4.43(c) shows subgrains formed in an α plate surrounded on both sides by β_{tr}.

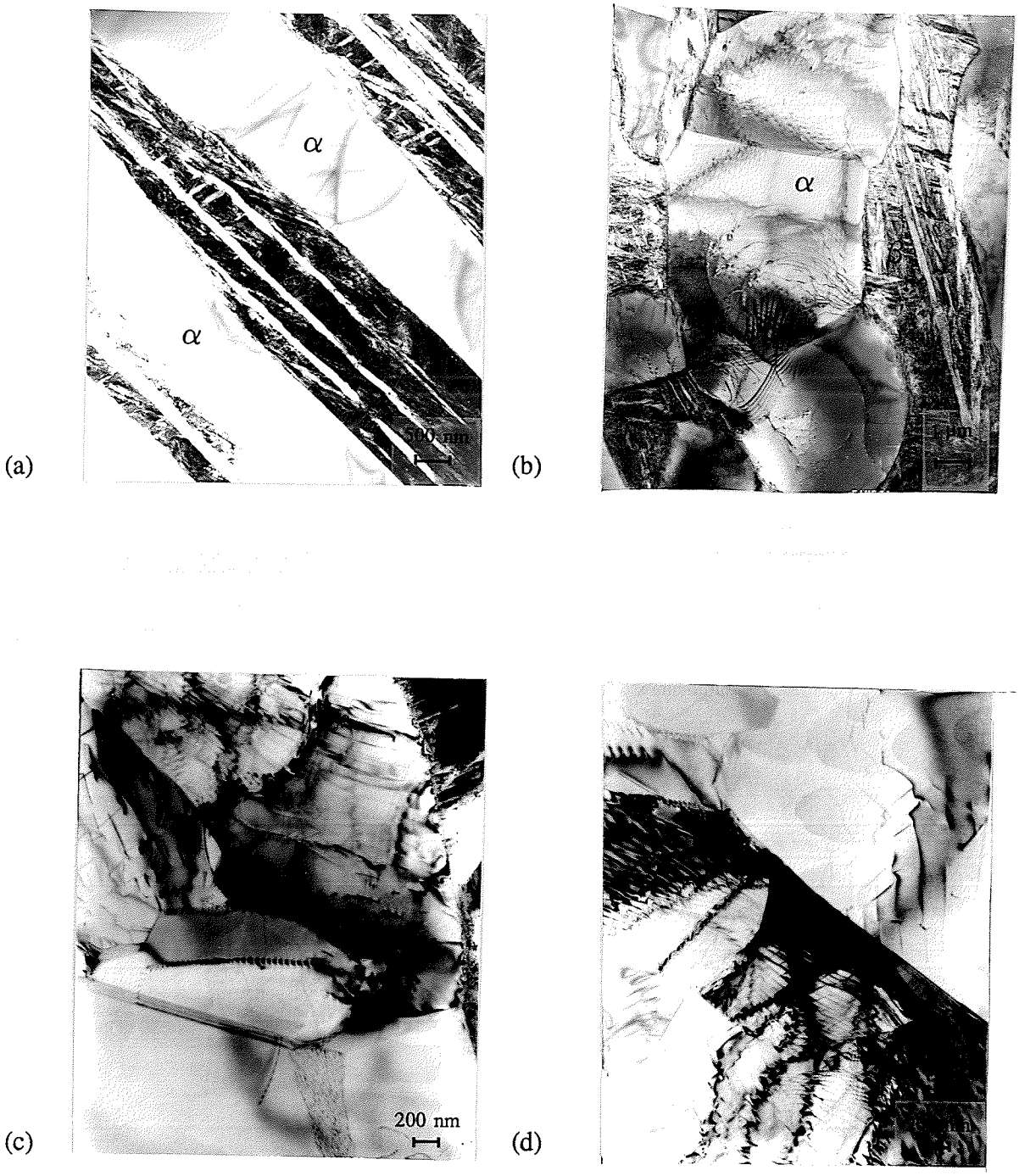

Figure 4.41: TEM micrographs of Ti-6Al-4V alloy with BA morphology water quenched from 925°C, (a)before deformation, after deformation to 1.0 strain at $5x10^{-4}$ s^{-1} showing (b)sheared α plate in a β_{tr} matrix, and (c) and (d) α subgrain formation.

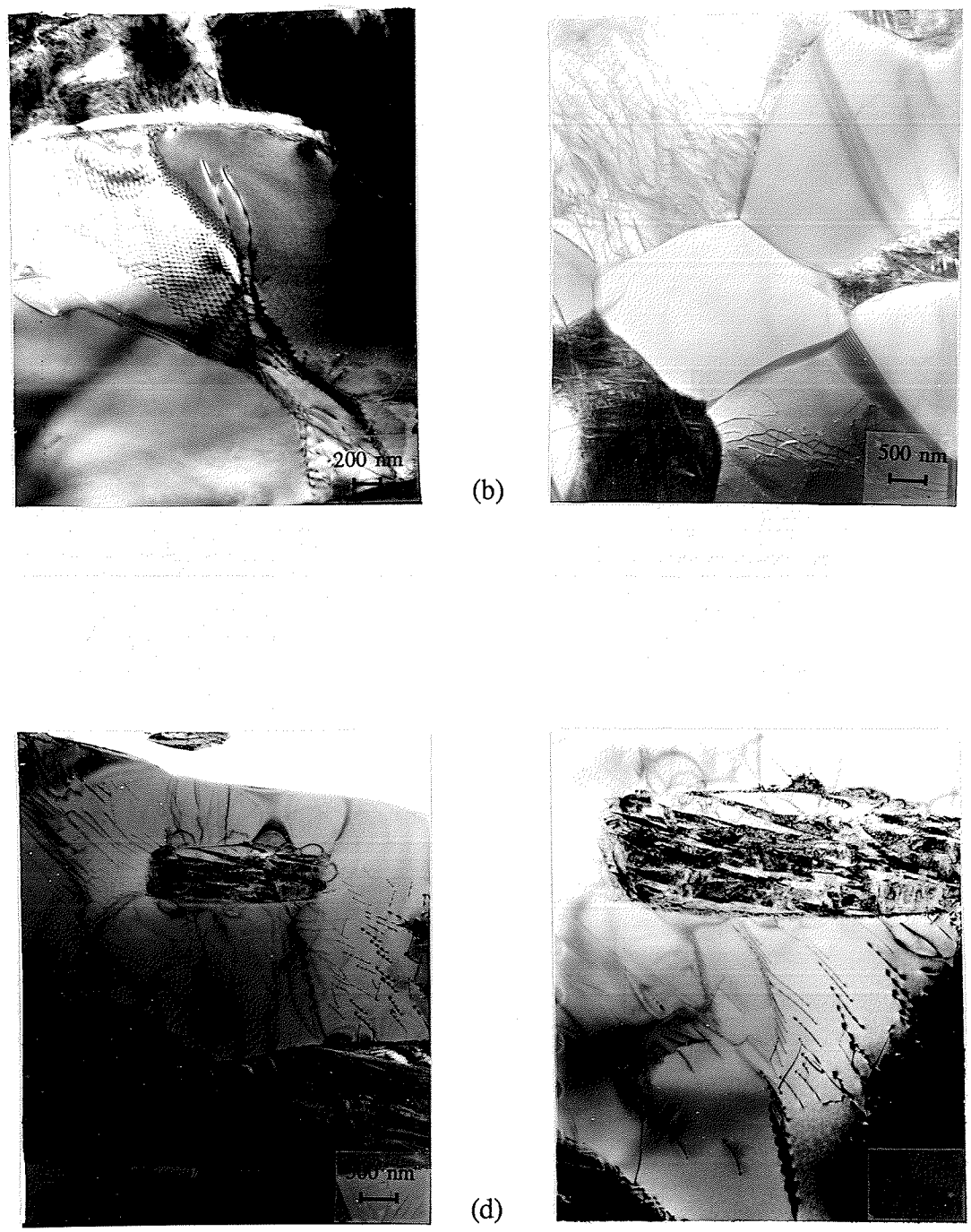

Figure 4.42: Deformed Ti-6Al-4V as in Figure 4.41. Illustration of (a) hexagonal network crossing an α lamella, (b) dislocation free α grain, and (c) and (d) β plate intersecting the mid point of an α plate.

In the early stages of deformation grain boundaries can act as sources of dislocations, but at later stages of deformation lattice dislocations can be injected into the grain boundary. At this point they become extrinsic grain boundary dislocations(EGBD's), being more mobile and not necessary to maintain the structure of the grain boundary. EGBD's disappear on heating so that water quenching a material under load at high temperatures should prevent their disappearance. Figure 4.43(d) shows some curved EGBD's interacting with the α/β grain boundary. Whether they are piling up with the grain boundary or being emitted from the grain boundary has not been determined. Figure 4.44(a) shows an $\alpha/\alpha/\beta$ triple point emitting dislocations that interact with an array crossing the α grain.

Also noted, qualitatively, for the material with the BQ morpholgy was the large number of β cusps and α/β interfaces. The number of α/β interfaces is purely a measure of the α plate break-up due to the cusping mechanism. The formation of β cusps during forging and subsequent annealing of lamellar α plates was described by Weiss *et al.* [33] for a Ti-6Al-4V alloy. Beta cusp initiation was observed to occur along α/α subboundaries of low and high misorientation, and followed by β penetration along these high energy paths. Their initial observations agree with those observed here. Figure 4.43(b) showed the β penetration along a subboundary partitioning an α plate. The next series of micrographs illustrates the possible steps observed in the α plate break-up. Figures 4.44(b) and (c) are brightfield and CDF images of what appears to be a disrupted area on the α/β grain boundary penetrating the α. The disruption is occurring at the tip of the convex portion of the β phase suggesting either β interjection into the α or grain boundary dislocation ejection into the α lattice. The α plate was dislocation free, so no subboundary path exists for the β to follow. Figure 4.44(d) shows a well developed β cusp following a subboundary and the dislocation tangles interacting with the subboundary. Upon separation, the α/α boundaries should become two well-rounded α/β interfaces with convex α grains. Figures 4.45(a) to (b) examine the α/β interfaces at these apparent

regions of α/α break-up. In 4.45(a), two α plates(light) are seen separated by interlinked β cusps. The β appears to have twisted suggesting α plate rotation. The β appears concave while the adjoining α is consequently convex in shape and is relatively pointed. Figure 4.45(b) shows two β/α/β boundaries and a distinct β/β boundary connecting the tips of the β/α/β boundaries. Figure 4.45(c) shows increased magnification of the β/α/β interface in Figure 4.45(b) indicating high dislocation density in the α. Dislocation emission was from the α tip and the α/β boundaries indicating possible sliding between α/β boundaries. Finally, 4.45(d) shows two α plates separated by β_{tr}. The α plates have two pairs of pointed interfaces suggesting that at one time they were coupled to eachother as an α/α interface.

Unlike the material with lamellar morphologies, the EQ material demonstrated no subgrain polygonization after strain to 1.0 at 925°C, $5x10^{-4}$ s^{-1}. The α and β morphology remained equiaxed with varied dislocation activity in the bulk lattice. Figure 4.46(a) provides a low magnification brightfield image of the two phase microstructure showing large dislocation networks crossing an α grain between two β_{tr} grains. Figure 4.46(b) and (c) shows a variety of single dislocations in the α grain interior, some bowed out under stress, and others gliding on specific planes. No dipoles were observed. Figure 4.46(c) shows rounded α/β boundaries with possible β interjection along the α/α boundary. The two α grains appear overlapped in the micrograph suggesting accommodation after grain boundary sliding. All of the α/β grain boundaries contain considerable intrinsic dislocations.

An α/α grain boundary in Figure 4.46(d) shows intrinsic grain boundary dislocations(IGBD'd) parallel to the interface. Extrinsic grain boundary dislocations(EGBD's) are seen emanating from the grain boundary at a 45 degree angle to the IGBD's. No dislocation activity was observed on the other side of the α/α grain boundary.

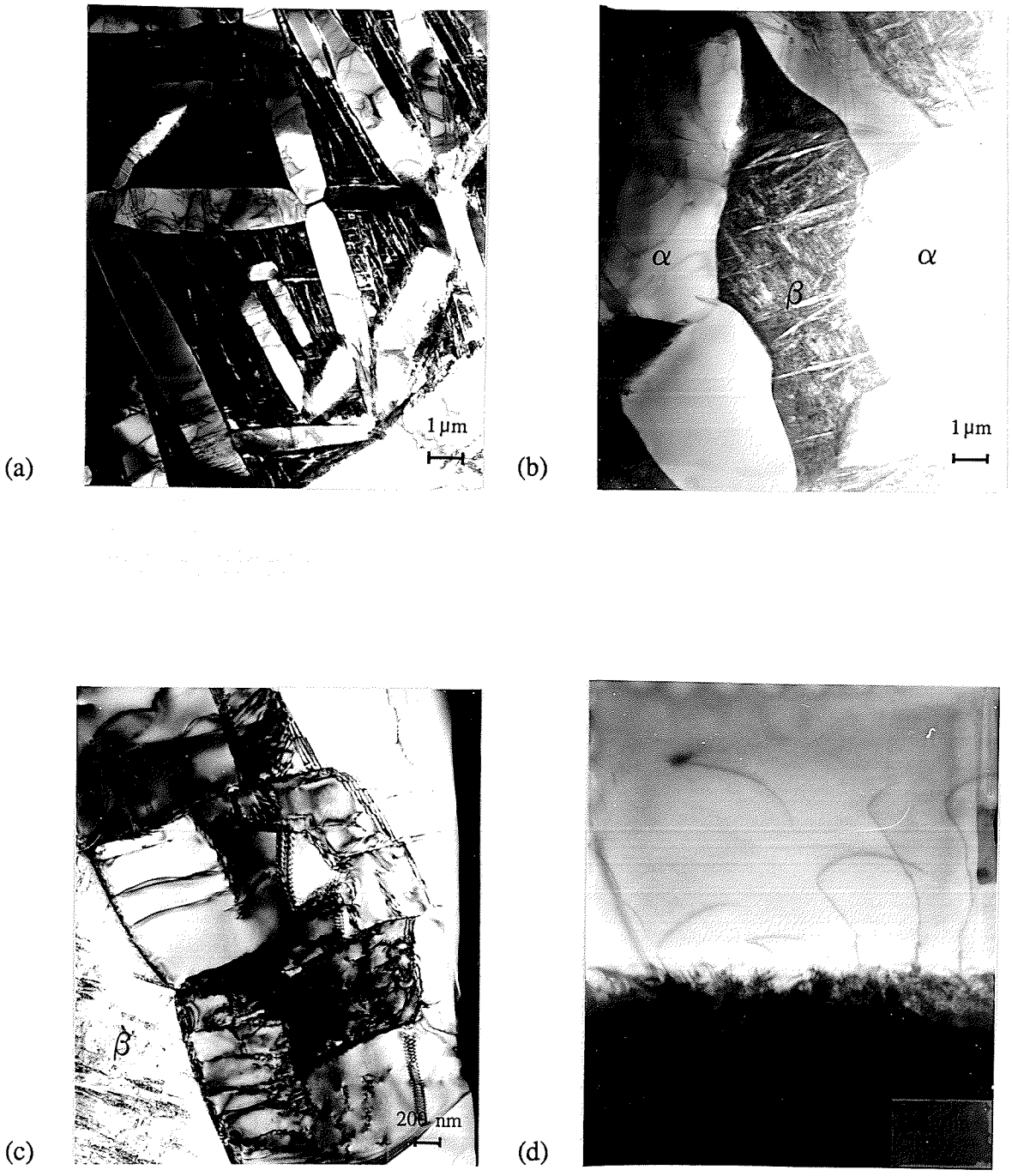

Figure 4.43: TEM micrographs of Ti-6Al-4V alloy with BQ morphology water quenched from 925°C, (a)before deformation, and after deformation to 1.0 strain at $5x10^{-4}$ s^{-1} showing (b)partially cusped α plate in a β_{tr} matrix, (c) α subgrain formation, and (d)α/β interface.

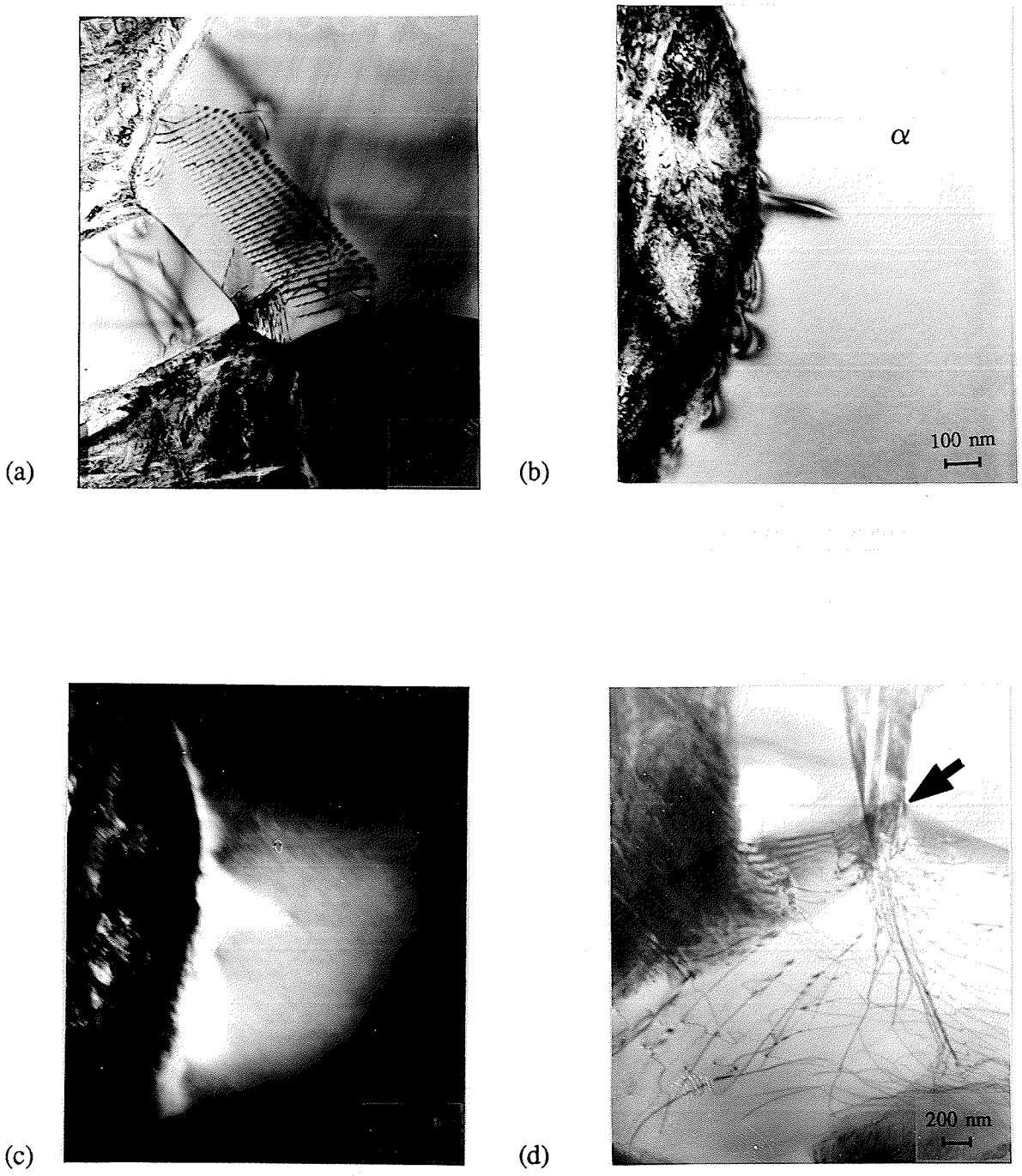

Figure 4.44: Deformed Ti-6Al-4V as in Figure 4.43. (a) Dislocation generation at α/α/β triple point (b)Brightfield and(c)CDF image of earlier stages of β penetration into α. (d) Dislocation generation as β phase interjects along α/α subboundary.

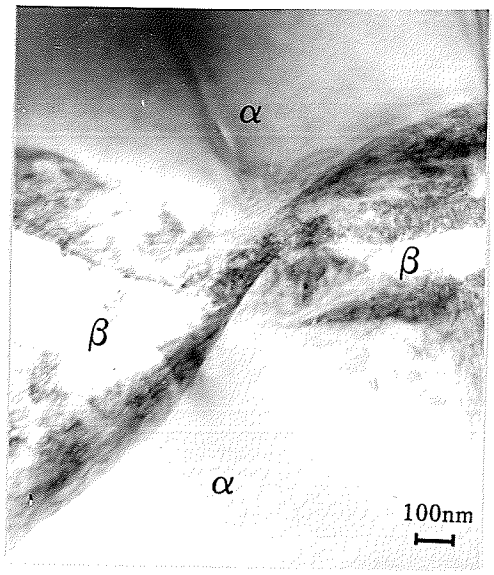

(a)

(b)

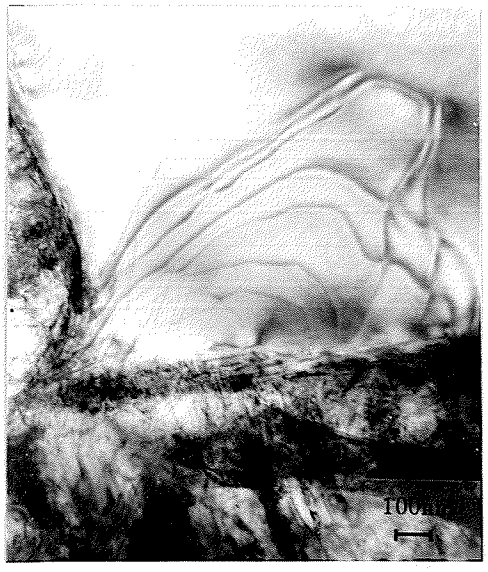

(c)

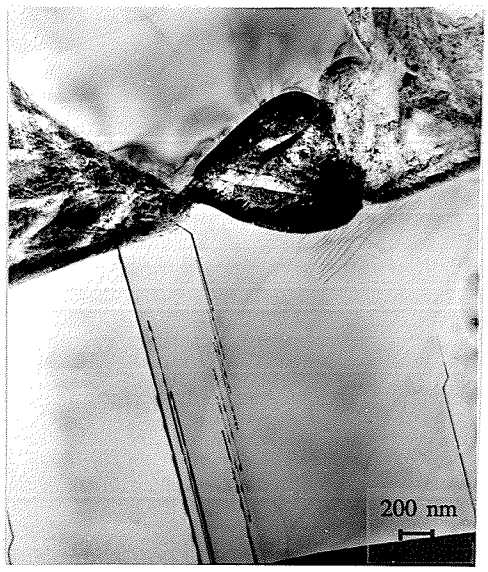

(d)

Figure 4.45: Deformed Ti-6Al-4V as in Figure 4.43 showing(a)β cusp coupling, (b)new β/β grain boundary formed with α/α separation, (c)newly separated α plate α/β grain boundary interaction, and (d)multiple cusping and break-up of α plate.

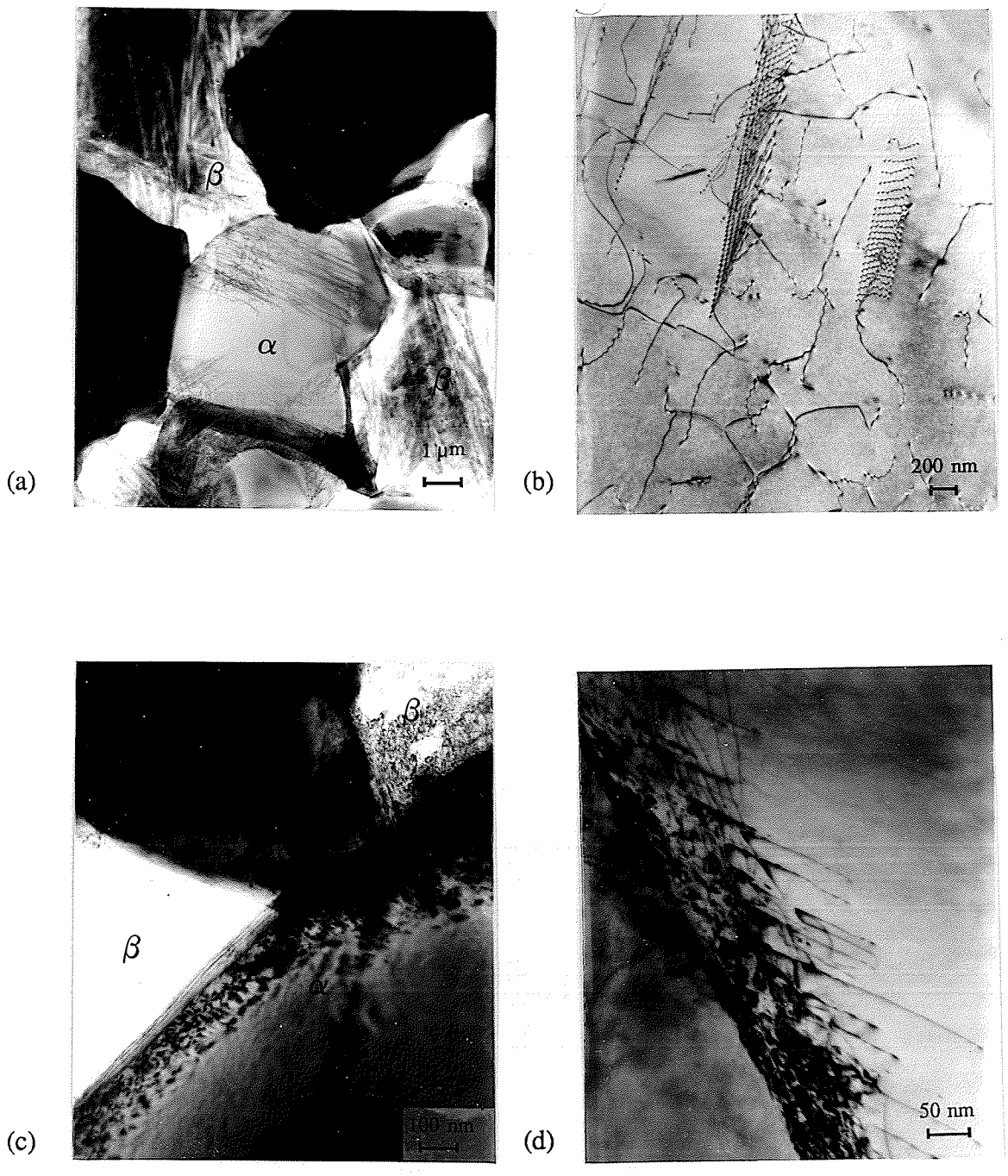

Figure 4.46: TEM micrographs of Ti-6Al-4V alloy with EQ morphology water quenched from 925°C, after deformation to 1.0 strain at $5x10^{-4}$ s^{-1} showing (a) α grains in a β_{tr} matrix, (b)dislocations in α grain interior, (c) α/α overlap, and (d) α/α IGBD's and EGBD's interface.

CHAPTER 5

DISCUSSION

The results obtained by mechanical testing and metallographic examinations will be discussed with emphasis on the lamellar morphologies in order to examine the similarities and differences in their behaviour with material characterized with the EQ morphology at typically superplastic conditions.

5.1 Mechanical Testing

5.1.1 Criteria for Superplasticity

Before discussing the experimental results, it is important to restate the mechanical requirements for superplasticity. The following criteria represents what has been observed to be the most agreed upon parameters in the literature. Superplastic materials are characterized by total elongations greater than 200 percent and m values greater than 0.3. These parameters represent the lower limits of superplasticity.

5.1.2 Continuous Tensile Tests

As proposed in Chapter 3, the purpose of the continuous tensile tests was to determine the general flow characteristics of the Ti-6Al-4V alloy with BA, EQ, and BQ morphologies.

The flow curves followed two apparent patterns: (1) strain hardening; (2) strain softening. It is generally accepted that a specimen subject to ideal superplastic deformation is supposed to exhibit neither strain hardening nor strain softening [79]. The behavior observed in this investigation obviously indicates non-ideal conditions.

Material with BA and BQ morphologies exhibited strain softening at all temperature and strain rate conditions while material with the EQ morphology only strain softened at strain rates of 5×10^{-3} s^{-1}. Microstructural evidence presented earlier indicates that the strain

softening in material with the BA and BQ morphologies can be attributed to break-up of the α plate-like morphology. This includes a redistribution of the β phase resulting in increased β continuity. The refinement of α phase for material with the EQ morphology also applies to strain rates of $5x10^{-3}$ s^{-1}. Strain hardening and strain softening has been reported to occur in Ti-6Al-4V alloy with typically equiaxed α and β phases when tested at the conditions used in this investigation [31,58,82].

The ultimate true stress at fixed temperature decreased with strain rate at all the test temperatures, as shown in Figure 4.13. This trend follows the general relation for flow stress when no strain hardening or softening is present . From equation (2.1) when n is zero,

$$\sigma = k\dot{\varepsilon}^{m} \tag{5.1}$$

which demonstrates a sensitivity of deformation to the strain rate, which is typical of superplastic materials. At the same temperature and strain rate conditions ultimate true stress was highest for the material with the BA and EQ morphologies, respectively.

At constant strain rate the flow stress also demonstrates a temperature dependance that can be used to calculate activation energy, as is discussed in section 5.3. Generally, the ultimate true stress decreased with increasing temperature for material with all morphologies tested, demonstrating a dependency on temperature and increasing volume fraction of β. This behaviour is in agreement with work on equiaxed Ti-Al-V alloys done by Ro *et al.* [58], and with work by Mackay *et al.* [8] on equiaxed Ti-6Al-4V. Figure 5.1 summarizes the variation of ultimate true stress with initial volume fraction of β for the three morphologies at $5x10^{-4}$ s^{-1} observed in this work to the results reported by Mackay *et al.* and Ro *et al.* at strain rates of $4x10^{-4}$ s^{-1} and $6.67x10^{-4}$ s^{-1}, respectively. Mackay's group observed that flow stress reached a minimum when volume fraction of β was 35 percent. Further increase in volume fraction of β resulted in an increase in flow stress. Unfortunately, they did not investigate higher volume fractions of β, because their curve

shows a decrease in flow stress with increased volume fraction of β. Ro *et al.* indicate that the maximum flow stress, which corresponds to the true ultimate flow stress here, decreased with increasing volume fraction of β. They were able to isolate the temperature effect on volume fraction of β by using different overall alloy compositions and all their results are for 900°C.

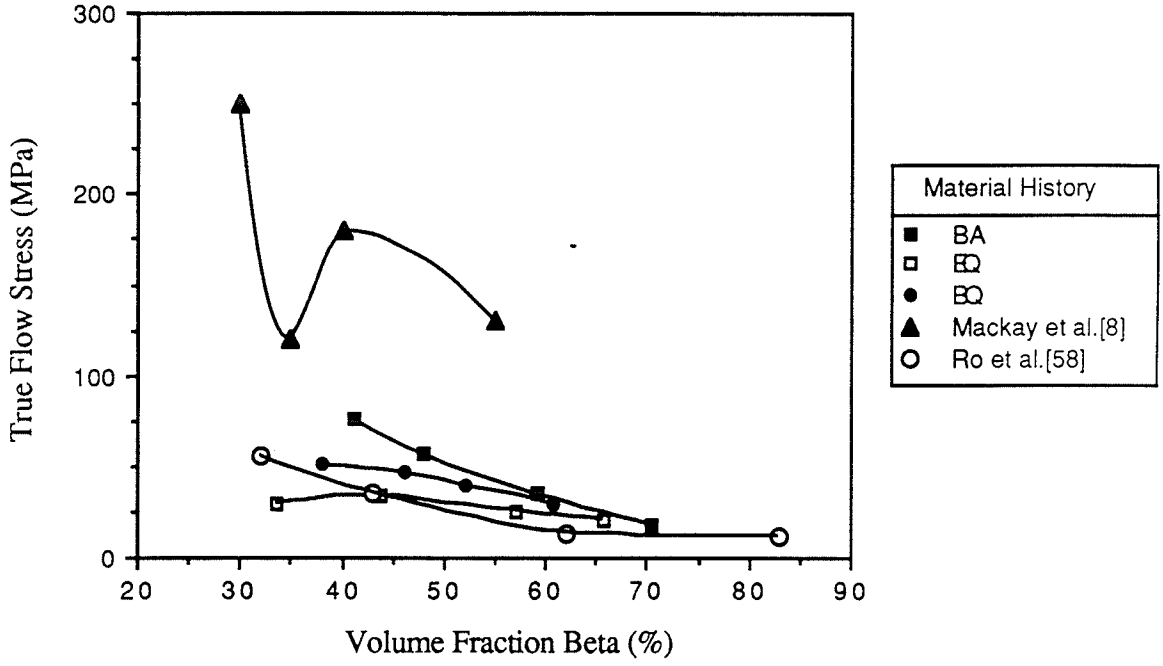

Figure 5.1: Effect of initial volume fraction of β on the true flow stress of (1) Ti-6Al-4V alloy with BA, EQ and BQ morphologies at $5x10^{-4}$ s^{-1}, (2)Ti-6Al-4V at $4x10^{-4}$ s^{-1} [8], and (3) Ti-xAl-xV alloy at $6.67x10^{-4}$ s^{-1}[58].

A linear relationship between flow stress, σ_f, and volume fraction of α, V_α, and β, V_β, would indicate that the material behaves with an iso-strain rate relation, so that

$$\sigma_f = \sigma_\alpha V_\alpha + \sigma_\beta V_\beta \tag{5.2}$$

and,

$$\dot{\varepsilon}_{total} = \dot{\varepsilon}_\alpha = \dot{\varepsilon}_\beta \tag{5.3}$$

where, σ_α = flow stress in α
σ_β = flow stress in β
$\dot{\varepsilon}_{total}$ = total strain rate
$\dot{\varepsilon}_\alpha$ = alpha strain rate
$\dot{\varepsilon}_\beta$ = beta strain rate.

This appears to apply for the 45 to 65 percent β range.

The other important parameter generated from the continuous tensile tests is the total elongation to failure. This parameter expresses the ductility of the material, and is valuable in providing forming limits for actual superplastic forming applications. The total elongation to failure data for material with the EQ morphology demonstrates results similar to those observed in the literature. Maximum elongation to failure occurred in the temperature range of 900°C to 925°C and at a strain rate of $5x10^{-4}$ s^{-1}. This agrees with results obtained by both Hamilton [64] and Jain *et al.* [31]. Overall, though, the highest elongations attained in this work are low when compared to the maximum values presented by Hamilton and to the results generated by Jain et al. on the same apparatus for sheet Ti-6Al-4V specimens. Jain *et al.* achieved elongation values at 900°C, $5x10^{-4}$ s^{-1} greater than 1000 percent. The reasons for the reduced specimen elongations could be due to chemical composition variations, grain size differences, tensile sample shape, and an observed α case on the specimens. Specimens in this study spent one hour at temperature, in the

positive pressure argon chamber, before deformation. It appears that either the increased exposure time or the purity of the commercial argon used in the chamber increased the probability of the α case formation visible in Figure 4.27(a) as a stabilized equiaxed α layer at the surface of the cross-section. Nevertheless, the trends in the variation in percent elongation with temperature are the same as those in the literature, thus indicating the importance of temperature and volume fraction of α and β phases.

The ductility exhibited by the material with the BA and BQ morphologies was noticeably reduced over the complete range of temperature and strain rate. The initial high aspect ratio α morphology directly affected the ductility of the material. When considering the ductility requirement in the superplastic criteria, increasing the initial α aspect ratio lowered the total elongations to failure of the Ti-6Al-4V alloy in one case as low as 135 percent. This behaviour was observed at the 875 and 950°C temperature. Other conditions resulted in elongations greater than 200 percent, indicating that the material met the ductility requirement for superplasticity. It should be noted that elongation to failure measurements should not just include total measurements, but include the uniform and non-uniform portions of the total elongations. The results from Figures 4.19 to 4.26 indicated that the uniformity of tensile sample cross-sectional areas vary considerably with deformation conditions. For any superplastic forming applications, uniformity in formed shapes is critical.

The most important observation from the results is that in the specific temperature - strain rate range of 900 to 925°C - 5×10^{-4} s^{-1}, the maximum ductility was attained regardless of the phase morphology. This is important, because Ti-6Al-4V specimens with morphologies controlled by different hot working histories are then expected to be most ductile at these conditions. This observation also reaffirms the importance of temperature, volume fraction of phase, and strain rate in controlling the overall deformation mechanism.

5.1.3 Strain Rate Sensitivity

The strain rate sensitivity, m , varied with strain for all the tensile tests. Figures 4.15 to 4.18 show that the highest initial m values are attained for the Ti-Al-4V alloy in the EQ condition while the lamellar morphologies exhibit the lowest initial m values. The changes in m can be considered with respect to the strain hardening and softening characteristics. For material with the lamellar morphologies, strain softening was accompanied by an increase in m values with strain. Strain softening in material with the EQ morphology was characterized by both increases or reduction of m values with strain. For material with the EQ morphologies, strain hardening was accompanied by a decrease in m values with strain. TABLE 5.1 summarizes the results of linear regression curve fits on Figures 4.15 to 4.18 by determining the relation between the change in m values with true strain($\delta m/\delta\varepsilon$) and flow softening(S) and hardening(H). The r^2 values represent the sample coefficient of determination, which approximate what fraction of the values considered adhere to a linear fit. The difference in m value behaviour between material with the EQ and the lamellar morphologies indicates that the variation in m is almost satisfactory in predicting the material's tendency to strain harden or soften. At 875 and 900°C-$5x10^{-3}$ s^{-1}, material with the EQ morphology strain softens, but $\delta m/\delta\varepsilon$ is positive. The remainder of the data indicates that $\delta m/\delta\varepsilon$ is positive when the material strain softens and negative when the material strain hardens. If the magnitude of $\delta m/\delta\varepsilon$ and its correlation coefficient are considered, the $\delta m/\delta\varepsilon$ values for material with the EQ morphology are all around 0.0, which indicates little variation of m values with strain. The stability of m represents the stability of the microstructure, and for superplastic flow, grain size stability is usually required[9]. It is therefore expected that the $\delta m/\delta\varepsilon$ values near zero should be reflected in the enhanced ductility of the material, but as will be seen in the next section, the ductility of the material is subject to other considerations. From the observed microstructural changes it can be stated that the break-up and refining of α with increasing strain is reflected by an increase in m values. Consequently, a decrease in m with strain is expected to be due to

TABLE 5.1: Relation between the change in strain rate sensitivity with strain($\delta m/\delta \varepsilon$) and strain hardening(H) and strain softening(S) flow characteristics.

Condition Temp./Morphology	Strain Rate (s-1)	$\delta m/\delta \varepsilon$ (10^{-2})	r^2	S/H
875/BA	$5x10^{-3}$	30	0.767	S
	$1x10^{-3}$	24	0.965	S
	$5x10^{-4}$	21	0.974	S
	$1x10^{-4}$	21	0.920	S
875/EQ	$5x10^{-3}$	1.4	0.070	S
	$5x10^{-4}$	-4.9	0.602	H
	$1x10^{-4}$	-5.4	0.410	H
875/BQ	$5x10^{-3}$	21	0.990	S
	$1x10^{-3}$	26	0.980	S
	$5x10^{-4}$	22	0.921	S
	$1x10^{-4}$	23	0.966	S
900/BA	$5x10^{-3}$	19	0.958	S
	$1x10^{-3}$	28	0.980	S
	$5x10^{-4}$	22	0.988	S
	$1x10^{-4}$	23	0.966	S
900/EQ	$5x10^{-3}$	-1.5	0.167	S
	$1x10^{-3}$	-10	0.697	H
	$5x10^{-4}$	-18	0.986	H
	$1x10^{-4}$	-6.6	0.608	H
900/BQ	$5x10^{-3}$	27	0.975	S
	$1x10^{-3}$	22	0.981	S
	$5x10^{-4}$	26	0.977	S
925/BA	$5x10^{-3}$	7.3	0.881	S
	$1x10^{-3}$	14	0.937	S
	$5x10^{-4}$	17	0.904	S
925/EQ	$5x10^{-3}$	-5.8	0.795	S
	$1x10^{-3}$	-19	0.816	H
	$5x10^{-4}$	-23	0.971	H
925/BQ	$5x10^{-3}$	17	0.976	S
	$1x10^{-3}$	14	0.879	S
	$5x10^{-4}$	27	0.976	S
	$1x10^{-4}$	20	0.929	S
950/BA	$5x10^{-3}$	16	0.934	S
	$5x10^{-4}$	12	0.982	S
	$1x10^{-4}$	16	0.980	S
950/EQ	$5x10^{-3}$	2.5	0.320	S
	$1x10^{-3}$	-19	0.955	H
	$5x10^{-4}$	-24	0.934	H
950/BQ	$5x10^{-3}$	13	0.922	S
	$1x10^{-3}$	11	0.874	S
	$5x10^{-4}$	21	0.962	S
	$1x10^{-4}$	13	0.905	S

grain growth even though no final grain size measurements were made in this study. Both observations have been confirmed by Ma and Hammond [52] and Gurewitz [79] for α/β titanium alloys.

5.1.4 Relation Between Strain Rate Sensitivity and Ductility

Considerable effort has been spent trying to relate strain rate sensitivity to ductility, yet in summaries of material characteristics of superplasticity, both m values and ductility values are usually indicated as prescribed by the superplastic criteria mentioned in section 5.1.1. Therefore, the two are still not synonymous. Generally, the highest ductility is expected for conditions that exhibit the largest m values as shown by the Woodford plot in Figure 2.8. The data generated in this study show that the assumption that m is constant [20] is not always true and the variation of m values with strain must be considered [92].

From the experimentally determined initial m values and the total elongations to failure, it can be shown that they do not determine the overall material ductility. Since m values were observed to vary with strain, some relationship in this variation relates to the total strain. Ghosh and Ayres[43] proposed that the final m near near fracture controls the total elongation. They calculated m values of 0.3 and 0.2 to represent the slower and faster rates of neck formation respectively. The termination of useful flow in ductile materials generally occurs by a process of strain localization during which the load necessary for continued deformation within a neck rapidly falls short of that needed outside the neck and thus leads to failure. From the first m values observed at a true strain of around 10 percent in Figures 4.15 to 4.18, which will correspond to the initial strain rate sensitivity, the material with the BA and BQ morphologies had initial m values ranging from 0.25 to 0.35. Based upon Ghosh and Ayre's work this indicates that necks should have formed at slow to more rapid rates. The necking profiles presented in Figures 4.19 to 4.26 indicate that for material with the BA and BQ morphologies that necks have formed. With increasing strain, the flow softening prevalent in these materials indicate a decrease in

load carrying ability. Nevertheless the m values tend to increase with increasing strain and it can be shown contrary to Ghosh and Ayre, what appears to be the final m value before failure does not determine the final elongation to fracture. Figures 4.16(b) and (c) indicate that for material with the EQ morphology at $5x10^{-3}$ s^{-1}, the final m value has decreased below 0.4, while material with the BQ morphology at the same conditions has a final m value around 0.45. The corresponding elongations to the final m values are 219 and 215, respectively.

It is therefore concluded that the instantaneous value of m influences the rate of neck formation, but in order to relate m values to total elongations the total m value with strain history must be considered. In doing so, the ability to predict total elongations from m values is lost, because the actual strain is being measured. These results indicate that m values appear to be better suited to determine the uniformity of deformation and microstructural evolution.

5.1.5 Validity of Tensile Test Procedure

Observations of instabilities prevalent in the tensile testing of material with the BA and BQ morphologies indicate that the strain rate in the necked region can be greater than that in the overall gauge length, since the reduction in area cross-section at the neck is occurring more rapidly than the bulk of the gauge length. It can be shown that at a time, t, the effective strain rate is expressed as,

$$\dot{\varepsilon}_P \approx \frac{1}{A}\left(\frac{\delta A}{\delta t}\right) \qquad (5.4)$$

where, A = tensile sample cross-sectional area.

The development and growth of external non-uniformities reduces the effective gauge-length, thus increasing the local strain rate. Furthermore, development of a triaxial

stress condition in the neck region may increase the level of flow stress as reported by Sagat and Taplin [93]. Another problem that arises is in the microstructural comparisons after deformation. Break-up of α was observed for material with the BA and BQ morphologies, but near fracture tips the α grain size was qualitatively smaller than that in the gauge length, thus demonstrating possible recrystallization. The actual strain rate is higher in these regions and so the temperature - constant strain rate conditions assumed at the beginning of the test are incorrect for the duration of the test. Cross-section measurements must be made in order to determine the actual strain for the deformed microstructure being considered.

5.2 The Role of α and β Morphology and Volume Fraction in Ti-6Al-4V Alloy During Superplastic Deformation

The experiments performed were designed to determine the role of morphology of α and β phases on superplasticity of the Ti-6Al-4V alloy for fixed volume fractions of α and β.

5.2.1 Starting Microstrucures

It was observed that the volume fraction of α and β controls the grain size in material with the EQ morphology. An increase in intrinsic treatment temperature, before deformation, (1) increased the volume fraction of beta phase, (2) increased the grain size of the β phase, and (3) had little effect on the α grain size. These observations are in agreement with the work done by Ro *et al.* [58] if the total grain concept is used. Using the total grain concept, Ro *et al.* reported that the average grain size over the whole alloy is a minimum when the volume fraction of α and β phases is equal. The average grain size is expressed as the sum of the mean sizes of the phases multiplied by the fraction of the phases. When this calculation is made for the material with the EQ morphology, the

average grain sizes for 66.3, 56.2, 43.0, and 34.2 percent α are 5.06, 3.95, 3.99, and 9.16 μm, respectively.

For material with the BA and BQ morphologies, no β phase measurements were made so the total grain concept can not be applied to the measured aspect ratios. Generally, for material with the BQ morphology, the α aspect ratios and plate thicknesses remained similar regardless of the volume fraction of α and β, which corresponds to the behaviour observed for α grain size in the EQ material. Material with the BA morphology was characterized by an α plate that was about two and a half times thicker than for the material with the BQ morphology, while the corresponding aspect ratios were relatively similar.

5.2.2 During Deformation

The volume fraction measurements made for the special deformation case of 925°C, 5×10^{-4} s^{-1} to an actual true strain of 1.0 indicated that the β volume fraction remained constant for the material with the EQ morphology but increased slightly for material with the BA morphologies, and increased considerably for material with the BQ morphology. The reported thermodynamic instability for plate-like microstructures [87] could be responsible for the increase in the β volume fraction.

The tendency for the material with the lamellar morphologies to break-up depends upon the cusp penetration rate, which appears to vary with temperature, volume fraction of α and β phases, and α plate thickness. This agrees with the observations made by Weiss *et al.* [33] who linked the cusp penetration rate to the diffusion of the alloying elements aluminum and vanadium through the volume or along the interfaces. The alloying element diffusion is definitely a function of both the α and β volume fraction and temperature. The best indicator to establish the effect of diffusion is the activation energy.

5.3 Activation Energy

The apparent activation energy, Q, can be calculated to evaluate the rate controlling mechanisms during deformation. Figure 4.13 illustrates the variation of true ultimate stress with strain rate at various temperatures. Figures 4.15 to 4.18 demonstrate the variation of m with strain. This data is now applied to equation 2.4 to evaluate the temperature dependence of deformation with constant strain rates. Figure 5.2 shows the Arrhenius plots constructed for material with the BA, EQ and BQ morphologies tested at $5x10^{-4}$ s^{-1}. TABLE 5.2 summarizes the apparent activation energy values for all the strain rate conditions. The results indicate three distinct ranges of values for material with the three distinct morphologies: (1) BQ, 100 kJ/mol; (2) BA, 125 to 200 kJ/mol; (3) EQ, 200 to 300 kJ/mol.

For material with the EQ morphology, the apparent activation energy values ranged from 192 to 274 kJ/mol. These values fall into the range of 223 to 298 kJ/mol calculated by Arieli et al.[78] for Regime II at various strains.

For material with the BA morphologies, the Q value peaks at 183 kJ/mol for a strain rate of $5x10^{-4}$ s^{-1}, which was the strain rate maximum ductility was observed. This value is close to the minimum Q value attained by material with the EQ morphology at $5x10^{-3}$ s^{-1}. It should also be noted that at these conditions material with both morphologies displayed similar total elongation values in the 200 percent range, and both exhibited long cavitaties parallel to the tensile axis.

Material with the BQ morphology behaved anomalously, when compared to the other two morphological states. It was observed that the maximum ductility attained by material with the three morphologies occurred at a strain rate of $5x10^{-4}$ s^{-1}, but the corresponding Q values for this strain rate were usually higher than at lower or higher strain rates, when the material had BA or EQ morphologies. For material with the BQ morphology, the Q value at $5x10^{-4}$ s^{-1} achieved a minimum of 81.3 kJ/mol. This suggests a different operating mechanism during deformation for material with the BQ morphology.

TABLE 5.2: Summary of the Apparent Activation Energy Values, Q for the Ti-6Al-4V Alloy with BA, EQ, and BQ Morphologies at Constant Strain Rates

Morphology	BA	r^2	EQ	r^2	BQ	r^2
Strain Rate(s^{-1})	(kJ/mol)		(kJ/mol)		(kJ/mol)	
$5x10^{-3}$	158	0.994	192	0.923	122	0.984
$1x10^{-3}$	139	0.998	274	0.940	101	0.975
$5x10^{-4}$	183	0.990	249	0.933	81.3	0.935
$1x10^{-4}$	148	0.980	-	-	101	0.992

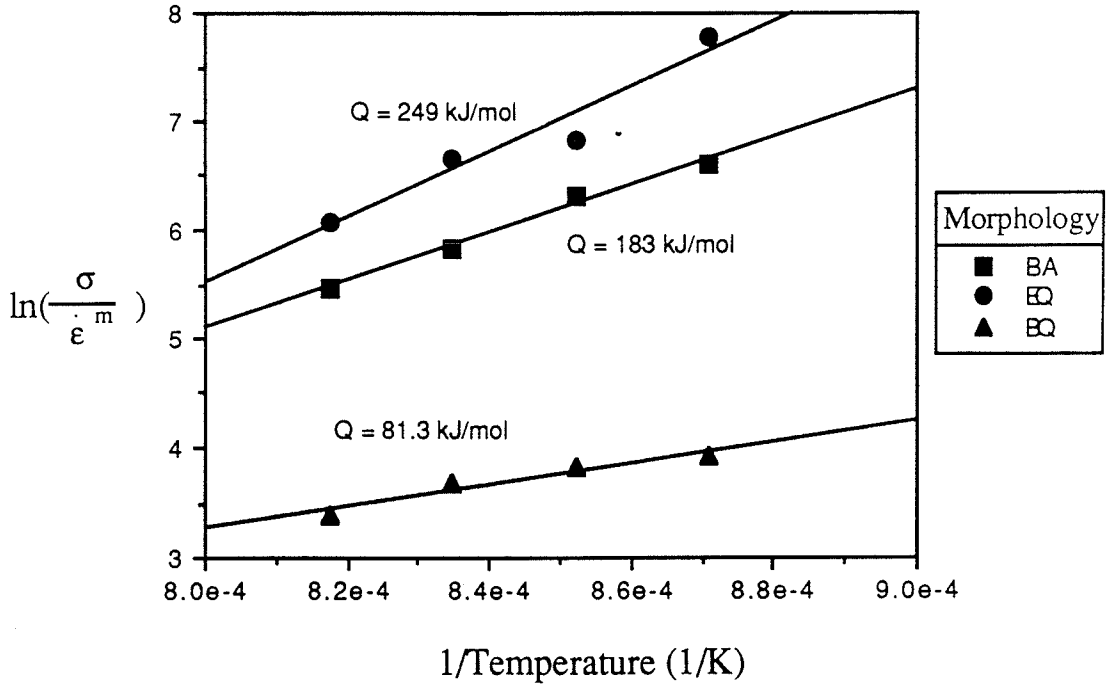

Figure 5.2: Apparent Activation Energy(Q) for Ti-6Al-4V alloy with BA, EQ, and BQ morphologies at a constant strain rate of $5x10^{-4}$ s^{-1}.

The relative relation of the Q values to various deformation mechanisms for Ti-6Al-4V has been presented in the literature and it is informative to use these values in interpreting the results presented here.

The base Q values from which all comparisons are made are the activation energies for self-diffusion in the α and β phases of superpure titanium. Dyment and Libanati [94] determined the activation energy values for self-diffusion in the α and β phases to be 169.147 and 152.818 kJ/mol, respectively. Malcor and Montheillet [49] calculated Q values for Ti-6Al-4V with equiaxed and lamellar morphologies in the hot working range of $5x10^{-3}$ to 5 s^{-1}. They obtained Q values from 546 to 600 kJ/mol which were similar to the results obtained by Sastry *et al.* [82] for equiaxed Ti-6Al-4V. Their conclusions were that dynamic recrystallization was occurring. Hamilton [64] stated that activation energy values for grain-boundary self diffusion, expected to be part of the accommodation mechanism during grain boundary sliding, should be lower than those determined for self-diffusion in the α and β phases.

So based upon the literature, Q values determined for material with the BQ morphology are low enough to signify grain boundary self diffusion. Material with the BA morphology had Q values in the range expected for lattice self diffusion. Finally, material with the EQ morphology had Q values typical of superplastic deformation [78]: higher than that reported for lattice self-diffusion, but lower than those observed for dynamic recrystallization. The TEM work performed in this investigation should be able to support the inferences made by the Q value determination, only if the literature is correct and if Q can be determined experimentally in the manner it was.

TEM work indicates that material with the BA morphology undergoes α plate break-up, characterized by both β cusping of α-plates and by dynamic recovery of α, as evidenced by the observation of polygonized α and dislocation free α grains. The degree of α break-up is considerably more for material with the BQ morphology, which is characterized by thinner plates than the material with the BA morphology. TEM

observation showed that β cusping of α plates and α subgrain formation were also characteristic of deformation of this material, but the observed number of cusps formed was considerably higher than for material with the BA morphology. As well, extensive αββ dislocation activity emphasizes the role of the grain boundary during deformation such that apparent α/β grain sliding is accompanied by αββ triple point dislocation emission. The dislocation motion would accommodate the grain boundary sliding [31]. Finally, for material with the EQ morphology the TEM work showed α developed dislocations in its grain interior and at α/α grain boundaries, but no polygonization was seen. Optical and scanning electron microscopy indicated that appearance of β between α/α grains is reflected in the observed increase in continuity of the β after deformation. The higher activation energies for the material with EQ morphology suggest that dynamic recrystallization should occur, but this is not so. It in fact appears that the interpretation of the observed Q value for material with the EQ morphology is difficult, because more than one deformation mechanism could be operating. Since the material with EQ morphology did demonstrate increased connectivity of β, similar to the interjection of β along α/α subgrains in material with the BQ and BA morphologies, it indicates that the overall accommodation mechanism for the deformation of EQ could be due the superposition of grain boundary diffusion and some dislocation mechanism. The evidence indicates that dislocation slip, observed across the α phase in the three material morphologies, could be the mechanism. Determining which process is rate controlling depends upon what stage the phase morphology is at during its evolution to a more equiaxed state [96].

5.4 Similarities Between Alpha Plate Break-up and Reported Beta Continuity After Superplastic Deformation

5.4.1 Observations

According to the results of the TEM analysis, the high aspect ratio α plates in material with the BA and BQ morphologies undergo break-up by beta cusping and dynamic recovery. Since grain boundary sliding is such an essential aspect of superplasticity, high

aspect ratio α-plates will affect the grain boundary sliding. If grain boundary sliding is deterred, then the ductility inherent in superplastic properties will also be deterred. The apparent difference between the material with the lamellar morphologies and material with the EQ morphology is that for grain boundary sliding to occur, high aspect ratio α plates must first develop α/α suboundaries that enhance α break-up by β penetreation along these boundaries. This initial step is not necessary for material with the EQ morphology, because α/α grain boundaries already exist. The β phase can therefore interject along these boundaries without having to wait for their formation. This accounts for the increase in β continuity for material with the BA, EQ, and BQ morphologies reported here, and by others[32,58,64,79], after superplastic flow of Ti-6Al-4V. The similarity in behaviour between material with the plate and EQ morphologies is further strengthened by two topological models which will be considered next.

5.4.2 Topological Explanation for Alpha Break-up

Weiss *et al.* [33] identified two mechanisms responsible for the break-up of α plates under forging conditions. One was characterized by β penetration along α/α sub boundaries, while the other was characterized by β penetration along heavily sheared zones in the α plate. Figure 5.3 demonstrates how the β phase forms shallow cusps at α/α grain boundaries with relatively low misorientation, and deep cusps at high angle boundaries. The depth of β penetration depends upon the plate thickness, with thinner plates(1 to 3 μm) separating more readily. They expressed the angle of cusp penetration as a function of the α/α and α/β interfacial energies as follows:

$$\frac{\gamma_{\alpha/\alpha}}{\gamma_{\alpha/\beta}} = 2\cos\theta. \qquad (5.5)$$

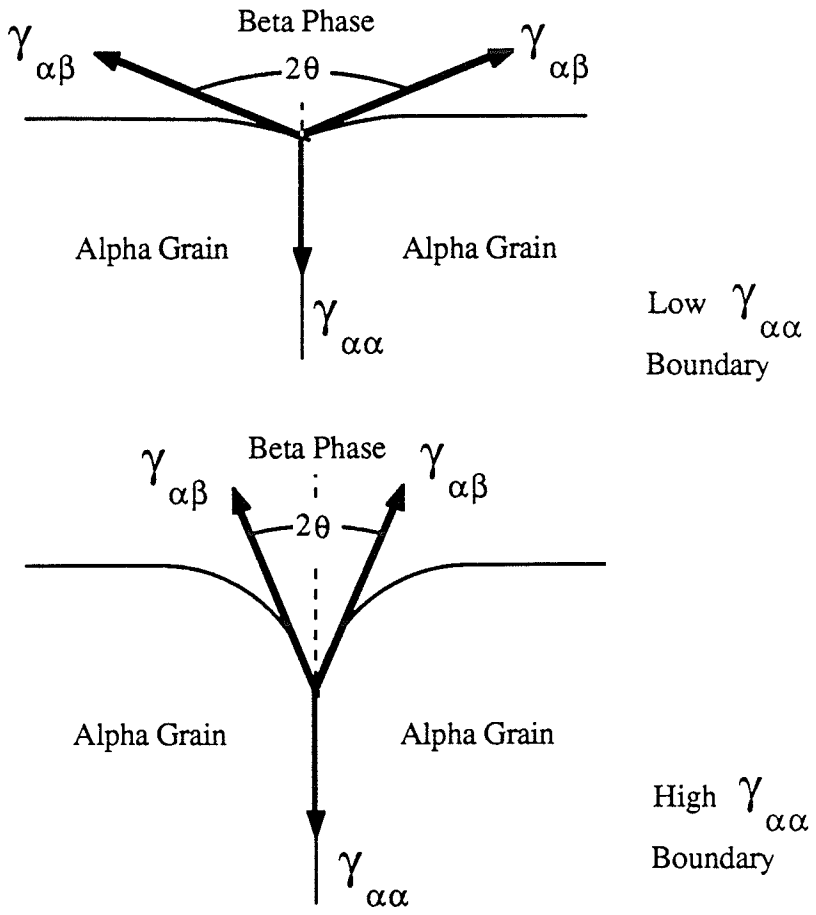

Figure 5.3: Illustration of the influence of the α/α interface energy on the penetration of beta phase into alpha grain boundaries [33].

These observations are similar to a model presented by Springarn and Nix [95] for the deformation of equiaxed two phase alloys at superplastic conditions. They modified the Ashby-Verall model by considering the traction developed across the grain boundaries. Figure 5.4 shows how their model predicts the interphase boundary shapes of a two phase alloy. The faster diffusing phase would become curved and eventually "pinch off" and separate the grains of the slower diffusing phase. The similarity between the Figures 5.3 to 5.4 is obvious, but what is not included in either model is the final step in the α phase separation. The SEM and TEM observations in this study provide the basis to qualitatively modify the models just presented in order to consider this final step.

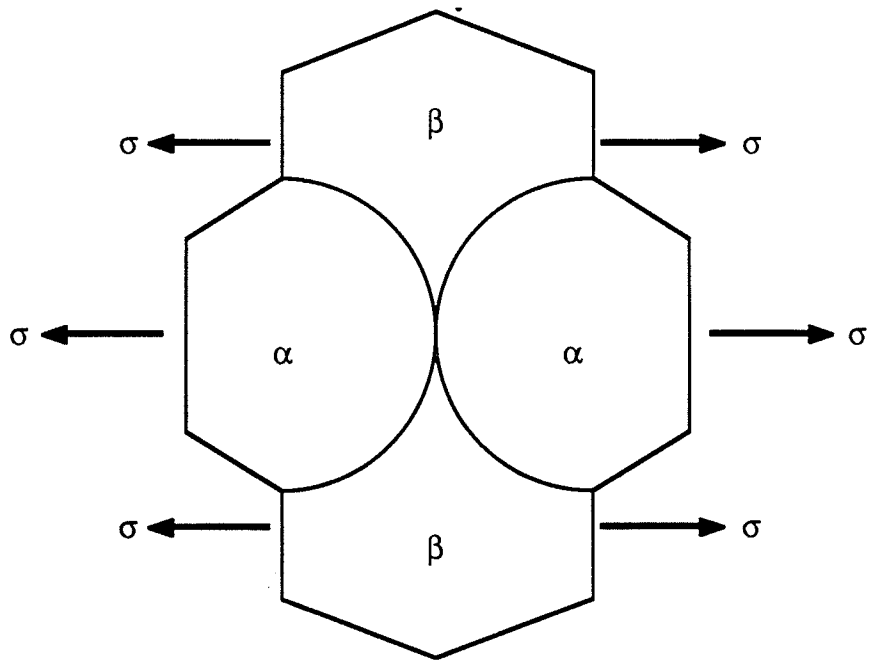

Figure 5.4: Two phase undergoing diffusional creep, showing pinching of α grains by the higher diffusive β phase[95].

5.4.3 Modification of Topological Models to Fit Observed Data for α Plate Break-up

The SEM and TEM observations indicate that initially α plate break-up follows the pattern demonstrated by Weiss *et al.* [33]. Beta phase penetration occurs along α/α sub boundaries, and complete separation of the α phase occurs. Two different models can be proposed based upon two different, but plausible, interpretations of the final separation

Figure 5.5(a) is a biaxial representation of an α plate undergoing β cusping from two sides. During this action it must be noted that the entire material has an applied load on it. Further penetration of the β occurs until just before a point of instability is reached as shown in Figure 5.5(b). Instability occurs when the α phase under traction begins to deform faster than β. This is illustrated in Figure 5.5(c), and was experimentally observed in TEM as ilustrated in Figure 4.45(a). This stage of deformation resembles Ashby and Verall's saddle point configuration, shown in Figure 2.11(b). Final α/α separation illustrated in Figure 5.5(d), and experimentally observed and illustrated in Figure 4.45(b) shows a new β/β grain boundary, as expected from Ashby and Verall's model in Figure 2.11(c). It should be noted that the α phase now has a pointed interface that can restrict α/β grain boundary sliding.

Another possible explanation can be given if one considers a triaxial representation of the α/β interaction. Figure 5.6 is a schematic of the field observed and illustrated in Figure 4.45(d). Figure 5.6 represents the final configuration of separated α/α filled by three β grains emerging from another plane to fill the space created by the α/β sliding. These observations prescribe in part to Gifkins' model presented in section 2.5.2, where the emerging grains are characteristically round. This also accounts for the pointed α phase boundaries and the new β/β boundaries predicted by the first model illustrated in Figure 5.5.

In summary, initial TEM observations suggest that qualitatively, both modified explanations for α break-up at the conditions tested appear probable. Each of the modified models share a common topological feature with either Ashby and Verall's diffusion based

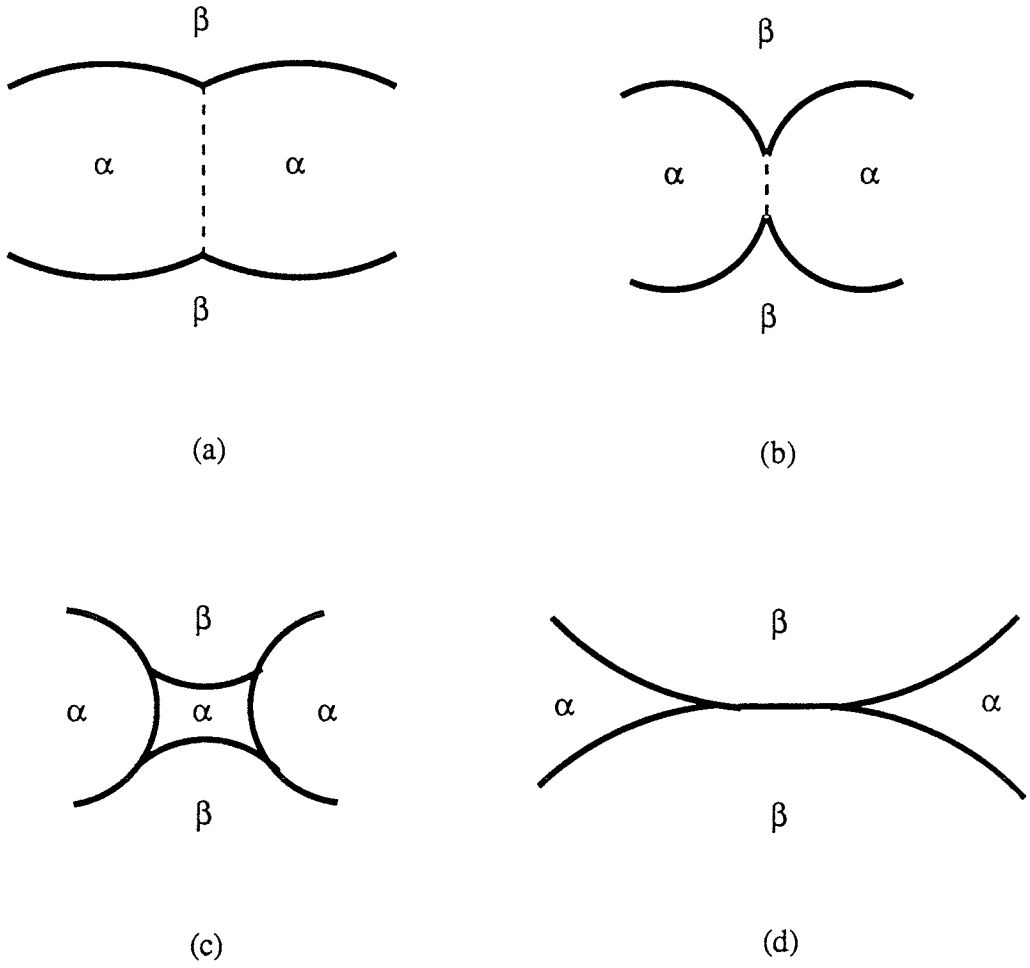

Figure 5.5: Modified model for the break-up of an α plate. (a) β penetrates along an α/α sub boundary; (b) until a noticeable β cusp forms. (c) At some stage in the deformation the α plate with reduced thickness begins to deform before the β completely pinches it off.(c) The final configuration consists of a β/β grain boundary perpendicular to the two new α grains.

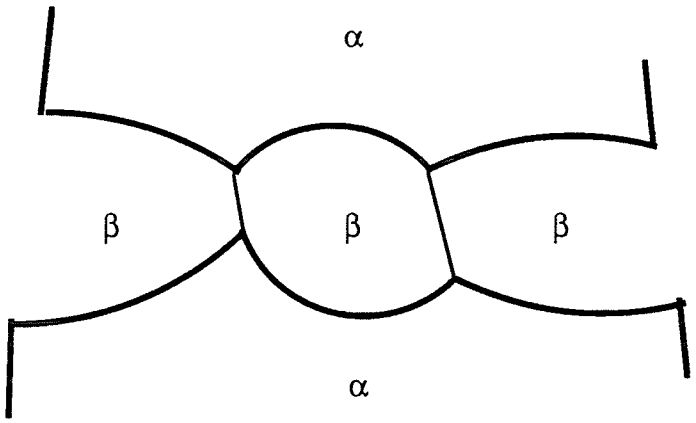

Figure 5.6: Alternative final configuration for α/α separation that is due to emergence of three β grains .

model or Gifkins' dislocation based model, suggesting that common features could be borrowed from each to explain the overall behaviour observed here. The importance of the findings lie in the observed tendency of the α plates to become more equiaxed and the β phase to become more continuous during deformation. This behaviour was observed to be enhanced at the specific temperature - strain rate conditions of 900/925°C - $5x10^{-4}$ s^{-1}. The literature indicates that during superplastic deformation of equiaxed Ti-6Al-4V alloy, the α grains remain equiaxed and β becomes more continuous. This can be restated to infer that the grains tend to this equiaxed state during deformation. Gifkins proposed that to remain equiaxed it is not necessary for dislocations to migrate across a grain during superplastic deformation [85]. For a non-ideal material, it is expected that not all grains are equiaxed at any one time, and so dislocations are expected to cross these grains. Dislocations were observed crossing the grain interiors of material with the EQ, BA and BQ morphologies in the TEM study. It thus appears then that the mechanisms operating during α phase separation for the BQ and BA morphologies also operate during deformation for the EQ

morphology. This includes grain boundary diffusion and dislocation slip. The evolution of the microstructure to an equiaxed one determines which mechanism is controlling the plastic flow. The apparent activation energy values for the Ti-6Al-4V alloy with the three morphologies suggest that for each morphology, varying proportions of different mechanisms are operating at the same temperature - strain rate conditions. This explains the differences in the observed mechanical properties and supports the belief that multiple mechanisms are needed to accommodate grain boundary sliding, but the morphology of the Ti-6Al-4V phases determines the contribution from each mechanism.

CHAPTER 6
CONCLUSIONS

The effect of morphology of α and β phases on the superplastic properties of the Ti-6Al-4V alloy has been investigated. It has been shown that the superplastic properties, specifically flow stress, total elongation and strain rate sensitivity can be altered substantially in Ti-6Al-4V alloy by beta processing before deformation in the temperature - strain rate range of 875 to 950°C - $5x10^{-3}$ to $1x10^{-4}$, respectively. In particular, the results of the tensile testing show that increasing the α aspect ratio from 1.5 to the 10 to 20 range (1)increases the ultimate true stress, (2)usually reduces the total elongation to failure, and (3)reduces the initial strain rate sensitivity to about 0.3. The plastic flow was characterized by strain hardening in material with the equiaxed α–β morphology and strain softening in material with the plate-like α phase. Strain softening was also observed in the equiaxed material at $5x10^{-3}$ s^{-1}. Constancy of strain rate sensitivity with strain is characteristic of no strain hardening or softening. The strain rate sensitivity as determined provides a measure of the tendency for instabilities to form, but does not immediatly present a direct relation to overall ductility. The optimum temperature-strain rate conditions for the superplastic deformation of the Ti-6Al-4V alloy tested is 900 to 925°C - $5x10^{-4}$ s^{-1}. This is supported by the observation that regardless of the α and β phase morphology, the largest total elongation was attained at these conditions.

The apparent activation energy value associated with the superplastic flow of the equiaxed Ti-6Al-4V of 192 to 274 kJ/mol are in agreement with those attained by Arieli and Rosen [78] for similar condiitons. Apparent activation energy values for the deformation of the material with the BQ (81.3 to 122 kJ/mol) and BA(139 to 183 kJ/mol) indicate grain boundary diffusion and lattice self diffusion, respectively.

Microstructural evidence indicate that α plate break-up occurs for materials with high aspect ratio plates by β phase penetration along α/α subboundaries. During

deformation the β becomes more continuous. Experimental evidence indicates that the 1.0 μm thick α plates characteristic of the BQ material become equiaxed more readily than the 3.0 μm α plates characteristic of the BA material.

TEM observations after deformation at 925°C - $5x10^{-4}$ s^{-1} to an actual true strain of 1.0 indicated that β penetration contributes to α break-up, which mechanically accounts for the measured decrease in true stress and the increase in strain rate sensitivity with strain. Topological models for superplastic deformation are similar to the β cusp penetration-separation model proposed by Weiss *et al.* [33] for forging conditions. TEM observation suggested that these models could be qualitatively modified to account for two interpretations of the complete α/α separation. It appears that the similar topographical features but differing mechanical properties evident during deformation at specific temperature - strain rate conditions indicate that grain boundary diffusion, dislocation slip and grain boundary sliding operate, such that the contribution of each is dependant upon the phase morphology.

CHAPTER 7
RECOMMENDATIONS FOR FURTHER STUDY

The work presented in this thesis provide, the basis to make suggestions for further study.

The deformation of Ti-6Al-4V alloy with lamellar phase morphology at typically superplastic temperature and strain rate conditions results in noticeable break-up of the α plates. What is not really known is the quantitative effect of the break-up of the α phase, specifically the change in aspect ratio, on the true stress and strain. Interrupted tensile tests could be run to fixed strains at which time the tensile specimens could be water quenched under load.

During the tensile testing it appeared that most material with lamellar α plates experienced a major instability at about 10 percent true strain. The continued strain is then characterized by development of a more equiaxed microstructure during the remainder of deformation. It would be interesting to (1) determine the microstructural source of the instability and (2) see if the overall superplastic properties could be improved. A suggestion is to prestrain the tensile samples at an initial strain rate typical of Regime III to a strain just before strain softening occurs , stopping the test to allow for static grain refinement, and then continuing the deformation.

One final suggestion is to use the data generated here to investigate the validity of the models used successfully by Paton and Hamilton [11], Ghosh and Hamilton [23], and Wert and Paton [18] to predict the large strain behaviour of Ti-6Al-4V. Their work focuses on equiaxed microstructures, but it is qualitatively understood from their models that increases in aspect ratio should decrease the superplastic properties.

REFERENCES

1. F. Hargreaves, J. Inst. Metals, 39 (1928) 301-327.
2. F. Hargreaves and R.J. Hill, J. Inst. Metals, 41 (1929) 257-283.
3. C.M.H. Jenkins, J. Inst. Metals, 40 (1928) 41-54.
4. C.E. Pearson, J. Inst. Metals, 41 (1929) 257-283.
5. E.E. Underwood, J. Metals, 14 (1962) 914-919.
6. T.G. Langdon, Met. Trans., 13A (1982) 689-701.
7. J.W. Edington, Met. Trans., 13A (1982) 703-715.
8. W.D. Nix, "Superplastic Conference Proceedings" edited by S.P. Agrawal, publ. ASM (1984) 3-12.
9. C.H. Hamilton, A.K. Ghosh, and J.A. Wert, Metals Forum, vol.8, no.4 (1985) 172-190.
10. J. Pilling and N. Ridley, "Superplasticity in Crystalline Solids", publ. by the Institute of Metals (1989).
11. N.E. Paton and C.H. Hamilton, Met. Trans., 10A (1979) 241-250.
12. W.G. Johnston and D.F. Stein, Acta Met., 11 (1963) 317-318.
13. D.L. Holt and W.A. Backofen, ASM Trans. Quart., 59 (1966) 755-768.
14. W.A. Backofen, I.R. Turner and D.H. Avery, ASM Trans. Quart. 57 (1964) 980-990.
15. F.A. Mohamed, S.Shei, and T.G. Langdon, Acta Met., 23(1975) 1443-1450.
16. B.P. Kashyap, A. Arieli and A.K. Mukherjee, Journal of Materials Science,20(1085) 2661-2686.
17. A.K. Ghosh, "Superplastic Conference Proceedings" edited by S.P. Agrawal, publ. ASM (1984) 23-31.
18. J.A. Wert and N.E. Paton, Met. Trans., 14A(1983) 2535-2544.
19. M. Peters , P.J. Winkler and W. Bunk, Ti-'84 Conference: Munich, FRG, AIME(1984) 681-688.
20. P. Griffiths and C.H. Hammond, Acta Met., 20 (1972) 935-945.
21. D. Lee and W.A. Backofen, Transactions of the Metallurgical Society of AIME, 239 (1967) 1034-1040.

22. M.E. Rosenblum, P.R. Smith and F.H. Froes, Ti-'80 Conference, ed. by H. Kimura and O. Izumi, publ. AIME, (1980) 1015-1024.

23. A.K. Ghosh and C.H. Hamilton, Met. Trans., 10A (1979) 699-706.

24. C. Hammond and J. Nutting, Met. Sci. Journal, 10 (1977) 474-490.

25. P.A. Farrar and H. Margolin, Transactions of the Metallurgical Society of AIME, 221 (1961) 1214-1221.

26. P.J. Fopiano, M.B. Bever and B.L. Averbach, Trans. of the ASM, 62 (1969) 324-332.

27. J.C. Williams and E.A. Starke Jr., "Deformation, Processing, and Structure", ed. by G.Krauss, publ. ASM, (1982) 279-354.

28. G. Sridhar, R. Gopalan, and D.S. Sarma, Metallography, 20 (1987) 291-310.

29. E.W. Collings, "The Physical Metallurgy of Titanium Alloys", publ. ASM (1984) 90.

30. B. Diak, this work.

31. M. Jain, M.C. Chaturvedi, N. Richards and N. Goel, Mater. Sc. Eng.,(In press).

32. K. Ito, T. Morimoto, S. Takemoto, and N. Niwa, Kobe Steel Report, 47 (1988) 219-224.

33. I. Weiss, F.H. Froes, D. Eylon and G.E. Welsch., Met. Trans., 17A (1986) 1935-1947.

34. M.T. Cope and N. Ridley, Material Science and Technology, 2 (1986) 140-145.

35. A.K. Ghosh and C.H. Hamilton, Met. Trans., 13A (1982) 733-743.

36. C.H. Hamilton and A. K. Ghosh, Ti-'80 Conference, ed. by H. Kimura and O. Izumi, publ. AIME, (1980) 1001-1014.

37. N. Furushiro and S. Hori, Ti-'80 Conference, ed. by H. Kimura and O. Izumi, publ. AIME, (1980) 1061-1070.

38. R.G. Sherman and H.D. Kessler, Trans. of the ASM, 48 (1956) 657-675.

39. J. C. Williams and M.J. Blackburn, Trans. of the ASM, 60 (1967) 373-383.

40. C.G. Rhodes and J.C. Williams, Met. Trans., 6A (1975) 1670-1671.

41. C.G. Shelton and B. Ralph, "The Metallurgy of Light Alloys" (1983) 180-183.

42. A.Arieli, B.J. Maclean and A.K. Mukherjee, Res Mechanica 6(1983) 131-159.

43. A.K. Ghosh and R. Ayres, Met. Trans. 7A(1976) 1589-1591.

44. A.K. Ghosh and R. Raj, Acta Met., 29(1981) 607-616.

45. A.H. Choski and A.K. Muherjee, Met. Trans., 19A (1988) 1621-1624.

46. D.S. McDiarmid, A.W. Bowen and P.G. Partridge, Materials Science and Engineering, 64(1984) 105-111.

47. B.P. Kashyap and G.S. Murty, Trans of the Japan Inst. of Metals, vol.22, no.4 (1981) 258-266.

48. F.H. Froes and W.T. Highberger, Journal of Metals, May(1980) 57-64.

49. J.G. Malcor and F. Montheillet, MST(1988) 399-404.

50. C.C. Chen and J.E. Coyne, Met. Trans., 7A(1976)1931-1941.

51. N Paton, Journal of Engineering Materials and Technology, Oct.(1975)313-315.

52. J. Ma and C. Hammond, Journal of Material Science, 21(1986) 475-487.

53. S.Sagat and D.M.R. Taplin, Acta Met. 24 (1976) 307-315.

54. D.S. Wilkinson and C.H. Cáceres, Acta Met. 32 (1984) 1335-1345.

55. M.M. Farag and G. Piatti, Mat. Sci. and Eng., A123 (1990) 271-280.

56. Y. Maehara and Y Ohmori, Met. Trans., 18A (1987) 663-672.

57. C.H. Cáceres and D.S. Wilkinson, Acta Met. 32(1984) 415-422.

58. Y. Ro. et al. Trans. ISIJ, 26 (1986) 322-327.

59. G. Heriot, B. Baudelet and J.J. Jonas, Acta Met. 24 (1976) 687-694.

60. J. Gurland, Transactions of the Metallurgical Society of the AIME, 212(1958) 452-455.

61. D. Hull and D. J. Bacon, "Introduction to Dislocations, 3e"Permagon Press: Toronto (1984) 112.

62. S. Furishiro and S. Nadiv, Ti-'80 Conference, ed. by H. Kimura and O. Izumi, publ. AIME, (1980) 899-906.

63. M. Peters and G. Luetjering, Ti-'80 Conference, ed. by H. Kimura and O. Izumi, publ. AIME, Warrendale(1980) 925-935.

64. C.H.Hamilton, "Superplastic Conference Proceedings" edited by S.P. Agrawal, publ. ASM (1984) 13-22.

65. C.D. Ingelbrecht, D.S. Mcdiarmid and A.W. Bowen, Royal Aircraft Establishment, Technical Report 86502, August(1986).

66. T.Nishimura, Y. Sugimura, Y. Ito and H. Kusamichi,Ti-'80 Conference, ed. by H. Kimura and O. Izumi, publ.AIME, (1980) 973-979.

67. J. Belzunce and M. Suéry, Scripta Met., 15 (1981) 895-898.

68. J. Lian and B. Baudelet, Scripta Met. 21(1987) 331-334.

69. J.W.D, Patterson and N. Ridley, Journal of Metals Science, 16 (1981) 457-464.

70. D.M.R. Taplin and T. Chandra, Journal of Material Science 10 (1975) 1642-1643.

71. Jimmin Ma and C. Hammond, Ti-'84 Conference: Munich, FRG, AIME(1984) 703.

72. J.R. Leader, D.F. Neal and C. Hammond, Met. Trans., 17A (1986) 93-106.

73. C.H. Hamilton, A.K. Ghosh, M.M. Mahoney, Advanced Processing Methods for Titanium, C.H. Hamilton and D.F. Hasson, eds., TMS-AIME, (1982) 129-144.

74. M.A. Greenfield and H. Margolin, Met. Trans., 2A(1971) 841-847.

75. M.A. Greenfield and H. Margolin, Met. Trans., 3A(1972) 2649-2659.

76. C.I. Smith, B. Norgate and N. Ridley, Met. Science, May(1976) 182-188.

77. C.W. Humphries and N. Ridley, Journal of Material Science, 13(1978) 2477-2482.

78. A. Arieli, B.J. Maclean and A.K. Mukherjee, Ti-'80 Conference, ed. by H. Kimura and O. Izumi, publ.AIME, (1980) 1047-1056.

79. G. Gurewitz, Doctoral Thesis, University of California Davis, 1983.

80. R.Z. VAliev and O.A. Kaibyshev, Acta. Met. 31(1983) 2121-2128.

81. A.Arieli and A.K. Mukherjee, Met. Trans. 13A(1982) 717-732.

82. S.M.L. Sastry, P.S. Pao, K.K. Sankaran, Ti-'80 Conference, ed. by H. Kimura and O. Izumi, publ.AIME, (1980) 873-886.

83. M.F. Ashby and R.A. Verall, Acta Met., 21(1973) 149-163.

84. R.C. Gifkins, Met. Trans., 7A(1976) 1225-1232.

85. R.C. Gifkins, Journal Material Science, 13(1978) 1926-1936.

86. A. Dutta, N.C. Birla, A.K. Gupta, Trans. of the Indian Institute of Metals, vol.36, no.3.(June 1983) 169-177.

87. G.V. Shakanova, I.B. Rodina, F.V. Tulyankin, A.L. Pilipenko, N.A. Sarahagin and N.V. Bukharina, Ti-'80 Conference, ed. by H. Kimura and O. Izumi, publ.AIME, (1980) 849-861.

88. G.F. Vandervoort, "Metallography: Principles and Practices", McGraw-Hill, New York (1984) Chapter 2.

89. C.H. Hamilton and A.K. Ghosh, Met.Trans., 10A(1980) 1494-1496.

90. G.F. Vandervoort, "Metallography: Principles and Practices", McGraw-Hill, New York (1984) Chapter 6.

91. H. Abrams, "Stereology and Quantitative Metallography: STP 504", publ. ASTM, (1971) 138-182.

92. Chin Liu, Met.Trans., 17A(1986) 685-690.

93. S. Sagat and D.M.R. Taplin, Metal Science, March(1976) 94-100.

94. F. Dyment and C.M. Libanati, Journal Mat. Science, 3(1968) 349-359.

95. J.R. Springarn and W.D. Nix, Acta Met., 26(1978) 1389-1398.

96. G.A. Salishchev and R. Ya Lutfullin, Superplasticity and Superplastic Forming Conference, Blaine Washington , publ. TMS/AIME(1988) 103-107.